DEVELOPMENT OF GOLD NANOROD NIR ACTIVE SURFACES FOR HUMAN MESENCHYMAL STEM CELL DETACHMENT

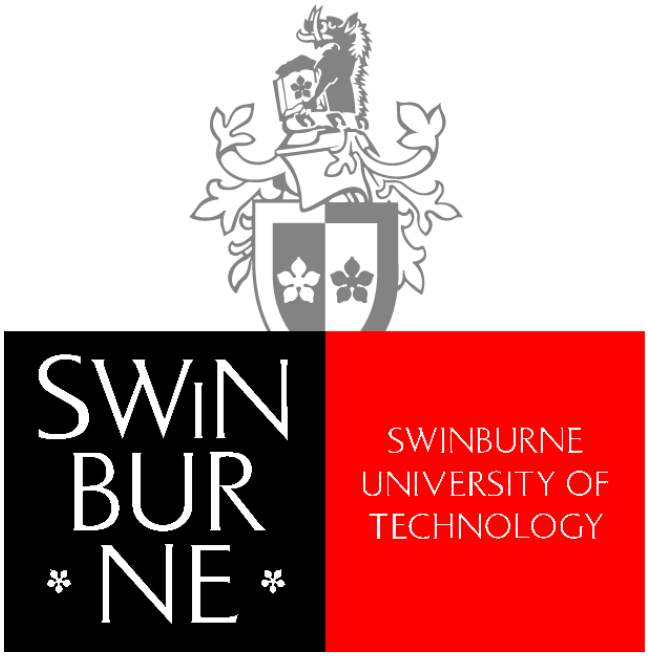

A thesis submitted for the degree of

Doctor of Philosophy

By

Yashaswini Vegi

ARC Training Centre in Biodevices

Faculty of Science, Engineering and Technology

Swinburne University of Technology

11 October 2019

“I'm writing a first draft and reminding myself that I'm simply shovelling sand into a box so that later I can build castles.”

Shannon Hale

Abstract

Stem cell therapies have shown the potential to dramatically improve patient outcomes in a variety of diseases and traumas including osteoarthritis, acute kidney injuries and bone non-union. Mesenchymal stem cells (MSCs) in particular have high therapeutic potential due to their ability to differentiate into a range of clinically useful cell types, availability and immunomodulatory property. Before transplantation, the MSCs are typically harvested from a donor or patient, and expanded to very large cell numbers. These large numbers of stem cells are required for successful therapy as each dosage requires millions of cells based on the disease to be treated. However, lack of methods and protocols to recover MSCs from culture substrates without damaging them is one of the factors impeding the widespread implementations of these therapies. Traditionally, cells are recovered from a cell culture substrate using enzymes such as trypsin. However, such enzyme-based cell recovery protocols are not ideal as the enzymes are derived from animal products and are expensive. They also non-specifically cleave a variety of cell surface proteins which can lead to dysregulation of cell function and even cell death.

This thesis outlines and develops an alternative enzyme free method for cell detachment. This method is based on the application of gold nanorods and near infra-red laser (NIR) to trigger non-toxic cell detachment from the culture surface. Surface-plasmons generated by irradiating surface electrons on the gold nanostructures with near infra-red light can induce nano-localised fluctuations in temperature which trigger cell detachment from the modified cell culture substrate. In collaboration with St. Vincent's Hospital, Melbourne, a new gold nanorods based coating for 2D substrates and microbeads have been developed in order to create biomaterials suitable for cell recovery on a clinically relevant scale.

Experiments have shown that strongly adherent NIH-3T3 mouse fibroblast cells and human mesenchymal stem cells (hMSCs) undergo efficient photothermal cell detachment from substrates functionalized with gold nanorods when irradiated with 785 nm laser diode. Not only were the cells viable post-NIR irradiation detachment, they also maintained their immunophenotype, and were successfully differentiated into adipogenic and osteogenic cells. While most of the results were equivalent to the

trypsinized cells, an increase in the hMSCs proliferative capacity and osteogenic differentiation potential was observed in the NIR irradiated cells. In addition to this, laser detached cells were seen to retain their surface proteins compared to enzymatically detached cells.

Another hurdle faced by the stem cell therapeutic industries is the production of stem cells on a large scale in order to treat diseases. While the demand for higher cell numbers are being overcome by using 3D cell culture techniques such as the microcarriers, the challenge to detaching the cells from their surface without compromising integrity by non-enzymatic means still remains.

In order to evaluate if this gold nanorods and NIR irradiation technique is applicable on a 3D surface, proof of concept studies were conducted on microcarriers coated with functionalized gold nanorods and cultured with hMSCs. These studies showed successful cell detachment when irradiated with NIR laser. Post-irradiation, a high cell detachment and viability was observed in the cells detached from the gold nanorods coated microcarrier surface.

All results suggests that it was possible to detach stem cells from a culture surface without the application of trypsin. With further studies it may also be feasible to apply this technique in large stem cell production industry.

Acknowledgements

As any other project, the amount of work that had to be done to complete this thesis successfully was tremendous. The completion of this thesis would not have been possible without the all the support and encouragement I have received from my supervisors, peers and friends.

First and foremost, I would like to express my gratitude to my supervisors, Prof Simon Moulton and Dr Nicholas Reynolds, for agreeing to supervise my PhD project. Your inputs, encouragement and guidance have been invaluable, and I am lucky to have such a great team. Nick, I appreciate your patience for having to deal with me dropping by your office randomly to ask questions regarding the project. I would also like to thank my industrial partner – St. Vincent's Hospital (Melbourne) and industrial supervisor, Prof Peter Choong for co-funding this project and for their help in driving the project forward.

I am truly grateful Prof Paul Stoddart, Prof Sally McArthur and Prof Gianni Renda for giving me the opportunity to be a part of the ARC Training Centre in Biodevices. This has been a gateway for me to gain experience in interacting with industries and devising my own project, which I never would have thought to be possible. I especially appreciate the guidance and mentoring from Paul. His input regarding optical physics and general advice has been vital during the course of my project.

I would like to express my gratitude to Dr Elaine Saunders for agreeing to be my mentor for the last four years. You have helped me to gain a better understating about the intricacies of a scientific career. I have also enjoyed your invitations to Woodend to take a break from my work and I am looking forward to future visits.

Dr Nerida Cole, I very much appreciate you help and guidance, especially during the last few months of my thesis. Your input regarding my work and thesis draft have been invaluable. And this, I believe, has made me a better researcher. Someday I hope to be as knowledgeable as you are.

There are endless number of people that I would like to acknowledge for their support and guidance throughout this entire project. I would like to thank Dr Mirren

Charnley for her help and advice with some of the biological procedures, especially with FACS studies. I found our discussions regarding the project and any other topic quite insightful and enjoyable. Dr Carmine Onofrillo, from St. Vincent's, for his help with PCR techniques. Dr Karyn Jarvis and Dr Blanca Del Rosal Rabes for allowing me drop by their office frequently, reading my manuscripts and/or to seemingly deal with my endless question regarding the project as well as life. Katharine Adcroft for assisting me with the lab protocols and helping me set up my experiments during the very early stages of my thesis.

I would also like to thank my friends and fellow PhD students at Swinburne University of Technology. It was enjoyable to bounce ideas off each other and solving problems together. Special thanks to Steve Béguin, Joelle Hawa, Benjamin Mooney, Jonathon Miegel, Umamageswari Suparamaniam, Joanna Nkyekyer, Shaun Gietman and Errol Phuah.

On a personal level I am sincerely grateful to my family, especially my Mum and Dad, who have supported me throughout this entire journey. A special shout out to my cousin, Akshat Mannam, for his unconditional support and strength for the past few years. To my friends Norbert Béguin, Catherine Hughes, Marion Dubois and crew from the rowing club especially Edwina Griffiths and Zoe Maxwell, I would have been a lab rat without you guys.

Statement of Original Authorship

I, Yashaswini Vegi, hereby declare that the research reported within this thesis entitled "*Development of gold nanorod NIR active surface for human mesenchymal stem cell detachment*", to the best of my knowledge is my original work unless otherwise stated. Any external work reported has been appropriately attributed and duly referenced to the original authors.

Yashaswini Vegi

ARC Training Centre in Biodevices
Faculty of Science, Engineering and Technology
Swinburne University of Technology
Melbourne, Australia

Dated this day, 11th October 2019

Table of Contents

List of Figures

List of Tables

List of Abbreviations

MSCs	Mesenchymal stem cells
EDTA	Ethylenediaminetetraacetic acid
GMP	Good Manufacturing Practices
Au NRs	Gold nanorods
PA-Au NRs	Poly amine conjugated gold nanorods
NIR	Near Infra-Red
ESC	Embryonic stem cells
hESC	Human embryonic stem cells
iPSC	Induced pluripotent stem cells
Oct3/4	Octamer-binding transcription factor 4
Sox2	Sex determining region Y-box 2
Klf4	Kruppel-like factor 4
c-Myc	Cellular Myc
DNA	Deoxyribonucleic acid
RNA	Ribonucleic acid
HSCs	Hematopoietic stem cells
ASCs	Adipose-derived stem cells
TCPS	Tissue culture polystyrene
PSCs	Perivascular stem cells
IFP	Infrapatellar fat pad
DMEM	Dulbecco's Modified Eagle's medium
BM-MSCs	Bone marrow-derived: large and more mature cells
NIP	Nestin-positive islet-derived multipotential stem cells
CFU	Colony-forming unit

CD	Cluster of differentiation
ALP	Alkaline phosphate
hMSCs	Human derived mesenchymal stem cells
GAG	Glycosaminoglycans
BMP	Bone morphogen proteins
RUNX2	Runt-related transcription factor 2
Cbaf1	Core-binding factor subunit alpha-1
cAMP	Cyclic adenosine monophosphate
SPP1	Osteopontin
BGLAP	Osteocalcin
OL1A1	Type I collagen
C/EBPα	CCAAT/enhancer binding protein gene
PPAR-γ	Peroxisome proliferator-activated receptor γ
Perf-1	Perforin 1
IBMX	Isobutylmethylxanthine
TGF-β	Transformation growth factor β
MAP	Mitogen-activated protein kinase
ERK-1	Extracellular signal-regulated kinase-1
HMG	High-Mobility-Group
AKI	Acute kidney injuries
CAM	Cell adhesion molecules
RGD	Arginylglycylaspartic acid
TGF-β	Transformation growth factor β
MAP	Mitogen-activated protein
ERK	Extracellular signal-regulated kinase
HMG	High-Mobility-Group

Sox	Sry-related HMG-box gene
Acan	Aggrecan
AKI	Acute kidney injuries
ECM	Extra cellular matrix
CAM	Cell adhesion molecules
RGD	Arginine-glycine-aspartate
GFOGER	Glycine-phenylalanine-hydroxyproline-glycine-glutamate-arginine
IKVAV	Isoleucine-lysine-valine-alanine-valine
HUVECS	Human umbilical vein endothelial cell
HRPTECS	Human renal proximal tubular epithelial cells
MCF-7	Michigan Cancer Foundation-7, breast cancer cell line
HeLa	Cervical cancer cell line
ErbB 2	Receptor tyrosine-protein kinase
EGFR	Epidermal growth factor receptor
HCC	Hepatocellular cancer
PCV	Porcine circovirus
BAEC	Bovine aortic endothelial cell
pNIPAAM	Poly-N-isopropylacrylamide
LCST	Lower critical solution temperature
SFM	Serum free media
DPBS	Dulbecco's phosphate-buffered saline
PEDOT	Poly(3,4-ethylenedioxythiophene)
SWNT	Single-walled carbon nanotube
ROS	Reactive oxygen species
CTAB	Cetyl trimethylammonium bromide

UV	Ultra violet
CW	Continuous wave
PDT	Photodynamic therapy
LLLT	Low laser level therapy
RRD	Rhegmatogenous retinal detachment
LITT	Laser-induced thermal therapy
MRTI	Magnetic resonance thermal imaging
LASIK	Laser-assisted in situ keratomileusis
hUMSCs	Human umbilical cord mesenchymal stem cells
HaCaT	Human keratinocytes
hBM-MSC	Human bone marrow derived mesenchymal stem cells
CCO	Cytochrome c
NO	Exogenous nitric oxide ligands
NADH	Nicotinamide adenine dinucleotide
ISO	International standard organization
LSPR	Localised surface plasmon resonance
LPR	Longitudinal plasmon resonance
TPR	Transverse plasmon resonance
EGFP	Enhanced green fluorescence protein
PTT	Photothermal therapy
PEG	Polyethylene glycol
KB cells	Keratin forming tumour cell line from oral epithelium
HepG2	Liver hepatocellular carcinoma cell line
DOX	Doxorubicin hydrochloride
SiO_2-Au NRs	Silica coated gold nanorods
NHS	N-hydroxysulfosuccinimide

JEG-7	Human choriocarcinoma cells
L-929	Mouse fibroblasts
PGA	Poly glycolydes
PLGA	Poly(lactide-co-glycolydes)
MDBK	Madin-Darby bovine or canine kidney cells
CHO	Chinese hamster ovary cells
VERO	Cercopithecus aethiops kidney epithelial cells
BHK	Baby hamster kidney cells
HEK-293	Human embryo kidney cells
NS0	Mouse myeloma cells
SEM	Scanning electron microscope
EM	Electromagnetic
SiO_2-Au NRs	Silica coated gold nanorods
ProA-Au NRs	Protein A conjugated gold nanorods
PA-Au NRs	Polymer coated amine functionalized gold nanorods
PEI	Polyethylenimine
PBS	Phosphate-buffered saline
UV-Vis	Ultra violet visible
BSA	Bovine serum albumin
CCM	Cell culture media
IR	Infra-red
DMEM	Dulbecco's Minimum Essential Medium
α-DMEM	Alpha Dulbecco's Minimum Essential Medium
FBS	Foetal bovine serum
Anti-Anti	Antibiotic-Antimycotic
NA	Numerical aperture

Calcein AM	Calcein acetoxymethyl ester
PI	Propidium Iodide
FMNH	Flavin mononucleotide
NADH	Nicotinamide adenine dinucleotide
NADPH	Nicotinamide adenine dinucleotide phosphate
FADH	Flavin adenine dinucleotide
IBMX	3-isobuty-1-methyl-xanthine
Ig	Immunoglobulin
Fab	Fragment antigen binding
FC	Fragment crystallisable
FACS	Fluorescence activated cell sorting technique
FITC	Fluorescein isothiocyanate
APC	Allophycocyanin
PE-Cy7	R-phycoerythrin cyanine dye 7
dNTP	Nucleotides
RT-qPCR	Quantitative reverse transcription polymerase chain reaction
cDNA	Complementary DNA
mRNA	Messenger RNA
GAPDH	Glyceraldehyde 3-phosphate dehydrogenase
FABP4	Fatty acid binding protein 4
DAPI	4′,6-diamidino-2-phenylindole
HL60	Human leukaemia cell lines

Scientific Communications

Oral Presentations

25th Annual Australasian Society for Biomaterials and Tissue Engineering Conference (ASBTE 2017) in conjugation with 7th Indo-Australian Conference on Biomaterials, Implants, Tissue Engineering and Regenerative Medicine (7th Indo-Australian BITE & RM), Canberra, Australia, 18th to 20th April 2017, *"A Scalable, Enzyme Free Method for Mesenchymal Stem Cell Recovery"*.

2018 European Materials Research Society Spring Meeting (EMRS 2018), Strasbourg, France, 18th to 22nd June 2018, *"Plasmonic Surfaces as a Scalable, Enzyme Free Method for Mesenchymal Stem Cell Recovery"*.

Poster Presentations

2018 International Conference on Nanoscience and Nanotechnology (ICONN 2018), Wollongong, Australia, 29th January to 2nd February 2018, *"A Scalable, Enzyme Free Method for Mesenchymal Stem Cell Recovery"*.

Intellectual Property and Industry Research Outputs

Provisional patent

Vegi Y, Choong P, Moulton S, Reynolds NP: (2017), AU2017901378 (Prov. Patent), *Method and substrate for cell recovery*.

Registered Patent

Vegi Y, Moulton S, Reynolds NP: (2018), WO2018187840 (International Patent Co-operation Treaty), *Method and substrate for cell recovery.*

Chapter 1: Introduction

1.1 BACKGROUND

Stem cell therapies have the potential to revolutionize the treatment of a number of the world's most socioecomically devastating diseases and traumas, including cardiovascular disease, arthritis, Alzheimer's and a variety of cancers. Typically stem cells are harvested from healthy tissue, cultured in the lab and then transplanted to the diseased tissue. Due to the transplanted stem cells ability to transform into various different cell types (a process known as differentiation), they can begin to regenerate healthy tissue at the disease site. The widespread clinical implementation of these therapies is currently prevented by a lack of methods to generate large numbers of healthy stem cells that possess the necessary ability to regenerate diseased tissues. One of the reasons for this is the reliance of harsh enzymatic treatments (i.e. trypsinization) used to detach the cells from culture substrates before implantation. These enzymes can damage the cells preventing them from transforming into other cell types, or even killing them reducing the overall effectiveness of any subsequent transplantation. In my thesis, I have developed new non-enzymatic photothermal methods for cell detachment, that can recover cells from culture substrates with high efficiency without effecting their ability to transform into other cell types or reducing their viability.

Mesenchymal stem cells (MSCs) emerged as one of the most potent stem cells for clinical applications due to their ability to differentiate into cell types relevant to some of the most prevalent diseases in the modern world (i.e. osteoblasts for bone tissue engineering, chondrocytes for cartilage tissue engineering and myocytes to treat cardiovascular disease). Their immunomodulatory properties means that they can be harvested either from an autologous (from the patient) or allogenic (from a donor) sources. Finally, compared to other stem cells, MSCs are free of ethical concerns and can be harvested from a variety of sources (e.g. bone marrow, fat, synovial membrane, umbilical cord blood, and periodontal ligaments [1]) using simple non-invasive surgical procedures like arthroscopy (key hole surgery).

1.2 CONTEXT

Mesenchymal Stem Cells (MSCs) are anchorage dependant cells that need to adhere to a surface to proliferate, maintain viability and their ability to differentiate.

This adhesion is controlled by various protein molecules and mechanisms between the cells and the substrate. After harvesting, MSCs are typically expanded to sufficient numbers on flat plastic cell culture dishes, this causes two problems:

a. **The cells need to be removed from these plastic substrates before transplantation.**

The conventional method for harvesting of cells from a substrate, is by using enzymatic reagents (EDTA-trypsin) and in some cases mechanical force (cell scraping) (not applicable for microcarriers). EDTA-Trypsin, used in research labs, are mostly animal derived (porcine). But the production of medical grade MSCs demands application of strict GMP (good manufacturing practices) guidelines. GMP guidelines recommend the usage of clinical grade non-animal origin reagents (xeno free). This recommendation was put forward to avoid zoonotic disease transmission that is possible while using reagents from animal sources [2]. Currently TrypLE select (Invitrogen) is considered as the "gold standard" for harvesting clinical grade MSCs. TrypLE express is a recombinant fungal serene protease that acts like trypsin. The main advantage of TrypLE express is that it is of animal free origin, thereby making it GMP compliant. Another similar product is TrypZean solution from Sigma [2, 3]. However, all these enzymatic cell detachment methods show limited specificity and digest important proteins expressed on the surface of the MSCs limiting their clinical value and in some cases causing cell death (enzymatic treatments typically result in a drop in viability of up to 20%, such losses are unacceptable for stem cell therapies when every additional cell is essential).

b. **The amount of cells required for a therapeutic effect is extremely high, meaning that huge cell culture surface areas are required for clinical significance.**

The therapeutic industry faces a bottleneck in the production of relevant cell numbers due to its reliance on traditional flat tissue culture plastic surfaces with limited surface area. For example, up to 50 million MSCs are needed to treat one osteochondral defect (a leading cause of osteoarthritis) in a normal adult [4]. Tissue culture plastic can culture approximately 40,000 MSCs per cm^2, meaning that a flat surface with an area of 1250 cm^2 is required for one treatment (and often multiple treatments are required per patient). Currently approximately 4 million people in Australia are suffering from osteoarthritis [5]. If all of these people were to require one

round of MSC therapy this would require 5 $\times 10^9$ cm^2 (500000 m^2) of tissue culture plastic. This surface area is equal to approximately 20 times the surface area of the MCG (Melbourne Cricket Ground) and is obviously unrealistic. This problem is currently being overcome by using microcarriers to support MSC growth. Microcarriers are biocompatible spheres which MSCs can adhere to and when cultured in stirred tanks in high concentrations can provide massively increased surface areas for cell culture (cf. flat plastic). As with flat plastics harvesting the cells from the microcarriers without reducing their clinical potential is highly challenging.

The goal of my thesis is to develop new protocols to detach cells, from cell culture substrates (both flat 2D substrates and microcarriers), that do not use damaging proteases like trypsin. This was achieved using a photosensitive gold nanorod functionalised surface that can be modulated by the application of near-infra red radiation.

1.3 PURPOSES

This thesis was designed with two main objectives:

a. **To explore novel methods that would allow detachment of stem cells from a cell culture surface, that does not involve trypsinization.**

This was demonstrated by using gold nanorods (Au NRs) coated surface and near infra-red laser (NIR). The exposure of Au NRs to NIR irradiation (wavelength of 785 nm) may have a thermal interaction, which lead to the detachment of cells from the Au NRs culture surface. After experimenting with various Au NRs (silica coated Au NRs, Protein A-conjugated Au NRs and Poly amine conjugated Au NRs) I decided to use poly amine conjugated gold nanorods (PA-Au NR). The reason behind the application of PA-Au NRs was mainly due to the nanoparticle's ability to form an even coating on the cell culture surface compared to other Au NRs.

NIH 3T3 mouse fibroblasts were chosen for pilot studies and human MSCs were used for main studies. Six parameters of cell behaviour, pre irradiation (in presence of Au NRs) and post irradiation, were evaluated: cell viability, cell proliferation capacity, immunophenotype, differentiation, gene expression and extra cellular matrix quantification. Cell viability of non-irradiated cells cultured on Au NRs and post NIR irradiation was studied.

Cell viability studies showed that Au NRs coated surface had no significant toxic effect on the cells. Following that, the cells were cultured on Au NRs coated surface and the entire surface was then exposed to a continuous wave near-infrared laser with a wavelength of 785 nm for 1 hour. The nanorods excitation due to NIR irradiation lead to the detachment of cells from the culture surface. Au NRs have surface plasmons which can be excited when exposed to electromagnetic waves. The excitation of the surface plasmons results either in photothermal (heat) or photochemical (reactive oxidation species or ROS) interaction between the gold Au NRs and the cells. This interaction may have led to cellular detachment from the Au NRs coated surface.

Post-irradiation, the detached cells were re-cultured, and studies showed no significant effect of laser detachment on the cell viability or proliferative capacity. hMSCs, detached via NIR irradiation, displayed a similar immunophenotype, differentiative capacity and gene expression as those of the cells detached via trypsin.

b. To study if the novel detachment method is applicable on microcarriers.

After obtaining successful detachment of cells from the flat surface I coated glass microcarriers with PA-Au NRs. Quantification of the amount of Au NRs present on the microcarrier surface was performed using dark field microscopy and mass spectrometry. Following this, cells were cultured on the PA-Au NRs coated microcarrier surface. Before NIR irradiation, the cells showed no significant difference in cell viability or proliferative capacity when compared to cells grown on non-coated surface. When cells grown on Au NRs coated microcarriers were exposed to continuous wave NIR irradiation of 785 nm, detachment of cells from the microcarrier surface were observed. Post-irradiation, the cells showed good viability and proliferative capacity.

1.4 THESIS OUTLINE

The research conducted in this thesis is extensively described in the following chapters:

Chapter 2 provides a background overview regarding the topics that are required to be understood in order to critically analyse the experiments and data gathered throughout the thesis. The literature review outlines the basics of stem cells and their applications in therapeutic industry with attention paid to mesenchymal stem cells. Subsequently, a review was conducted on current cell detachment techniques. This

review highlights the drawbacks and gaps in development of an appropriate cell detachment technique. Following this I described the principles and applications of near infra-red laser and Au NRs in therapeutic industries. This rationalizes the reasoning behind the usage of these two techniques for cell detachment. Finally, I describe the bottleneck facing therapeutic industries due to the limitations in the number of stem cells produced, the cell harvesting method and the different methods being investigated to tackle this problem. While microcarriers maybe the answer, it still faces the problem of detaching the cells from its surface.

In chapter 3 various experimental techniques including their working principles are described. This information is provided to in order to understand the reasoning behind each technique used in the context of this thesis.

Chapter 4 deals with surface coating a 2D surface using different functionalized gold nanorods. In this chapter I describe the materials, methods and techniques used to obtain an evenly coated Au NRs surface. Studies regarding Au NRs characterisation, surface coating, temperature evaluation were performed using UV-Vis spectrometer, scanning electron microscope and thermal camera respectively. I also detailed the parameters and characteristics of the laser used during my entire thesis.

In chapter 5 various biological studies were performed with NIH-3T3 mouse fibroblasts and human derived mesenchymal stem cells. I studied the viability of these cells on different concentrations of Au NRs coated surface. Studies were conducted to determine if the cells cultured on Au NRs coated surface could be detached via NIR irradiation and if the detached cells were viable. The laser detached hMSCs were also studied to determine if the laser irradiation altered their immunophenotype, differentiative capacity and gene expression. In addition to this I also made a comparative study in extracellular matrix degradation between cells released via trypsin and NIR irradiation.

Chapter 6 describes the proof of concept studies carried out to determine if Au NRs could be coated on microcarriers and if cells cultured on these microcarriers, post irradiation with NIR would display cell detachment. Glass based microcarriers were coated with gold nanorods and experiments were carried out to observe if the cell detachment observed on the 2D surface could be replicated on 3D surface. Quantification of gold nanorods on the microcarrier surface was performed by using

dark field microscopy and mass spectrometry. Cell viability of MSCs were studied pre and post irradiation using Live/Dead staining and PrestoBlue assay.

In chapter 7, I summarised all the key findings presented in the previous chapters and recommended some future works that may help in scaling up the cell detachment techniques.

Chapter 2: Literature Review

Regenerative medicine is an emerging branch of medical science that aims to restore and replace diseases or damaged human tissues and organs [6]. This field can be divided into tissue engineering, cellular therapies, artificial implants and artificial organ development. Stem cells offer an exciting opportunity in the development of cellular therapies due to their unique ability to transdifferentiate into all human cell types. To date stem cell therapies have been developed in various regenerative medical applications[6] and used to treat various diseases and conditions including cartilage defects [7], osteoarthritis [8], liver cirrhosis [9], Crohn's disease [10] and osteogenesis imperfecta [11].

One major bottleneck that is preventing the widespread application of stem cell therapies is a lack of protocols and materials available to provide the large numbers of clinically viable cells required for successful clinical outcomes. For example, a study conducted by Broekman *et al.,* to treat chronic obstructive pulmonary disease required between 1-2 $\times 10^6$ stem cells/kg of body weight. If a patient weights 50 kg, the total cell numbers required for the treatment would be between 50-100 $\times 10^6$ cells per infusion [12]. Higher number of infusions would require larger amount of cells which means there is a need to expand cells on a larger scale. On a commercial scale the vast majority of stem cells are cultured on 2D flat surfaces with limited surface area and are dissociated from these surfaces by trypsin. While flat surfaces produce limited number of cells and take up large space, trypsin is known to cause cellular dysfunction. Stem cells, which hold a promising future for cellular therapies, are required in larger quantities with an intact quality in order to be used for human therapeutics.

In the current chapter, I provide an in-depth insight about stem cells and their therapeutic uses, cell detachment techniques that are currently being used and developed, interaction of light with tissues, gold nanorods and their applications, 2D cell culture and cell expansion using 3D cell culture. The information supplied in this chapter would provide necessary knowledge to critically analyse the data gathered in the following chapters.

2.1 STEM CELLS

Although the term "Stem Cell" was coined by Alexander Alexandrowitsch

Maximow in 1908, it was not until 1963 stem cells were truly discovered in mouse bone marrow by Siminovitch *et al* [13, 14]. Siminovitch *et al*., were actively conducting studies to determine if cells derived from mouse haematopoietic tissues displayed colonial formation without being rejected, when injected intravenously into the irradiated mice. The results from their studies showed the presence of rapidly forming colonies on the mice spleen. This showed that the haematopoietic cells could extensively proliferate, self-renew and differentiate, which are the characteristics of stem cells. The successful isolation of haematopoietic stem cells from human cord blood in 1978, paved the way for their potential use in the treatment of various disease [15]. Since then, there have been many major breakthroughs in the area, including the discovery of other types of autologous adult stem cells, human embryonic stem cells in 1998 [16] and invention of induced pluripotent stem cells in 2006 [17].

Stem cells can be defined by (i) their self-renewal and proliferative capacity (unlike nerve cells, muscle cells and blood cells) (ii) their ability to remain undifferentiated (iii) and their capacity to differentiate into different cell lines. The plasticity of these stem cells makes them invaluable in the cell therapy industry [18, 19].

A cell's capacity to differentiate into different cell types is termed as cell potency (Figure 1). Different degrees of potency observed in various stem cells are [20]:

1. Unipotency: The least potent of the stem cells, unipotent stem cells have the ability to differentiate into only one cell type. Epithelial stem cells are one of the prime examples of unipotent progenitor stem cells. [21]
2. Multipotency: These stem cells have the ability to differentiate into multiple cell lines. Since these cells are derived from a single germ layer, they are restricted to differentiating into a limited family of cells. Mesenchymal stem cells are the most well-known multipotent stem cells [20].
3. Pluripotency: Pluripotent stem cells can differentiate into cell lines arising from all the three different germ layers (endoderm, ectoderm and mesoderm). The prime examples of these cells are embryonic stem cells (ESC) and induced pluripotent stem cells (iPSC) [20].
4. Totipotency: These cells have the ability to differentiate into all types of cell lines hence also names as "omnipotent" cells. They are derived from a first

few division of an embryo or zygote after fertilization [20].

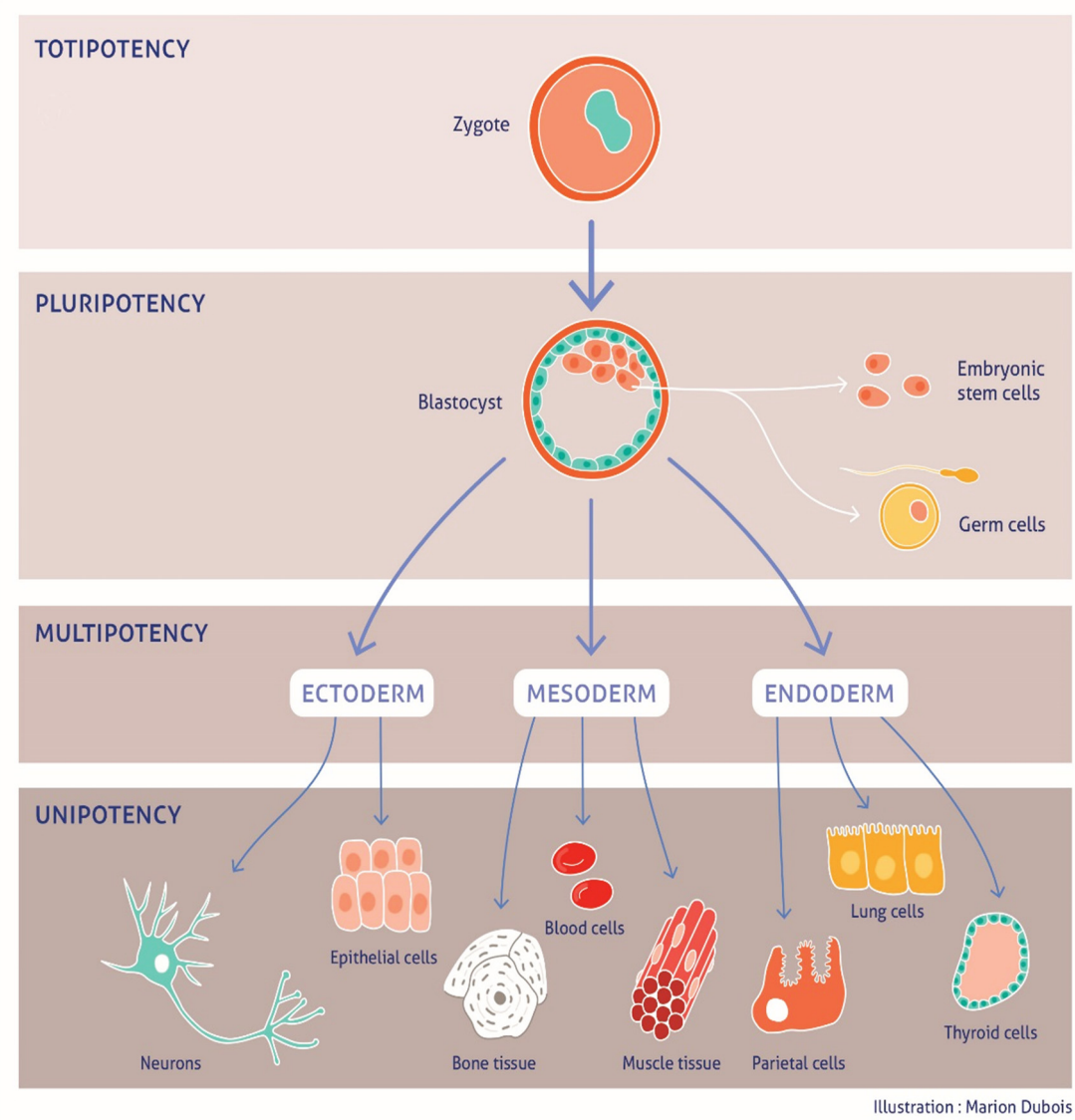

Figure 1: Stages of stem cell potency. Pluripotent stem cells have the ability to differentiate into any cell type. Pluripotent stem cells can differentiate into cells belonging to all the three germ layers. Multipotent cells differentiate into cells belonging to the germ layer they are derived from. The least potent of all the stem cells, unipotent stem cells are pre-committed to differentiate into a particular cell type.

2.1.1 Stem cell locations: The "Niche" property

Stem cells are of importance due to their ability to proliferate and differentiate into different cell lines in order to maintain the tissue function. During physiological stress these cells are expected to replace, and repair injured or apoptotic cells. To perform these functions the cells are maintained in a microenvironment where they are protected and maintain sufficient communication with each other. While unregulated proliferation can lead to stem cell exhaustion and tumorigenesis, uncontrolled differentiation would lead to deficiency of stem cell pool [22, 23]. The stem cell

"niche" was first proposed by Schofield in 1978 [24] and it can be described as a microenvironment that supports the stem cells. The stem cell niche are made of cellular components that anchor the stem cells, secrete growth factors and cytokines, maintain cell-cell interaction, regulate their self-renewal and maintain the differentiation capacity of the stem cells [25-27].

The ability of cells to revert to a reversible dormant state, is known as cell quiescence. The stem cell quiescent state is regulated by their microenvironment in the niche region, where tissue homeostasis, proliferation and differentiation is tightly regulated [22]. The exposure of these cells to extrinsic signals, in response to injury or disease, causes the cells to re-activate from their quiescent state, homing them to the injured site and differentiate terminally into a required cell type to recover the damaged tissue [28].

2.2 TYPES OF STEM CELLS

Stem cells can be classified into three types based on their origin: embryonic stem cells, adult stem cells, and induced pluripotent stem cells.

2.2.1 Embryonic Stem Cells

Formation of a zygote in mammals occurs when a female ovum is fertilized with a male sperm. In early development in mammals prior to implantation, a fertilised ovum undergoes cell division to form a blastocyst comprising 40-150 cells. A blastocyst consists of an outer layer of cells called the trophoblast which surrounds a fluid-filled cavity, the blastocoel and an inner cell mass. If the blastocyst is implanted and development continues, the trophoblast will form the extra-embryonic structures such as the placenta, while the inner mass will eventually develop in to the foetus [29].

Embryonic stem cells (ESCs) are derived from the inner cell mass from *in* vitro culture of mammalian blastocysts 5-6 days after fertilization. Due to their ability to differentiate into tissues of the three primordial germ layers, these cells are pluripotent in nature [30, 31]. Human ESCs have a comparatively extended replicative life span as a result of high levels of telomerase activity, which allows cells to divide without reaching the Hayflick limit at which point the cell division ceases and the cell becomes senescent [16]. Hayflick limit states that, in an *in vitro* cellular culture, human cells have a finite lifetime and following a certain number of population doubling, the cells are programmed to stop proliferation and enter cellular senescence [32].

ESCs are cultured on feeder layers which are either made up of mouse embryonic fibroblasts [16] or human derived embryonic fibroblasts combined with adult fibroblast cells [33, 34]. The risk of cross-contamination due to the presence of feeder layers prevents the transfer of ESCs to a clinical setting. In addition to this the research in hESCs is strictly limited and regulated due to issues pertaining to ethical controversies, political and religious factors [35].

2.2.2 Induced Pluripotent Stem Cells (iPSC)

The ethical dilemma surrounding the use of pluripotent ESCs and the difficulty in obtaining them in stem cell research has demanded an alternative for cell therapeutics. In 2006 and 2007, Takahashi and Yamanaka made a breakthrough by successfully re-programming somatic mouse cells and adult human dermal fibroblasts to revert back to an undifferentiated state by modifying the cell genetic material using a retrovirus. These cells behave like/similarly to ESCs[17, 36]. Retrovirus are viruses that encode their genetic material as RNA. Upon entering the host cells, the RNA is transcribed into viral DNA and are multiplied. Followed by a multiple step new retroviruses are formed in the host cells and spread to the surrounding cells [37].

The over expression of 4 transcription factors namely, Oct3/4, Sox2, Klf4, and c-Myc causes cells to revert back to their pluripotent stage. This was exploited by inserting the genes for these transcription factors into the fibroblasts using retroviral vectors. The resulting cells overexpressed these proteins. Studies have shown that, iPSC show similar morphology, telomerase activity, gene expression, surface marker expression, similar doubling time and the ability to differentiate into cells related to 3 germ layers to that of ESCs [36, 38]. Despite this ground-breaking discovery, the use of viruses to manipulate the genetic materials carries a number of risks for use in patients. These include the potential for the virus to remain active and/or for the unregulated expression of genes to have deleterious effects. For example c-Myc is known to be oncogenic and it's over expression in the recipient may lead to the development of tumours [39]. Studies have already shown the reactivation and expression of retroviral c-Myc gene in the iPSC. This outcome is less desirable due to c-Myc's known oncogenic potential [40]. Consequently, while promising, the use of genetically manipulated cells will require extensive development and rigorous testing before meeting clinical requirements.

2.2.3 Adult Stem Cells

Totipotency in stem cells disappears after earlier divisions of oocytes. With each foetal developmental stage, the oocytes give rise to different distinctive stem cells with restrictive proliferative and differentiative capacity. Adult stem cells, also known as somatic stem cells, can be found residing in various tissues of a human body and like any other stem cells they are responsible for maintaining the homeostasis and repairing injures/diseased tissue. Stem cells such as mesenchymal stem cells (MSCs) and hematopoietic stem cells (HSC) are known to be multipotent in nature due to their ability to differentiate into various cell lines. The least versatile adult stem cells are the oligopotent progenitor cells. Progenitor cells are partially differentiated cells that are committed to differentiation into specific lineage [41]. Progenitor cells are descendants of stem cells, but are more constrained in their capacity for replication and their differentiation potential.

One remarkable advantage of adult stem cells is the ability to use the patient's own cells for therapy. As the cells are autologous they do not give rise to tissue rejection or have the limitations described above for embryonic or induced pluripotent stem cells or have ethical restrictions [42]. Adult stem cells that are patient-derived can be expanded to the numbers required for a clinical intervention and differentiated into the required cell type for the treatment. Their utility is demonstrated by clinical studies that have been conducted to treat a wide range of conditions including myocardial infarction, ischemic stroke, bone tissue regeneration, degenerative eye disease etc., [43-46]. However, there are a number of disadvantages to this approach. The major difficulties are their limited availability as they are present in low numbers in adult humans and isolating these cells from differentiated cells in the same tissue is challenging. Research and clinical applications most commonly use mesenchymal stem cells and haematopoietic stem cells. Stem cell studies in this thesis was conducted by using human MSCs.

The most common methods for harvesting adult stem cells from various sources are as described below:

1. Bone marrow is a rich source of pluripotent mesenchymal stem cells. Bone marrow is usually obtained surgically from iliac crest of a donor by aspiration using a bone marrow aspirate needle with or without ultrasound guidance. The bone marrow is dispersed in cell culture media and then

filtered through a fine sieve membrane to remove cell aggregates. Nucleated stem cells are then isolated, cultured and expanded [47]. The requirement for invasive surgery to harvest the bone marrow is a major drawback of this technique.

2. Adipose-derived stem cells (ASCs) can be easily harvested by liposuction from various regions of the body. Following its collection, the lipoaspirate is allowed to settle in order to separate blood from the fat. The blood is pipetted off and the lipoaspirate is then washed several times to remove blood residue. The fat is separated from the aqueous layer by phase separation and collected by aspiration. The isolated fat is washed and enzymatically digested frequently with collagenase. The digest is then centrifuged to separate the mature adipocytes and lipids from the stromal vascular fraction (SVF), a heterogeneous mixture of blood cells, fibroblasts, pericytes, endothelial cells and ASCs. The ASCs are enriched by selection for plastic adherence before expansion. [48, 49].

   When compared to harvesting stem cells bone marrow, stem cells derivation from adipose tissues is less invasive, with less post-operative pain. In addition to this lipoaspirate are known for their high yield of stem cells. 10^7 stem cells can be harvested from 300 mL of lipoaspirate [50].

3. Another type of mesenchymal stem cells are perivascular stem cells (PSCs). PSCs can be harvested from infrapatellar fat pad (IFP) and the extraction technique is similar to that of ASCs [51].

4. In addition to the sources and methods mentioned above, adult stem calls stem cells can also be derived from synovial membrane [52], periodontal ligaments [53], skin [54], umbilical cords blood [55] and skeletal muscles [56] etc. Detailing the extraction of the stem cells from every source is beyond the scope of this thesis.

In Table 1 lists different types of stem cells recognised, their proliferation potential and the differential potential shown by each of the cells.

Table 1: A list of different adult stem cells found in human body.

Name	Derived location	Proliferation Potential	Differential Potential	Reference
Embryonic stem cells	Inner cell mass of blastocysts	Up to 8 months	Cells have the potential to differentiate into ectodermal, endodermal and mesodermal cell lines	[16, 57, 58]
Neural stem cells	Dentate gyrus of the hippocampal region and lateral ventricle wall, olfactory lobes	60 cell doubling	Neurons, astrocytes, oligodendrocytes,	[59-62]
Bone marrow derived mesenchymal stem cells	Bone marrow	Proliferates extensively	Osteocytes, adipocytes, chondrocytes	[63-66]
Umbilical cord mesenchymal stem cells	Wharton's jelly of the umbilical chord	80 population doubling	Osteocytes, adipocytes, chondrocytes, neurons, glial cells and cardiomyocytes	[66-69]
Adipose derived adult stem cells	Adipose tissues	100 population doubling	Chondrocytes, osteocytes, adipocytes, neural progenitor cells, smooth muscle cells, cardiomyocytes,	[48, 50, 70-73]
Synovial membrane derived mesenchymal stem cells	Synovial membrane and synovial fluid	30 population doubling	Adipocytes, osteocytes, chondrocytes and sometimes myocytes	[52, 74, 75]
Dental pulp stem cells	Pulp in human teeth	>140 population doubling	Odontoblast like cells	[76-78]
Skin derived stem cells	Dermis	Not stated	Neuroectodermal and mesodermal lineage cells including neurons, smooth muscle cells, adipocytes, astrocytes and glial cells	[79-81]
Blood derived mesenchymal precursor cells	Blood	Not stated	Osteocytes, adipocytes, fibroblasts	[82]
Umbilical cord blood	Umbilical cord	Up to 14 weeks	Shows embryonic stem cell characteristics. Can undergo angiogenesis or differentiate into, endothelial/myogenic cell lines, islets like cells, neural like cells	[83-85]
Skeletal muscle stem cells	Muscles (e.g., brachioradialis muscle, pectoral muscle)	Up to 20 population doubling or 3 months in cell culture	Skeletal muscle fibres, smooth muscle cells, adipocytes, osteocytes, neural cells	[86-90]

2.3 AUTOLOGOUS VS ALLOGENIC STEM CELL THERAPY

Stem cell therapy can simply be defined as the application of stem cells, in a patient, to treat various diseases. As mentioned previously, they can be used for autologous therapy as well as allogenic therapy:

1. Autologous stem cell therapy: In this system, the stem cells are extracted from the patient to be treated, expanded ex-vivo to a relevant scale and then induced back into the patient.
2. Allogenic stem cell therapy: In this process, the stem cells originate from a single donor. These stem cells are expanded on a large scale and are used to treat a number of donors.

The difference between the two stem cell therapy are stated in the Table 2 below:

Table 2: Autologous Vs allogenic stem cell therapy. Table adapted from Malik *et al*., [91]

	Autologous Stem cell therapy	**Allogenic Stem cell therapy**
Immune rejection risk	Low	High
Cell survival rate and integration	High	Low
Quality of cells	Dependant on the patient. The quality and the quantity of the stem cell decrease with the increase in the age of the donor.	Usually high as cells are extracted from healthy young donors. This increases the quality and quantity of stem cell yield.
Risk of cross-contamination	Low	High
Off the shelf	No	Yes
Number of doses in a batch	Up to 2000	One dose is equivalent to a batch
Number of procedures during treatment	Two procedures: extraction of stem cells and re-administration after expansion	Single procedure: only administration of stem cells
Automation and scaling up	Difficult as each batch/dose is different from other and can risk cross-contamination. May required different production protocol for each patient/	Easier as all doses in a batch are homogeneous thereby allowing the application of same protocol.
Manufacturing cost of each dose	High	Low

2.4 MESENCHYMAL STEM CELLS

Though the presence of non-haematopoietic stem cells in the bone marrow was first suggested in 1867 by German pathologist Julius Cohnheim, it was not until a century later that mesenchymal stem cells (MSCs) were discovered [65]. In the mid-1960s, Friedenstein identified the presence of MSCs in the bone marrow of a guinea pig. During his investigation, the murine whole bone marrow samples were placed in a plastic culture dish and after 4 hours the non-adherent cells were removed. He observed heterogeneous, tightly adherent fibroblast-like cells with a spindle shape that clustered in colonies [92]. He showed that these cells were multipotent and were able to differentiate into osteoblasts, chondrocytes, adipocytes and hematopoietic supporting stroma when a single colony forming unit (CFU)was re-transplanted in vivo [93].

This finding has been confirmed by many *in vitro* studies showing the ability of these cells to differentiate into adipocytes, osteocytes, chondrocytes and myoblasts [64, 94-96]. It was in 1991, the term “mesenchymal stem cells” was officially coined by Caplan for these derivatives of bone marrow cells. This was due to their capacity to differentiate into diverse groups of mesodermal tissues and phenotypes [97].

In addition to differentiating into cells from mesoderm, studies have also shown that MSCs have the capacity to differentiate into ectodermal and endodermal tissues such as hepatocytes, neutral cells and endothelial cells [98-100]. This property makes them trans-differential in nature (Figure 2). According to Jopling *et al*., it is the ability of these stem cells to regress to their dedifferentiated stage and switch lineage. [101]

Although MSCs were thought to be present only in bone marrow, recent studies have shown that these cells can be isolated from various human tissues such as skin, dental pulp, fat, umbilical cord, muscles, placenta, skeletal muscles, ligaments, veins , brain, guts, blood vessel [102]. Despite their presence in various tissues, MSCs derived from bone marrow are the most studied cells. The frequency of MSC in bone marrow aspirate of an adult is between 1:50,000 – 1:100,000 or 0.001% to 0.01% [63, 103].

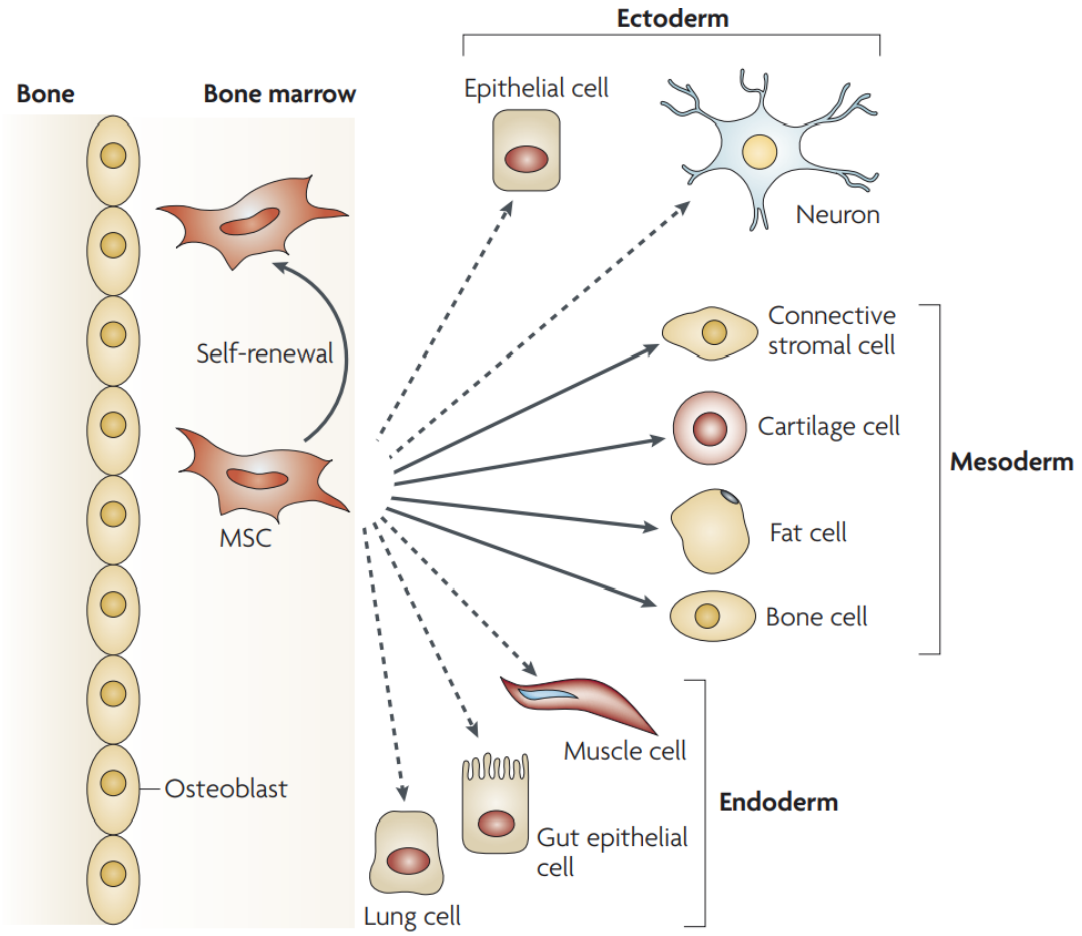

Figure 2: Mesenchymal stem cells have the ability to self-renew and differentiate into mesodermal cell lines such as osteogenic, adipogenic and chondrogenic cell types. In addition to this recent studies have also shown the MSCs to transdifferentiate into cell types belonging to ectoderm and endoderm.. Image adapted from Uccelli *et al*., [104]

As stated earlier MSCs are isolated from whole bone marrow by disposing off the non-adherent cells from the tissue culture plastic. Post collection, these cells exhibit quiescent state and morphologically spindly shaped. The adherent cells are then cultured in DMEM media supplemented with foetal bovine serum and growth factors. At passage 0, MSC are slow to replicate due to a lag phase but with successive passages these cells expand rapidly and appear homogeneous [105, 106].

2.4.1 MSC characterisation

Though considerable progress is being made in characterising MSCs, no particular universal or MSC specific marker has been identified. The Mesenchymal and Tissue Stem Cell committee of the International Society for Cellular therapy made a proposition statement outlining the minimum criteria required for the cells to be defined as mesenchymal stem cells [107]. The proposition states: “First, MSC must be plastic-adherent when maintained in standard culture conditions using tissue culture

flasks. Second, ≥ 95% of the MSC population must express CD105, CD73 and CD90, as measured by flow cytometry. Additionally, these cells must lack expression (≤ 2% positive) of CD45, CD34, CD14 or CD11b, CD79a or CD19 and HLA class II. Third, the cells must be able to differentiate to osteoblasts, adipocytes and chondroblasts under standard in vitro differentiating conditions."

The surface markers, also known as cluster of differentiation (CD) molecules, are useful for identification and characterisation of cells and sub cell populations.

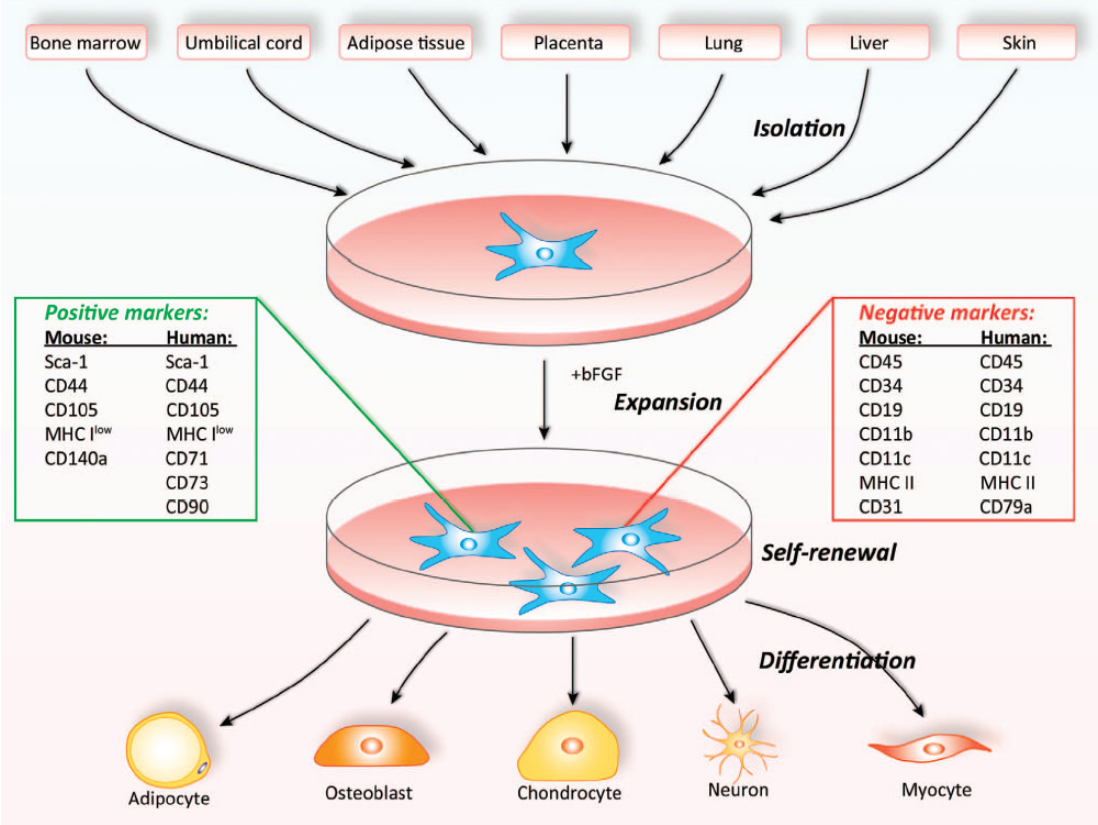

Figure 3: MSCs can be isolated and expanded from various organs. The characterisation of these stem cells can be performed by using various positive and negative CD markers. Following their expansion, the MSCs can be induced to undergo different types differentiation. Image adapted from Chen *et al*,. [108]

Cell adherence to tissue culture plastic has been a standard criteria. But a decade since the release of the proposition, additional surface markers (in addition to CD105, CD 73, and CD 90) for characterising MSCs have been identified (Figure 3). These surface markers can be easily identified by through specific antibody binding and immunofluorescent detection by flow cytometry. Mesenchymal stem extracted from bone marrow are uniformly positive and negatively for the surface markers stated in Table 3 below [109]:

Table 3: Markers for bone marrow derived MSCs (reproduced from Samsonraj *et al*.,[109])

Positive Cell Surface Markers	Negative Cell Surface Markers
CD29 - Integrin β1 chain (ITGB1)	CD11a Integrin α L chain (ITGAL)
CD31 - Platelet endothelial cell adhesion molecule (PECAM1)	CD11b - Integrin α M chain (ITGAM)
CD44 - Hyaluronan receptor	CD13 - Aminopeptidase N (ANPEP)
CD49a – e - Integrin subunit α (ITGA1 - 5)	CD14 - Myeloid cell-specific leucine-rich glycoprotein
CD51 - Integrin subunit α V chain (ITGAV)	CD19 - B-lymphocyte surface antigen B4
CD54 - Intracellular adhesion molecule (ICAM1)	CD31 - Platelet endothelial cell adhesion molecule (PECAM1)
CD58 - Lymphocyte function-associated antigen (LAF-3)	CD34 - Transmembrane phosphoglycoprotein
CD61 - Integrin β3 chain (ITGB3)	CD45 - Lymphocyte common antigen; protein tyrosine phosphatase, receptor type, C (PTPRC)
CD71 - Transferrin receptor (TFRC)	CD133 - Prominin-1 transmembrane glycoprotein (PROM1)
CD73 - Ecto-5'-nucleotidase (NT5E)	
CD90 - Thy-1 (THY1)	
CD102 - Intracellular adhesion molecule (ICAM2)	
CD104 - Integrin β4 chain (ITGB4)	
CD105 - Endoglin, TGFβ R III (ENG)	
CD106 - Vascular cell adhesion molecule (VCAM1)	
CD120a -Tumour necrosis factor receptor 1A (TNFRSF1A)	
CD120b - Tumour necrosis factor receptor type II, TNF IIR (TNFRSF1B)	
CD121a - Interleukin-1 receptor (IL1R1)	
CD124 - Interleukin-4 receptor (IL4R)	
CD140a- Platelet-derived growth factor receptor alpha (PDGFRA)	
CD140b - Platelet-derived growth factor receptor beta (PDGFRB)	
CD146 MCAMMelanoma cell adhesion molecule	
CD166 - Activated leukocyte cell adhesion molecule (ALCAM)	
CD200 - OX-2 membrane glycoprotein	
CD221 - Insulin-like growth factor 1 receptor, IGF-R (IGF1R)	
CD271 - Nerve growth factor receptor (NGF-R)	
SSEA-4 - Stage specific embryonic antigen-4 (SSEA4)	
STRO-1 - Stromal antigen 1	
W8-B2/MSCA-1 - MSC antigen 1	
CD217 – Interleukin-17 receptor (IL17RA)	

Of all the markers mentioned above CD 217, has emerged as a definitive marker for bone marrow extracted MSCs. CD 271 is highly expressed by the multipotent BM-MSCs and can be used in purification and detection of the stemness of cells [110, 111]. Differentiation of MSCs into specific lineage leads to downregulation and upregulation in the expression of specific markers. Downregulation in CD 73, CD 105 and CD 106 are common in MSC differentiate into osteo, adipo or chondrocytes [112]. Osteogenic and adipogenic differentiation shows a common down regulation in CD90, CD97, CD98, CD155 and an upregulation in CD63, 73, 122, 160. Individually, osteogenic differentiation leads to a down regulation of CD29, CD44, CD61, CD99, CD, 276 and CD 304. Similarly, adipogenic differentiation causes a downregulation of CD9 and CD54. Chondrogenic differentiation leads to a downregulation in CD44, CD81 and CD166 [113].

2.4.2 MSC Differentiation

Mesenchymal stem cells have the capacity to undergo osteogenic, adipogenic and chondrogenic differentiation which belong to mesoderm lineage. The differentiation in these stem cells occurs due to complex responses to external stimuli that trigger lineage specific signalling pathways leading to specific gene expression regulation. In vitro differentiation of MSC can be performed by administering selected molecules that are physiologically responsible for the differentiation into osteocytes, chondrocytes, and adipocytes:

Osteogenic differentiation

It has been reported that exposing undifferentiated MSC to ascorbic acid, dexamethasone, heparin and β-glycerophosphate and induces osteogenic differentiation of bone marrow MSCs *in vitro* [114-117].

The effects of exposing cultured cells to ascorbate is dependent on the type of cells and concentration. Concentrations of ascorbic acid in the range 50-500 μM promote MSC proliferation and differentiation, while concentrations above this threshold induce apoptosis [114]. Ascorbic acid induces an upregulation of alkaline phosphate (ALP), osteocalcin and promotes the deposition of type I collagen. Ascorbic acid is an essential cofactor in the hydroxylation of collagen. This property of ascorbic acid may be responsible for an increase in collagen accumulation thereby stimulating osteogenic differentiation [118].

Dexamethasone is a synthetic glucocorticoid hormone that is essential for osteogenic differentiation in MSC. The effect of dexamethasone on MSCs is dependant of its concentration. While lower concentration of Dex (~10 nM) induces high proliferation rate in hMSCs, ~ 100 nM causes cells to cease proliferation and induces osteogenesis in hMSCs [115, 119]. The exposure of cells to dexamethasone causes a significant upregulation RUNX2, the master regular of the osteogenic differentiation, which in turn will regulate the expression of proteins responsible for the mineralization process [120, 121].

Heparin is a hyper-sulfated glycosaminoglycans (GAG). Exposure of hMSCs to heparin with other molecules promotes osteogenesis and decreases adipogenesis. Similar to the other molecules (ascorbic acid and dexamethasone), the presence of heparin causes an upregulation of ALP that induces bone mineralization. The exposure of cells to heparin causes an enhancement in the bone morphogen proteins (BMP) signalling, which in turn is responsible for an increased ALP expression [117].

β-glycerophosphate is an inorganic phosphate intracellular signalling molecule. This molecule responsible for providing the phosphate which is required by the cell to produce hydroxyapatite mineral. Studies conducted by Tada *et al*., shows that β-glycerophosphate activates cyclic-AMP/protein-kinase-A pathway signalling pathway, which in turn helps in increasing bone morphogenic protein 2 (BMP-2) [122].

Differentiation of MSCs can be determined by the change in morphology and either upregulation or downregulation of osteo specific markers such as ALP, RUNX2/Cbfa1 [123]. Under the influence of these proteins the morphology of the MSCs undergoes a change by displaying aggregation or a nodular formation [63]. Alkaline phosphate (ALP) is also an early marker. An increase in ALP expression is usually seen after 4 days of osteogenic induction and peak expression of ALP is observed at 14 days [123]. Studies involving *ALP* gene knockout in mice showed the development of various defects in mice. The mice developed diseases such as rickets. The mice developed defects such as skeletal defects, development of seizures, apnea [124, 125] and increase in fat absorption through intestinal tissues [126].

RUNX2/Cbfa1, is a master transcription factor that bind to the runt domain in the DNA [127]. It is known to regulate the expression of genes responsible for the induction of the osteogenic program and for the production, extrusion and organization

of the mineralized matrix [128] such as osteopontin (*SPP1*), osteocalcin (*BGLAP*), type I collagen genes (*COL1A1*) and bone sialoprotein (B SP) [123, 129]. Murine studies demonstrated that, inactivation of these genes leads to the absence of ossification and osteogenic differentiation, leaving the animal with cartilaginous skeleton devoid of bone formation [130].

Adipogenic Differentiation

In vitro adipogenesis can be induced in MSCs by adding dexamethasone (glucocorticoid), isobutylmethylxanthine (cAMP agonists), insulin and indomethacin to cell culture media [131-135].

As explained in osteogenic differentiation section, the concentration in dexamethasone is responsible for the fate of cell differentiation. Studies have shown that the presence of dexamethasone in osteogenic media does increase the adipogenic gene expression even if the cells differentiate into osteogenic line [131]. Dexamethasone acts to increase adipogenesis by inducing C/EBP-δ, which is a part of CCAAT/enhancer binding protein family. Perf-1, which is known to inhibit adipogenesis, is supressed by dexamethasone. This also leads to an elevating the expression of PPAR-γ thereby inducing adipogenic differentiation [135].

Isobutylmethylxanthine (IBMX) is a phosphodiesterase inhibitor which elevates the cAMP in a cell. The increase in cAMP leads to an enhanced expression of PPAR-γ and C/EBPα thereby promoting differentiation in the cell [134].

Insulin hormone regulates intracellular signalling that leads to cellular adipogenesis. Insulin is responsible for activation of Akt-TSC2-mTORC1 pathway. This pathway increases the level of triglyceride accumulation in the cells, thereby enhancing the adipogenic differentiation [136].

Indomethacin is an anti-inflammatory drug which when added with the other molecules mentioned above promotes terminal adipogenic differentiation in stem cells. This is because indomethacin promotes an enhanced expression of PPAR-γ which drives differentiation of stem cells into adipogenic cells [133].

Differentiation of the cells become apparent when lipid rich vacuoles accumulate within the cytoplasm of cells. These lipid rich vacuoles develop, merge and fill the cells to form an adipocyte [63]. Though many transcription factors are necessary for adipogenic differentiation, CCAAT/enhancer binding protein (C/EBPα) family and

peroxisome proliferator-activated receptor γ (PPAR-γ) are the most important ones [137].

Of both the transcription factors, PPAR-γ is known as the master regulator for adipogenesis. PPAR-γ expression has been observed in pre-adipogenic cells. During early adipogenesis, PPARγ activates the fatty acid binding and adipo specific genes that causes the MSCs to exit from its cell-cycle progression and trigger adipogenesis. C/EBPα transcription factor, which is expressed later in the differentiation process, is said to be induced and upregulated by PPARγ. C/EBPα further upregulates the expression PPARγ. This creates a positive feedback loop between the two transcription factors resulting in the promotion of adipogenic differentiation and maintenance [138]. Effectors of adipogenesis as lipoprotein lipase (LPL), fatty acid binding proteins (FABP4/aP2), leptin are expressed during different stages of adipogenesis [139].

Murine studies have shown that decrease in PPAR-γ upregulation results in decreased adipogenesis. Embryonic stem cells with PPAR-γ downregulation increased osteogenic differentiation and decreased adipogenesis. Selective knock out of PPAR-γ in mice lead to loss of brown and white adipocytes [140].

Chondrogenic differentiation

Chondrogenesis can be triggered in bone marrow derived MSCs by administering a multifunctional cytokine called transformation growth factor β-3 (TGF-β) to the cells [63, 141].

TGF-β is known to initiate intracellular signalling cascade, such as mitogen-activated protein (MAP) kinases, with upregulated cartilage specific gene expression. Major subtypes of MAP kinase such as p38 kinase and extracellular signal-regulated kinase-1 (ERK-1) are known to play various roles in chondrogenesis. While p38 kinase is known to enhance chondrogenesis, ERK-1 repressed this differentiation process [142].

Chondrogenesis differentiation is often regulated by three transcription factors namely L-Sox 5, Sox 6 and Sox 9. The SOX trio belong to Sry-related family of HMG (High-Mobility-Group) box DNA-binding proteins. Of all the three, Sox 9 is known to maintain chondroprogenitor phenotype and is highly upregulated during chondrogenesis [143]. During chondrogenesis Sox 9 is known to activate and upregulate the expression of many extracellular matrix components such asCOL2A1,

Col9a1, Col11a2 and Acan (aggrecan) [144]. Studies have also shown that there is a direct correlation between Sox9 and Col2a1. Co-transfection of Sox9 with 4X4-p89Col2a1 by plasmid transfection has been shown to activate Col2a1 expression in nonchondrocytic cells [145].

Murine embryos with Sox9 mutation have shown the inability to form cartilaginous tissues and lack chondrogenic marker expression [143]. Mutation of Sox 9 in human leads to various diseases such as campomelic dysplasia (skeletal dysmorphia), XY gonad dysgenesis (male to female sex reversal), hypertrichosis and alopecia areata (loss of hair) [144].

2.5 ROLE OF MSC IN STEM CELL THERAPIES

The ability of MSCs to self-renew and differentiate into various cell lines has made them invaluable for research toward regenerative cellular therapies. They are known to be multipotential due to their ability to not only differentiate into mesodermal cell lines but also ectodermal and endodermal cell line such as neurons, hepatocytes, cardiomyocytes, pancreatic cells, skeletal muscles, and skin.

In addition to this, MSCs are well documented for their immunomodulatory properties especially the immunosuppressive effect displayed by the stem cells during allogenic transplants [146, 147]. Gea-Banacloche *et al.*, states that "immunomodulation encompasses all therapeutic interventions aimed at modifying the immune response" [148]. In simple terms it can be explained as manipulating the immune system by introducing intrinsic or extrinsic agents to alter, increase or decrease the immune response from a body. According to various studies, the introduction of MSCs regulates various immune factors such as:

- inhibition of T-cell maturation and proliferation [149, 150]
- inhibition of cytotoxic T cells proliferation leading to decrease in cytotoxic effect

This immunomodulatory potential has made MSCs very attractive in regenerative cellular therapeutic industry. This allows the cells to be transplanted into a "third party" with minimal chances of eliciting immunogenic reaction. Various clinical trials are currently underway to study the application if MSCs can be used in disease and trauma treatment.

- The ability of MSCs to differentiate chondrocytes has been used to treat cartilage defects and regeneration [7], osteoarthritis [8], regenerating hyaline like cartilage [151] and regeneration of articular cartilage [152]. For example, a successful preliminary study was conducted in 2013 to treat patients suffering from knee osteoarthritis by injecting the patients with autologous bone marrow derived MSC. An improvement in cartilage quality was observed in after 1 year and further improvement was seen after 2 years of treatment [8, 153]. Similar studies conducted to treat osteoarthritis using allogenic MSCs were also successful and showed improvement on cartilage quality over time [154]. Neither of the studies required surgical intervention.
- The osteogenic differentiative capacity of MSCs have been used in clinical trials to treat bone disorders such as osteogenesis imperfecta, atrophic tibial diaphyseal non-union etc. In children suffering from osteogenesis imperfecta, induction of MSCs has shown an increase in growth and bone mineralization [11, 155]. Bone non-union can be caused in long bones due to bone fractures and the inability of the bone to heal. Studies have shown that MSCs in combination with hydroxyapatite can accelerate the rate of heal [10]. Biomaterials seeded with MSCs can be used to reconstruct or replace damaged bones.
- The immunomodular ability of MSCs makes it suitable for treating various autoimmune and inflammatory diseases such as graft Vs host disease, Crohn's disease, multiple sclerosis, systemic lupus erythematosus and systemic sclerosis [156].
- Clinical studies have been performed to treat acute-on-chronic- liver failure and liver cirrhosis by transplanting allogenic MSC into patients [9, 157]. Studies have shown that the while presence of allogenic MSC did not have any negative immune effect on the patients, the survival rates increase due to improved liver function. Zhao *et al*., also noted the with the increase in time the patience, effect with liver cirrhosis, also showed significant improvement [9].
- Studies were conducted where allogenic MSCs were used to treat patients suffering from acute kidney injuries (AKI). Preliminary results from phase 1 of the clinical trials not only showed an improvement in renal function

with a 40% decrease patient re-admission rates but also a reduction in the patient's dependence on haemodialysis [158]. Cardiac surgeries creates complications with kidneys and leads to post-operative kidney injuries. Inducing allogenic MSCs helps in reducing these complications.

2.6 CELL ADHESION

MSCs differ from other cells present in their *in vivo* microenvironment due to the fact they are highly adherent to typical cell culture substrates (tissue culture polystyrene etc), this adherent property of MSCs allows them to be separated and purified from the biological milieu after extraction. Furthermore, cell adhesion is required for the survival of many cell types both *in vitro* and *in vivo*. Failure to adhere causes the activation of apoptosis in these cells mainly because they are dependent on cell-ECM and cell-cell adhesion to maintain viability, regulation of cellular activities and proliferation. This process, known as anoikis, is induced when the cells lose cell-ECM and cell-cell contact [159, 160].

The 3D structure and the normal function of a tissue is dependent on the adhesive properties of the cells. Cell adhesion or cell attachment can be defined as the process by which the cell interacts with its microenvironment. This can either be a surface or another cell. Adhesion is also required by the cells, as transmembrane signalling processes, which take place between the cell and the ECM, regulates the cell behaviour and fate [161]. Cell adhesion consists of multiprotein complexes made up of 3 classes of proteins[162]:

1. Extracellular matrix (ECM) proteins
2. Cell adhesion molecules (CAM)/adhesion receptions
3. Cytoplasmic plaque/peripheral membrane proteins

Extracellular matrix is a complex dynamic structure made up of different proteins (collagen, fibronectin, laminin, elastin), polysaccharides and GAGs (heparan sulfate) etc. RGD or arginine-glycine-aspartate is tri amino acid ligand present on many ECM proteins and in the cellular microenvironment [163]. Cellular adhesion molecules (CAM) are transmembrane glycoproteins which dictate the attachment between cell-cell or cell and ECM [164]. While CAMs are subdivided into different types of transmembrane glycoproteins, integrins are considered as the main receptor

involved in cell-ECM adhesion and cadherins are the main proteins involved in cell-cell adhesion [163].

2.6.1 Cell-ECM adhesion

Integrins act as communication channels that mediate the interaction of the cells with the adjacent surface (Figure 4). Integrins are heterodimer transmembrane proteins that are subdivided into α and β subunits. These subunits form 25 diverse parings which help in the formation of ligands with CAMs such as fibronectin, laminin and collagen in the extracellular matrix. The interaction between the integrins and CAMs are via RGD peptide motif (fibronectin, collagen), IKVAV peptide (laminin) ligands and GFOGER (collagen, laminin) present. The binding of these heterodimeric proteins to the peptide ligands helps in establishing a connection between the cells and its environment. Integrins have a low affinity to their ligand due to non-covalent bond formation between the integrins and adhesion molecules. Though the bond is weak, it has two distinct advantages. While the presence of the numerous ligands between the integrins and adhesive molecules (collagen, laminin and fibronectin) helps the cells to anchor firmly to the matrix, the weak covalent links help the cells to break away from the extra cellular matrix when required to migrate [163, 165-168]. Integrins also transmit signals to the interior of the cells and also receive signals from within the cells [169].

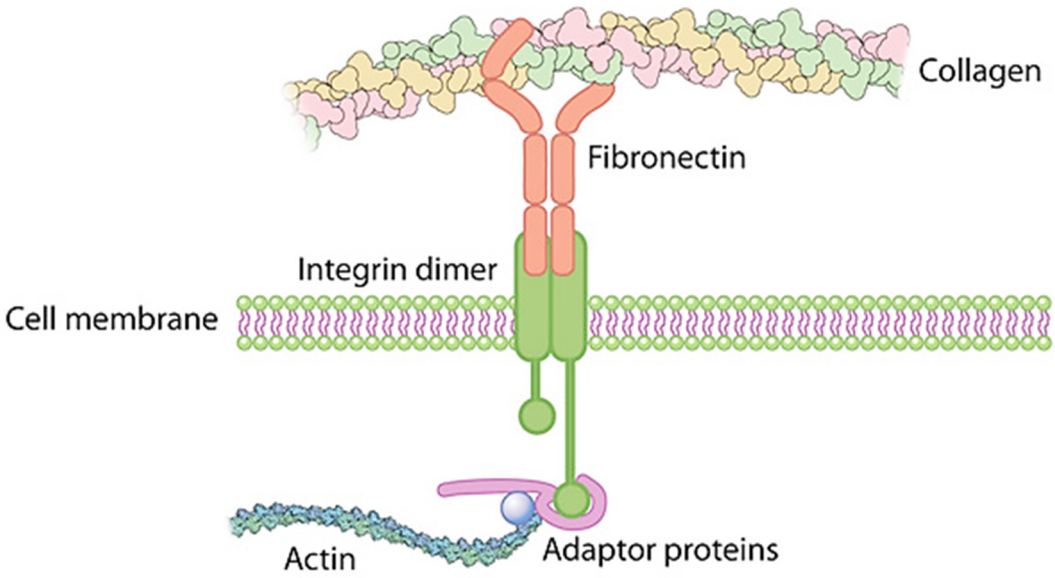

Figure 4: Binding of integrins dimers to ECM. The β integrin subunit of the integrins binds to the actin filament of the intracellular cellular cytoskeleton. Both α and β integrin subunit from adhesion bonds outside the cell by binding to the to the proteins in the ECM that is present outside the cell. Image adapted from O'Connor *et al.* [170]

The behaviour of integrins and the interior of the cell, in response to EMC, is bidirectional. Not only does the binding of integrins to ECM invoke a change in the interior of the cell, but the interior of the cell also concentrates or clusters integrins near the ECM and mechanically pushes it to increase the adhesiveness [171]. The β sub unit of the integrin is connected to the actin filaments of the cytoskeleton by a complex of proteins.

Cell spreading and cell adhesion are also directly proportional to the number of focal adhesions present in a localized area [172]. Focal adhesions can be defined as dynamic multi-protein containing structures which form a mechanical link between the cytoskeleton of the cells and the ECM. FA is mediated through intracellular actin bundles and integrins. Actin filaments, plays an important role in FA as well as in cell migration. Cell migrations and adhesions are controlled by lamellipodium and filopodia. Being the most abundant protein the cell, actin proteins are the main structural components of lamellipodium. Lamellipodium is a flat protrusion, that is present in the leading edge of the cell, and protrudes towards the required direction. Filopodia is a finger like extension from the lamellipodium and the cytoskeleton, containing bundle of parallel actin filaments, that is projected from the cell membrane. The cell movement caused by both protrusions is driven by the polymerization and depolymerisation of actin filaments. Adhesion of the cells to the substrate is dictated by the adhesive proteins such as integrins present in the ECM and the protrusions from the cells. Lamellipodium form an anchorage with the integrins which gives rise to a weak and short lives adhesion called nascent adhesion. This connection can be used by the actin cytoskeleton to either push the cell forward by depolymerisation of the actin and thereby disassembling the nascent adhesion or form a strong FA with the ECM by actin polymerizerization [173, 174].

The focal adhesion of the cells is mainly dependent on RGD-integrin density. Many studies have been conducted by the Spaz group to investigate the effect the number of integrin-adhesive RGD ligands, per unit area on a surface, has on cells. If the density of RGD ligands is higher in presence of cells, a focal adhesion formation was observed in the cells. During the presence of low density of RGD ligands, it was noted that, the cells had lower adhesion. This is mainly caused by the smaller focal adhesions and as previously described lower adhesion or non-adhesion of cells lead to cell quiescence or to cell apoptosis [175, 176].

2.6.2 Cell-cell adhesion

Cell-cell adhesion or interaction is necessary for tissue and organ formation. Adhesion between cells is mediated by various CAMs that include integrins, immunoglobulin super family and cadherins. Of all these molecules cadherins are the most dominant cell adhesion molecules. Cadherins are adhesion molecules that belong to a superfamily of transmembrane glycoproteins. Cadherins are classified into N-cadherin, P-cadherin and E-cadherin. Cell-cell adhesion in vertebrates is dependent on the presence of Ca^{2+}. Absence of Ca^{2+} can lead to loss in cell-cell adhesion and disintegration of tissues. Cadherins mediate Ca^{2+} dependant homophilic as well as heterophilic cell-cell adhesion. [163, 177, 178].

Adhesion between cells take place in the form of intercellular junctions. Intercellular junctions are divided into 4 types as shown in Figure 5:

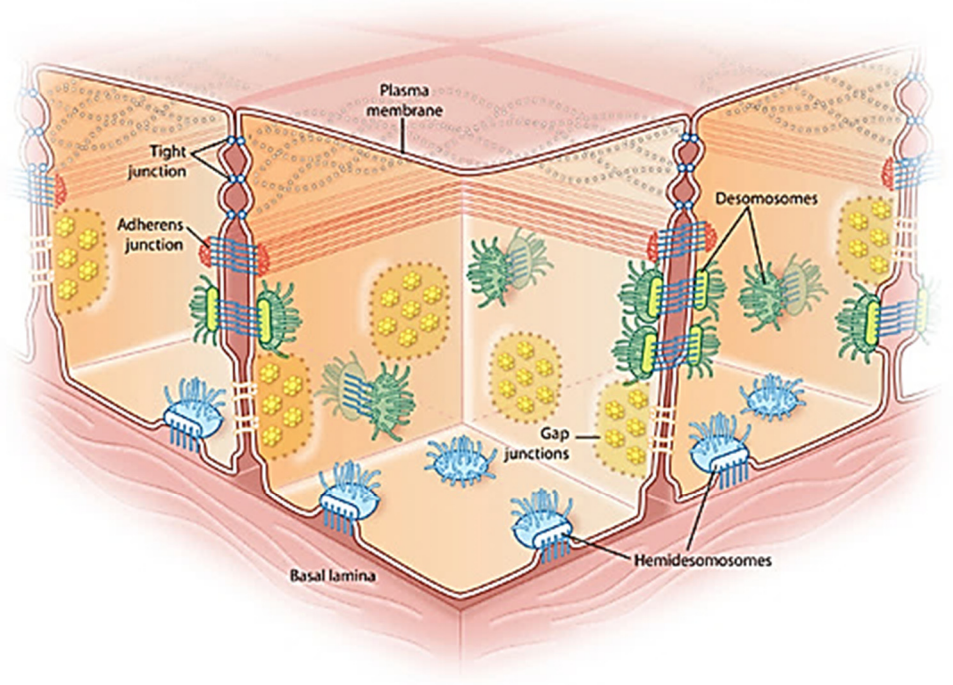

Figure 5: Adhesion mechanism between cell-cell and cell-ECM. Different mechanisms and molecules come into play for intra cellular and extra cellular adhesion to take place. Image reproduced from O'Connor *et al.*[170]

- Tight junctions: These junctions connect different cells together with the help of occludin and claudin transmembrane proteins. As indicated in the name, these junctions form a tight seal which prevents the passage of

fluids, molecules and ions in the cellular gaps present between two adjacent cells. The mixture of integral membrane proteins present in the apical and basolateral membranes of the cells are also prevented by these junctions. This helps in maintaining the specialized function such as the endocytosis (apical surface) and exocytosis (basolateral membrane) [179].

- Adherents junctions: These junctions are present below the tight junctions. Transmembrane glycoprotein E-cadherins, catenin and actin filaments are the main function units of adherents junction. The cell-cell adhesion mechanism through adherents junctions takes place due to intra and extracellular mechanism. In intra cellular mechanism, a bundle of actin filaments are bound to the membrane via cantenins and they form a belt like structure in the cytoplasm of the cells. These cantenins bind with the cytoplasmic domain of the E-cadherins. Cell-cell adhesion takes place when the extra cellular domain of E-cadherins (from one cell) forms bonds with the E-cadherins of the other cells [162, 179].
- Gap junctions: Gap junction are cylindrical hollow intercellular channels formed by transmembrane proteins called connexions. These constricts have a diameter of 1.5-2 nm. Gap junctions allow the direct passage of water soluble molecules and ions from one cell to another [180].
- Desmonal junctions: Similar to adherents junctions, desmonal junctions have intracellular and intercellular functions. The intracellular complex is made up of intermediate keratin filaments, and desmoplakin and plakophilin. The intermediate keratin filaments are coupled to the plasma membrane via desmoplakin which in turn is attached plakophilin. Desmoplakin and plakophilin also known as cytoplasmic plaque proteins. The intercellular complex is made up of desmosomal cadherins. While the cytoplasmic domain of the desmosomal cadherins are bound to the cytoplasmic plaque proteins, the extracellular domain forms a strong adhesive bond with the desmosomal cadherins extending from other cells [181].

From above it can be stated of all 4 junctions, adherents junction and desmonal

junctions play a major role in cell-cell adhesion. This is mainly because these junctions in one cell indirectly form connections with the cytoplasm of the other cells (via actin filaments and intermediate keratin filaments). In both the junctions, cadherins are the important molecules that help in maintaining adhesion between the cells.

2.7 CURRENT METHODS OF CELL DETACHMENT

While cell attachment is necessary for anchor-based cells to proliferate and differentiate when cultured *in vitro*, it is also necessary to detach these cells from the culture surface for stem cell therapy applications. While enzymatic methods such as trypsinization and cell scraping can be used in labs for cellular research, GMP guidelines recommend avoiding the application of animal origin solutions (porcine trypsin). This was done to avoid possible cases of animal transmitted disease or contamination. In addition to this, trypsin is known to cause cellular dysfunction and disintegration of cell surface molecules. When using stem cells for clinical treatment, it is necessary for the stem cells to be healthy, viable and undamaged in any way.

In this section I describe in detail about the effects of trypsin and cell scraping on cells, the other products available in market and the current research currently undertaken to find an alternative solution for cell detachment.

2.7.1 Trypsinization

Trypsin

Trypsin is a digestive enzyme and its inactive precursor, trypsinogen is synthesized and produced by acinar cells in the pancreas [182]. The activation of this proteolytic enzyme takes place only in specific places in order to prevent the unwanted destruction of cellular proteins. When needed trypsinogen is activated and released into the lumen of the small intestine via the bile duct [183]. Trypsin, in humans, is secreted in 3 isotypes. While the cationic and the anionic forms predominate (occurring in a ratio of 2:1), the mesotrypsinogen isotype is found in traces. Mesotrypsinogen, being an inhibitor resistant protein, accounts for only 5% of the total enzyme secreted.

During the process of digestion, acting with other proteases, the dietary protein molecules are broken down to their component peptides and amino acids by trypsin. Though trypsin and chymotrypsin have remarkably similar chemical structure and composition, they show subtle differences in substrate specificity. It has been shown

that trypsin specifically breaks down peptides containing arginine and lysine residues, whilst chymotrypsin is specific to tyrosine, phenylalanine, tryptophan, methionine, and leucine.

Trypsinization Process

Trypsinization is the process of dissociation of cells from their culture surface by using trypsin. Trypsin displays an advantage of being a discriminating proteolytic enzyme i.e., it attacks and cleaves only a certain number of chemical bonds. Due to this advantage researchers and industries have widely employed trypsin as a reagent to cleave certain molecule. This advantage has allowed researchers and industries to widely employ trypsin as a reagent to cleave certain molecules such as arginine and lysine [184]. When it comes to use of trypsin in cell therapeutic industries, trypsin isolated from bovine or porcine pancreases is the most commonly used reagent due to its cost and availability.

During cell culture, when the cells have reached confluence (i.e., when 80-90% of the culture surface area is covered by proliferating cells), they need to be subcultured. Cells generally form a monolayer and are adherent to the base of the culture substrate. Trypsin is added to the cells in order to dissociate them from the surface of the culture plate. The concentration of trypsin can vary from 0.025% to 0.5% depending on the sensitivity of the cells. Exposing the cells to trypsin causes the reagent to cleave the cell-substrate, cell-ECM and cell-cell bonds [185] [186]. While some cells lines may only need 2 minutes of trypsin exposure time (HUVECS, T3T, HRPTECS), other strongly adherent cells may need relatively longer incubation times (L929 fibroblasts for 6 min, MSC for 6-10 min) with trypsin.

Disadvantages of Trypsinization

Though trypsinization is a commonly used and convenient method of detaching cells, it has various negative effects on the cells. Being a proteolytic enzyme, trypsin cleaves specific amino acids within the backbone of protein molecules (protein digestion). When added to cells, the surface proteins, such as fibronectin, laminin and collagen are digested by trypsin leading to dysregulation of cell functions [187]. The enzyme cleavage by trypsin is severe enough to effect the structural integrity of the bilayered cell membrane [188].

A study conducted by Huang *et al*., on breast cancer cell line (MCF-7) and

cervical cancer cell line (HeLa) demonstrated that trypsinization causes damage of cell membrane proteins leading to the dysregulation of cell function. The expression of 36 different proteins, found on various cell lines, were significantly altered after trypsinization. Proteomic results also found that trypsinization down-regulated the expression of growth and metabolism related proteins and up-regulated apoptosis-related protein expressions. Though many of the trypsin induced protein expressions were reversible, some of the proteins remained dysregulated even after 24 hours [189].

Dysregulation of surface proteins due to enzymatic cell detachment could potentially lead to numerous diseases. For example, malignant transformation of epithelial cells can occur as a result of the introduction of mesenchymal membrane protein expression (N-Cadherin) and the loss of E-cadherin expression [190, 191]. Cadherins are protease sensitive i.e., they disintegrate rapidly when exposed to calcium free trypsin [177]. ErbB 2, a member of epidermal growth factor receptor (EGFR) family and a transmembrane glycoprotein, has an extracellular and intracellular ligand binding domain. Studies have shown that mutation caused in ErbB-2 receptor can direct to hepatocellular cancer (HCC) and gastric cancer [192, 193].

In a study that was conducted on hMSCs by Tsuji *et al*., trypsin was responsible for the reduction of many CD markers which indicate the multipotency of the cells. Depending on the time of exposure markers such as CD140a, CD55, CD105 and CD140b were affected by trypsinization. Though the cells recovered all these cell surface markers at/by 5 days post trypsinization, this process is disadvantageous to be applied for stem cell therapy [194]. During stem cell therapy, it might be necessary for the stem cell to be applied immediately to the patients (autologous transplant) or to be stored for further treatment (allogenic transplant). This does not allow the cells to recover the surface antigens and may lead to further clinical complications such as loss of immunophenotype of the cell.

In addition to all the above mentioned disadvantages, there is always a possibility of xeno contamination when using animal derived trypsin. One of the prime examples of such contamination was reported in 2009. Two batches of Rotarix® (a rotavirus vaccine produced by Glaxo Smith Kline) was contaminated with porcine circovirus-1 (PCV-1). This contamination was caused due to the application of contaminated (non-irradiated) porcine trypsin by the manufacturers of Vero cell line banks. These Vero cell lines were used in the production of the vaccines leading to PCV-1 contamination

in the final vaccine product. During the same time, studies conducted by Merck showed the presence of porcine circovirus-2 (PCV-2) DNA fragments in 11 batches of rotavirus vaccine called RotaTeq®. This contamination was associated with the usage of gamma irradiated porcine derived trypsin [195]. These cases have shown that, when animal derived products are used, there is a possibility of the final product being contaminated with xeno material even after application of stringent sterilization techniques or due to human error.

When trypsin is used for therapeutic stem cell cultures, care has to be taken so that no trace of trypsin remains in the final product. This can be achieved by repeated washing re-suspension and centrifugation of cells in cell culture media. But this process is time consuming and labour intensive. Any traces of trypsin would lead to an immunogenic reaction from the patient due to the animal protein [196].

In short, application of trypsin for stem cell therapeutics displays many drawbacks. But in addition to trypsinization there are other alternatives available for cell detachment.

2.7.2 Cell Scraping Technique

Though not used on an industrial scale, the cell scraping technique is mainly used by researchers in labs to remove cells from their surface. This process involves the mechanical scraping of the cells, to disassociate them from the surface.

A study was conducted by Canavan *et al*., to compare the detachment of bovine aortic endothelial cell (BAEC) using trypsinization and cell scraping technique. Observation using a microscope and immunoassay, on cells dissociated by both trypsin and cell scraping, revealed a striking difference in regards to their appearance and ECM protein staining. While cells detached by trypsinization were separated from each other and had a rounded appearance, cells detached by cell scraping method retained their original form. ECM protein fluorescence emitted by cells detached using cell scraping was stronger as compared to the ones detached by trypsinization showing it's structural integrity [197]. The one advantage of scraping process over trypsinization is the presence of ECM and surface proteins, which during trypsinization, is digested away.

Disadvantages of Cell Scraping:

Though a simple process, cell scraping has its own drawbacks due to it being a

mechanical process. The viability of the cells may be reduced if:

1. The cells are scraped too fast
2. Too much pressure is applied while scraping the cells
3. Repeated scrapings are required to overcome strong adhesion

The above conditions can lead to lyses of the cells resulting in their apoptosis. In addition to these disadvantages, cell scraping can only be used on a flat surface making it unsuitable for any other structure. Therefore, this cell scraping technique is not well suited in 3D cell cultures.

2.7.3 Other Commercial products

Commercial products alternative to trypsin and cell scrapers are available in the markets. Some of them are:

Non - Enzymatic Cell Detachment Reagents

Various companies have developed non-enzymatic reagents for dissociation of cells from their surface. Examples are shown in Table 4:

Table 4: List of non-enzymatic products available in the market

Company	Product name	Use *in Vitro*	Therapeutic use
BI-Biological Industries	Cell Dissociation Solution (non-enzymatic)	Yes	No
Promocell	Cell Dissociation Solution ACF	Yes	No
DNR Molecular Biology	Animal Component-Free Cell Dissociation Solution Non-enzymatic	Yes	No
Stem cell technologies	Gentle Cell Dissociation Reagent	Yes	No
Stemmera	Non-Enzymatic Cell Dissociation Solution (1×)	Yes	No
Sigma-Aldrich	Cell Dissociation Solution Non-enzymatic 1×	Yes	No
Thermo Fischer Scientifics	Cell Dissociation Buffer, enzyme-free	Yes	No
Alstem Cell Advancements	EZStem™ Enzyme-free Stem Cell Dissociation Solution	Yes	No

Although the products in Table 4 can be used for stem cell culture, they are exclusively made and approved by FDA for *in vitro* use and not for therapeutic

purposes. Some of these enzyme free products are produced from bacterial fermentation. The principal of these products is based on chelation of free calcium and magnesium ions in the solution [198]. All the products come with a restricted use warning, stating that they should not be used for human therapeutics [199-206].

Though enzyme free solutions are favoured due to their ability to preserve the structural integrity of the cell, it comes with certain disadvantages. According to a study by Chowen *et al*., the viability of the human mesenchymal stem cells dissociated by using enzyme free solution, were lower compared to that of those dissociated by trypsin. The percentage of cells reattached after dissociation was also reduced for an enzyme free solution as compared to trypsin. It was also observed that the number of cell apoptosis occurrences, after 24 hours, increased for cells detached by enzyme free solutions post-cryopreservation [198].

Thermo Scientific Nunc UpCell Surface

Thermo Scientific has created a range of culture dishes, called Nunc UpCell Surface, which are coated with a very thin layer of thermoresponsive polymers (Figure 6). The polymer coating on these surfaces is a well-known and researched polymer called Poly-N-isopropylacrylamide (pNIPAAM). pNIPAAM is a thermoresponsive polymer i.e., by reducing the temperature of the polymer, the structure of the polymer changes.

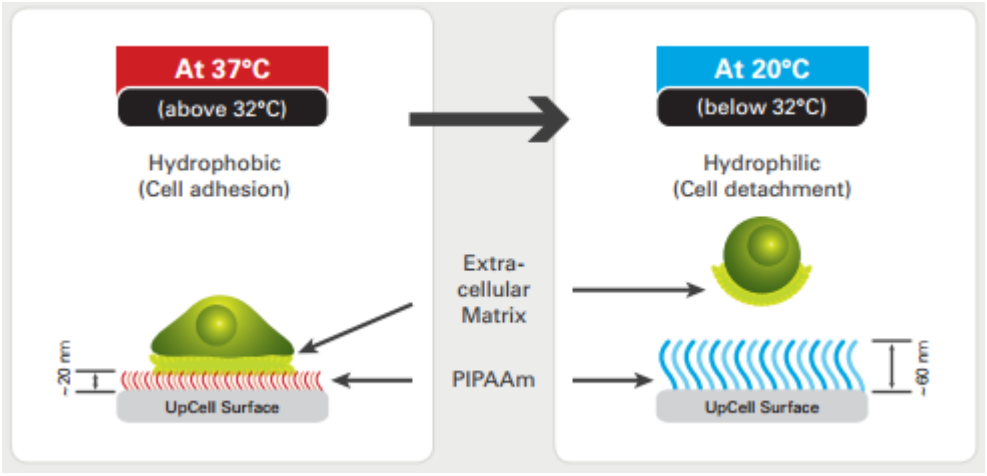

Figure 6: Cell release mechanism with the change in temperature [207]

When the surrounding temperature is 37°C, the polymer is hydrophobic which encourages the attachment of cells. But when the temperature is reduced to below 20°C, the polymer becomes hydrophilic due to water binding and the polymer expands. This change in structure facilitates the release of the cells from the surface of the

polymer (Figure 6). Due to the absence of any enzyme the extra cellular matrix is preserved and no proteins are destroyed in the process of cell detachment. Depending on the requirements, these products can be used to harvest cells in the form of single cells or as a complete cell sheet. [207]

Disadvantages:

Though this product has a vast potential it does come with its disadvantages.

1. Dimensions: All the products in the UpCell line are designed only as 2-D lab ware. The polymer coated on tissue culture Petri dishes and multi well culture dishes. This reduces its applications were large volumes of therapeutic cells are required.
2. Cost: The cost of the product is extremely high. For example
    a. A pack of UpCell 6 cm culture dishes (containing 30 pieces) costs AUD($) 1,195 [208].
    b. A pack of UpCell 3.5 cm culture dishes (containing 30 pieces) costs AUD($) 951 [209].
3. Reusability: All the products are designed for single use only. More than a single use is not warranted by Thermo Fischer Scientific.
4. Use in therapeutics: According to Thermo Fischer Scientific, the products are intended only for research purposes and cannot be used for clinical and diagnostic purposes.

2.7.4 Other studies developed in labs

Research has been conducted over the years in various labs to develop new methods which can have the potential to replace the use of enzymes for cell detachment. Some of them are detailed below:

pNIPAAM

One of the most looked into material is the use of poly-N-isopropylacrylamide (pNIPAAM). Many researchers have been extensively looking into the use of pNIPAAM for cell detachment since the 1990's. Their trials to detach cells from the pNIPAAM surface have been highly successful. The Okano lab managed to release cells such as corneal epithelial cells [210], hepatocytes [211], renal epithelial cells [212, 213], vascular endothelial cells [214], epidermal keratinocytes [215], cardio

myocytes [216] and periodontal ligament cells [217]. In the majority of the above cases, Okano labs, managed to get cell layer sheets without any damage to the cells and the complete release of cells from their attached surface.

Cells typically have a preference to attach and grow on hydrophobic surfaces compared to hydrophilic surfaces. Yamada *et al*., states that "Cell attachment and adherence are prevented by difficulty of displacing absorbed water molecules oh highly hydrated hydrophilic surfaces" [218]. As most of the cell culture is performed at 37 ^{o}C, the pNIPAAM polymer being hydrophobic above 32 ^{o}C (allowing cell attachment) and hydrophilic below (encouraging cell detachment), gives an ideal condition to culture cells. Cross-linked pNIPAAM was grafted on tissue culture polystyrene (TCPS) and cells were grown on the surface. When the temperature was decreased below the lower critical solution temperature (LCST) (around 20 ^{o}C), spontaneous detachment of cells was observed [218, 219].

The precise mechanism leading to the detachment of cells from pNIPAAM is still the subject of debate. The most accepted proposal put forward by Okano *et al*., suggested that the cell release mechanism, from the thermoresponsive polymer, is a two-step mechanism comprising of a passive mechanism and an active mechanism. While in passive mechanism the hydration of pNIPAAM substrate chains induce cell detachment, active mechanism is dependent on the metabolic process taking place inside the cell. The metabolic process leads to a change in the shape of the cells and complete detachment of the cells from the polymer surface.

Though the polymer chains are hydrated at 25 ^{o}C, the initial step of passive mechanism comes into effect only when the temperature is around 20 ^{o}C. In this process, though the primary process of cell detachment comes into play but complete detachment of the cells does not come into effect. This is due to the lack of metabolic activity from the cells. To complete the cell detachment process, the temperature has to be raised to 25 ^{o}C. It is at this temperature were the cell detachment process is significantly enhanced. At this point the cellular metabolism takes place leading to a change in morphology of the cell and the release of the cells from the polymer surface. Okano also observed that lowering the temperature below 20 ^{o}C inhibits the detachment process. This is caused by the decrease in metabolic process .[220]

Though the above theory is widely accepted, there has been studies which oppose it. Several studied have been conducted which have successfully detached cells

at temperature lower than the LCST [221, 222]. A study undertaken by Reed *et al*., showed that the release mechanism of bovine aortic endothelial cells is faster at 4 ^{o}C than at room temperature (13 minutes faster than at 25 ^{o}C). The release times were between 8.8 minutes and 6.8 minutes when using two different solutions: serum free media (SFM) and serum free media with a DPBS wash [223]. This study contradicts the conclusion given by Okano labs. Reed *et al*., also observed a 100% detachment of cells from the TCPS surface. It was suggested that the dissimilarity might be due to the difference in media used by both the facilities. While Okano's facility used serum free media, Reed's facility used media with serum. The author states that the additives present in the media with serum encourages cell attachment compared to serum free media. The absence of such additives may have allowed the cells to detach faster.

But the claims by Reed *et al*., was also backed up by Cooperstein *et al*. A study conducted by Cooperstein *et al*., was specifically designed to test the involvement of metabolic activity and the effect of temperature of the cell detachment process from the pNIPAAM surface. This study, unlike Reed *et al*., used serum free media. The results obtained refutes Okano *et al*., two step mechanism. Cooperstein *et al*., states that the not only do the cells detach at 4 ^{o}C, the mechanism of cell detachment is independent of the metabolic activity of the cells. In addition to this cell detachment from pNIPAAM coated surface was observed to be faster when the cells were exposed to cold medium (4 ^{o}C) than at room temperature. This may have been due to the faster hydration of the pNIPAAM chains at low temperature media (in room temperature) compared to warm temperature media. It is postulated that the hydration and expansion of the polymer leads to the rupture of the cellular anchorage. This mechanism results in the detachment of cell from the pNIPAAM surface [224].

Conductive polymers based cell detachment

Presson *et al*., used a the conductive polymer poly(3,4-ethylenedioxythiophene) (PEDOT) to study if it could be used for detaching cells from the polymer surface [225]. In its unadulterated form, PEDOT is known to exhibit high conductivity and insolubility. Polymerizing EDOT-S in water containing an aqueous solution of inorganic sodium persulfate ($Na_2S_2O_8$) and a catalytic amount of iron (III) chloride ($FeCl_3$) leads to the formation of water soluble PEDOT-S. PEDOT-S exhibits self-doping and electro conductive properties (12 S/cm) [226]. However, PEDOT-S, as a thin film, is unstable in aqueous medium due to its weak adhesive property towards

the substrate. In order to overcome this problem, PEDOT-S:H was synthesized. PEDOT-S:H showed improved self-doping capacity, enhanced conductive (30 S/cm) and adhesive property [225].

A thin layer of PEDOT-S:H was applied on a surface and suspended in electrolytes. Electrodes for voltage application was attached to the coated surface. After culturing human epithelial cells on PEDOT-S:H coated surface, a potential of 1V was applied across the setup. Cellular detachment was seen but so was disintegration of the polymer. The application of potential lead to the cracking and flaking of the polymer. Only 50% of cell detachment was observed in this method when compared to trypsin. In addition to this there is a problem of separating disintegrated polymer contaminants from the cell culture media after detachment [225].

Light based cell detachment

Sada *et al*., used single-walled carbon nanotube (SWNT) and laser exposure to for cell detachment. SWNT was spray coated on a glass surface and cells were cultured on the surface. Following cell proliferation, they were exposed to NIR pulse laser of 1064 nm. The exposure of SWNT to the NIR irradiation produces a shockwave due to photoacoustic response. This shockwave "catapulted" the cells along with the SWNT from the cell culture surface. By using this process single selective cell detachment was possible [227]. But this method has many short comings. Not only does the SWNT detach from the surface along with the cells, the cells endure the shock generated during the detachment process. The study has also shown a decrease in the viability of the cells post detachment. In addition to this, other studies have shown that SWNT themselves are cytotoxic to the cells thereby decreasing the cell viability [228-231].

A study conducted by Wang *et al*., used boron doped silicon wafers with a p/n junction [Si (p/n)] and visible light to produce a photovoltaic effect for cell detachment. Photovoltaic effect can be defined as the application of light to generate electricity on a semiconductor surface. The p/n junction was incorporated into the boron doped Si wafers by using phosphorus oxychloride as the source and exposing it to a furnace at 900 ^{o}C. Pre-osteoblastic MC3T3-E1 fibroblast cells were cultured on the p/n junction [Si (p/n)] wafers and then exposed to visible light with a wavelength of 400−800 nm with intensities varying between 10-50 mW/cm^2. A complete cell detachment from the semiconductor surface was observed at power exceeding 30

mW/cm^2. The authors state that the photovoltaic effect induces a deabsorption mechanism in the proteins present between the cells and the surface leading to cell detachment [232].

2.8 FUNDAMENTAL OPTICAL PROPERTIES OF ELECTROMAGNIC SPECTRUM

Biophotonics and biomedical optics are multidisciplinary fields that involves in the manipulation and application of different wavelengths of electromagnetic waves for biological research, diagnostics and therapy [233]. In some of the studies detailed above (section 2.7.4) the application light, in the form of laser, demonstrated detachment cells from a chemically manipulated cell culture surface. Laser, that produces these electromagnetic waves, is also the one of the chief instruments used in our current studies. In this section, our aim is to detail a general introduction on light/matter interaction, fundamentals of laser/tissue interaction and their applications in biomedical field.

2.8.1 Light-matter interaction

Light can be defined as an electromagnetic radiation that is made up of oscillating electric and magnetic disturbances. It has the ability to travel through both vacuum and medium [234]. While electromagnetic radiations are characterized as waves, wavelength can be defined as the distance between two peaks of these waves. Electromagnetic radiation is grouped into various categories depending on its wavelength. The categories are: gamma rays, x-rays, ultra violet light, infra-red light, microwaves, radio waves, and visible light. When directed at a target, light can undergo either reflection, refraction, absorption or scattering. These properties mediate the physiochemical and thermal effect of the electromagnetic waves on the cells. Through the cells and cellular organelles, the light pathway determines the effect of electromagnetic radiation on the cell culture substrate and the cells. While reflection, refraction and scattering may lead to photothermal reaction, absorption of the electromagnetic waves by the cells may induce photochemical effect in the cells (more details in section 2.10). Therefore, it is necessary to understand the properties of the electromagnetic waves when they interact with mediums such as air, liquid media and cells.

Reflection and refraction

Both reflection and refraction occurs when light propagating from one material (e.g., air or liquid) encounters the surface of the second material (target medium). Reflection of light is defined as the return of light after it's incident with the target medium material and in this phenomenon the angle of incidence is less than or equal to the angle of reflection (Figure 7). Refraction is the ability of light to partially reflect or transmit through the second material due to its different refractive index. The amount of light reflected or transmitted through a material is dependent on the refractive index of two materials, angle of incidence and the polarization of the radiation [235]. Snell's law can be applied to define the relationship between the angle of incidence and angle of refraction [236].

$$n_1 \sin \phi = n_2 \sin \psi$$

From the above equation ϕ is considered as angle of incidence, ψ is considered as angle of refraction, and n_1, n_2 are the refractive index of the propagating and target medium. When light normally incidents on a plane surface the amount of incident energy transmitted across the surface (T) can be calculated by [236]:

$$T = \frac{4\, n_1\, n_2}{(n_1 + n_2)^2}$$

In addition to this the amount of light reflected (R) by the surface of incidence can also be calculated by [236]:

$$R = 1 - T = \frac{(n_1 - n_2)^2}{(n_1 + n_2)^2}$$

Absorption

Absorption of light occurs when the energy of the electromagnetic wave is converted in different forms of energies such as heat or fluorescence by the absorbing medium. While transparent mediums allow the complete passage of light without any conversion of energy, this phenomenon is not observed in opaque mediums [237]. Absorption of light is dependent on various factors such as electronic constitution of the atoms and molecules of the medium, wavelength of the radiation, thickness of the absorbing material and internal parameters such as temperature and concentration of the medium. According to Beer – Lambert's law, absorption can be equated as [236]:

$$I(d) = I_0 \exp(-\mu_{abs}\, d)$$

Were I is the intensity of light, d is the thickness of the medium, $I(d)$ is the intensity of transmitted light expressed in the form of W/cm^2, I_0 is the incident light intensity and μ_{abs} is the absorption coefficient expressed as cm^{-1}. μ_{abs} of a material can be further calculated by using absorption cross section (σ_{abs}) and the density of absorbing molecules (ρ_m) [236].

$$\mu_{abs} = \sigma_{abs}\rho_m$$

Absorbance is a dimensionless quantity that defined as the ratio of absorbed light intensity to incident light intensity (I_0). When a medium is exposed to light, certain wavelengths in the electromagnetic radiations are absorbed by the medium. This phenomenon is known absorption spectrum or optical depth. Optical depth (τ_λ) of the material is defined as [236]:

$$\tau_\lambda = In\left(\frac{I_0}{I}\right) = \mu_{abs}d$$

Scattering

Tissues are made up diverse and complex sub-cellular organelles with different sizes and shapes leading to a wide range of scattering properties [236]. Scattering in a material can be noted following absorption and heat generation. The phenomenon of scattering is observed when an incident beam of photons hits a material. All non-reflected light, is either scattered or refracted, causing a change in the course of the photon beam without the loss of energy (Figure 7) [238]. Scattering of light can be calculated using Rayleigh's and Mei's scattering theory. While Rayleigh's scattering theory is applicable for particles whose size is small compared to that of the wavelength of light, Mei's scattering theory is used for calculating the scattering of light on spherical particles of any size to that of the wavelength [235].

The scattering efficiency of a medium can be expressed as [236]:

$$I(d) = I_0 \exp(-\mu_s d)$$

From the above equation I is defined as the intensity of light, I_0 is the light attenuated due to scattering, μ_s (cm^{-1}) is the scattering coefficient, d is the distance from the attenuated light and $I(d)$ is the intensity of the light transmitted (W/cm^2). The above equation is only applicable in calculating the unscattered beam of light of an uncollimated beam. The scattering efficiency for a collimated beam of light can be calculated using the Bouguer-Beer-Lambert Law [236]:

$$I(d) = \left(1 - R_f\right) I_o \exp(-\mu_t d)$$

The scattering coefficient μ_{sca} of a material can be obtained by calculating the scattering cross section and σ_{sca} and the scattered density of particles ρ_p [236].

$$\mu_{sca} = \sigma_{sca}\rho_p$$

The average distance travelled by the photons or the scattering mean free path can be equated as [235]:

$$l_s = \frac{1}{\mu_{sca}}$$

The total attenuation (μ_t) of the medium can be obtained by summing the scattering coefficient (μ_{sca}) and absorption coefficient (μ_{abs}) [236]:

$$\mu_t = \mu_{sca} + \mu_{abs}$$

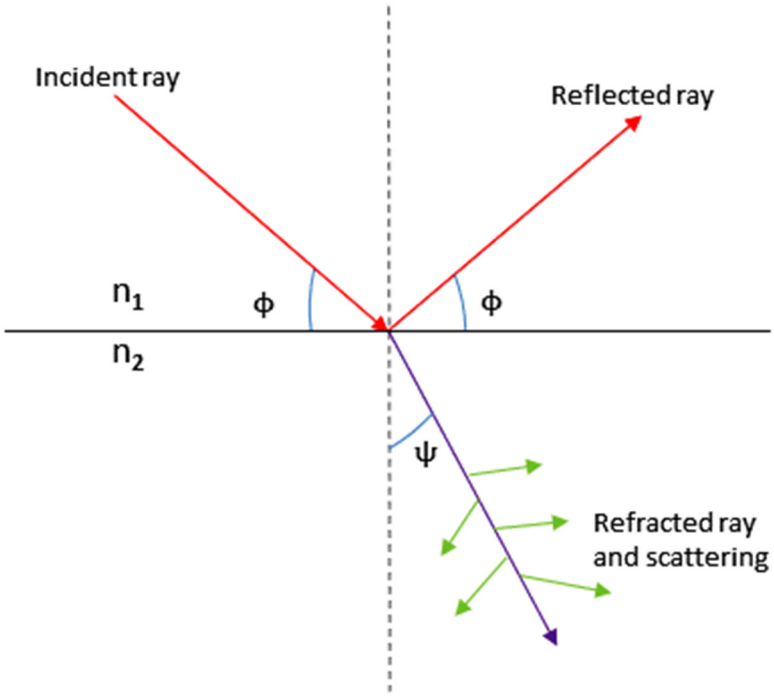

Figure 7: Schematic representation of reflection, refraction and scattering of light. Figure adapted and formatted from Tuchin *et al.,* [236]

2.8.2 A brief introduction to lasers

Acronym for **L**ight **A**mplification by **S**timulated **E**mission of **R**adiation, lasers are known for their ability to generate an intense narrow beam of light. Since their introduction in 1960, lasers had a wide spread impact and contribution in the field of biomedical engineering [239]. The light generated are of wide variety that are present in the electromagnetic spectrums (infrared light, UV light and X-rays).

Construction of a functional laser requires three basic components [240]:

1. Energy source: As depicted in the name, the energy source in a laser is the construct which provides the energy necessary for the generation of the laser light. The energy can be sourced from electricity, other lasers, arc lamps etc.
2. Lasing medium: The lasing medium, also known as gain medium, is a source that determines the wavelength of the electromagnetic wave generated by the laser. It can made up of solids, liquids or gases.
3. Optical resonance cavity: These are cylindrical structures which run parallel to the lasing medium. While one end of the tube is made up of highly reflective mirror, the other end is made up of highly reflective but also partially transmitting mirror. The transmitting end allows the laser light to pass for functional use.

In order to initiate the process of laser light emission, the electrons in the lasing medium are excited by supplying them with energy. This process is known as pumping. Pumping causes the excited electrons to move to the highest energy state called the singlet state. After a short period of time in the singlet state, the electrons emit a minor amount of energy and decays to a lower energy state called the meta-stable state [240].

The life time of electrons in the metastable state is much longer than in the singlet state. This causes an accumulation of electrons in the meta-stable state, leading to population inversion. When stimulated by a photon, the electrons in the meta-stable state release two photons and fall back to the ground state. These photons interact with other neighbouring electrons in the meta-stable state thereby producing double the number of photons. The electrons, that fall back to the ground state can be continuously excited to release photons [240].

The continuous excitation and decay of electrons in the laser medium leads to an intense and coherent build-up of photons in the resonance cavity. This leads to a phenomenon called photon cascade event. The presence of the reflective mirrors in the resonance cavity, causes photon amplification. The photons reverberate across the lasing medium leading to continuous excitation/decay of electrons and an enhanced generation of photons in a very short period of time. The end result is a controlled and coherent release of monochromatic beam of light (photons) through the partially reflective mirror [240].

Lasers are divided into two types: continuous wave (CW) and pulsed lasers. Laser interaction with biological tissues are characterised by four parameters [237]:

i) Wavelength: As previously stated, electromagnetic radiations are made up of waves that are characterized by the distance separating one high peak of a wave from other. Wavelength is represented by λ. The wavelength of a laser determines the distance penetrated in the tissue exposed to laser.

ii) Pulse duration: The measurement of the total amount of time an electromagnetic wave is emitted for.

iii) Energy density: This is the total amount of energy delivered per unit area. Energy density is also known as fluence or radiant exposure and is represented by J/cm^2 .

iv) Power density: This represents the ratio of power across of cross-section. Power density is also known as irradiance or intensity and is represented as W/cm^2 .

Of the above four, energy density and power density are important in biological applications to express the energy applied on the biological surface [241].

2.9 INTERACTION BETWEEN LASERS AND TISSUES

While a number of chemical and physical interactions takes place between lasers and biological tissues, there are four main groups of interactions (Figure 8). They are photochemical interactions, thermal interactions, photoablation and photodisruption [237].

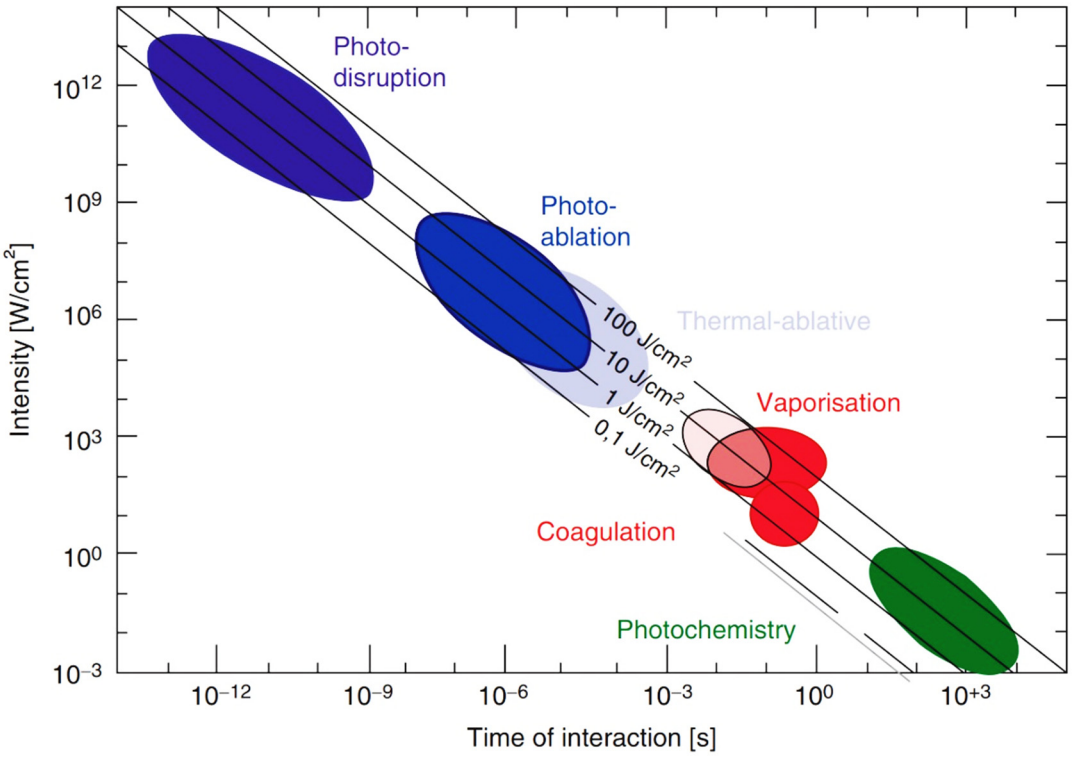

Figure 8: Graphical representation of laser-tissue interaction. The graph illuminates the photophysical effects encountered by the tissues in correlation with intensity and time of laser exposure. Figure adapted from Steiner *et al.,* [238].

Interactions between the laser and tissues, that can be used in medical applications, take place at energy density between 1 J/cm^2 to 1000 J/cm^2 and at a power density between 10^{-3} to 10^{15} W/cm^2.

Photochemical interaction

Light induced chemical reactions within tissues or macromolecules leads to photochemical reaction. Photochemical interaction can be triggered at a low power density such as 0.01-50 W/cm^2, in the presence of continuous wave for long exposure time and the interactions follows a specific pathway. This property can be used in photodynamic therapy and biostimulation [237].

Photodynamic therapy (PDT) involves in the usage of light activated exogenous chromophores or photosensitizers. While chromophores can be defined as biological

molecules that can absorb light of a defined wavelength [242] photosensitizers are the chromophore molecules that, when activated by light, cause a chemical reaction and lead to transfer of energy to the surrounding non-absorbing molecules [243]. Upon exposure of the chromophore to light, the molecules absorb the photons, thereby promoting excitation in the molecules. As an energy transforms takes place in these molecules, they move from ground stated to triplet state and this causes them to transfer the energy to oxygen. This in turn causes the oxygen to change into a highly reactive oxygen species which is toxic in nature [244]. The toxicity of the oxygen species, to the tissues, is due to its ability to induce cellular apoptosis by damaging DNA molecules [245]. PDT is used in treating cancer by inducing chromophores in tumour cells and irradiating the induced cells with laser. The laser irradiation triggers a photochemical reaction in chromophores leading to selective tumour necrosis.

Biostimulation or Low Laser Level Therapy (LLLT) is the photo stimulation of biological tissues with low level irradiation of visible red or near infra-red laser, thereby enhancing the biochemical reaction in the tissues. Many studies have shown that LLLT can be used in cellular proliferation [246, 247], wound healing [248, 249], nerve stimulation [250, 251], arthritis treatment [252] and anti-inflammatory properties. According to Hawkins *et al*., when biologicals are exposed to lasers, the mitochondria and cell membranes absorb the photons. The energy present in the photon is used by the cells to effectively increase the production of adenosine triphosphate production (ATP). The increase in ATP leads to an enhanced DNA formation which triggers higher neurotransmission. A cascade of metabolic reactions are triggered as a response to the inter and intra cellular biochemical reactions. These response can be used for faster wound healing, pain reduction and better inflammatory response [253].

Thermal interaction

Thermal interaction in tissues is induced when there is a significant increase in local temperature. In laser medicine, thermal interaction is caused when tissues exposed to laser converts the photons into heat energy. When the laser pulse duration is less than the thermal relaxation time of the tissue, negligible tissue damage is observed. But when the pulse duration is greater than the tissue thermal relaxation time, permanent thermal damage to the irradiated tissue and its surroundings often occurs. Optical penetration depth can be defined as the distance penetrated (thermal

diffusion length) by any electromagnetic radiation in a material.

The photothermal effect can be induced by either CW or pulse laser and when the power density of the laser is between 10-10^6 W/cm^2. Thermal effects such as coagulation, vaporization, carbonization, and melting can be distinctly differentiated by the duration and peak value of the tissue temperature. The effects and types of thermal damage caused by exposing tissued to an increasing temperature is listed in the Table 5 below:

Table 5: Effects of temperature increase on tissue properties

Temperature	Effect on tissues
37 ^oC - 42 ^oC	No measurable effect on tissues
42 ^oC – 50 ^oC	Hypothermia, bond destruction, membrane alteration and tissue necrosis
50 ^oC – 60 ^oC	Protein and collagen denaturation, tissue coagulation and necrosis
Temperature > 80 ^oC	Change in chemical equilibrium of the tissues due to increased permeabilization of membrane
100 ^oC	Vaporization of water in tissues leading rupture and thermal decomposition of tissues or ablation
Temperature > 100 ^oC	Carbonization of tissues

Thermal interaction is used in various biomedical applications such as thermal decomposition, treatment of retinal detachment, cauterization and laser induced interstitial therapy [237]. One of the most commonly application is photo cauterization to treat rhegmatogenous retinal detachment (RRD). RRD occurs when the retina is detached or torn from its designated spot. This leads to accumulation of vitreous fluids in the sub retinal spot. In order to threat this condition, the laser beam is focused over the damaged area thereby welding it to the wall of the retinal. The welding effect is caused when the photons from the laser is converted into heat energy, leading to coagulation between the damaged retinal and wall. While this process also leads to necrotic tissue formation in the treated area, the necrotic mass is gradually replaced by new tissues that are rich in pigment cells [254].

Another application of photo cauterization due to laser is sutureless surgeries. As stated in table 4, exposure of laser to tissues can result in protein and collagen

denaturation and tissue coagulation. This coagulation property of tissues can be used to bind the treated areas and seal the wound. When compared to conventional surgical process which needs the application of sutures, laser based cauterization results in low bleeding, faster healing time and circumvention of foreign materials and infection [255].

Thermal interaction of lasers with tissues are also used for laser-induced thermal therapy (LITT). LITT is a minimally invasive technique which can be used to treat tumours in various organs by inducing tissue necrosis. The necrosis is the result of thermal coagulation induced by the heat produced during the laser/tissue interaction. This technique is especially helpful in treating tumours forming in surgically challenging locations such as various locations of the brain. LITT when combination with MRI produces magnetic resonance thermal imaging (MRTI). This property is used by the surgeons to qualitatively monitor the thermal heat in real-time during the surgery while treating the tumours in remote locations [256, 257].

Photoablation

Photoablation is the process of breaking molecular bonds by using high intensity of light for a very short period of time. Photoablation of biological tissue can be achieved only via UV laser as the energy deposition of the light is usually higher than the specific threshold of the biological material. When tissues are exposed to a UV laser, the photons absorbed by the molecules allow the electrons to gain energy high enough to break covalent bonds. This leads to dissociation of the molecules, fragmentation of tissues and finally ablation of the exposed tissue. Also known as ablative decomposition, the depth and geometry of the ablation is defined by pulse energy and spatial parameters of the laser in use. The power density of photoablation ranges from 107 – 1010 W/cm2 while the pulse duration ranges between 10 – 100 ns [237]. Photoablation process is mostly applied for corneal refractive surgery [258].

In medical settings, photoablation is applied in LASIK refractive surgeries. An acronym for laser-assisted in situ keratomileusis, LASIK can be used to correct various optical defects such as myopia, hyperopia and astigmatism. In this procedure, a flap with a hinge is created on the cornea of the eye and folded back. This leads to the exposure of stromal tissues which can be photoablated with excimer laser (UV laser) of 193 nm wavelength. In order to treat myopia using LASIK, the tissues in the central cornea are ablated. This resulting in flattening of the central cornea and hence reducing

the refractive power. Hyperopia can be treated by ablating the tissues from the peripheral cornea resulting in an increase of curvature of the cornea and refractive power [259].

Photodisruption

Photodisruption is induced in a sample, when they are exposed to lasers with higher pulse energies. In this method the samples are split due to mechanical disruption. The optical breakdown of the samples occurs inside the tissues instead of the surface of the tissues. When exposed to the laser the tissue undergoes mechanical impacts such as plasma formation, shock wave generation, cavitation and jet formation leading to the ablation of the tissue. Photodisruption can be achieved at power densities ranging between $10^{11} – 10^{16}$ W/cm^2 with exposure period of 100 femtoseconds to 100 nanoseconds [237].

Photodisruption can be used to perform minimally invasive intraocular microsurgeries. In photoablation section describes how LASIK refractive surgeries can be used in vison correction. Initially, this procedure requires the creation of a lamellar flap on the cornea in order to access the stroma. The creation of the flap is a critical step as any damaged to the flap would lead to a myriad of complications. The flap is created by using the photodisruptive mechanism. In order to create the flap, pulses using the femtosecond laser at NIR wavelength of 1053 nm are delivered onto the cornea with a distance of 3 μm between each point. An optical breakdown is induced due to the plasma formation which is generated due to ionized tissues. The plasma generated results in intrastromal cavitation bubbles. The bubbles merge and form and cleave the intrastromal tissues. The cleaving of tissues is extended all the way to the surface, thereby leading to a flap formation [260].

2.9.1 Interaction of NIR wavelength with biologicals

As previously described, different regions of the electromagnetic spectrum can be applied in medical field to treat various conditions. But it was also observed that applications of certain wavelengths, such as the UV light (even for a very short period of time) leads to thermal disruptions (photoablation and photothermal disruptions). It is for this very reason research is being conducted to investigate the application of NIR wavelength for non-destructive medical applications.

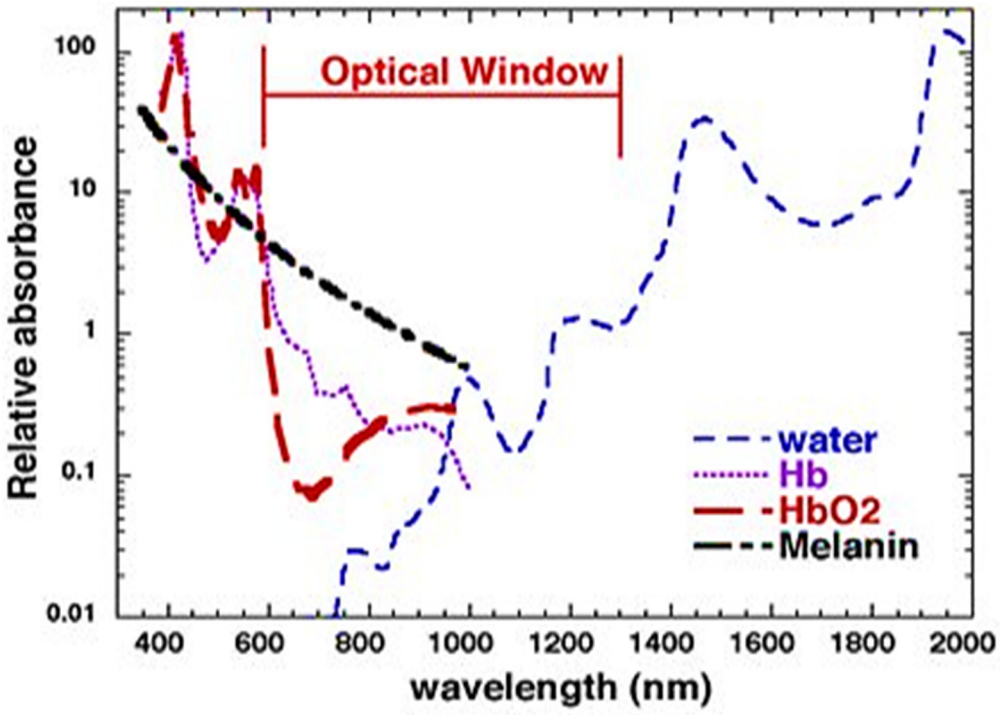

Figure 9: Illustration of optical or therapeutic window. A low absorption co-efficient can be observed by water, and haemoglobin in the NIR region. Image reproduced from Huang *et al* [261].

The ability of the light to penetrate a tissue is strongly dependent on its absorption co-efficiency. The proteins, macromolecules and water that make up the tissue are mainly responsible for the absorption of light by the tissue [237]. Major body constituents such as water, haemoglobin and chromophores have low absorption co-efficiency in this window which in turn allows the NIR wavelength to have better light/tissue interaction [262]. At NIR wavelengths between 600-1300 nm (Figure 9), absorption of light is minimized, therefore light at this wavelength has higher penetration capacity compared to the other wavelengths. This phenomenon, also known as “therapeutic window” or “tissue optic window”, is mainly due to the tissue’s property of low light scattering and less absorption [263]. This property is responsible for less heat deposition therefore limiting tissue damage due to thermal reaction.

2.10 EFFECTS OF NIR IRRADIATION ON CELLS

As stated earlier in this chapter, mesenchymal stem cells are known for their ability to differentiate into various cell lines. Currently many studies are being undertaken to study the biological and chemical effects of photobiomodulation of MSCs. Photobiomodulation is defined as the application of low energy lasers that emit light between the visible and near infra-red region (NIR) on biologicals [264].

Studies have shown that irradiating various cells lines with low level light irradiation (LLLI) has diverse effects on the cell's proliferation rate and differentiation abilities. Most of these studies were conducted using NIR wavelengths (630 nm – 980 nm) at a power density ranging from 0.2 – 12 J/cm^2 for a varying period of time. Stimulation of cells such as porcine Achilles tendon fibroblasts [265], human skin fibroblasts [266], synovial fibroblasts [267], human keratinocytes (HaCaT) [268], satellite cells [269], HeLa cells [270] and lymphocytes [271] amongst many others have shown an increase in the cell proliferation rate. Furthermore an increase in production of type I collage in porcine Achilles tendon fibroblasts was observed [265].

Studies have been conducted on stem cells obtained from various organs such as human umbilical cord mesenchymal stem cells (hUMSCs) [272], bone marrow derived mesenchymal stem cells (hBM-MSC) [273], adipose derived stem cells (hADSCs) [274], and irradiated with LLLI. All the irradiated cells have shown an increase in proliferation and migration. There was also an increase in osteogenic differentiation in rat (bone derived) and human MSCs (adipo derived) when exposed to wavelengths of 632.8 nm [275], 620 nm [276], 630 nm [277]and 810 nm [273].

In an *ex vivo* study conducted by Abramovitch-Gottlib *et al*., MSCs were cultured on a 3D coralline biometrics structure and irradiated with LLLI of 632.8 nm. They were studied for over 28 days for change in proliferative rate compared non-irradiated MSCs. In this investigation the irradiated MSCs showed an earlier phosphorous peak formation, significant enhancement in ALP activity and higher expression of calcium incorporation in the newly formed tissues compared to non-irradiated samples [275].

Biostimulation of cells by photobiomodulation is also dependant on various factors such as the wavelength, power density, energy density and the cell lines use. Modification of these variable leads to a different outcome in different cell lines [278].

Evans *et al*., showed that a higher proliferation rate was induced in human skin fibroblasts irradiated with 635 nm and while no such induction was observed in 808nm [279]. But in a study conducted by Tuby *et al*., the mesenchymal stem cells and cardiac stem cells when exposed to 804 nm irradiation showed an increase in their proliferative rate [280]. A study conducted by Li *et al*., showed that the daily irradiating of MSCs with a power density ranging from 1.5 J/cm^2 -2.5 J/cm^2 with a wavelength of 630 nm resulted in an enhanced colonial formation of MSCs. It was also observed that the proliferation rate was higher when MSCs were plated at low density and irradiated with low irradiance intensity compared to high plating density and irradiance [281].

Despite many studies being conducted, the mechanism of change in cell proliferation and differentiation rate, due to irradiation, is poorly understood. But it is understood that exposure of cells to LLLI induces photochemical reaction (specifically biostimulation and photobiomodulation) due to the absorption of photons by the chromophores that are present in the mitochondria and on the cellular membrane [282]. The terminal end of the respiratory chain in the mitochondria, cytochrome c (CCO) or the complex IV trans membrane protein are known to be specifically affected by the NIR irradiation [283]. Exogenous nitric oxide ligands (NO), which act as inhibitors, are known to bind themselves to the CCO. NIR irradiation of cells causes the displacement of NO from CCO, leading to an increase in its metabolic activity and membrane potential. This helps in an increased generation of ATP molecules, NADH and cAMP, leading to an elevation in the DNA and RNA synthesis [272, 282, 284].

Studies have demonstrated that, irradiating cells directly or during non-invasive photodynamic therapy (PDT) (human fibroblast, hepatocellular carcinoma cell line) with UV and NIR light leads to the generation of reactive oxidative species or ROS [285, 286]. A reactive oxidative species (ROS) is a highly reactive natural by-product of mitochondrial metabolism (aerobic metabolism). ROS is produced during the production of ATP molecules. It is known to promote cell signalling, regulate cell cycle, protein synthesis and enzyme activation [282]. Due to the increase in mitochondrial metabolism, post NIR irradiation, the generation of ROS is also elevated. Elevated levels of ROS leads to pathological dysregulation in cells inflicting DNA damage, inactivation of enzymes, protein oxidation and lipid peroxidation [287]. Studies have shown that stem cells undergoing self-renewal process display low level of ROS as opposed to those of the differentiated cells which contain more oxidative

species [288]. The anti-oxidants, which inhibit the effects of ROS, are seen significantly decreased in the differentiated cells. This may confirm that while low levels of ROS helps in maintaining the stemness of the cells, high levels of ROS may lead to a cascade of reactions in the cells promoting cell differentiation. In addition to this ROS is also responsible for upregulation of various genes which may cause an increase in cellular proliferation and migration [282].

Many of the above studies have shown that NIR irradiation of cells leads to an increase in proliferative rate, migration rate and sometimes an enhanced differentiative capacity. Pre-conditioning of cells, prior to stem cell therapy, by irradiating them with NIR wavelength may help in increasing the proliferative regenerative capacity of the cells. This may yield to higher and faster yield of stem cells and with better wound healing capacity. But it should also be noted that, if ROS is generated during the pre-conditioning of the cells, it would detrimental to the cells viability and therapeutic capacity.

2.11 NANOPARTICLES – GOLD NANORODS

According to International Organization for Standardization (ISO), nanoparticles are defined as 3D particles which has diameter range between 1 nm – 100 nm [289]. There is a rapid growing scientific interest in the research of nanoparticles due to their wide variety of potential applications especially in the biomedical field. In a bulk state, regardless of the size, the physical and the chemical properties of a component remain constant. But in nanoscale, the properties of the component are dependent on the it's molecular and atomic constructions [290]. Nanoparticles can be created in various shaped (spherical, rods, tubes, hollow capsules), sizes and can be made of different materials (metals, magnetic and semi-conductors). In our particular studies, I will be looking into gold nanoparticles especially the gold nanorods (Au NRs).

While gold nanospheres has an absorption resonance peak limited to 550 nm, the longitudinal plasmon resonance (LPR) adsorption of Au NRs is highly dependent on the aspect ratio of the nanorods themselves, as such the LPR can be tuned between around 650-1350 nm by selecting NR with specific aspect ratios [291]. The wavelengths of NIR lasers have the capability to penetrate up to 10 cm of the soft tissues due to the scattering properties of the soft tissue and the low absorption by

water and blood [292]. This property of NIR wavelength along with the ability to fine tune Au NRs to the required LPR, making them useful for a wide variety of biomedical applications some of which are detailed in section 2.11.4 of this chapter.

2.11.1 Localised Surface Plasmon Resonance (LSPR)

Before discussing the synthesis and applications of Au NRs, it is necessary to understand surface plasmon resonance and localised surface plasmon resonance. Surface of many conducting materials (most commonly noble metals such as gold and silver), contains large numbers of surface bound delocalised electrons that are not associated with specific atoms. When exposed to electromagnetic radiation (such as NIR irradiation), a collective coherent oscillation is induced in the free electrons due to the absorptions of the photons. This produces standing waves of varying electron density that spreads across the conducting surface also known a surface plasmon resonance (SPR). These surface waves can be thought of as analogous to waves spreading out on the surface of a lake when a stone is thrown in [293].

While surface plasmon resonance can take place over a wide area of the metal-dielectric interface, localised surface plasmon resonance is generated in smaller metallic nanoparticles. The smaller size of the nanoparticles can greatly increase the optical resolution. This phenomenon is due to the strong surface electromagnetic field generated around the nanoparticle and its exponential decay over distances similar to the particle size. The strong electromagnetic field is caused by the resonant photons which are confined within the plasmonic nanoparticles and causes the local surface plasmon oscillation [294].

While nanospheres display only one absorption resonance due to single absorption spectrum, the anisotropic shape of the Au NRs display two types of absorption resonance. This is caused by the presence of two absorption spectrums in nanorods namely the longitudinal plasmon resonance (LPR) and the transverse plasmon resonance (TPR) as shown in Figure 10.

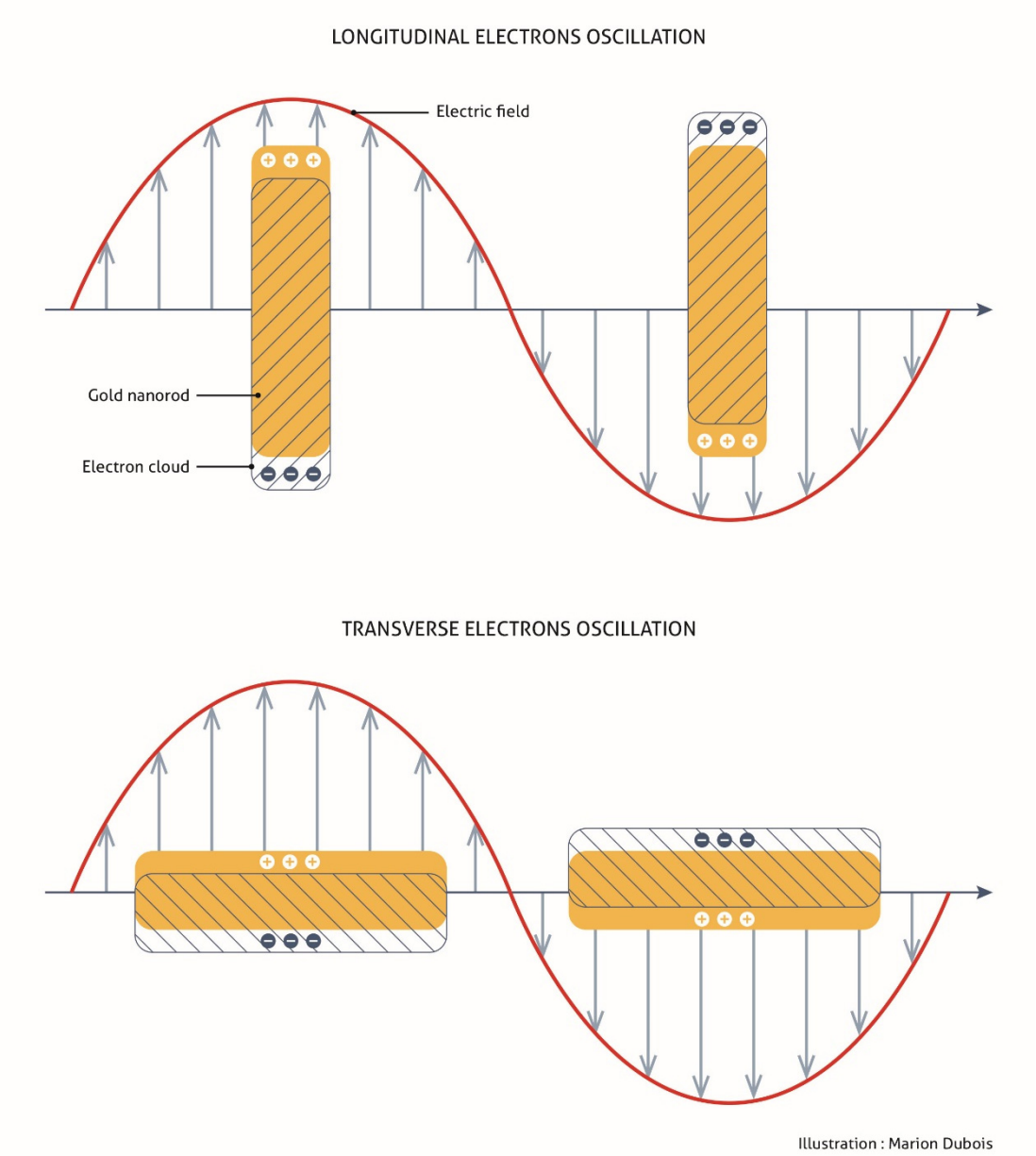

Figure 10: Two different types of plasmon resonance generated in Au NRs due to surface plasmon resonance in both the axis. While LPR is generated due to longitudinal electron oscillations and TPR is caused due to transverse electron oscillations.

The LPR corresponds to the length and the TPR corresponds to the width of the Au NRs. TPR of Au NRs remain relatively constant (between 500 - 520 nm) and they are insensitive to the change in the size or refractive index of the particles. In contrast to this is LPR in Au NRs are highly dependent on their aspect ratios. The TPR can be customised to show a red-shift, between 550 nm to 2000 nm, by tuning the aspect ratio of the Au NRs [295, 296].

LPR peaks in Au NRs are highly sensitive to conditions such as aspect ratio, shape, size and change in refractive index (due to the change in aspect ratio) in the

local dielectric environment (Figure 11). LSPR peak shifts or broadenings can also be cause by nanorods aggregation, assembly and functionalization [295, 296].

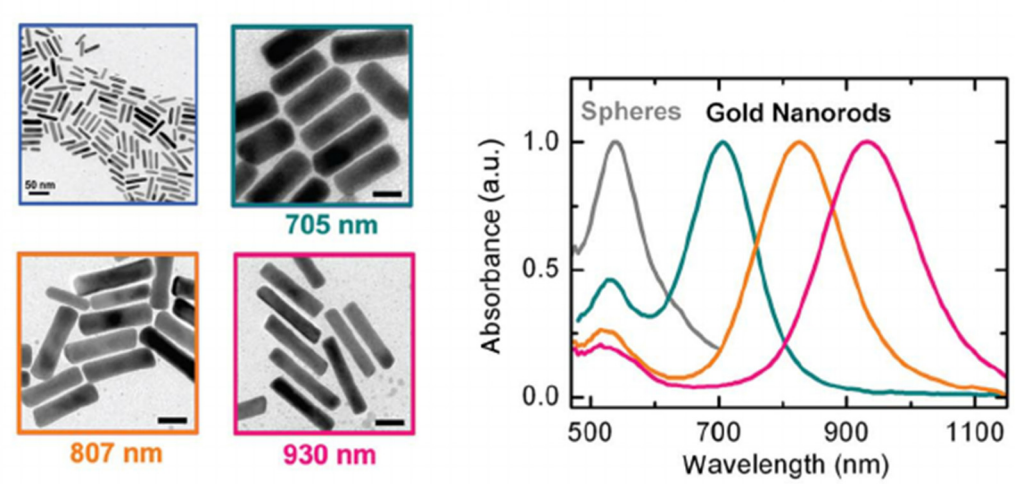

Figure 11: The LSPR of Au NRs varies with the aspect ratios and size of the nanoparticles. In the figure it can be noted that with the increase in the aspect ratios of the Au NRs, the wavelength also increases. Figure reproduced from Li *et al.,* [297]

2.11.2 Synthesis of Au NRs

Various methods have been developed to synthesize Au NRs. Some of the most common ones are:

Electrochemical method

First demonstrated by Wang *et al*., electrochemical redox reaction between two electrodes leads to the synthesis of Au NRs [298]. In this process a gold metal plate and platinum metal plate of same dimensions are used as anode and cathode. The electrodes are immersed in electrolytic solution made up of cationic surfactant, hexadecyltrimethylammonium bromide (CTAB) and tetraoctylammonium bromide (TCTAB), hexane and acetone. While both CTAB and TCTAB are known for their rod inducing capacity, CTAB is mainly used to stabilize the Au NRs and prevent the nanorods from aggregating after they are synthesized. The electrolytic cell was setup in an ultra-sonicator bath at a temperature of 38 ^{o}C and a controlled current electrolyses was induced by applying a typical current of 3 mA for 30 minutes. This resulted to the synthesis of Au NRs with various mean aspect ratios (1.8, 3.0 and 5.2) and different LSPR (600 nm, 710 nm and 873 nm). Later on, Wang *et al*., demonstrate that the aspect ratio of Au NRs can be controlled by gradually immersing silver plate, behind the platinum electrode. The major axis length of the rods formed was controlled by the amount and speed of silver ions dispersed in the electrolytic solution during the redox

reaction [299]. The disadvantages of this method is its low reproducibility, limitation of plasmon band to 850 nm in many cases, low yield rate and the formation of spherical nanoparticles [300].

Template method

This electrochemical method relies on the deposition of gold in the nonporous aluminium or polycarbonate membrane. The nanopores in the membranes act as the template for the formation of Au NRs. The process of creating Au NRs using this method is done in 5 stages. Stage 1 involves in electrochemical growth of Au nanoparticles in the pores, leading to stage 2 were the gold is electrodeposited within the pores of the membrane. Stage 3 and 4 involves in selective dissolving of membrane in the presence of polymer stabilizer like poly(vinylpyrrolidone). The final stage involves in sonicating the Au NRs in water or organic solvent. The diameter and length of the Au NRs can be controlled by controlling the pour diameter and gold deposition rate. The disadvantage of using this method is the low Au NRs yield. This is mainly due to the limited amount of pours present across the surface area of the membranes [301].

Photochemical synthesis

A good yield of Au NRs can be obtained when gold chloride solution mixed with acetone, cyclohexane, silver nitrate, CTAB and TCTAB is irradiated with UV light with a wavelength of 254 nm for 30 hours [302]. The irradiation time period can be reduced to 30 minutes when Au^{3+} is reduced to Au^{+} in the presence of ascorbic acid during the irradiation [303]. Similar to photochemical method, the aspect ratio of the Au NRs can be controlled by the amount of silver ions present in the solution. In the presence of higher amount of silver ions, the aspect ratio of the Au NRs increases with the decrease in their width and vice versa. Low amount or absence of silver ions results in formation spherical nanoparticles [302].

Seeded method

Of all the synthesis techniques, seeded technique has emerged as the most popular approach to create Au NRs. This is due the ability to easily control the aspect ratio of the particle, generation of high quality of nanorods and high yield rate. Though seeded method has been used for many decades to synthesize gold nanoparticles, Jana *et al*., were the first develop a seeded method to synthesize Au NRs [304]. Seeded

method is a two-step process. The first step involves in the creation of spherical gold nanoparticles also known as seeds. Following this, the spherical gold nanoparticles change into Au NRs [305].

Jana *et al*., prepared the gold nanospheres or "seeds" by reducing $HAuCl_4$ (Gold (III) chloride trihydrate) and tri-sodium citrate to citrate capped $HAuCl_2$ in the presence borohydride. Citrate capping acts as a stabilizing agent for the gold nanospheres. When $HAuCl_2$ was added to a solution of $HAuCl_4$, CTAB, and ascorbic acid at a pH of 2.8, spheroidal and rod like gold nanoparticles were formed. These particles had aspect ratio ranging between 4-18. Though Au NRs formation was observed the yield rate for this procedure was only 4% [304]. The same group improved the yield to 90 % by modifying the pH to 3.5 [306]. Nikoobakht *et al*., increased Au NRs yield to 99 % by performing two modifications to the above method. In the first modification, the citrate capping was replaced by CTAB capping on the seeds as the stabilizing agent. Secondly silver ions were added to the solution to control the aspect ratio of the synthesized Au NRs. This resulted in the high yield of Au NRs with aspect ratios varying from 1.5 – 4.5 [300].

In most of the above described methods, CTAB is used to induce rod formation during the Au NRs production. There are two theories behind the rod induction capacity of the CTAB:

- Collision theory: This theory states that rate of nanorods formation is dependent on the rate of collision between the cationic $AuCl_2$-CTAB micelles and the gold seed. During higher collision rates, the micelles collide with the tip of the nanorods instead of the sides of the nanorod, thereby giving rise to longer nanorod morphology [307].
- Zipping theory (Figure 12): This theory states that CTAB surfactants prefer to adsorb on to the sides of the nanorods. During this process the hydrocarbon tail of CTAB, along the nanorods, are bound together by van der Walls force thereby forming a bilayer chain. This prohibits gold ions from interacting with the sides of the nanorods thereby forcing them to merge at the edge of the Au NRs. This process regulates the size of the nanorods [308].

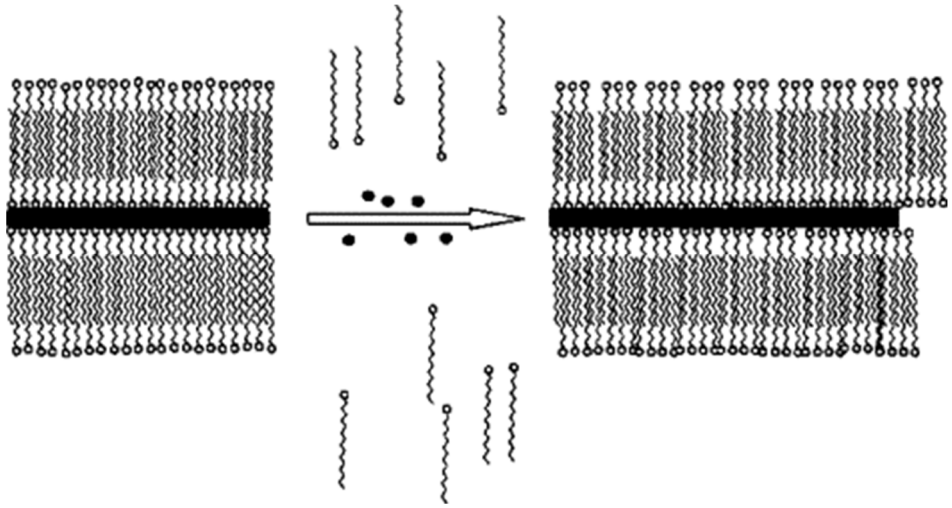

Figure 12: Au NRs formation by "zipping". CTAB bilayer is formed on the sides of the nanorods. This forces the gold seeds to interact with the edges of the nanorods thereby increase the nanorod length. Figure adapted from Gao *et al*., [308]

2.11.3 Effect of lasers on gold nanorods

When exposed to electromagnetic waves, a unique localised surface plasmon resonance (LSPR) occurs on the surface of the Au NRs. The LSPR of the nanoparticles is dependent on various parameters of the material such as its dielectric constant, shape, size and the particle-particle coupling (interaction between the particles). The exposure of surface plasmons to electromagnetic light waves causes photon-electron and electron-electron interaction which leads to the generation of localized heat by the nanoparticles [309]. In short, the light energy is converted into thermal energy by a series of photophysical steps. This phenomenon is also known as photothermal effect. The heat generated by the Au NRs is influenced by many variables such as the volume of Au NRs present, the power density delivered by the laser, laser wavelength and the type of laser used (pulsed vs continuous wave).

Studies have shown that exposure of Au NRs to different pulse dependant lasers can induce not only LSPR on the surface of the particle but also causes size and morphological changes in the nanoparticles. When exposed to low energy lasers, the temperature in the nanoparticle lattice is only raised by few tenths of degree. The increase in the temperature is dependent on the size of the particle and intensity of the laser. Exposing nanorods to high intensity femtosecond, nanosecond or continuous NIR lasers induces size and shape transformation (from rods to spheres to nanoparticle fragmentation in few cases) in the nanoparticles, a decrease in LPR intensity and increase in TPR intensity [301, 310]. While the decrease in the LPR intensity is caused

due to decrease in the of the rod length, the increase in TPR is caused due to the transformation of the Au NRs to spheres. The decrease in LPR peak also creating a blue shift in the LSPR wavelength [311]. Chang *et al*., observed the formation of new "φ-shaped" particles, which are considered to be responsible for the intermediate stability of the nanostructures during rod to sphere transition [299]

2.11.4 Biological applications of Gold Nanorods

Gold nanorods have emerged as a new type of nanostructure which has wide variety of uses in the field of biology and biomedicine due to its radiative and non-radiative properties. Gold nanorods are being used in bio sensing, drug delivery, gene delivery, diagnostics, therapy and disease detection. Some of the biological applications of Au NRs are:

Drug delivery

The possibility of gold nanorods to have tuneable optic absorption, low toxicity, ability to carry wide range of organic molecules by conjugation, has made them one of the most often cited material in the field of nonmedical research. Modification of the surface of the gold nanorods by surface conjugation according to need, allows it to carry specific drugs or biomolecules. The main advantages of drugs delivered through nanoparticles are target specificity, delivery of higher concentration of drugs on the required target and control over the release of drugs. Internal stimulations such as change in pH or external stimulation like application of light or heat can help in controlling the drug release [312].

Many studies involving in effective loading of therapeutic drugs and anti-cancer drugs onto functionalized Au NRs using different approaches are currently being conducted. The release profile of the drugs are dependent on the strength of the drug-nanoparticle binding. While strong binding of drugs to the polymer shell can lead to difficulty in drug release, weak binding may cause the drugs to be prematurely released or leaked before the nanoparticles reach the intended target [313]. Drugs are conjugated on to the Au NRs via various physical and chemical reactions such as electrostatic interactions [314], diffusion of drug molecules into the outer Au NRs shells [315] and covalent interaction (for example: carboiimide chemistry and hydrazone linkage) [316, 317].

Targeting the gold nanorods for *in vivo* applications are done by two ways: active targeting and passive targeting [312]. In the case of passive targeting, the drugs are attached to the nanoparticles and are released into the blood stream. The nanorods are designed to reach and accumulate in and around the required location by "homing of the vectors" on the extravasation (leakage) in the blood vessels of unhealthy tissue. The drug release may occur due to change in surrounding environment such as temperature, pH or homeostasis etc [312, 318].

In active targeting the ligands are conjugated on the carriers so that it recognizes and actively binds to the specific cell surface receptor [319]. Drug carrying nanoparticles can be designed with a cell specific ligand. When released into the body these ligands will bind to the targeted cells which have complementary ligands. For example, it is known that in the presence of a metastatic tumour, there is an up regulation in the expression of transferrin receptors, and they possess transferrin-receptor mediated endocytosis mechanisms. Transferrin can be conjugated to the nanoparticles loaded with drugs and injected into the body. In this way there will be an increase in the uptake of nanoparticles by the target due to the ligands [320].

Gene delivery

In order to replace defective DNA, gene therapy is used. It is the process by which the foreign DNA is safely and efficiently introduced into the somatic cell. Gene delivery is traditionally done in two ways: via viral vectors and by using synthetic carriers. Though viral mediated delivery has been highly successful, it has resulted in side effects such as cytotoxicity, immunogenic reaction, limited DNA carrying capacity, restricted targeting, and high costs [321]. These side effects have led to increased desirability to use synthetic materials with gold nanorods receiving attention in recent years.

Experiments were done by Wu *et al* [322]., to see the possibility of remotely controlling the delivery of gene to a specific target. In this experiment the thiolate gene of enhanced green fluorescence protein (EGFP) DNA was covalently bound to gold nanorods. These EGFD-gold nanorods were later exposed to HeLa cells and then irradiated by using NIR irradiation technique. On incubating the cells for specific observation under fluorescent spectroscopy, EGFP expression by the cells were observed, proving that the gene delivery had been successful.

Photothermal therapy for cancer

Photothermal therapy (PTT) is a minimally invasive therapeutic process in which the photon energy is converted into heat energy to kill cancer cells. This property also makes them a high level contrasting agent, allowing for easy tracking [323]. In the present environment gold nanospheres, gold nanoshells, gold nanorods, gold nanocages and carbon nanotubes are being used for the treatments. The gold nanoparticles show higher intrinsic absorption efficacies, this leads to higher and faster rates of the heating effect compared to gold nanoshells or gold nanocages. The multi functionality, tuneable optic properties and ease of preparation makes gold nanorods favourable for therapeutics [324].

2.11.5 Cytotoxicity and surface modifications

Though highly recommended as a nanomaterial, it is always advisable to check the cytotoxicity of gold nanorods. As explained previously, the most popular methods to synthesizing gold nanorods is by the process called seed-mediated growth method. In this process CTAB is used as a surfactant to direct the shape of the nanorods in solution phase [300, 325]. CTAB is regarded as an indispensable part for synthesizing the nanorods. Though CTAB molecules can be removed by the process of repeated centrifugation and dialyses, excess removal may lead to the collapse and aggregation of the nanorods. The surface of the gold nanorods can be modified in a way that CTAB is either replaced or is capped by biocompatible molecules to reduce the cytotoxicity.

Low concentration of CTAB-stabilized Au NRs showed strong cytotoxicity to the cells. In vitro studies on toxicity by Au NRs showed that while free CTAB molecules are harmful to human cells, bound CTAB molecules are non-toxic[326]. Functionalizing or coating Au NRs with materials that follow the following rules can help in decreasing the cytotoxicity to the cells: (i) ability to firmly attach to the surface to the CTAB coated Au NRs, (ii) physical and chemical stability, (iii) non-toxic and biocompatible (iv) easily functionalization that allows further conjugation of chemicals or biomolecules, (iv) optical transparency for excitation and emission of light, (v) ease of maintaining the coating thickness and (vi) has no effect on the LSPR of the Au NRs post coating [327].

A study by Niidome *et al*., showed that by simply adding mPEG-SH to the CTAB solution, PEG modified gold nanorods will be formed. *in vivo* cytotoxicity testing of this PEG functionalised materials showed 90% viability of the cells [328].

Huff *et al*., investigated the internalization of CTAB coated gold nanorods and mPEG-DCT modified gold nanorods by the KB cells (Keratin forming tumour cell line from oral epithelium). It was observed that a high density of CTAB gold nanorods were internalized within a few hours. As opposed to CTAB gold nanorods, mPEG-DCT modified gold nanorods were internalized at a reduced level. This study demonstrated that CTAB encourages the cells to internalize the gold nanorods which explains the reduced cell viability [329].

The CTAB triggered cell apoptosis is not a well understood phenomenon. A study conducted by Pan *et al*., states that the cellular interaction of CTAB may activate a mitochondrial apoptosis dependant pathway. In their studies, exposing HepG2 cells (liver hepatocellular carcinoma cell line) to CTAB showed an increase in AMP-activated protein kinase (AMPK) which in turn activates the p53 protein [330]. AMPK is known for regulating the cellular energy and metabolism and is activated when the energy is low. The increase in AMPK in the cellular environment leads to the increase in p53 proteins. p53 protein activation is a reaction which occurs when the cells are exposed to metabolic stress and DNA damage. The activation of p53 leads to myriad of pro-apoptotic reactions such as arrest of cellular growth, cell senescence and cell death [331].

Silica is most commonly used material for the functionalization of Au NRs. Silica is biocompatible in nature and is known to improve the stability of the Au NRs and is almost non-cytotoxic to the cells [327]. In addition to this, biomolecules ligands can be easily conjugated to the silica surface. The thickness of the silica coating causes a shift in the LSPR spectra of the Au NRs. Increase in the thickness of the Si coating causes a red shift in the LSPR due to the increase in its refractive index [327]. Studies have shown that silica coated Au NRs (SiO_2-Au NRs) can be potentially used in vivo as an effective cancer drug carrier. The silica shell of the SiO_2-Au NRs acts as a payload for cancer drugs such as doxorubicin hydrochloride (DOX). These gold nanorods can be delivered to a required location and the drug release can triggered by irradiating the DOX- SiO_2-Au NRs with NIR irradiation. Exposing the DOX- SiO_2-Au NRs with NIR irradiation induces a photothermal reaction on the nanoparticles.

This photothermal heat weakens the interaction between the DOX and the silica shell, leading to drug release in the intended target [332].

EDC/sulfo-NHS is the most commonly used strategy to conjugate biomolecules to Au NRs. [1-ethyl-3-(3-dimethylaminopropyl) carbodiimide hydrochloride] is a cross linking agent that helps in the formation of amide bonds with carboxyl groups or amine groups. Bio conjugation with EDC can be performed in water but the reaction has to be carried out quickly to avoid the hydrolyses of ester bond. Sulfo (N-hydroxysulfosuccinimide) or Sulfo-NHS can be added as an intermediated stabilizing agent by forming an active ester functional group with carboxylates or amines [333].

Functionalized Au NRs are also commercially available from companies such a s Nanopartz and nano ComposiX amongst many others. Many of the Au NRs (designed biological purposes) sold by these companies are claimed as CTAB free and are functionalized with a wide variety of chemicals that help in easy conjugation of ligands, biomolecules and DNA.

2.12 APPLICATION OF LASERS AND GOLD NANORODS IN CELL DETACHMENT

To date there have been only two examples using gold nanostructures to promote the detachment of cells. In 2012, Kolesnikova *et al.*, demonstrated that the selective detachment of cells by using gold nanoparticles was possible. This was done by exposing the NIH-T3T cells grown on gold nanoparticles base to visible green laser light (520nm). Gold nanoparticles were micro patterned on to a PDMS surface and NIH-3T3 fibroblast cells were cultured on them. After cell proliferation the, samples were exposed to 532 nm, at 500 mW and 1000 mW for 2 and 5 minutes. Cell detachment was observed on the laser exposed area. It is hypothesised that after strong photo absorption in the presence of green laser light, the absorption peak shifts towards the red region. During this period there is a nanoparticle aggregation due to dipole-dipole interaction between nanorods. This may have led to the nanoplasmonic effect which may have triggered a photothermal or photochemical response leading to cell detachment [334]. The study also showed the generation of reactive oxygen species (ROS) following the irradiation. The author postulates that the generation of ROS may be responsible for the detachment of cells which may be detrimental to the cell viability.

In 2016, Giner-Casares *et al*., also used gold nanoparticles and NIR laser (980 nm) to detach cells. Gold covered surfaces were fabricated by dip coating a solution of inverse polymer micelles composed of a polystyrene-polyvinylpyridine block co-polymers with Au ions doped inside their hydrophobic core. These block co-polymers formed a 2D ordered hexagonal array on the substrates (a process the authors term micellar block copolymer nanolithography). This array was then exposed to a short burst of oxygen plasma to remove the polymers leaving behind an array of gold nanoparticles (diameter = 15 nm). In a final step the Au array was exposed to a solution of gold salts, ascorbic acid, and cetyltrimethylammonium bromide (CTAB) to promote the chemical growth of high aspect ratio gold nanostructures with SPR in the NIR region of the electromagnetic spectrum. The final dense array of branched nano structures possessed lengths of 40–60 nm and a mean diameter of 30 nm and a SPR between 600 to 1100 nm. Five different cells (HeLa, A549, HUVECS, T3T and J774) were used to test the detachment process. The cell detachment for each of these cells was successful when the surface was irradiated with NIR of 980 nm. It was observed that each different cell line required different exposure times. HUVECS took the least time (5 minutes), J775 and A594 took the highest time to detach (40 minutes), with detachment rate ranging from 80 % - 100 %. The viability of the detached cells valued between 75 – 100 %. When the detached cells were re-seeded for culture, relevant amounts of adhesion and proliferation was observed [335].

In this paper it is postulated that the photothermal effect may be the likely phenomenon responsible for cell detachment. Though NIR induces a mild heating in the bulk culture media, there is expected to be a higher increase in temperature between the interface of nanoparticles and cells. This localized effect may have been responsible for the detachment of the cells while avoiding any permanent damage to them.

2.13 A BRIEF HISTORY OF 2D AND 3D CELL CULTURE

While detachment of cells from cell culture surface using non-enzymatic detachment is necessary to prevent damage to the cells, expansion of cells on a larger scale is also important. Stem cell therapy, to treat various diseases, require hundreds of millions of stem cells which are difficult to produce on a 2D surface. Therefore, 3D cell cultures such as microcarriers are being investigated and used to produce required

stem cell numbers. While a 3D microcarrier system can be used on large scales, an appropriate cell detachment technique, that does not involve in enzymes, is still being investigated. Below is a review of different cell culture techniques, their advantages/disadvantages and detachment methods used to recover cells from microcarrier surface.

2.13.1 2D cell culture

Since over a century, 2-dimensional (2D) cell culture is recognised to be the most predominant from of cell culture technique. This technique relies on culturing cells on a flat plastic or glass surface. It is a simple but efficient technique that allows the cells to grow and proliferate as a monolayer in the presence of media rich in nutrients and growth factors [336]. Some of the main advantages of the 2D cell culture is the low cost required in maintaining the cells, the ease of maintaining them and of performing various functionality tests on the cells in a flat environment [337]. But 2D cell culture also has many disadvantages. It is well established that extracellular matrix, present outside the cell membrane, not only acts as a scaffold for the cells to adhere, but also as helps the cells in regulation of proliferation, differentiation, migration, cell polarization, organization and in survival of the cells [338]. The 2D cell culture does not represent the cell-cell and cell-matrix interaction present in the *in vivo* environment of a tissue. There is a distinct change in the morphology, organization and cell signalling, which all together effect the functionality of the cells [337].

Birgersdotter *et al.*, states that 2D surfaces enforce an unnatural geometry on the cell culture leading to mechanical constrains on the cells. In addition to this, studies have also shown changes in the gene expressions, gene splicing, protein modification and overall biochemistry in the cells. Birgersdotter *et al*., also states that culturing cells in a 2D environment has an effect on the intracellular pathway in the cells, leading to the loss of polarity and proliferation rate of the cells [339]. Polarity of a cell is defined as the intrinsic asymmetrical placement of different cellular components which is necessary from the cells to perform specialized functions. Furthermore, there is also a loss of tissue specific architecture, biochemical signalling, mechanical signalling and a loss of cell-cell communication. In addition to this, the data obtained during pharmaceutical drug trials are skewed due to the inability of the 2D cell culture to mimic the complexity of a dynamic in vivo 3D environment [340].

2.13.2 Effect of 2D cell culture on pharmaceutical industry

In the pharmacological industries, any new drug candidate must undergo stringent testing through pre-clinical and clinical trials (phase I, II and III). In order to be approved by the European and American regulatory authorities the drug must pass these trials. Preclinical studies involve examining the effect of numerous variants of drugs on a target. This step is performed to narrow down and optimise the relevant compound which exhibits efficacy toward the target [341]. Preclinical studies are usually conducted in a 2D *in vitro* model and relevant animal *in vitro* models to explore the safety and efficacy of the drug [342]. This preliminary analyses involves in studying pharmacodynamics and pharmacokinetics of the drugs such as the effect of concentration, toxicity, metabolic activity, adsorption and excretion of the drug by the target [341, 343]. If the drug passes pre-clinical trials, the clinical studies involved in testing the usefulness and effect of the drugs on human are conducted [342, 343].

However, the studies conducted in the preclinical trials are often insufficient to determine the effect of the drugs on a patient. Kola *et al.,* states that between 1991-2001 only 11% or 1 in 9 drugs made it through the clinical phase and were approved by the European and American regulatory authorities [344]. While billions of dollars are spent on getting a drug approved, it was noted that many of the drugs fail in either phase II or III (the most expensive phase) [343]. These failures are mainly attributed to lack of clinical efficacy (approximately 30% of failure) and safety/toxicity (30% of failure rate) [344].

In order to lower the failure rates, it is crucial to develop an *in vitro* cell culture testing method that mimics and predicts the outcomes of the drugs in an *in vivo* system. This system would help to weed out the inefficacies and toxicity of the drugs during the very early stages of testing. While 2D monolayer cell culture testing system is the norm for preclinical trials, studies have suggested limitations to this system. Properties such as cell-cell, cell-ECM signalling pathways that are necessary for an in vivo cell proliferation, differentiation and other functions are limited in 2D monolayer [343]. These limitations can be overcome by using a 3 dimensional (3D) cell culture system in which the cell behaviour are morphologically and physiologically more true to the in vivo cell system [345].

2.13.3 3D cell culture

In order to overcome the short comings of the 2D cell culture system, many studies are being conducted to culture cell in a 3D system. The earliest known 3D cell culture was carried out by A.W. Hamburger and S.E. Salmon in 1977 [346]. Human tumour stem cells when cultured on soft agar showed colony formation. Since then there have been many studies in which cells have been successfully cultured in 3D. There are many 3D cell culture systems such as hydrogel scaffolds which can mimic the native ECM environment [347], roller bottle cell culture system, hollow fibre cell culture systems and microcarrier cell culture systems. Some of the main differences between the 2D cell culture and 3D cell culture systems are detailed in Table 6.

2.13.4 Problems with cell numbers in stem cell therapeutics

It has been stated previously that stem cell therapy is being used in clinical trials to treat cardiovascular disease [348, 349], neural disease [350, 351], liver cirrhosis [352, 353], autoimmune disease [354] etc. But several challenges have been identified that needs to be addressed for the mesenchymal stem cells to be applied to its full potential in the therapeutic industry. Some of the major issues are the stem cells' limited harvest numbers, limited proliferative, differentiative capacities and slow proliferative rate. While bone marrow is considered to be one of the most reliable sources for MSCs, only of a very small percentage of the isolated nuclear cells i.e., 0.001% to 0.01% are MSCs [63].

MSCs expansion should be maintained at low densities in order to preserve their self-renewal capacity and rapid growth. MSCs have a limited rapid proliferative capacity and they decrease or cease to proliferate after approximately 50 population doublings at low densities. Passaging cells at high densities lead the cells to cease expansion only after 15 population doublings. It is theorised that the slow proliferative rate of cells in higher densities may be due to either cell to cell contact or cell secretions in the medium [355]. In addition to this, at higher passage rates, the MSCs have shown to enter the Hayflick's limit. At this stage they enter a senescence state were the morphology of the cells are enlarged and irregular [356].

The increase in passage rate also has an impact on the MSC's differentiation capacity. Studies have shown that even though the MSCs can differentiate into osteoblasts at passage 15 [357], they lose their ability to differentiate in to adipocytes,

Table 6: Comparison of a 2D cell culture to a 3D cell culture. Table reproduced from Kapałczyńska *et al*., and Edmondson *et al*. [337, 345]

Variables	2D cell culture	3D cell culture
Time taken for cell culture	Minutes to hours	Hours to days
Culture quality	High performance, reproducible, simple to culture, easy to study, can be cultured for a longer period	Poor performance and reproducibility, complex to culture, difficult to study and to culture for a longer period of time
In vivo emulation/simulation	Does not represent original microenvironment of a tissue or organ as cells grow flat sheet like in a monolayer	Mimics the functionality of tissues and organ due to aggregated structure.
Cell interactions	Lack of cell-cell interaction and cell to extra cellular environment as observed in in vivo microenvironment and niches	Enables proper cell-cell interaction and cell to extra cellular environment as observed in in vivo microenvironment and niches
Cell characteristics	Alteration in the original cell morphology, loss of phenotype and polarity	Retention of original cell morphology, phenotype and polarity
Access to essential components	Even access to all the cells in the monolayer to the nutrients, oxygen and metabolites which is stark contrast to in vivo environment	Variable access to of nutrients, oxygen and metabolites to the cells representing the in vivo environment. The supply may not reach the core of the aggregates.
Molecular mechanism	Change in gene expression, topology reaction and biochemistry in the cells	Cells express genes, topological reactions and biochemical reactions similar to that of in vivo environment.
Cost	Cheap, cosmetically available standardised tests and media	Expensive, standardised tests are not available.
Gene/Protein expression	May display variable expressions compared to an in vivo model	Gene/protein expression profiles is similar to that of in vivo models
Cell cycle stage	All cells display similar cell cycle stage due to equal exposure to nutrients	Different cell cycle stages are seen due various cells in the aggregates undergoing, proliferation, quiescence, hypoxia and necrosis.
Polarity [339]	Cells lose their polarity when cultured on a 2D surface	Cells cultured on a 3D surface have their polarity restored, independent of the time they were cultured on a 2D surface

thereby losing their multipotency [358]. All these factors limit the expansion of stem cells. In short, I need to proliferate a large densities of stem cell while they are in their earlier passages in order to obtain cell with high proliferation and differentiation capacity that can be used for therapeutics.

While currently the dosage of stem cells for the treatment of some disease (graft vs host diseases) varies between 10^6 to 10^7 MSC/kg body weight per week [359, 360], other disease such as cardiac repair, diabetic treatment or immunotherapy require numbers greater than 10^{10} cells [361, 362].

While most of the stem cell culture expansion are performed in a flat planar T-flask, this system has its own detriments such as the limited surface area for further cell expansion. T-flasks have surface area ranging between 25 cm^2 to 175 cm^2 leading to a maximum yield of $1.76 * 10^7$ cells from a single large flask [363]. While this system is feasible to culture cells for an autologous stem cell therapy, large quantities of T-flasks would be necessary to achieve the required cell numbers due to the required cell numbers [364]. For example, one T-175 flask yields approximately 1.76×10^7 cells. In the above statement I have stated that cell therapeutic treatment would require nearly 10^7 cells/kg. Assuming a person is 50 kg, I would require 50×10^7 cells for a single person which in turn requires approximately 45 to 50 T-175 flasks or an entire 40 stack of Nunc tray (Figure 13) that needs to be automated and machine manipulated due to its size [365].

Figure 13: Thermo Scientific Nunc Cell Factory Bioprocessing System showing 4×40 stacked T flasks in an incubator. Image adapted from Thermo Scientific [366]

But, in case of allogenic cell therapy, were cells from a single donor is used to treat multiple patients, the stacked T flasks would not be sustainable to provide the amount of cell required. Want *et al*., estimated that in order to treat 250,000 patients with cardiac disease it would require nearly 10^{16} stem cells. This approximately requires 286 million T-175 tissue culture flasks [367]. In addition to these issues, culturing cells in a 2D culture is labour intensive (in absence of automated system), time consuming, prone to infection due to manual replacement of media and the cell passaging are done after short period time as a result of limited surface area. This process is less sustainable and cost inefficient [368]. Culturing cells on flat surfaces is quite restrictive and is not reliable to ease the bottle neck in producing the necessary cell numbers. In addition to this I have also earlier stated that culturing cells in a 2D surface causes them to lose their multipotency and culturing cells in the T-flasks also results in generation of large amount of plastic wastes.

In order to meet the demand for higher number of cells, expansion of cells on a larger scale is necessary. There are products in the market such as stacked flask (previously mentioned), roller bottles, hollow fiber modules and microcarrier technologies.

Roller Bottles

An initial scale up method, the roller bottles are mainly used for culturing anchor dependant cells on a large scale. These bottles are hollow cylinders with cells attached to the inner surface and set on a roller (Figure 14). During the rotation, the cells inside the bottle are exposed to atmosphere and growth media alternatively [369]. A high output of cells can be obtained when numerous roller bottles are stacked together. Though a simple technology, this system has the disadvantage of being labour intensive, expensive, difficulty in manipulation and requiring large space for scaling up [369, 370]. In addition to this studies have shown that the output obtained from 1 litre of microcarrier system is equal to 18 roller bottles [370]. This method cannot be necessarily considered as a 3D cell culture system due to the cell adhering to the flat surface of the bottle.

Figure 14: Roller bottle bioreactor system (Integra CELLROLL System)

Hollow fibre bioreactor system

Cell culture in hollow fiber was first performed by Kanzek *et al*., in 1972. In this process, L-929 (mouse fibroblasts) were cultured on hollow cellulose acetate capillaries and JEG-7 (human choriocarcinoma cells) were seeded on to silicon poly carbon capillaries and perfused with media. After 2 weeks the cell count was estimated to be 17×10^6 for L-929 and 217×10^6 for JEG-7 after 28 days. The entire cell expansion was performed in an area that was less than 3 cm^3 [371]. In present day, hollow fibre bioreactors are, as stated by Whitford *et al*., "high-density continuous perfusion system" [372]. This system is made up of thousands of semi-permeable hollow fibres that arranged parallel to each other (Figure 15). The space between the fibres known as the extra capillary space and cells are seeded and cultured in the extra capillary space. The semi - permeable hollow fibres are flushed with cell culture media allowing the exchange of nutrients between the cells and the capillaries. The advantage of this system is it's high surface, non-shear environment and the porous nature of the fibre. This porosity of the fibre and the perfusion helps in recapturing the in vivo like 3D cellular environment [372].

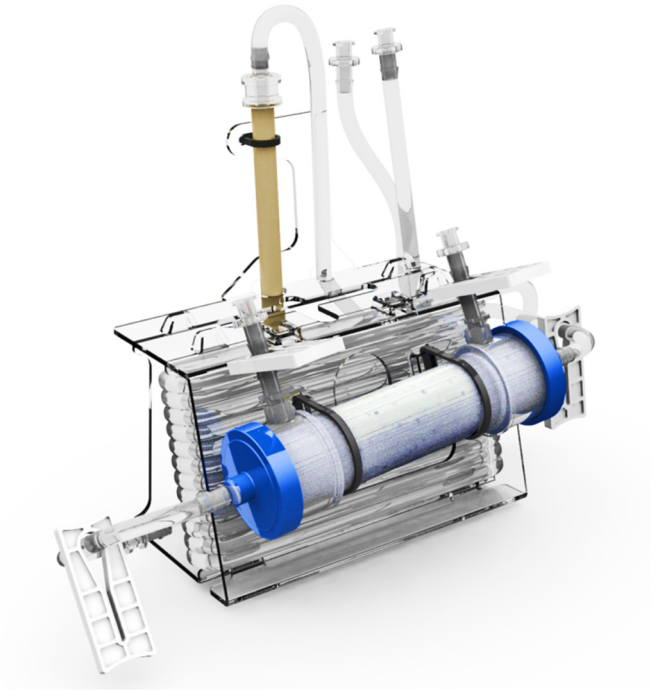

Figure 15: A hollow fibre bioreactor system for cell culture from FibreCell Systems [373]

The non-homogeneity of this system causes several short comings such as limited potential to scale up due to the necessity of perfusion system design, inconvenience in sample collection due to fibrous nature of the system, difficulty to maintain and control the inner environment of the system [365].

2.14 MICROCARRIERS

The studies regarding growing cells on beads were first performed in 1967 van Wezel *et al*., who were also the first to coin the term "micro-carriers". According to the studies the negatively charged cells were cultured on positively charged cross-linked dextran (sephadex) or DEAE-Sephedex which had low density, transparency and high surface to volume ratio. The studies concluded that, at the end of the culture period, though the growth rate of the cells were similar to that of monolayer culture, a higher density of cells can be obtained by changing the cell culture media [374].

Microcarriers are spherical particles usually between 100-500 µm in diameter made up of polystyrene, glass, macroporous gelatine, glucose, poly glycolydes (PGA), poly (lactide-co-glycolydes) (PLGA) polymers as well as co-polymers [375]. They are made of materials that help and support cell adhesion and proliferation. Typically, these microcarriers have diameters much larger than the cultured cells, and when dispersed in cell-culture media present a very large surface area for cells to attach and

proliferate. The curved nature and the porosity of the of the microcarriers not only acts as 3D system to the cells but also increases the surface to volume ratio. The large surface to volume ratio of microcarriers allows for increased cell expansion yielding higher number of cells in a bioreactor system without having to resort to large and bulky stacked industrial T-flasks [375]. In addition to this the surface area, in a particular bioreactor, can be easily expanded by adding more microcarriers into the bioreactor system, thereby also reducing the plastic waste generation [376].

Additionally, the volume of cell-culture media required per cell is much lower for microcarrier based systems compared to traditional 2D culture systems, offering significant potential for cost-savings upon scale up. For example, 5 mg of Cytodex 1 microcarriers requiring 1 mL of media generates a surface area of 30 cm^2. A T-25 flask, however, has a surface area of (25 cm^2) and required around 7 – 10 mL. As mentioned earlier, the output generated by a 1 litre microcarrier system is equivalent to 18 roller bottles. This also saves 21% of material cost in comparison to the roller bottle system [370].

According to Malda *et al*., the surface area provided by 1 gram of microcarriers is equivalent to 15 75cm^2 flasks [377]. Microcarrier systems have mainly advantages such as the ease of scalability, dynamic environment, gaining a homogeneous cell culture system, ability to stringently regulate and control parameters such as the pH, gas levels, shear rate, temperature, agitation of the cell culture media and the distribution of nutrients across the culture medium. In addition to this samples of cell culture can be tested periodically without having to sacrifice the entire cell culture unlike the 2D and hollow fibre cell culture system [376-378].

Different types of microcarriers such as Cytodex type1[379], Cytodex type 2, Cytodex type 3 [375], macroporous gelatine, CultiSphere G microcarriers, CultiSphere S microcarriers [380-382]and SoloHill Plastic P102-L [382] etc., are commercially available. Almost all of the above mentioned microcarriers are specifically designed for cell culture. Different types of microcarriers available in the market are listed in Table 7 along with their chemical makeup and physical properties.

Table 7: Microcarriers available in the marker. Table adapted and modified from Badenes *et al*.[383]

Product	Material	Density	Diameter (µm)	Manufacturer
Cytodex 1	Dextran	1.03	190 ± 58	GE Health Care
Cytodex 3	Dextran	1.04	175 ± 36	GE Health Care
Cytopore 1	Cellulose	1.03	240 ± 40	GE Health Care
Cytopore 2	Cellulose	1.03	240 ± 40	GE Health Care
Cytoline 1	PE and Silica	1.32	10-400	GE Health Care
Cytoline 2	PE and Silica	1.03	10-400	GE Health Care
CultiSphere G	Gelatine	1.04	225±125	Percell Biolitica AB
CultiSphere S	Gelatine	1.04	225±125	Percell Biolitica AB
Fact III [384]	Polystyrene	1.02-1.03	90-150	Solo Hill
Hillex [385]	Polystyrene	1.09-1.15	160-200	Solo Hill
Plastic	Polystyrene	1.02-1.03	90-150	Solo Hill
Plastic Plus	Polystyrene	1.034-1.046	125-212	Solo Hill
Hillex II	Polystyrene	1.090-1.15	160-200	Solo Hill
Star-Plus	Polystyrene	1.0- 1.03	125-212	Solo Hill
Synthemax II [386]	N/A	1.026	125-212	Corning
Glass beads	Glass	1.04	150-1180	Sigma - Aldrich

The potential drawbacks of using a microcarrier system are the microcarrier aggregation due to formation of cell bridges, limited supply of oxygen and nutrients, shear stress and difficulty in eliminating the accumulating waste products from the cell culture. These disadvantages may lead to decrease in cell viability and proliferative capacity [387]. Another disadvantage are the methods involved in detaching the cells from the microcarrier surface which are discussed in section 2.14.4.

2.14.1 Bioreactors

Microcarrier cell culture technique is technically based on culturing anchor dependant cells on microcarriers in a fluid suspension system. This culture system can yield a result of 200 million cells per mL [388]. While a small lab based microcarrier can yield around 3 $\times 10^6$ cells/ml, a 1000 litre scaled up bioreactor system can easily yield around 1 trillion cells in a single batch [389]. Currently the bioreactors can be commercially scaled up to a maximum of 6000 litres [390]. When cells are cultured in

such large scale, appropriate measures should be taken to design a perfusion system which can maintain a continuous flow of nutrients, growth factors and expunge toxic metabolites [383]. The bioreactors can be either be a traditional stirred suspension-based bio reactor or a Wave bioreactor.

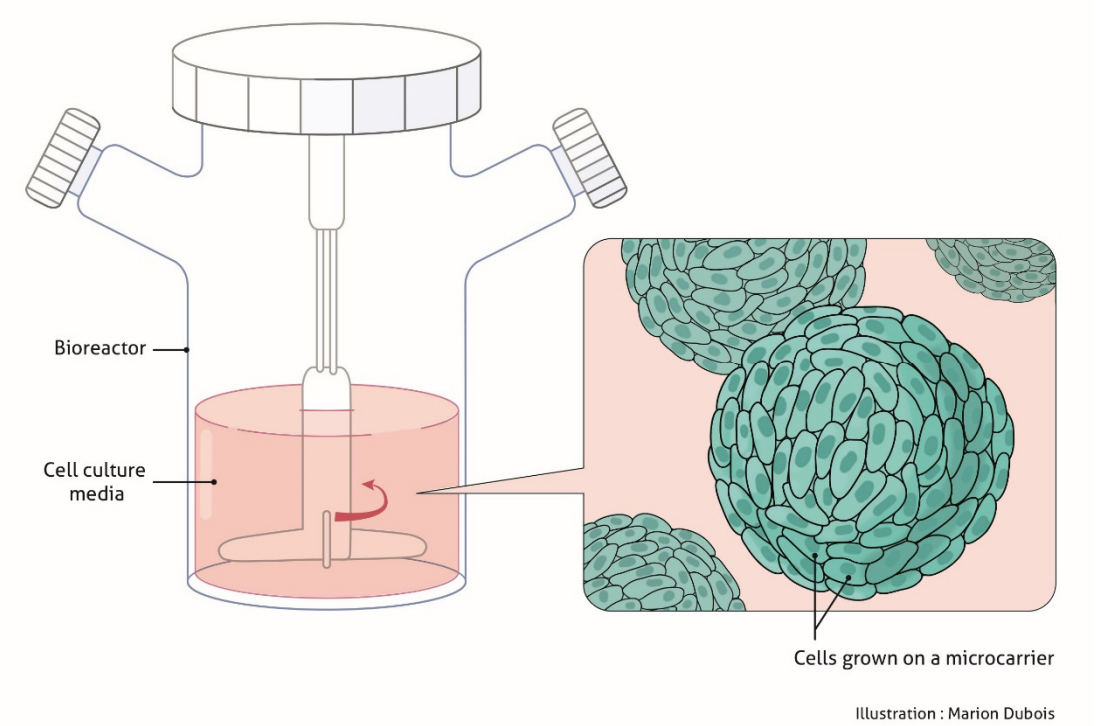

Figure 16: Schematic representation of a bench top or a small scale stirrer based bioreactor. Microcarriers with cell are dispersed in the cell culture media present in the bioreactor. The stirrer continuously stirrers the cell culture media, thereby keeping the microcarriers in suspension.

A stirrer based bioreactor, as represented in Figure 16, is made up of two components: (i) a spinner flask (small scale or lab based) or a large stirrer tank, for holding the microcarriers and the cell culture media and (ii) a magnetic stirrer bar or an electrically driven ball shaped rotating agitator or an impeller to help in agitation [390]. The continuous spinning of the magnet or the rotation of the ball generates turbulence which keeps the microcarriers afloat.

A Wave bioreactor system is manufactured in the form of single bags that have been scaled only to 500 litres (as opposed to 6000 litres in a stirrer tank). In this system the bags are placed on a rocking platforms and the microcarriers are kept in suspension by the rocking motion [389, 390].

2.14.2 Applications of microcarriers

The variable properties of microcarriers such as materials, size and shape

facilitates them to be used for various biological applications. Microcarriers are currently being used for large scale production of vaccines, recombinant proteins and expansion of cell lines (as previously mentioned).

Vaccine production

Shortage and ethical issues surrounding the usage of animals for development of vaccines has forced researchers to look for an alternative method for vaccine production. This problem has been partly overcome by the usage of microcarriers for vaccine production. Large batches of vaccines can be produced by culturing cells (animal or human) on microcarriers and infecting them with the required virus. These cells act as substrates for the viral vectors. Vaccine production on microcarriers are divided in to two phases. An exponential proliferation of cells is seen in the first phase. Second phase involves in maintaining the cell numbers but an increase in viral multiplication in the cells [391].

While many cell lines such as Madin-Darby bovine or canine kidney (MDBK), Chinese hamster ovary (CHO) cells, human diploid lung fibroblast (MRC-5) can be used, the non-tumorigenic mammalian VERO cell obtained from the kidney of African green monkeys are the most widely used cell lines for vaccine production on microcarriers [392]. Vaccines for many diseases such as polio [393], influenza [394], rabies [395], measles [396] and Japanese encephalitis [397] etc., are produced using microcarriers.

Recombinant protein production

Commercially available recombinant proteins can be produced in many organisms such as bacteria, yeast, insect and mammalian cells [398]. Enhanced protein production from any of these organisms can be obtained by manipulating the gene expression. Gene manipulation leads to an increased recombinant gene expression leading to higher protein output by the organism. Though microbes are often used for the production of proteins, studies have shown that these proteins have can have limited effectiveness due to incorrect protein folding. This is reduced in mammalian cells [399].

Production of proteins using cells and microcarriers follows a well-established protocol. The cells that are used for culture undergo first and second transfection of recombinant genes. The transfected cells are then exposed to a selection media which

only allows the survival of cells that express the selector gene. These cells are cultured and expanded to form colonial population. Each of the colonies are examined for their quality and quantity of recombinant protein produced. The cell lines that pass the evaluation are then cultured on microcarriers in bioreactors for higher recombinant protein output. Cell lines such as CHO, baby hamster kidney (BHK), human embryo kidney (HEK-293), human retinal cells and mouse myeloma (NS0) have regulatory approval for recombinant protein production [400].

Studies conducted by Knibbs *et al*., has shown a 5-fold increase in protein production by the COS-7 (CV-1 in Origin with SV40 genes) fibroblast cell line when compared to that of a monolayer culture in a polystyrene flat surface. In addition to this while cells cultured on the polystyrene surface stopped producing proteins and detached after 10 – 14 days, cells grown on microcarriers stayed anchored up to 24 days and constant production of recombinant proteins were observed [399].

2.14.3 Effect of bioreactor conditions on microcarrier based cell culture

Continuous stirring of the microcarriers in a stirred tank bioreactor is the most commonly used bioreactor as it allows (i) the entire surface of the microcarriers to be available for cell expansion, (ii) creates a homogeneous state of suspension which gives the cells a uniform environment to grow (iii) reduces aggregation of cells over numerous microcarriers (iv) and allows proper exchange of gases, nutrients and oxygen throughout the bioreactor [401]. Stirred tank bioreactors consist of a container which holds the cell culture media, and a mechanical stirrer. Cells cultured on microcarriers are usually placed in the bioreactor and the stirrer is rotated at a speed optimal for cell growth. Many factors such as stress, strain, rotation speed etc., influence the viability of the cells in the bioreactor.

But it should be noted that the agitation rate greatly influences the growth, pluripotency and final yield of the cells. This is usually caused due to the sensitivity of the cells to hydrodynamic shear forces. The production of hydrodynamic shear is the result of using stirrer suspension bioreactor. The strength of the shear stress is directly proportional to the speed of the propeller agitation. Depending on the agitation, the hydrodynamic shear keeps microcarriers suspended in a constant homogeneous dynamic environment [402]. While large shear forces may result in decreased protein productivity, cell injury or lyses of the cells [403, 404], low shear forces leads to cell/microcarrier aggregation, limiting oxygen and nutrient distribution,

decreasing cell viability and non-homogeneous mixture cell culture environment [402]. The cellular effect of agitation rate is variant for different cell types. For example, while cell types such as CHO-K1 and BHK-21 cells can withstand and proliferate at 200 RPM (12.2 dyn/cm^2), the proliferation rate of Vero was completely inhibited at this speed due to hydrodynamic stress [405]. A study conducted by Cormier *et al.*, showed an increase in proliferation of mouse embryonic stem cell (mESC) when the culture was exposed to 80 RPM (4.5 dyn/cm^2) and 100 RPM (6.1 dyn/cm^2). However at an agitation rate of 120 RPM (7.8 dyn/cm^2), no proliferation, extensive cell damage and cell derby likely caused due to ruptured cell membrane was observed. The damage to the cells was caused due to the excessive shear stress generated due to the high agitation rate [406].

Stem cells are known to be sensitive to their surrounding environment as change in the environment may trigger differentiation. A study conducted by Toh *et al*., observed that when mESC were expose to shear stress greater than 0.0016 dyn/cm^2 there was a significant increase in the expression of Fgf5 gene (associated with epiblasts). Though the mESC were still pluripotent, their ability to self-renew decreased while their commitment towards a lineage increased. Studies conducted by Liu *et al.*, showed the difference in gene expressions of hMSCs when cultured in non-osteogenic media under low and high shear stress conditions. While a slight insignificant increase in ALP, Runx2 and COLIα gene expression was observed under low shear stress (0.34 dynes/cm^2), high shear stress (4.2 dynes/cm^2) significantly increased all the gene expressions thereby promoting osteogenesis in the stem cells [407].

In addition to this, the agitation conditions are variable for different cell lines and often existing literature is contradictory. Leung *et al*., showed that human embryonic stem cells displayed a decrease in yield and expression of pluripotent markers when the agitation speed was greater than 30 RPM [408] however, Lock *et. al.* found that the same cells were not affected until the agitation speed increased above 80 RPM [409]. Using a 50 mL Stem Span spinner flask, Badenes *et al*., evaluated that optimal rotation speed for mesenchymal stem cell growth was between 30-70 RPM and the maximum number of cells was yielded at 44 RPM [383].

2.14.4 Cell detachment methods for microcarriers

The commercial applications of microcarriers in virus and recombinant protein production was relatively straightforward, largely due to the fact that in these technologies there is no requirement for recovering the cells cultured on the microcarriers. The cells can be simply digested, and the produced virus/protein extracted and purified using well established protocols. However, in technologies such as stem cell therapies successful commercial translation of microcarrier culture requires protocols to detach and recover the cultured cells in very high yields with no detrimental effects on their viability. As mentioned previously traditional enzymatic methods of cell detachment can have significant negative effects on cell phenotype and viability, and these effects are often exacerbated in microcarrier cultures (the vastly increased surface area : volume ratio typically requires higher concentrations of trypsin and longer exposure times). Thus, there has been considerable research into alternative methods for detachment and recovery from of cells cultured on microcarriers in stirred tanks [383].

The majority of the studies conducted to date have focused on developing methods for the expansion of cells on microcarriers, and less research into harvesting the cells from these microcarriers has been performed. Successful cell harvesting from a microcarrier requires a two-step process were cells are first detached from the microcarrier and then separated, typically by filtration, from the left over microcarriers [410].

Different cell detachments techniques from microcarriers were investigated by Weber *et al*. hMSCs-TERT cells (human mesenchymal stem cells - telomerase reverse transcriptase, immortal cell lines) were cultured on and detached from microcarriers using trypsin, accutase, collagenase or trypsin-accutase mixture. This study was performed on various commercially available microcarriers such as Cytodex 1, Cytodex 2, RapidCell, Biosilon and SoloHill Plastic P102-L. Cell detaching agents such as trypsin, accutase, trypsin-accutase mixture and collagenase were used. The study have shown that nearly 85 - 100% cell detachment and viability was obtained from RapidCell, Biosilon and SoloHill Plastic P102-L when exposed to trypsin, accutase and trypsin-accutase for 6-10 minutes. A poor yield was seen in Cytodex type 1 and Cytodex type 2 when exposed to collagenase for 40 minutes [411]. Nienow *et al* and Dos Santos *et al*., used a process where the cells cultured on microcarriers were

exposed to trypsin and then intensely agitated in the bioreactor for 5-7 minutes [410, 412]. While Nienow *et al* used SoloHill microcarriers, Dos Santos *et al* employed CultiSphere-S This harvest protocol showed an efficiency of 95% cell detachment from the microcarrier surface. To date there has been few studies of enzyme free methods of cell detachment from microcarriers.

Cells that do not have strong adhesion to the microcarrier surface can be harvested using hypotonic treatment were a hypotonic aqueous solution containing sodium chloride, potassium chloride and glucose was used to recover Chinese hamster ovarian cells from microcarriers. In this process exposure of the cells to the hypotonic solution resulted in osmotic shock causing the cells to adopt a less-adherent rounded morphology. When agitation was applied to the microcarriers the cells detached. However, the percentage of cells recovered from by this method was significantly less than for cells detached by trypsinization [413].

Yang *et al*., developed poly-N-isopropylacrylamide (pNIPAAM) grafted microcarriers using Cytodex type 3 as base surface [414]. pNIPAAM is a temperature sensitive "smart" polymer that is hydrophobic above 32 ^{o}C (allowing cell attachment) and hydrophilic below (encouraging cell detachment) [218, 415]. When the temperature of the cultured cells was reduced to below 32 ^{o}C, 82.5% detachment of hMSCs was observed. While the usage of animal based enzymes is being completely avoided in this method, the coating of microcarriers with pNIPAAM is non-trivial and difficult to scale-up to industrial levels.

Chapter 3: Experimental Techniques and Instruments

Over the course of this thesis, many different experimental techniques have been used to study the physical and biological aspects of materials used under different conditions. This chapter describes the working principles and mechanisms of the various methods used throughout this thesis.

3.1 NIR LASER

All the experiments in my thesis, involving NIR irradiation, were performed using a single near infrared laser. Prior to the cell culture experiments, characterisation of laser parameters was performed to determine the power density or irradiance (W/cm^2) and to profile the laser beam. A multi-mode fibre (AFW Technologies, Victoria, Australia) with a with a numerical aperture (NA) of 0.22, coupled with a continuous wave near infrared laser (NIR) diode of wavelength (λ) 785 nm (Optotech, Victoria, Australia) was used to excite the surface plasmonic resonance in the Au NRs. This setup was used for all the experiments in this project. An uncollimated beam, from the laser, had a fixed power of 40 mW. A beam limiting collimator with an NA of 0.57 (Thor Labs, New Jersey, USA) was attached to the distal part of the optic fibre which had a FC connector. The following equation can be used to calculate the NA of the optical fibre:

$$NA = \mathrm{n}\sin(\theta)$$

where n represents the refractive index of the medium and sin (θ) is the maximum half angle of the cone of light that exits the fibre. Experiments were set up with the fibre placed at a distance (d) of 6±2 mm from the sample. The final beam radius (r) emitted from the collimator was measured to be 3 mm. Assuming that the beam is a Gaussian beam, the total beam area was calculated using the formula:

$$A = \pi r^2$$

The area of the beam was calculated to be 7.06 mm^2. By dividing the power by beam area the irradiance across the laser exposed surface was obtained to be 566 mW/cm^2.

The exposure time and irradiance used for our studies were chosen after studying

the results obtained from Kolesnikova *et al* and Giner-Casares *et al*. While Kolesnikova *et al*. used power densities varying between 400 – 1000 mW, Giner-Casares *et al*., irradiated their samples with power densities ranging from 145 mW/cm^2 to 340 mW/cm^2 [334, 335] with the time of exposure ranging from 2 minutes to 40 minutes. Studies conducted by Krpetic *et al*., shows that cellular damage and apoptosis occurs when the cells are exposed for 2 minutes to power densities that exceeding 20 W/cm^2 [416]. While I decided to use an irradiance of 566 mW/cm^2 the time of exposure was finalized only after complete cell detachment was achieved from the cell culture samples after laser irradiation. The time of exposure is discussed in detail in chapter 4.

3.2 SCANNING ELECTRON MICROSCOPY

Scanning electron microscopy or SEM is the application of high energy electron beam on the surface of a sample to obtain images of its sub nanometre surface topography. Depending on their physical and chemical characteristics, a thin layer gold or platinum may be sputtered on the samples (prior to imaging) to enhance their signal to noise ratio. Upon the interaction of the high energy electrons with the samples, back scattered electrons, low energy secondary electrons and x-rays are produced from the samples. These electron particles are detected and collected by the electron detectors which are then processed into images of the sample topography. In this thesis two different SEMs (Carl Zeiss SUPRA 40VP SEM and RAITH 150 Two) and an accelerating voltage of 3-5kV was used to obtain images of the sample topography. Samples were imaged under SEM for the presence of Au NRs on their surface. Unless specifically stated, the samples were not sputtered with either gold or platinum.

3.3 SPECTROSCOPY

Spectroscopy is the quantitative measurement of the spectra produced when electromagnetic (EM) radiations interact with matter. The results are dependent on the properties of the samples, EM radiation interaction with the matter (absorption, emission and diffraction) and the EM regions used for analyses (ultra violet region, visible region or infra-red region) [417]. In this thesis Cary 50 UV-Vis spectrophotometer was used.

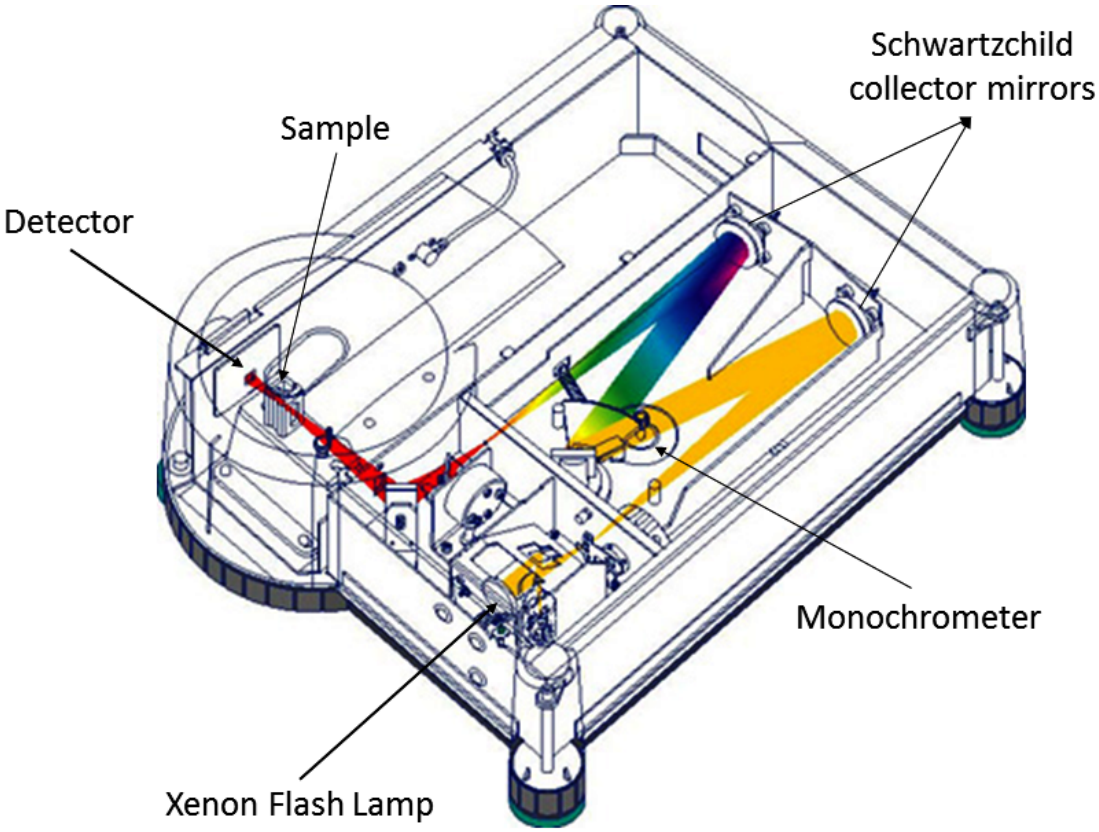

Figure 17: Schematic representation of Carry 50 UV-Vis spectrophotometry. Image adapted from [418]

As shown in Figure 17, Cary 50 UV-Vis spectrophotometry consists of a sample holder, detector, collection mirrors, monochromator and xenon (Xe) flash lamp. In addition to being the light source of UV-Vis radiation, the Xe flash lamp (when passing through the beam splitter) also acts as simultaneous reference beam corrector. By doing so the excess photometric noise and wavelength shift error, which is observed in traditional scanning methods, are removed. During the process of UV-Vis spectroscopy, the light (from Xe lamp) is collected and reflected from the Schwartzchild collector mirror to the monochrometer. Following this the light exits from the excitation monochrometer and passes through the sample placed in the sample holder. During this step while some light is absorbed by the sample the remaining light is collected and processed by the detector. The output obtained is the difference between the difference between the incident and final EM radiations collected [419].

It was previously discussed in chapter 2, that localised surface plasmon resonance (LSPR) in Au NRs occurs when the surface plasmons (delocalised electrons) on the Au NRs surface are disturbed by electromagnetic radiation. The

interaction between the electromagnetic radiation and the surface plasmons leads to coherent oscillations between surface plasmons due to absorption of photons. When this effect collectively takes places over a wider area of the Au NRs, LSPR is generated. During this phenomenon, reflection, absorption and scattering of the electromagnetic wave also occurs. While the some of the incoming electromagnetic wave is reflected away at the same wavelength (based on LPR and TPR of the Au NRs), scattering and absorption of the electromagnetic wave leads to transfer of energy into the lattice of the Au NRs. Depending on the dimensions of the Au NRs particles, the absorption band can arise in various regions of the visible-NIR region of the electromagnetic spectrum [420, 421]. The LPR on the surface of the Au NRs can shift when properties such as the aspect ratio, surface modification and the surrounding environment of the Au NRs are altered [422]. The position of the LSPR in Au NRs can be measured using a UV Vis Spectrometer.

3.4 IR BASED THERMAL MEASUREMENT

Temperature changes on the surface of Au NRs can be measured using invasive and non-invasive techniques. Non-invasive measurements can be obtained by using external devices that allows us to negate the usage of any additional agents in the samples. This prevents any interference of the temperature measurement in the experimental results. Temperature changes of Au NR-coated surfaces have been reported using luminescence thermometry (fluorescent dyes, quantum dots), thermopiles and thermocouples. [423-426]

Temperature measurements can also be obtained by studying the infrared (IR) or thermal radiation from the samples. Infrared radiation is emitted by any object which is above absolute zero (i.e., $T > 0$ K). An infrared camera can be used to obtain images which allow the temperature of a material to be determined. Infrared radiation emitted by the sample, is acquired by the camera and processed into false colour images which represent different temperatures [427]. A thermal resolution of 0.01 ^{o}C at 50 μm^2 can now be achieved using IR camera [428].

The instrument used to study the temperature on Au NRS coated surface was a FLIR ETS 320 Thermal Imaging Camera (RS Australia) (Figure 18). The instrument has a non-contact temperature measurement range of -20 ^{o}C to +250 ^{o}C with an IR spatial resolution of 320x240 (76,800 pixels). The IR camera is sensitive enough to

detect a temperature shift smaller than 0.06 ^{o}C and has a spectral range between 7.5 µm to 13 µm allowing measurement of long wavelengths with great details due to minimal atmospheric absorption.

Figure 18: FLIR EST 320 IR thermal imaging camera used for temperature characterisation.

3.5 LIVE/DEAD ASSAY

A quick assessment of the ratio of live cells to dead cells can be performed using fluorescent based Live/Dead assay. This technique is used to measure the cell viability and cytotoxicity based on the fluorescence displayed by the cells. The test uses two dyes to differentially label live and dead cells in a single step. One dye is calcein acetoxymethyl ester (Calcein-AM) which is highly membrane permeable. Though not fluorescent by itself, it is converted to the strong green fluorescent molecule calcein by esterases present in viable cells. The other dye, propidium iodide is excluded from viable cells as it is membrane impermeant. In dead or dying cells where membrane integrity is compromised the dye enters the cell, intercalates with DNA which increases its red fluorescence 30-fold. However, it may be taken up by cells with transient disruptions of the membrane.

The polyanionic dye, Calcein-AM (an acetoxymethyl ester of calcein), is a non-florescent macromolecule. Calcein AM is a lipophilic membrane permeable dye that can passively cross into a viable cell and be well retained within viable eukaryotic cells [429]. The esterase activity, in a viable cell, causes the calcein-AM to undergoes an enzymatic hydrolysis which results to a strongly enhanced green fluorescence(λ_{ex}490 nm and λ_{em}515) (Figure 19) [430]. Propidium iodide (PI) is a fluorescent nucleic acid stain (λ_{ex}535 nm and λ_{em}617 nm, Red) which was used to stain non-viable cells. PI enters the cells through damaged membranes of non-viable cells and undergoes enhancement of fluorescence upon bonding to nucleic acids (Figure 19). The viability of the cells can be revealed by studying the ratio between the green and red fluorescence. This simple assay was used to visually observe the viability of the cells cultured on the Au NRs coated substrates and the viability of the re-seeded cells detached after NIR irradiation.

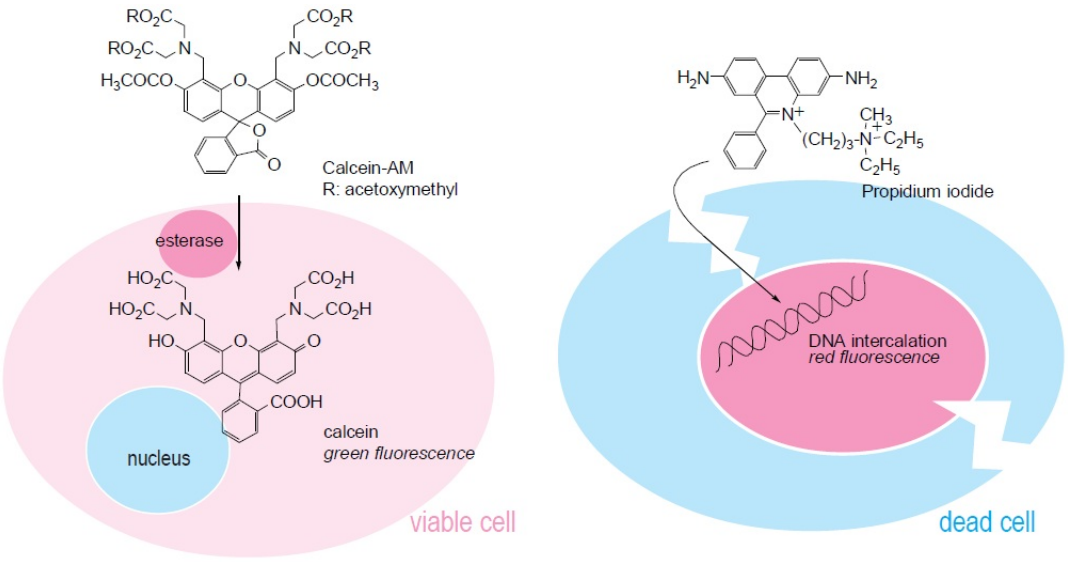

Figure 19: An illustration representing the working of Calcein-AM and PI in Live/Dead assay. The esterase in the viable cells converts calcine-AM to green fluorescent calcein. PI intercalates with the DNA of a dead or dying cell and displays red fluorescence. Image adapted from Dojindo Molecular Technologies, Inc. [431]

3.6 PRESTOBLUE ASSAY

Dyes such as PrestoBlue and alamarBlue are resazurine based and can be used for indicating cell viability and the metabolic activity of the cells [432]. These dyes are oxidation-reduction indicators which, in response to metabolic activity in cells, undergoes colorimetric changes and generate fluorescent signals.[433] In its oxidised state resazurine dye is usually non-fluorescent blue in colour. In its reduced state, resazurine, changes to resorufin which displays a strong fluorescence (λ_{ex}560 nm and

λ_{em}590 nm) [434].

Intracellular activities involving reductase and mitochondrial electron transport chain lead to the reduction of resazurine. During the process of cellular respiration, an oxidised resazurine accepts electrons from cytochromes, FMNH, NADH, NADPH and FADH, effectively reducing to resorufin. A shift in the colour of the dye is caused during this reduction reaction i.e., the colour changes from non-fluorescent blue to bright fluorescent pink (Figure 20), which can be measured using a fluorimeter [435].

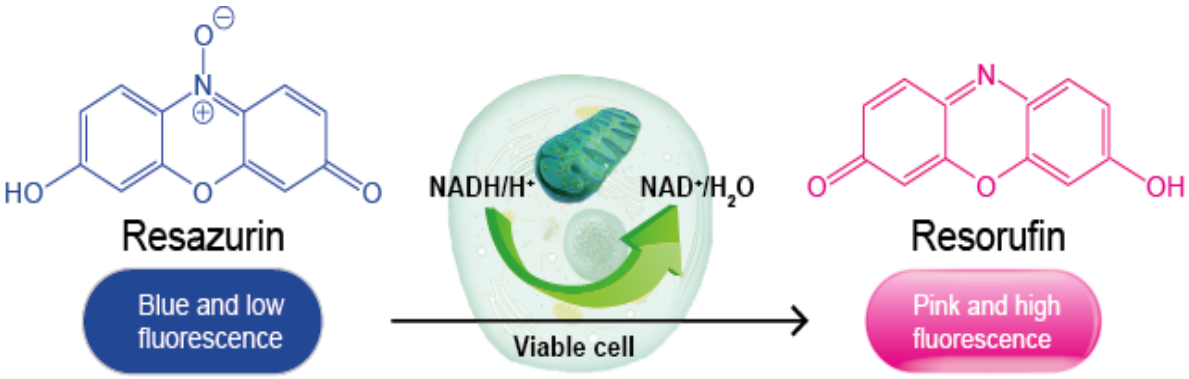

Figure 20: PrestoBlue assay principle. When non-fluorescent oxidised resazurine dye comes in contact with a metabolically active cell, it undergoes reduction and changes to fluorescent resorufin. Image adapted from ABP Bioscience, Inc. [436]

Unlike other metabolic assays resazurine dies are non-toxic and do not affect the metabolic activity of assayed cells. Though not used in the present studies, PrestoBlue also can be used continuous monitoring of the cells. Its short incubation time also makes PrestoBlue favourable as a cell viability test [437].

3.7 PRINCIPLES OF IMMUNOASSAYS

Immunoassays can be used to visualize and quantify proteins present either within the cell, or associated with the cell membrane. This assay relies on the in highly specific interaction between the protein (antigen) present in/on the cells and antigen-specific antibodies.

Antibodies are glycoproteins that belong to a large family of immunoglobulins (Ig) and are schematically represented as Y shape molecules (Figure 21), based on their structure determined by X-ray crystallography [438]. Immunoglobulins are divided into 5 different isotypes or classes namely: IgA, IgE, IgD, IgG and IgM. IgG is the most abundant antibody present in human serum and is commonly used in immunoassays. All the antibodies used in our experiments belonged to IgG isotope.

The Y shaped IgG contains 2 heavy chains and 2 light chains which may be considered as 3 protein fragments: 2 identical Fab (Fragment antigen binding) fragments and one Fc fragment (fragment crystallisable). The interaction between the antigen and the antibody takes place on the two Fab fragments of the antibody. The Fc fragment of the antibody is responsible for binding itself selectively to the Fc receptor of an effector or protein molecule. [439-441]

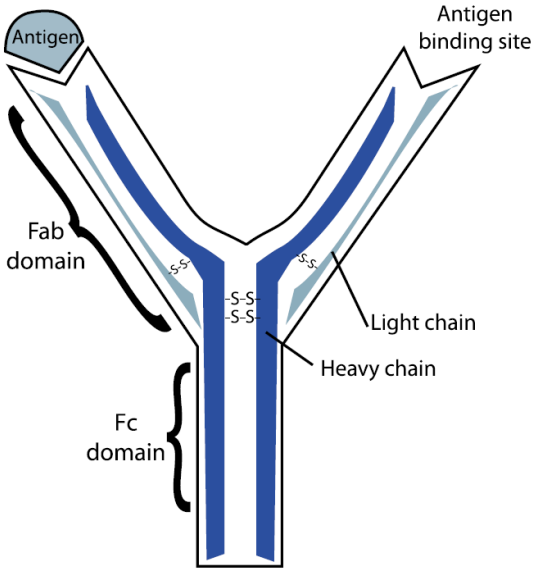

Figure 21: Structure of IgG antibody. 2 heavy chains 2 light chains of an antibody is clearly illustrated in the figure. The Fab fragment of the antibody binds to an antigen. Figure adapted from Koivunen *et al.,* [440]

Immunofluorescence is a fluorescent based immunostaining method, where a fluorophore is conjugated to an antibody. The antibody is then able to be detected by exposure to the appropriate wavelength of light under a microscope. There are two types of immunofluorescent staining techniques: direct and indirect techniques.

In the direct technique the primary antibodies are conjugated with the fluorophore as shown in Figure 22 a. These antibodies attach to a specific antigen and can be directly observed under a microscope. This technique has less staining time due to reduced number of steps and maybe reduced non-specific staining. The disadvantage of using this method is the finite number of fluorophores resulting in weak signals and the reduced flexibility when choosing the fluorescent colours. In addition to this, the antibodies used for this technique are also expensive compared to indirect technique, which is detailed below.

The indirect technique, uses unlabelled primary antibody and fluorescent

conjugated secondary antibody (Figure 22 b). While the primary antibody specifically binds to the target protein the fluorescent conjugated secondary antibody binds to the primary antibody. When compared to the direct technique, the indirect technique has the advantage of having amplified signals. This is due to the ability of multiple antibodies binding to a single primary antibody. In addition to this, the secondary antibodies are relatively inexpensive and can be used to detect various primary antibodies as long as they are anti-species to the primary antibodies. The availability of different conjugation offers an increase in flexibility in fluorophore selection. The number of steps involved in labelling the samples is one of the main disadvantages to this method. The complexity is also increased when multi-labelling is performed on a sample. Multi-labelling requires antibodies raised in different species in order to avoid cross-reactivity.

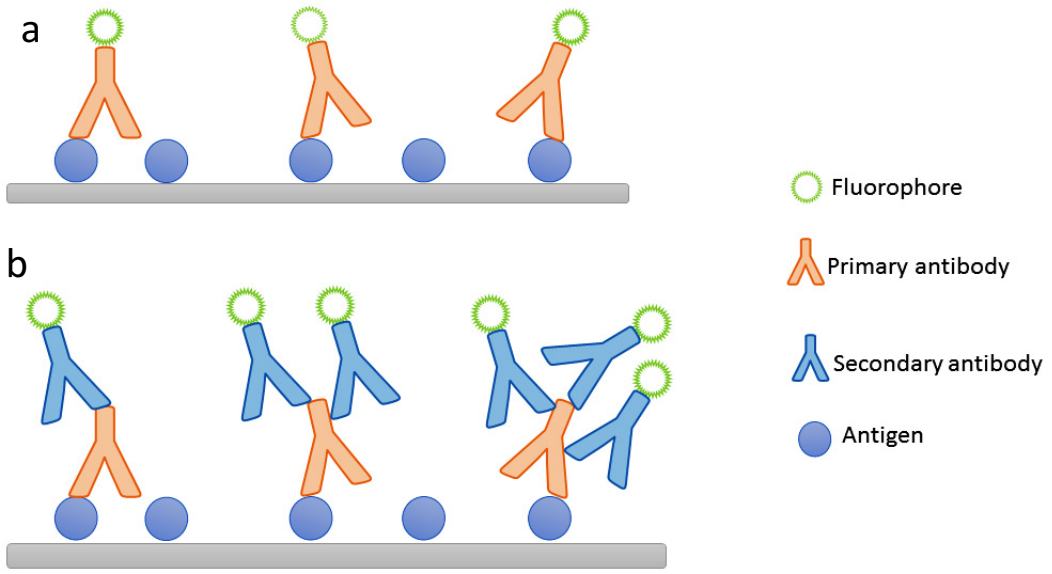

Figure 22: Immunostaining techniques (a) Direct immunostaining requires only one antibody conjugated with a fluorophore (b) Indirect immunostaining required a primary antibody and an anti-species secondary antibody conjugated to a fluorophore.

In my studies, immunoassay was used to measure surface proteins such as collagen, laminin and fibronectin present in the extra cellular matrix (ECM) present on the hMSCs. In addition to this, indirect immunostaining technique was also used in fluorescence-activated cell sorting (FACS or flow cytometry) to study the cluster of differentiation (CD) markers present on the surface of the hMSCs.

3.8 PRINCIPLES OF FACS

Immunophenotyping of hMSCs was performed using fluorescence activated cell

sorting technique (FACS) or flow cytometry. FACS is used for analysing intracellular molecules and cell surface expression by utilizing laser based technology and it's scattering properties to count and profile cell types in heterogeneous cell population. Flow cytometry allows analysis the purity, size, volume, viability of cells in large populations of heterogeneous cells and also perform multi-parameter evaluation of a single cell [442].

FACS, allows us to simultaneously collect data for a number of markers by using antibodies conjugated with fluorescent labels. The labelled antibodies bind to target proteins on the membrane or within the cell. The fluorescently labelled targets are detected by the FACS scanner and analysed to give detailed information of the phenotypes present in a population of cells [443-446]. FACSAria™ III, BD Bioscience was used for all the FACS studies performed in this thesis.

Cluster of differentiation and MSC indicative CD markers

Cluster of differentiation (CD) markers are used to identify patterns of cell surface molecules for immunophenotyping cells. CD surface markers or antigens are expressed by the surface of the cells. These CD antigens can be that can be recognised by a particular type of monoclonal anti-bodies. This process allowing us to detect the presence or absence of specific surface bound molecules on cell membranes, thereby allowing us to characterize the cells [447]. Multipotent hMSC have a between reported to be characterised by expression of a number of CD markers including CD29, CD44, CD71, CD73, CD90, and CD105, and the absence of the following CD markers: CD45, CD34, CD14 or CD11b, CD79a or CD19 [63, 448, 449]. The expression of these markers indicates the multipotency of the cells. If the bone marrow derived hMSC lack the expression of any of the above markers, it indicates the loss of hMSCs multipotency and the potential to differentiate into specific cell lines. The increase or decrease in certain markers tells us that the hMSCs have committed to differentiate into a specific lineage. CD44 is a cell adhesion receptor with multiple ligands such as hyaluronan, osteopontin, selectins and collagen. High expression of CD44 is reported in *in vitro* culture of hMSC and according Ramos *et al*., hMSCs should express CD44 as they are critical for biological action [450, 451]. hMSCs highly express CD90 markers and the presence of this marker also confirms the undifferentiated status of MSCs. Decrease in level of CD90 marker can be tallied as commitment of the hMSC to a specific lineage [452, 453]. Ecto-5′-nucleotidase, CD73 is known for its

involvement in hMSCs migration, hMSCs modulation to adaptive immunity and bone marrow stromal interactions [454]. Downregulation in the expression of CD73 marker indicates that the cells commitment to differentiate into a specific lineage [455]. Also known as endoglin, is a glycoprotein which acts as a receptor for TGF-β superfamily ligand. MSC committed to differentiation and those differentiated into adipose tissues have shown to express low amount of CD105 [456].

For my studies I used CD44, CD73, CD90, and CD105 as these panel of markers were recommended by the Mesenchymal and Tissue Stem Cell committed of International Society for Cellular therapy as a minimum number markers that is to be exhibited by the cells to be defined as hMSCs [107].

3.9 ADIPOGENIC DIFFERENTIATION ASSAY

The extent of adipogenic differentiation displayed by the hMSCs in these studies was quantified using AdipoRed™ Adipogenesis Assay Reagent (PT-7009, Lonza Poietics, Switzerland). The Adipo red staining kit is based on Nile Red staining. This dye can be used as a sensitive detector for localization and quantification of intracellular neutral lipid droplets. Nile red (Figure 23) is minimally fluorescent in water or polar solvents and undergoes fluorescence enhancement and a large blue shift in a non-polar environment. It is widely used for the detection of intracellular lipids. Adipogenic differentiation is identified by measuring an increase in lipid is interactive with hydrophobic environment (neutral lipid droplets) leading the dye to fluoresce. Under different spectral conditions, Nile red can be used as a general staining dye for detection of various lipidic species such as phospholipid, cholesterol, cholesteryl esters, and triacylglycerols [457]

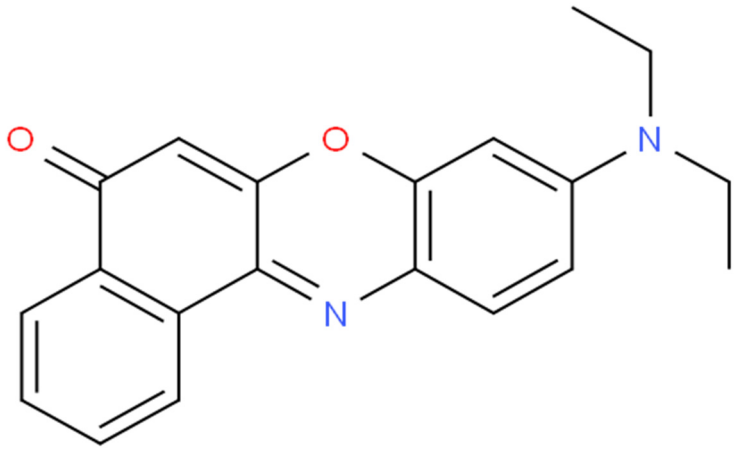

Figure 23: Chemical structure of Nile Red. Figure adapted from ChemSpider chemical database [458].

Neil Red has an excitation/emission of $\lambda_{ex}485/\lambda_{ex}535$nm and can be qualitatively observed under a fluorescent microscope and quantitatively measured using a plate reader.

3.10 OSTEOGENIC DIFFERENTIATION ASSAY

Osteogenic differentiation displayed by the hMSCs, in my studies, was measured using Alizarin Red S Staining Quantification Assay (#8678, ScienCell Research Laboratories, CA, USA). Alizarin Red S, (3,4-dihydroxy-9,10-dioxo-9,10-dihydroanthracene-2-sulfonate) is an organic chemical dye (Figure 24) that forms non-covalent bonds with the calcium ions in hydroxyapatite which is present in bone. [459]

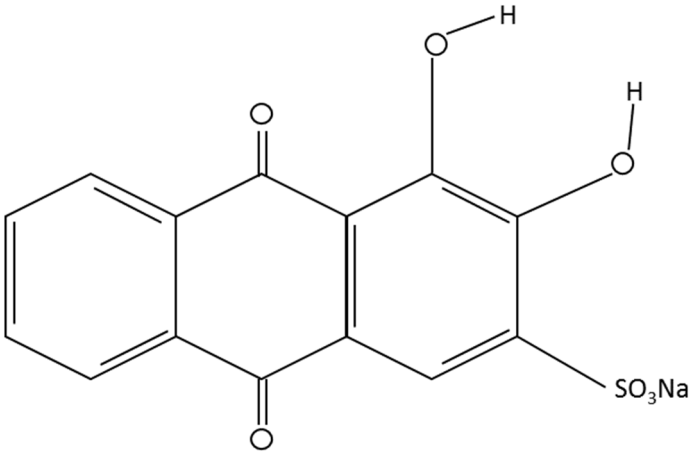

Figure 24: Structure of an Alizarin Red S dye structure. Figure adapted from PubChem open chemistry database [459]

The reaction between the Alizarin Red S and the calcium ion can occur in in two ways [460]:

a. The major bonding mode

In this process the reaction occurs via the formation of a salt bridge with two hydroxyl groups (OH(1) and OH(2)) (Figure 25).

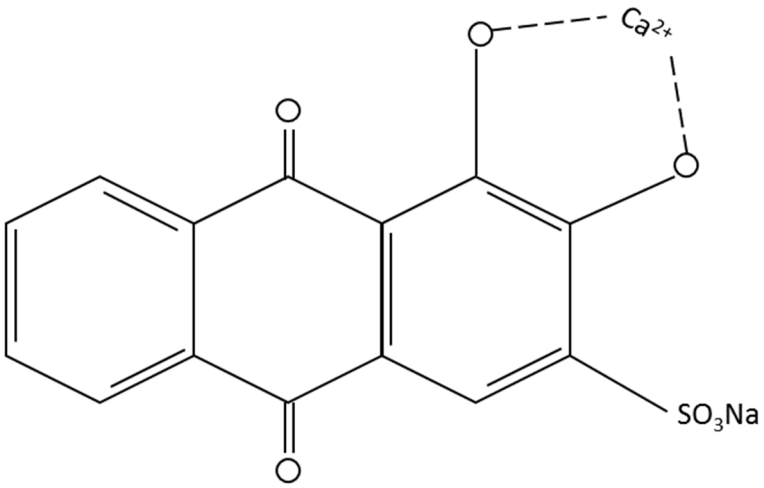

Figure 25: Major bonding of Alizarin Red S structure

b. The minor binding mode

This reaction occurs via a chelate formation with the carbonyl group (C=O(9) and (OH1) (Figure 26).

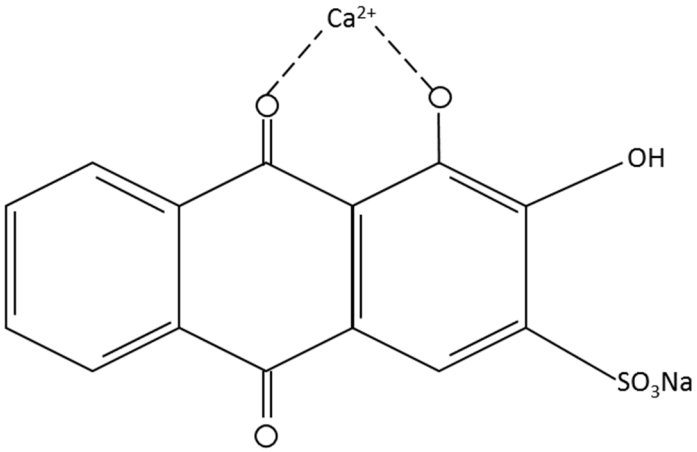

Figure 26: Minor bonding of Alizarin Red S structure

Alizarin Red S has been widely used to detect the calcium deposits in cell culture. It may be used for both qualitative and quantitative assessment of osteogenic differentiation. Qualitative measurement of calcium deposits (post Alizarin Red S staining) can be measured under a normal bright field microscope. Quantitative data can be obtained using a plate reader, by measuring the absorbance displayed by the cells at 405nm.

3.11 POLYMERASE CHAIN REACTION

An in vitro molecular method, PCR or polymerase chain reaction is an amplification technique which replicates and exponentially amplifies a copy of a selected sequence of nucleic acid (DNA) [461]. For a PCR reaction to take place, there are 5 essential components these are: DNA template, a thermostable DNA polymerase enzyme (Taq polymerase), primers, nucleotides (dNTP) and buffer. The components are then introduced to a thermal cycler, which cycles the reaction components through phases of heating and cooling:

1. DNA denaturation: This initial phase heats the DNA strand to a temperature of 94 ^{o}C for between few seconds to 2 minutes. When heated to this temperature double stranded DNA separates into single strands. In the denatured form, the DNA template can be targeted by the primers that will identify the selected replication start site for the Taq-Polymerase.
2. Primer annealing: Primers are short strands of complementary DNA which initiate the amplification. They are designed to bind at either end of the sequence to be copied. In the second phase of the cycle, the primers binds to each of the single separated strand of the targeted DNA region, thus addressing the Taq polymerase to a specific region of the DNA strand. The primers bind or anneal with the single stranded DNA when the temperature is lowered, typically to 40-60 ^{o}C. This process is quite rapid and this part of the cycle is usually for 15-60 seconds.
3. Elongation: The primers form a starting point for synthesis of DNA as the Taq polymerase enzyme can only add bases to double-stranded DNA. This step takes place between 60-70 ^{o}C and lasts between 1-2 minutes.

While PCR is used for DNA amplification, the method used for RNA amplification is known as reverse transcriptase PCR or RT-PCR. In this method the RNA is reverse transcribed to complementary or cDNA which then undergoes the same series of steps as DNA amplification.

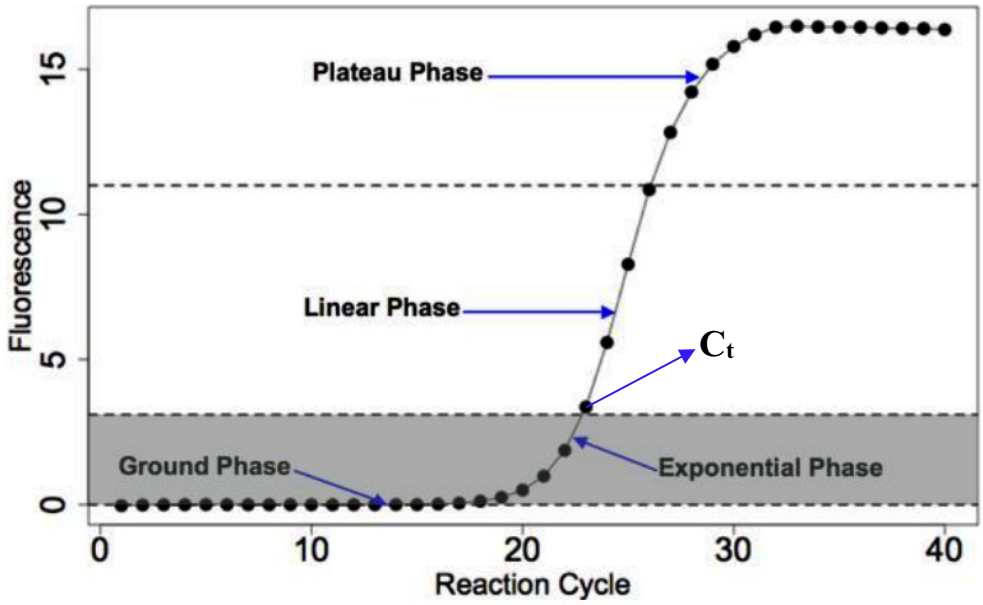

Figure 27: Different phases of PCR amplification, modified from Page *et. al.* [462]

Real time or quantitative real timer PCR (qPCR) reactions are split into four phases: ground phase, exponential phase, linear phase and plateau phase (Figure 27). The initial ground phase defines the reaction cycles in which the fluorescence signal is accumulated but there is insufficient PCR product for detection. This phase is used to calculate baseline. In the exponential phase, fluorescence can be detected due the amplification of the cDNA which doubles with each cycle. The number of cycles required to detect the exponential phase is represented by is represented by C_t. C_t can also be used to measure the original amount of cDNA present before the amplification process. In the log phase, the amplification of cDNA exponentially increased due to the cDNA doubling in every cycle. The quantity of DNA/RNA template decreases in the plateau phase due to the depletion of components required for amplification signalling an end to PCR reaction.

3.12 INDUCTIVELY COUPLED PLASMA MASS SPECTROMETRY

ICP – MS is a powerful technique that can be used to precisely measure an analyte element down to 1-10 ng per litre in a solution [463]. ICP-MS can be used to quantitatively detect the presence of trace elements in both biological and inorganic samples. As stated in the name ICP-MS is the application of inductively couples plasma to perform mass spectrometry (Figure 28).

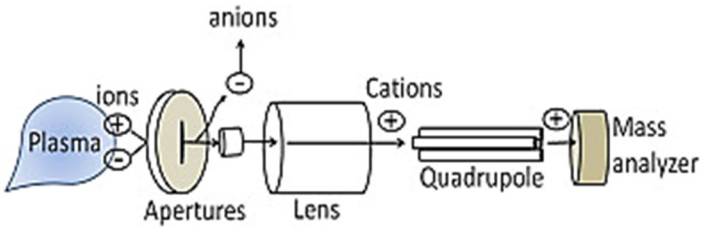

Figure 28: An illustration of components involved in ICP-MS. Image adapted from Singh *et al*., [464]

The plasma is generated when gases (e.g., argon) are heated with electromagnetic coil. These gases become electrically charged and ionised. The solid samples are converted into micro particles by irradiating them with laser (laser ablation) [465]. These samples are then sprayed into to the hot plasma, where they are decomposed into atoms and thereby generating ions. These ions are then passed through aperture and lenses in order to separate the positive ions from the anions. The positive ions then enter a quadrupole mass filter. In this filter the separation of the target ions from the rest takes place according to the mass to charge ratio. The target ions then strikes the mass spec detector where the data, regarding the relevant sample, is generated [464].

This method was performed to quantitatively analyse the amount of gold present on the microcarrier surface.

3.13 DARK FIELD MICROSCOPY

In a bright field microscope, contrast is generated in an image only when there is a significant difference in the refractive index of the samples and the surrounding medium. When the refractive index is close to the surrounding medium, as in the case of aqueous suspensions of glass micro-carriers it is impossible to generate sufficient contrast for a high quality image.

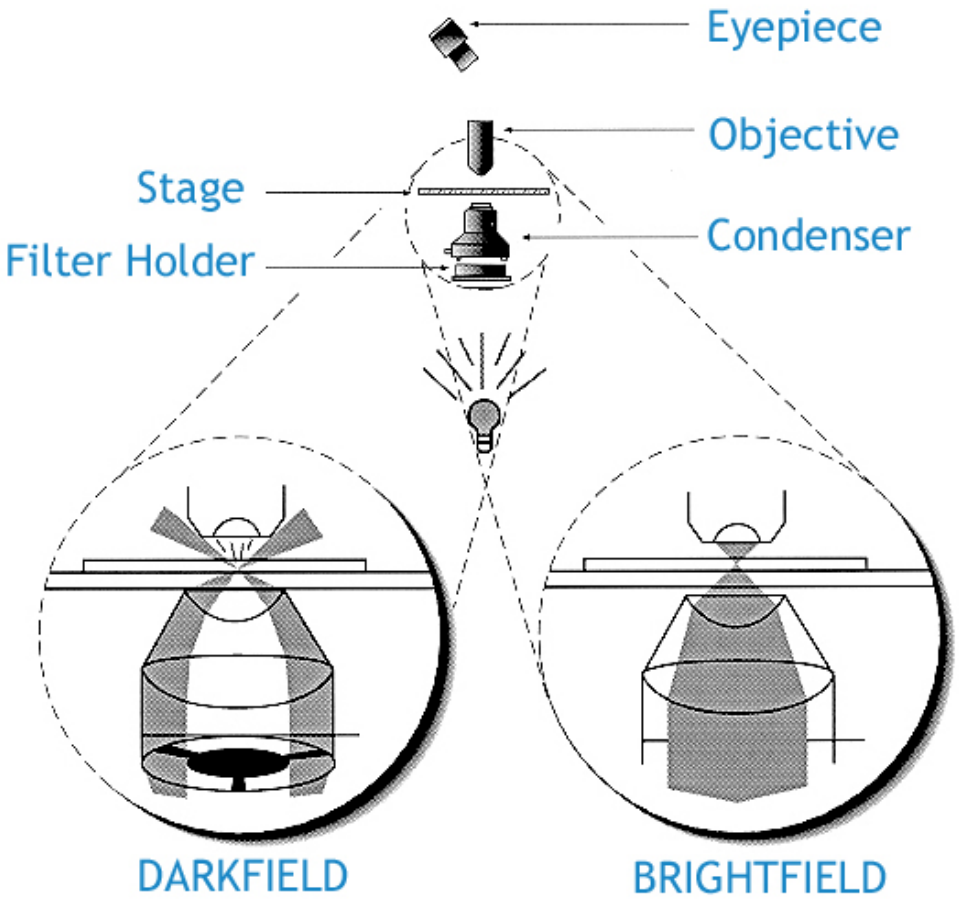

Figure 29: Difference in principles between a dark field and a brightfield microscope (Illustration provided courtesy of Washington State University)

The principle of the dark field microscope involves in only collecting the light rays that are scattered by the samples. As seen in Figure 29, a circular disk is used to block out the transmitted light from the light source. This creates a cone of light that is picked up by the condenser lens. While some rays of light from the samples are directly transmitted, others simply scatter after the impact with the sample. These scattered rays are picked up by the condenser lens, objective and then can be viewed as an image.

In this thesis dark field microscopy was used to qualitatively study the amount of Au NRs present on the surface of microcarriers.

3.14 PHALLOIDIN STAINING

The cellular cytoskeleton is a nano-fibrous network of many different protein filaments and other biomolecules that supports the internal structure, the shape of the cell and provides mechanical support to all eukaryotic cells. Actin filaments are a major constituent of the cellular cytoskeleton. Actin in its monomeric form is known as G-actin which when exposed to specific physiological conditions polymerizes to F-actin. The dynamic shape and functionality of the cells depends on the ability of the actin to polymerize and de-polymerize rapidly. Microfilaments also known as actin filaments or F-actin, forms a major part of the cytoskeletal structure of a cell [466, 467]. In eukaryotic cells, actin is found as a meshwork of membrane associated proteins which allow the cells to attach to associated substrates. Fluorescent staining of actin filaments is therefore a useful method of visualising the extent of cellular attachment to culture substrates such as micro-carriers.

Belonging to a group of phallotoxins, phalloidin is a bicyclic peptide produced by the mushroom *Amanita phalloides* [468]. Phalloidin forms complexes with both the monomeric (G-actin) and the filamentous (F-actin) forms of actin [469]. However, phalloidin shows considerably more phalloidin affinity towards F-actin filaments thus, is often used as a cytoskeletal stain. Binding of phalloidin to both monomeric actin and actin filaments prevents further polymerization or de-polymerization effectively establishing stability in the in the cytoskeleton, allowing fluorescent microscopic images to be recorded with relative ease [470, 471]. Phalloidin staining was used to study the morphological spread of cells across the 3D microcarriers.

3.15 STATISTICAL ANALYSES

Unless otherwise stated, statistical differences between all the variables in this thesis were determined using a Tukey comparison and statistical significance was performed using Student's t-test. Results were considered statistically significant only if they had a p value < 0.05. Gold nanorods and cell count was performed by using Image J software package.

Chapter 4: Gold Nanorods and Laser Characterisation on 2D Surfaces

Gold nanorods (Au NRs) have a broad range of potential biological applications because of their well-defined capacity for localised surface plasmon resonance and biocompatibility [294]. In addition to this, they are easily synthesised and functionalised [300], and their aspect ratios are tuneable for optical excitation in the biological window [294]. The NIR biological window is defined by the wavelengths of light (700 nm-1300 nm) that have maximum penetration of tissue. This property can be used in wide variety biomedical applications such as diagnostics and LLLT [257]. Consequently Au NRs are being widely investigated for many applications including theragnostics (diagnosis and therapy) [472], gene delivery [473], drug delivery [474] and diagnostic imaging [475]. Gold nanoparticles and light (in the NIR region) have the potential to allow the interaction of surface plasmon resonance effects with the basal and basolateral cellular adhesive functions as shown by Giner-Casares *et al* [335].

In this chapter parameters for producing and irradiating surfaces suitable for using NIR to non-enzymatically detach cells via surface plasmon effects were investigated/optimised. Three different types of Au NRs with different surface coatings, functionalization and conjugations were studied. They were characterised, tested for compatibility with hMSC culture medium and covalently/electrostatically attached to silica surfaces. The resulting Au NRs coated surfaces were characterised to determine the uniformity and density of Au NRs attachment using scanning electron microscope (SEM). In addition, the spectral properties of the Au NRs were determined and the laser parameters required for cell detachment were investigated. The effects of NIR irradiation of Au NRs-coated surfaces on the temperature of the system was also examined.

4.1 MATERIALS AND METHODS

4.1.1 Gold nanorod surface coating

Three types of commercially available Au NRs, with different dimensions, differing polymer coatings and functionalizations, were used to coat the silicon wafer (Melbourne Nanofabrication Centre, Australia)/glass surface (ProSci Tech,

Thuringowa Central, Australia). All the Au NRs had a SPR ranging between 770-790 nm. The surfaces produced were evaluated for uniformity and density of coating. While silicon wafers were used for SEM analyses of the surface topography post Au NRs coating, glass surfaces coated with Au NRs were used for cell culture. While imaging of Au NRs coated on glass surface is possible, it requires sputtering of gold or platinum layer to avoid the charging effect. In order to avoid the sputtering step, silicon wafers were used for SEM imaging. The surface chemistry of silicon wafer and glass is largely similar (containing high concentration of Si-O bonds).

Silica coated gold nanorods (SiO_2-Au NRs)

Silica coated Au NRs (SiO_2-Au NRs) was chosen due to their versatile application in therapeutics such as drug delivery, diagnostics, cancer therapy and their biocompatibility [332, 476]. Silica coated Au NRs functionalised with hydroxyl group were obtained from Creative Diagnostics (CR-780-1, New York, USA). The manufacturer's product specifications are: the Au NRs have dimensions of 42 nm in length, 11 nm in diameter and an aspect ratio of 3.8. The stock concentration was stated as 8×10^{11} Au NRs/mL. The SiO_2-Au NRs were electrostatically attached to the surface by pre-treatment of the wafers with Polyethylenimine (PEI) to impart a positive charge.

PEI solution was prepared by adding PEI (Sigma Aldrich, Missouri, USA) [1 mg/mL] to 0.5 M solution of sodium chloride (NaCl; Sigma Aldrich, Missouri, USA). The silicon wafers were immersed and incubated in the PEI-solution for two hours at room temperature, and excess NaCl-PEI was washed off from the surface using PBS solution.

Three different concentrations of SiO_2-Au NRs were prepared by diluting the stock solution in PBS: 4×10^{11} Au NRs/mL, 2×10^{11} Au NRs/mL and 1×10^{11} Au NRs/mL. These SiO_2-Au NRs solutions were pipetted onto the PEI-NaCl-coated substrates and were allowed to interact with the surface overnight. The following day, the surfaces were rinsed in PBS solution to remove excess unattached Si-Au NRs.

N-Hydroxysuccinimide – Protein A conjugated gold nanorods (ProA-Au NRs)

N-Hydroxysuccinimide functionalized Au NRs were used as NHS chemistry helps in conjugating the nanorods with various types of proteins. The protein conjugated Au NRs can be applied on surfaces to investigate if an even coating can be

obtained. Gold nanorods, encased in activated ester terminated polymers N-Hydroxysuccinimide (NHS) (C12-25-780-TNHS-50) were purchased from Nanopartz (Loveland, USA). According to the manufacturer's specification sheet, these Au NRs had a diameter of 25 nm and length of 87 nm with an aspect ratio of 3.5. The concentration of the NRs was stated as 5×10^{12} Au NRs/mL. In order to obtain "sticky" Au NRs that would attach to the cell culture surface, NHS-Au NRs were conjugated with Protein A (Figure 30). Protein A was chosen due to its higher concentration lysine in comparison to other proteins. Lysine has primary amine group which can promote non-specific binding of Au NRs to the surfaces.

The covalent immobilization of amine groups on the surface of NHS group is composed of two steps: hydrolysis and aminolysis. In this reaction the NHS ester group, present on the Au NRs surface is first re-activated by hydrolysing it in the presence of PBS solution at room temperature. Following hydrolysis, the NHS surface is then exposed to protein amines which are prepared in buffers of low ionic strength and pH below the isoelectric point of the protein ligand. Aminolysis is a one step process that involves in the NHS ester terminal reacting with the nucleophilic amino group of the Protein A. During this step the ester group is replaced with amine terminated protein via amide linkage [477]. The final product was protein A conjugated gold nanorods (ProA-Au NRs).

A solution of Protein A was prepared in PBS at 1000 μg/ml. The pH of the solution was maintained between 7.75-8.0 to ensure optimum reactivity between the NHS esters and the primary amines. The mixture was immediately added to the Au NRs and sonicated for 1 minute. To facilitate binding of amine-containing Protein A to the NHS ester, the solution was vortexed for 30 minutes at room temperature. In order to purify the Au NRs, the solution was centrifuged at 12000 rcf for 5 minutes and the supernatant was removed and replaced by an aqueous solution containing 1% PBS and 0.1 % Tween 20. After repeating the above step 3 times, the supernatant was completely replaced with phosphate-buffered saline solution (PBS solution, Sigma Aldrich, Missouri, USA). The Protein A conjugated Au NRs (ProA-Au NRs) were stored at 4 ^{o}C until further use.

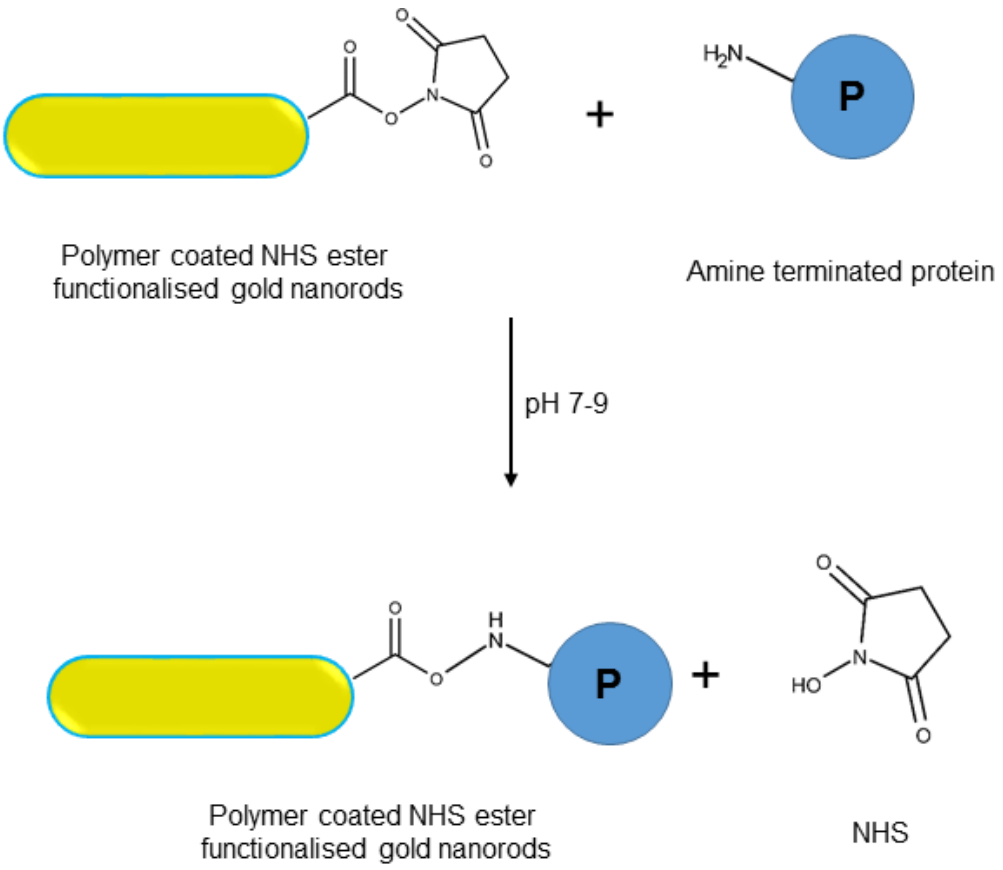

Figure 30: Reaction between the NHS functionalized gold nanorods and Protein A. When exposed to pH between 7-9, the NHS ester terminated group reacts with the primary amines within protein A and forms a covalent bond

Before being exposed on to the surface to obtain an Au NRs-coated surface, the ProA-Au NRs were sonicated (170W and 42kHz) in a ultrasonic bath (Codyson Digital Ultrasonic Cleaner CD-4820) for 5 minutes. This was performed to dissociate any possible formation of the Au NRs aggregates. The ProA-Au NRs solution was then diluted to 5 $\times 10^{12}$ Au NRs/mL, 2.5 $\times 10^{12}$ Au NRs/mL, 1.25 $\times 10^{12}$ Au NRs/mL and 0.62 $\times 10^{12}$ Au NRs/mL in PBS. Surfaces for further experiments were prepared by cleaning the surfaces in a UV ozone cleaner for 10 minutes. Following this, 80 µl of each concentration of ProA-Au NRs solutions was then added to individual silicon wafer/glass surface and spread evenly. These surfaces were air dried overnight at room temperature, allowing the ProA-Au NRs to attach to the surface, followed by rinsing them in order to remove any unattached Au NRs.

Amine functionalized gold nanorods (PA-Au NRs)

Amine functionalization was chosen due to its positive charge. The electrostatic difference between the anionic cell culture surface and the cationic amine was expected to lead to electrostatic interaction and binding. Amine functionalised Au NRs

(PA-Au NRs) were obtained from Nanopartz (C12-10-780-TA-50; Loveland, USA). The manufacturer's specification is that the Au NRs have a diameter of 10 nm and length of 38 nm with an aspect ratio of 3.8. The concentration of the stock solution was 4.3 $\times 10^{13}$ Au NRs/mL. The colloidal stock solution was diluted in PBS to the following concentrations: 2.6 $\times 10^{12}$ Au NRs/mL, 1.34 $\times 10^{12}$ Au NRs /mL, 0.67 $\times 10^{12}$ Au NRs/mL. Prior to adding the Au NRs solution, the silicon wafers were cleaned using a UV ozone cleaner for 10 minutes. 80 µl of each of the solutions was pipetted and spread evenly onto individual clean Si-wafer/glass substrates. The surface was allowed to interact with PA-Au NRs overnight. The following day, the surfaces were washed with PBS in order to remove any unattached Au NRs.

4.2 CHARACTERISATION

Three different types of Au NRs were tested: SiO_2-Au NRs, ProA-Au NRs and PA-Au NRs. The uniformity and density of the Au NRs on the silicon wafer surfaces attached using the three strategies was examined using SEM, absorption spectra and the change in the bulk temperature when NIR irradiated. This information was used to identify the coating method that resulted in the most appropriate surface coating for further studies to determine the spectral absorption properties, position of the surface plasmon resonance and the bulk photothermal effects caused by NIR irradiation on Au NRs coated surface (that is submerged in cell culture media).

4.2.1 Surface Characterisations

Scanning Electron Microscope

The nanoscale morphology of Au NRs coated onto the substrate surfaces was investigated via scanning electron microscopy (SEM; Carl Zeiss SUPRA 40VP SEM and RAITH 150 Two). Silicon wafers (1cm × 1cm) purchased from the Melbourne Nanofabrication Centre were used for the surface characterisation studies. The Au NRs coated substrates were mounted on the sample holder using conducting carbon tape and then placed in the SEM chamber. No gold sputtering was required for imaging as the surface was made of silica and coated with Au NRs, which itself is a naturally conductive material. Magnifications of 12,500, 25,000, 40,000 and 60,000 and accelerating voltages of 3-5kV were used to obtain images.

4.2.2 Au NRs characterization

Absorption Spectroscopy analyses

An ultraviolet visible (UV-Vis) spectrophotometer (Cary 50 UV Vis Spectrophotometer, Agilent, Santa Clara, USA) was used of determine the LPR wavelength of the Au NRs used in this project. The spectral data was collected between wavelengths (λ) of 400 – 1000 nm with a scan rate of 300 nm/minute at intervals of 0.50 nm. Baseline correction was applied to remove background noise. This range focuses primarily on NIR wavelength range as the LPR of nanorods used in our experiments is expected to occur in this region. Stock solutions of different Au NRs were diluted to 1:100 in water separately in a glass cuvettes. Their UV-Vis spectrum of the suspended Au NRs was in the spectrophotometer.

Similarly, absorption spectra were also collected for ProA-Au NRs and PA-Au NRs incubated in cell culture media. The Au NRs were diluted at a ratio of 1:100 in cell culture media and incubated for 24 hours at 37 °C in an atmosphere of humidified 5 % CO_2/ 95% air. After the incubation time period, the Au NRs dispersed in cell culture were transferred to separate glass cuvettes. A cuvette containing only cell culture media was used as the blank reference. The absorption spectroscopy measurements were performed on the Au NRs, suspended in CCM, using a Cary 50 UV Vis Spectrophotometer. This measurement was performed to determine if Au NRs exposed to cell culture media (CCM) would undergo any physical changes.

4.2.3 Temperature measurement of Au NRs coated surface

A two-dimensional radiometry technique was used to study the bulk temperature profile of the CCM when Au NRs coated samples (present in the CCM) were exposed to NIR irradiation. This study was conducted to investigate if the local heating effect generated the Au NRs (as a result of being exposed to NIR irradiation for a certain period of time) would lead to an increase in the temperature in the overall media.

A FLIR ETS 320 Thermal Imaging Camera (RS Australia) was used to measure the temperature difference. Principles and technical details of this instrument is detailed in chapter 3, section 3.4. Temperature measurements were made in a two-dimensional plane during the laser exposure. An entire well of 2 cm^2 surface area (one well in a 24 well plate) could be measure in this field of view.

The objective of this experiment was to study the change in bulk temperature of

the system during NIR irradiation. 2 different samples were used for temperature analyses:

1. Controls (glass surface) silicon wafer covered with cell culture media at room temperature
2. PA-Au NRs coated surface with cell culture media at room temperature.

The samples were exposed to NIR irradiation at a constant distance of 6±2 mm. The temperatures were recorded every 10 minutes after the samples were exposed to laser and the studies were performed for a total of 1-hour time period. During the measurement period, the leaser was turned off in order to focus the irradiated sample to the IR camera. FLIR+ Tools software was used to analyse the data obtained.

4.3 RESULTS AND DISCUSSION

4.3.1 Surface characterization using SEM analyses

Three different types of functionalized Au NRs, SiO_2-Au NRs, ProA-Au NRs and PA-Au NRs, were investigated in order to establish which one would provide a uniform Au NRs surface coverage. It is hypothesized that a uniform and high coverage by Au NRs is necessary as it gives a high contact surface area between the cells and the Au NRs. This may result in homogeneous cell detachment post NIR irradiation. Presence of Au NRs aggregation may result in non-uniform cell detachment.

SiO_2-Au NRs exposed to a PEI coated surface

PEI was used as a base solution for coating as it is highly cationic organic polymer with a high density of amine groups [478]. The biocompatibility and cationic property of PEI has been used for various *in vivo* and *in vitro* biological applications [479] [480]. The addition of NaCl solution to PEI promotes an aggregation in the PEI cationic complex [481]. This property of PEI-NaCl can be used to strengthen/enhance the cationic charge on the coated surface. Opposed to this, the surface charge of SiO_2-Au NRs is negative, making them anionic in nature.

In order to coat surfaces with SiO_2-Au NRs, I relied on the electrostatic attraction between the cationic PEI coated surface and the anionic silica functionalization of the Au NRs. It was expected that the opposite charges would result in a strong and evenly coated Au NRs on the surface.

Figure 31 shows the qualitative SEM images of PEI coated silicon wafers exposed to SiO_2-Au NRs. Figure 31 a-d show PEI-coated surfaces covered with SiO_2-Au NRs at different concentrations: 8×10^{11} Au NRs/mL, 4×10^{11} Au NRs/mL, 2×10^{11} Au NRs/mL and 1×10^{11} Au NRs/mL, respectively. It can be observed that the surface coated with the highest concentration of SiO_2-Au NRs (8×10^{11} Au NRs/mL) retains the highest concentration of Au NRs on it, although higher concentrations also result in the formation of NR clusters. While this cluster formation decreases for lower SiO_2-Au NRs concentrations, the distance between the Au NRs is also greater leading to uneven coverage of SiO_2-Au NRs across the PEI coated surface.

From the SEM images (Figure 31), it can be noted that the SiO_2-Au NRs coverage on the PEI-coated surface is poor (compared to other Au NRs coating shown below) regardless of the concentrations of SiO_2-Au NRs used. The results throughout the different repeated samples were never consistent or reproducible and the SiO_2-Au NRs coverage always varied even when the same protocol was used. As a reproducible evenly coated SiO_2-Au NRs coated surface could not be obtained, no further experimental studies were performed using silica-coated Au nanorods.

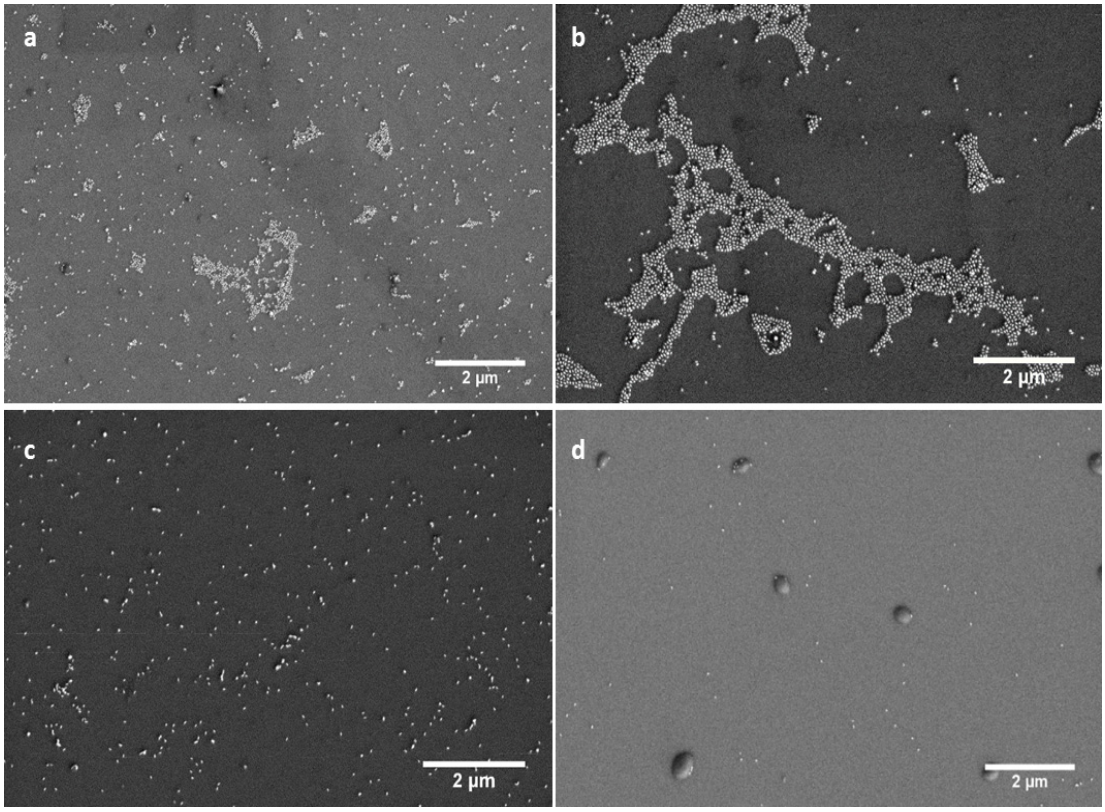

Figure 31: SEM images of SiO_2-Au NRs coated to PEI coated silicon wafers. (a) Stock concentration of SiO_2-Au NRs 8×10^{11} Au NRs/mL, (b) 4×10^{11} Au NRs/mL, (c) 2×10^{11} Au NRs/mL and (d) 1×10^{11} Au NRs/mL

ProA-Au NRs coated surface

Au NRs conjugated with Protein A via NHS chemistry were used to investigate if an even distribution spread of Au NRs could be obtained on a silicon surface compared to the SiO_2 Au NRs. Studies have shown that N-hydroxysuccinimide activated carboxylic acids are frequently used to covalently conjugate and immobilize various biomolecules such as enzymes, antibodies, peptides and various biomaterials to form stable peptide bonds [482]. The immobilization of proteins is dependent on various parameters such as the pH value, concentration of buffers, temperature, reaction time and ionic strength [483].

Figure 32 shows SEM images of different concentrations of ProA-Au NRs coated on a silicon wafer. The effects of dilution of the ProA-Au NRs solution on coating efficiency and quality determined using SEM are shown in Figure 32 and the average particle counts per unit area are shown in Figure 33 for the lower dilutions.

Particle count data was not obtained for the highest concentration as clumping (Figure 32 a) prevented accurate enumeration. Quantification (using the software package Image J) of the amount of ProA-Au NRs (Figure 33) showed an expected drop in the number of Au NRs/μm^2 when the concentration of the coating solution decreased from 2.5 $\times 10^{12}$ Au NRs/mL dilution to 1.25 $\times 10^{12}$ Au NRs/mL. Though clumping of Au NRs could still be observed in 2.5 $\times 10^{12}$ Au NRs/mL dilution samples, it was still possible to see an even coating of gold nanorods on the surface. Though an even coating of ProA-Au NRs could be observed in 1.25 $\times 10^{12}$ Au NRs/mL dilution and 0.62 $\times 10^{12}$ Au NRs/mL dilution, the coverage of the ProA-Au NRs on the surface is lower. The two lower dilutions were also not visually distinguishable in Figure 32 (c & d) and did not result in statistically different particle numbers per unit area (Figure 33).

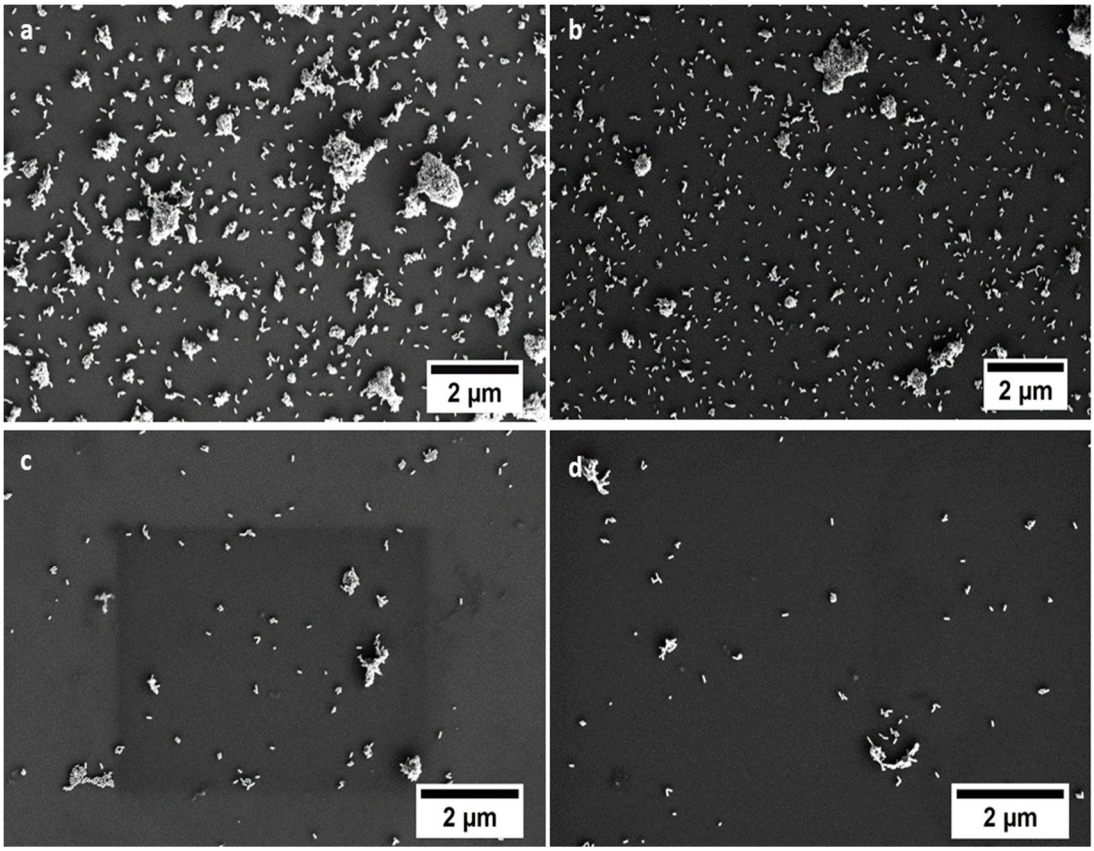

Figure 32: SEM surface images of different dilutions of ProA-Au NRs coated on silicon wafer. (a) 5 $\times 10^{12}$ Au NRs/mL, (b) 2.5 $\times 10^{12}$ Au NRs /mL, (c) 1.2 $\times 10^{12}$ Au NRs /mL and (d) 0.625 $\times 10^{12}$ Au NRs/mL

When these Au NRs are exposed to the silicon wafers, adhesion of the Au NRs to the silicon surface may be due to the non-specific adsorption between the ProA-Au NRs and the surface. Studies have shown that peptides bind to hydrophobic surfaces through hydrophobic interactions. The non-specific adhesion between the globular protein and the hydrophobic silicon/glass surface can be caused due to enhanced long-range hydrophobic attraction. These non-specific binding can be caused due to either electrostatic interaction or mechanical interaction [484].

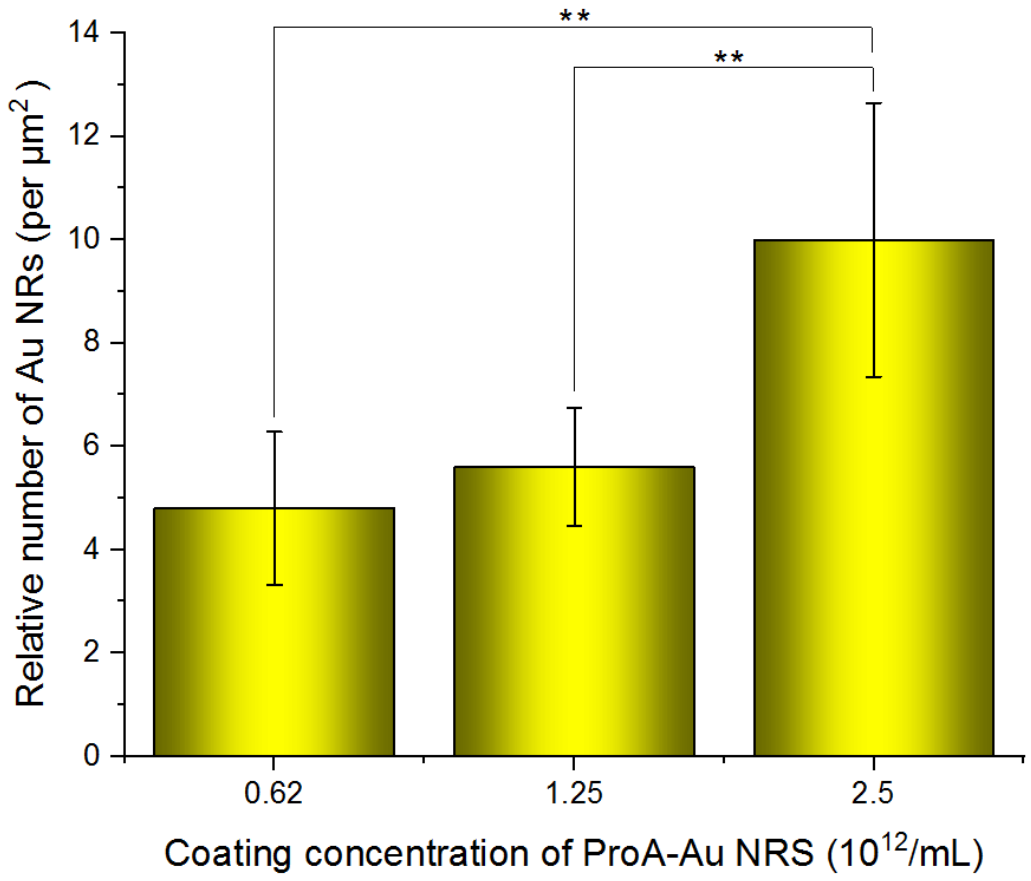

Figure 33: Number of ProA-Au NRs coating a μm^2 of the surface based on concentration of the solution. The highest number of Au NRs was observed for 2.5 $\times 10^{12}$ Au NRs/mL. *p<0.05, **p<0.01 and ***p<0.001. Standard deviation was used. Error bars show ± 1 standard deviation from the mean.

A higher number of gold nanorods are preferred in order to have a high surface area coverage. This would allow the cells to have optimum contact with the ProA-Au NRs thereby exposing them to evenly distributed LSPR across their plasma membrane. But a highly clumped coatings has the potential to generate localised areas of high temperatures when exposed to NIR light which may be detrimental to cell membrane integrity or cellular function [485, 486]. The folding properties in the proteins dictate aggregation of multiple proteins towards each other. These aggregation phenomenon between the proteins may be the reason that the Au NRs seem to show formation of clumps [487]. Based on the data obtained, samples coated with 2.5 $\times 10^{12}$ Au NRs/mL were selected for further studies. This was to ensure that sufficient particles were present to aid the cells to detach during NIR irradiation.

PA-Au NRs coated surface

The third gold nanorods used in these studies were PA-Au NRs. Figure 34 presents representative SEM images of different concentrations of PA-Au NRs coated

on silicon surface. Extremely high aggregation of Au NRs (Figure 34 a) can be observed with the stock solution (4.3 $\times 10^{13}$ Au NRs/mL). At dilution below 2.6 $\times 10^{12}$ Au NRs/mL aggregation of Au NRs were eliminated and a better individual distribution of Au NRs across the surface could be observed (Figure 34 b, c & d). Compared to the two lowest dilutions, 2.6 $\times 10^{12}$ Au NRs/mL (Figure 34 b) showed a better coverage of nanorods across the surface. As the dilution increases the images show a distinguishable difference or drop in the Au NRs count on the coated surface (Figure 34 c & d).

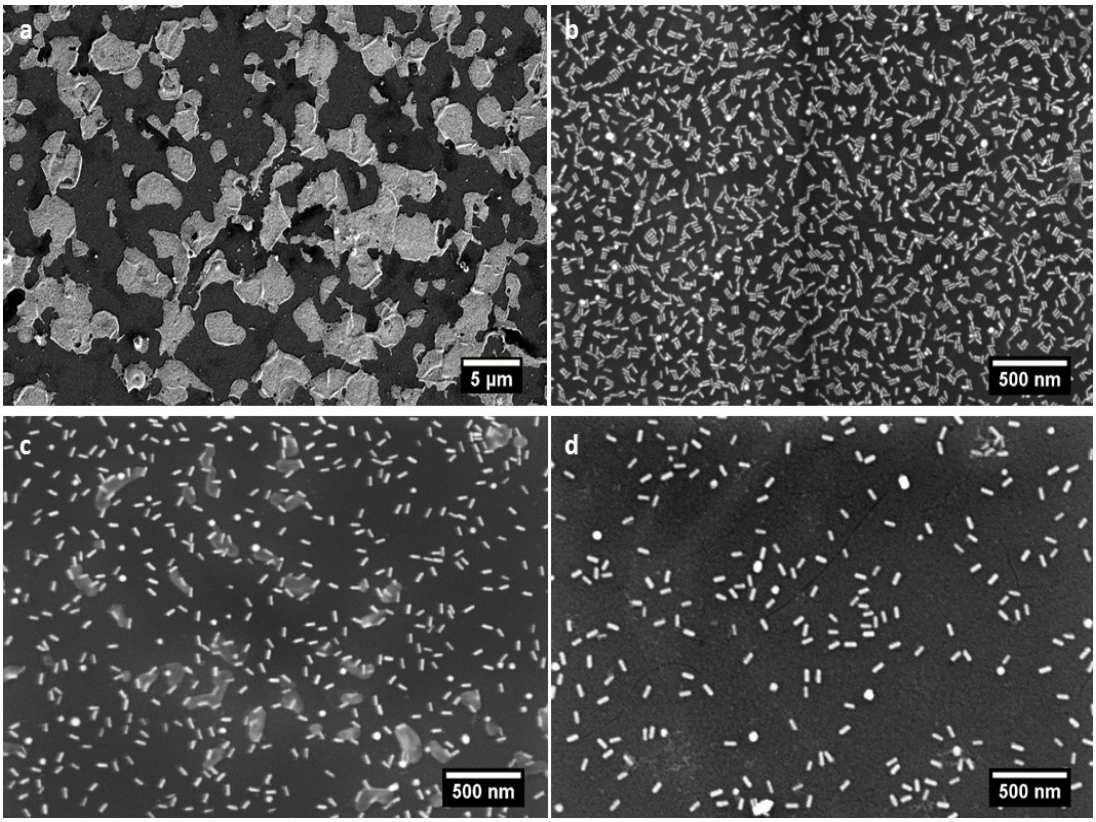

Figure 34: SEM images of silicon surface coated with PA-Au NRs. (a) Stock solution 4.3 $\times 10^{13}$ Au NRs/mL, (b) 2.6 $\times 10^{12}$ Au NRs/mL, (c) 1.34 $\times 10^{12}$ Au NRs /mL and (d) 0.67 $\times 10^{12}$ Au NRs/mL

Due to individual spreading of the nanorods below 2.6 $\times 10^{12}$ Au NRs/mL dilution, particle count for the PA-Au NRs was possible. Quantification of average number of particles per μm^2 based on dilution with standard error of mean was performed using the software package Image J (Figure 35).

Surfaces coated with 2.6 $\times 10^{12}$ Au NRs/mL showed the highest number of Au NRs and was statistically significant when compared to other two lower concentrations. While particle count for lower dilutions (0.67 $\times 10^{12}$ Au NRs/mL and 1.34 $\times 10^{12}$ Au NRs/mL) showed a variable in Au NRs numbers, the difference was not

shown to be statistically significant.

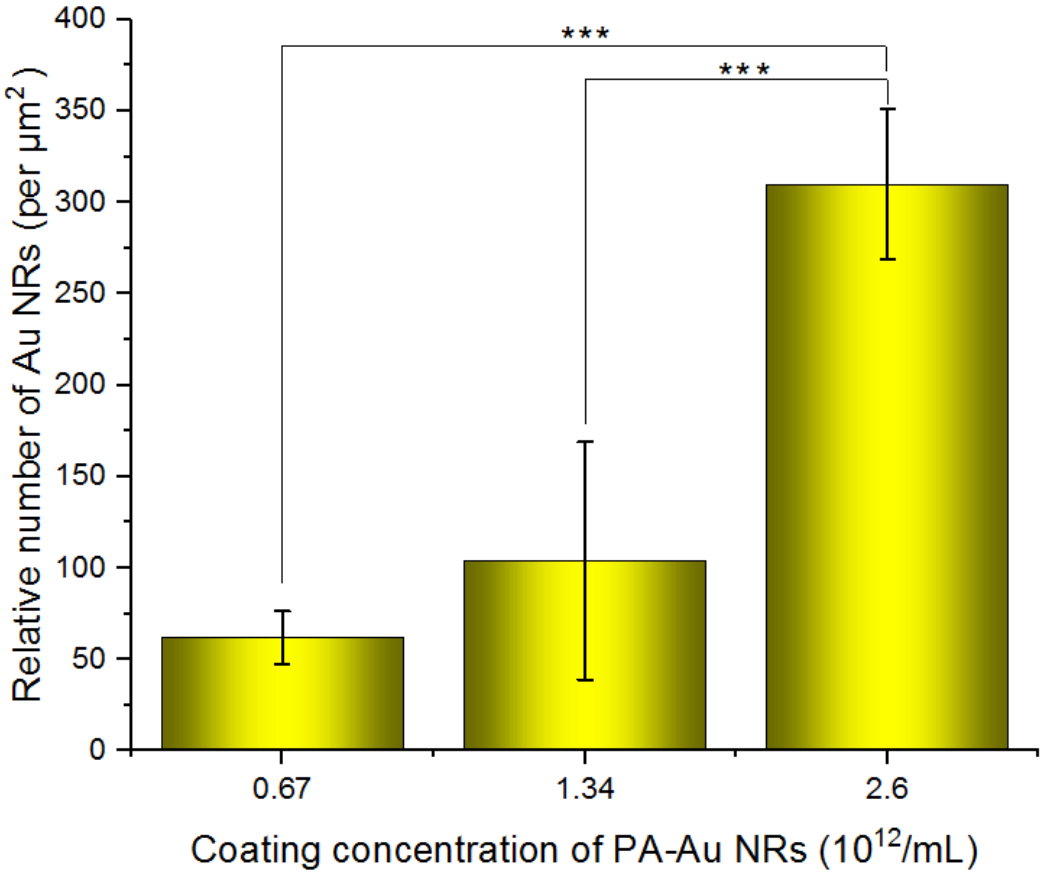

Figure 35: Quantification of the number of PA-Au NRs particles coated per µm^2 of the surface based on concentration of the solution. The highest number of Au NRs was observed for 2.5 ×10^{12} Au NRs/mL. *p<0.05, **p<0.01 and ***p<0.001. Standard deviation was used. Error bars show ± 1 standard deviation from the mean.

The surface adsorption of the PA-Au NRs was most likely caused by electrostatic interactions between the positively charge amine functional groups on the Au NRs and the negatively charged surface of the silicon wafers. The electrostatic interaction between the Au NRs and the silicon surface is driven by Van der Walls forces [488].

Similar to ProA-Au NRs, the surface that showed highest but even coating of PA-Au NRs was at 2.6 ×10^{12} Au NRs/mL and was used for cell culture studes (Chapter 5). Higher concentration with even spread of Au NRs was prefered due to it's high surface coverage area, allowing the cells to be exposed to high amount of Au NRs and hence LSPR when irradiated with NIR wavelength.

4.3.2 Absorbance spectral measurements

While SEM was used to observe the coating quality and effeciency of the Au NRs, UV Vis spectroscopy was performed to measure the absorbance spectra of the Au NRs.

In Figure 36, the absorbance spectroscopy of the Au NRs suspension in water showed prominent peaks at 780 nm for ProA-Au NRs and 775 nm for PA-Au NRs corresponding to LPR. Not only are these measurements consistent with the manufacturers specifications, they also agree with previous studies conducted by Tong *et al*., who showed similar SPR peak at similar aspect ratios (3.5-3.7) [489]. Small TPR were seen at 516 nm for ProA-Au NRs and at 508 nm for PA-Au NRs. The amplitude of TPR is ~ 5 times smaller than that of the LPR.

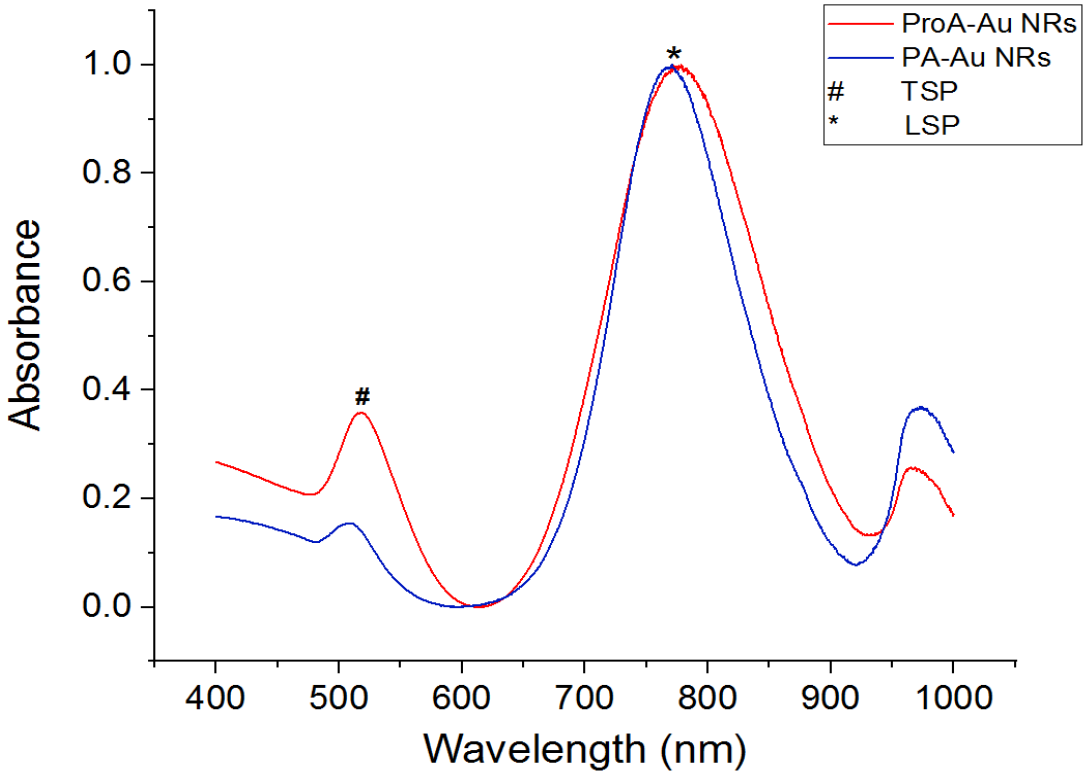

Figure 36: Absorption spectra of ProA-Au NRs and (red line) and PA-Au NRs (blue line). Both the Au NRs show spectral peaks between 775-780 nm. Data show in the figure has been normalised. The symbol # represents the TSP and * represents the LSP of the Au NRs.

Au NR spectra were also obtained in cell culture media (CCM) (Figure 37). The Au NRs were conditioned in CCM for 24 hours at 37 °C in an atmosphere of humidified 5 % CO_2/ 95 % air prior to spectral measurement. The presence of various biomolecules in CCM may cause structural alterations in the Au NRs resulting in the LPR shift in the nanoparticles [490]. While the electrolytes in the media may result in

Au NRs aggregation or colloidal instability, the binding of serum proteins to the nanoparticle surface can lead to shift in LPR and modification in particle dimensions, charge and chemistry [490, 491].

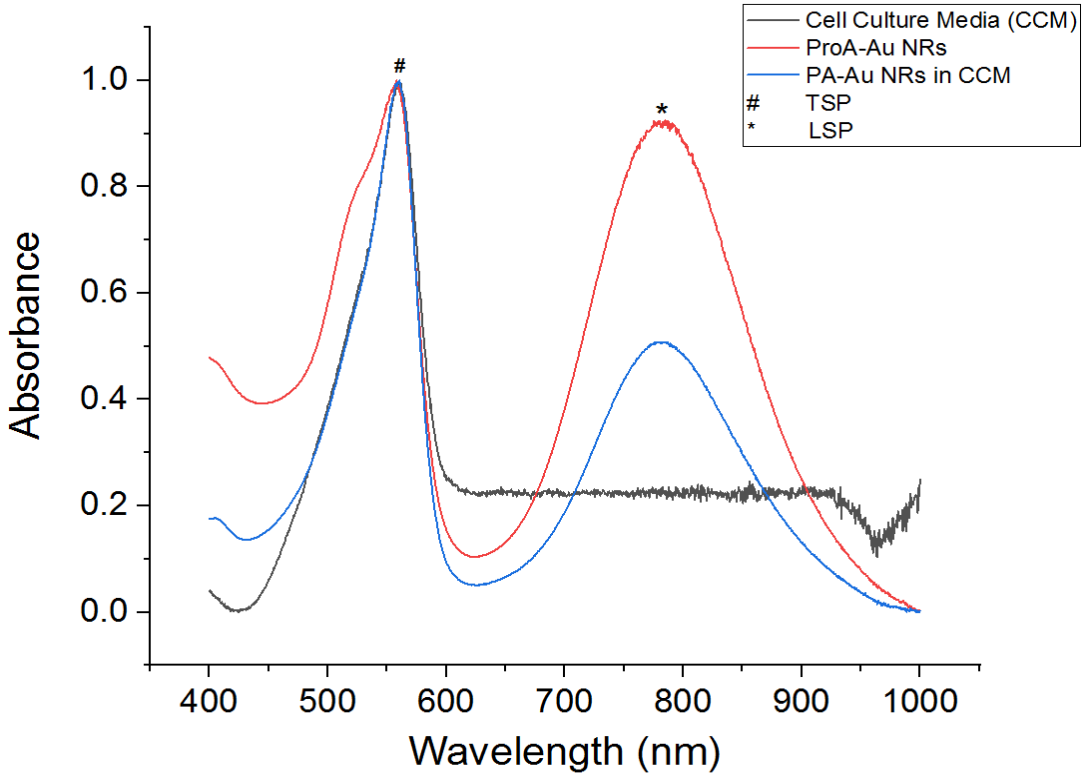

Figure 37: UV-Vis absorption spectra of various Au-NRs in cell culture media (CCM) after being incubated in CCM for 24 hours at 37 °C. Spectra for CCM (grey), ProA-Au NRs (red) and PA-Au NRs (blue) are shown. Both the nanorods show a slight shift in LPR peak post incubation in CCM. In contrast a prominent shift in TPR peak was observed in both the Au NRs. Data shown in the graph has been normalised. While # represents the TSP, * represents the LSP by the Au NRs.

In this spectrum obtained following the UV-Vis absorption spectroscopy studies for the particles incubated in CCM the ProA-Au NRs shows a prominent LPR peak at 786 nm the PA-Au NRs displays the same at 782 nm. This shows a very slight red shift in both the Au NRs by ~ 6-7 nm. A study conducted by Iosin *et al*., also observed the similar red shift in the gold nanorods when exposed to protein bovine serum albumin (BSA) [492]. The slight shift may have been caused due to the change in the aspect ratio, local refractive index or aggregation of the nanoparticles in the presence of the cell culture media. But this shift does not have a significant effect, as they fall on the same bandwidth as that of the NIR laser (785 nm) which would still result in plasmon excitation on the Au NRs. The slight red shift is not expected to have a significant effect on the studies conducted as the LPR still fall in the NIR area of the laser used.

A high absorbance maximum 560 nm which corresponds to the TPR was

observed (Figure 37) for all samples including that of the control CCM (absence of Au NRs). This indicates that this absorbance is associated with a component of the medium, potentially the phenol red pH indicator which has a strong absorbance maximum at 550nm at pH's above neutral [493]. In Figure 37, a prominent shoulder is displayed by the ProA-Au NRs which is absent in PA-Au NRs. This shoulder may represent the TPR of the ProA-Au NRs and it peaks at approximately 526 nm. This shift is ~10 nm from the TPR displayed by ProA-Au NRs in water. While this shift may indicate a change in the particle shape, it may have also been caused due to the background emitted by the phenol red present in the CCM. The ~10 nm shift cannot be considered as a significant shift.

4.3.3 Temperature characterisation

As already discussed in chapter 2, Au NRs have the ability to absorb electromagnetic waves and convert them into thermal energy. This is caused by the surface plasmons that are produced when the oscillations of the free delocalized electrons, present on the Au NRs, resonate coherently with the frequency of the electromagnetic waves. This excitation is caused due to energy absorption and scattering. The intense oscillation dynamics cause a shift in the kinetic energy of the electrons, which is the converted into heat [494].

While cells have shown to have optimal viability and proliferative capacity at 37 ^{o}C, studies have shown that temperature above 42 ^{o}C is detrimental to the cells. Increase of temperature around cells causes chromosomal aberration (leading to DNA damage), protein denaturation, insoluble protein aggregation, blebbing of the plasma membrane (correlating to cell death) and inhibition of ion transport etc [495, 496]. The detachment of cells from Au NRs surface via NIR irradiation is expected to be caused due to the heat generated by the Au NRs when exposed to NIR irradiation [335]. Since, the investigation of the temperature increase on the surface of Au NRs during NIR irradiation could not be performed, studies were performed to see if there was a change in bulk temperature of the CCM in presence and absence of Au NRs surface.

All cell detachment studies were performed at room temperature due to the dividing cells sensitivity to thermal damage. Studies have shown the negative effect of hyperthermia on dividing CHO cells at 45 ^{o}C [497]. Intermediate phase of cell cycle/division involves in cell growth (G1 phase), replication and synthesis of DNA and chromosomes (S phase) followed by resumed cell growth and protein synthesis

for onset of mitosis. Heating of cells have shown to induced chromosomal aberration and damage during the G1 and S phase of cell division. These aberrations lead to fragmentation in DNA double strands and cell apoptosis [496, 497]. While hyperthermia can induce cell death, hypothermia can slow down or cause a temporary arrest of cell cycle in mammalian cells [498]. This arrest in cell cycle can be reversed when the cells are reintroduced to optimal proliferative temperature (37 ^{o}C). This condition would be ideal for the experiments as an increase photothermal temperature is expected when exposing Au NRs to NIR irradiation. The cell culture media and the open system of the experimental setup at room temperature acts as a heat sink thereby rapidly dissipating the bulk temperature increase.

Figure 38 shows the quantitative data obtained when blank glass surface and PA-Au NRs coated glass surfaces, immersed in cell culture media, were irradiated with NIR laser for 60 minutes at room temperature. From Figure 38, it can be observed that the temperature on the blank glass surface constantly increased for 30 minutes following which the readings show a stabilization in temperature regardless of the time of exposure. As opposed to this, the surface coated with PA-Au NRs shows a steady increase in temperature. A temperature increase of 1.5 ^{o}C and 3.0 ^{o}C is observed on the blank surface and PA-Au NRs surface respectively.

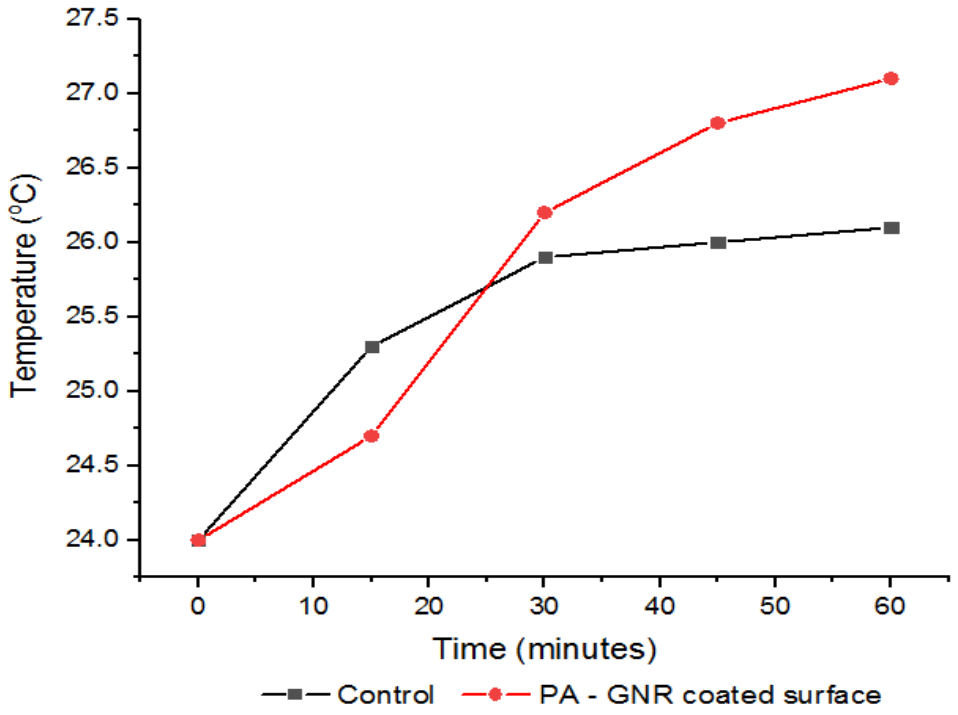

Figure 38: Change in temperature of the bulk media surrounding a control blank glass surface or a PA-Au NRs coated glass surface over time when irradiated with a NIR laser for 60 minutes.

Studies have shown that NIR irradiation of Au NRs causes an increase in temperature ranging between 30 ^{o}C - 60 ^{o}C near the nanorods [499-501]. The temperature closer or on the Au NRs may have been higher during the exposure time and this may not have been picked up by the thermal camera due to its lower resolution. It is also possible that higher temperature readings could not be observed due to the presence of the cell culture media. The cell culture media may have caused the heat to dissipate across the liquid thereby not allowing the thermal camera to pick up the accurate temperature.

4.4 CONCLUSION

Though Au NRs have been used for various biomedical applications, very few studies have been conducted in relation to applying them for cell detachment. While Giner-Casares *et al*., used gold seeding method to "grow" gold surface, Kolesnikova *et al*., used microcontact printing on polydimethylsiloxane (PDMS) to stamp gold nanoparticles on its surface. However, both these techniques are time consuming and difficult to scale up. Functionalized Au NRs are easily available and the functionalizations can be modified to achieve desired surface coating.

While various functionalized Au NRs were characterised, ProA-Au NRs and PA-Au NRs were selected for cell culture studies. This was due to the ability of these nanorods to spread evenly across the surface and their reproducibility. Neither of these properties were observed in SiO_2-Au NRs. Both the Au NRs (ProA-Au NRs and PA-Au NRs) displayed LPR between 780-788 nm in CCM after 24 hours of incubation, which is in the NIR region. In the following chapter, investigations regarding the cell cytotoxicity, the ability of the cells to detach from the Au NRs coated surface post-NIR laser irradiation and cell characterisation is detailed.

Chapter 5: Cellular Detachment and Cell Characterisation Studies

The remarkable ability of stem cells to differentiate into a variety of different cell types, and self-renew makes them desirable for the cell therapeutics industry and in clinical applications. Human mesenchymal stem cells (hMSCs) can be isolated from various sources in the body including adipose tissue [502], bone marrow [503], lung tissue [504], and the umbilical cord [505], and expanded *in vitro*. The enormous potential of MSCs as an effective treatment for tissue damage in a range of disorders has been reported in both animal models and in human trials. These have included autologous treatment of a range of autoimmune diseases [506], models of corneal damage [507], myocardial infarction [508], and spinal cord [509], and lung injury [510] amongst many. Bone marrow derived mesenchymal stem cells, were chosen for use in our studies as they have shown an especially wide variety of therapeutic applications in humans. Reported uses include a clinical trial of autologous bone marrow derived stem cells were improvements in liver function in patients suffering from end-stage cirrhosis were demonstrated [511]. Other trials have shown bone marrow derived hMSCs have therapeutic effects in musculoskeletal disease, repairing bone damage in osteonecrosis [512], repairing burns wounds [513], regeneration of periodontal tissue defects [514], and revascularisation in diabetic limb ischemia [515].

Adherent cells such as the mesenchymal stem cells are also widely known for their plastic - adherence properties. They require tissue culture plastic or other culture surfaces in order to proliferate and differentiate *in vitro* [516]. After either proliferation or differentiation the cells are required to be detached and recovered from their *in vitro* substrate for further use. The current industry "gold standard" for the detachment of cultured cells, including stem cells, from a surface is by exposing the cells to the proteolytic enzyme trypsin for a certain period of time. Trypsin is widely used in disaggregation of tissues and in cell culture as it robustly cleaves cell-substrate adhesion complexes, extracellular matrix and cell-cell adhesion junction complexes. Trypsin is a mammalian digestive enzyme that cleaves on the carboxyl side of arginine and lysine residues and proteolytically digests all but a few proteins [184]. As a result of its broad substrate specificity, exposure of cells to trypsin has been reported to result in dysregulation of cellular functions [517] as well as affect the structural integrity of

the membrane[517, 518].

In the pharmaceutical industry and in clinical settings, the deleterious effects of trypsin on the quality and/or viability of cells produced for human use may significantly reduce the effectiveness of therapeutic interventions. Consequently, it is of great importance to develop new, non-enzymatic approaches to harvesting cells that ensure the quality of the cells produced by preserving the integrity of the cell structure and function. In the literature review I described the alternative cell detachment techniques and their shortcomings. New methods for cell harvesting should be investigated and this technique must also be scalable to meet the rising clinical demands for new cell-based therapies.

The current chapter details the study performed on cells (NIH-3T3 mouse fibroblasts and human mesenchymal stem cells) that were cultured on gold nanorods surface and detached via laser irradiation. The NIH-3T3 fibroblasts cells were used for initial viability and detachment studies as these cells are known for their robust characteristics and adherent properties [519]. The NIH-3T3 fibroblast studies were performed in order to determine the appropriate Au NRs coated surface and NIR irradiation based cell detachment that can be applied directly on the hMSCs. Experiments were designed in order to evaluate that the hMSCs could be detached without compromising their stem cell characteristics required for development of novel therapeutic interventions.

All cell experiments were designed specifically to test (i) the viability of NIH-3T3 mouse fibroblast cells and hMSCs cultured on Au NRs (ii) the efficiency of cell detachment from the various Au NRs coated surfaces upon NIR exposure (iii) the viability of laser detached cells over a period of 7 days for hMSCs (iv) the effect of NIR exposure on cell surface protein expression (v) the effect of laser exposure on adipogenic differentiation potential (vi) the effect of laser exposure on MSC osteogenic differentiation ability (vii) the effect of laser exposure on gene expression and of the specific genes upregulated during differentiation of hMSCs by q-PCR.

5.1 MATERIALS AND METHODS

5.1.1 Cell culture

Cells for all experiments were grown to 80 – 85 % confluence in either 75 cm^2 or 25 cm^2 polystyrene tissue culture flasks (Corning Costar, New York, USA) under

standard conditions and collected for use by trypsinization. This was performed in order to achieve the appropriate cell numbers required for our experiments from the commercially supplied stock. Briefly, cells were treated with a recombinant animal component-free trypsin (TrypLE™ Express, Invitrogen, California, USA) according to the manufacturer's directions. Detachment was confirmed by microscopy, and the culture surface rinsed (2 × 5mL) with tissue culture medium. Pooled cells were collected by centrifugation at room temperature for 5 minutes at 1500 rpm (1000 g) and resuspended in fresh media. Cell numbers were estimated using a standard hemocytometer and the cells diluted in fresh warmed tissue culture medium to a seeding density of 10,000 cells per well for 96 well plates or 100,000 cells per well for 24 well plates. Cells were cultured for 24 hours at 37 °C in an atmosphere of humidified 5 % CO_2/ 95 % air before use unless otherwise stated.

For Au NRs-surface experiments that dealt with NIR irradiation and cell detachment, tissue culture plate wells (24 well plates, Corning Costar, New York, USA) containing either sterile glass surfaces coated with gold nanorods, control surfaces (sterile plain glass) were seeded at 100,000 cells/well with cells prepared as described above. All cell culture studies described in this chapter were conducted on ProA-Au NRs, PA-Au NRs coated surfaces (section 5.1.2) and blank surfaces. Au NRs coated and uncoated glass surfaces were sterilized by exposing them to 2 % (v/v) Antibiotic-Antimycotic™ (100×; Gibco, Thermofisher Scientific, Massachusetts, USA) in sterile phosphate buffered saline (PBS; Sigma-Aldrich ST Louis, Mo, USA) for 60 minutes. Following sterilisation, the samples were thoroughly rinsed with sterile PBS prior to use.

NIH-3T3 Cell line

NIH-3T3 fibroblast cells (ATCC CLR-1658) derived from NIH/Swiss mouse embryonic fibroblasts [520], obtained from the ATCC culture collection (ATCC, Virginia, USA) were stored in complete growth medium supplemented with 5 % (v/v) DMSO in liquid nitrogen until required. The base medium used to culture these cells was Dulbecco's Minimum Essential Medium (DMEM; Sigma-Aldrich ST Louis, Mo, USA) supplemented with 10% foetal bovine serum (FBS; Life Technologies, Carlsbad, Ca, USA), 0.5 % Glutamax (Thermofisher Scientific, Waltham, MA), 0.5 % Antibiotic-Antimycotic™ (Gibco, Thermo Scientifics). Cryopreserved cells were thawed in a 37 ^{o}C water bath for 1.5 minutes and gently resuspended in 5 mL of

temperature equilibrated culture medium using a sterile pipette prior to use. Suspended cells were collected by centrifugation at 1500 rpm for 5 minutes at room temperature and then resuspended in fresh cell culture medium before numbers of live cells were estimated by trypan blue exclusion in a haemocytometer. Cells were then plated at a density of 3000 cells/cm^2 as per manufacturers recommendations and incubated at 37 ^oC in an atmosphere of humidified 5 % CO_2/ 95 % air. The media was changed every 2 days and cells were cultured until they reached 80-85 % confluency. NIH – 3T3 fibroblasts between passage 11-25 were used for all experiments.

Human Mesenchymal Stem Cells (hMSCs)

Normal human bone marrow-derived mesenchymal stem cells were obtained from Lonza (cat # PT – 2501; Basel Switzerland) and were stored in liquid nitrogen until required. Cell culture media for hMSC culture was made up of Alpha Dulbecco's Minimal Essential Medium (α-DMEM; M4526, Sigma-Aldrich) supplemented with 10% foetal bovine serum (FBS; Life Technologies, Carlsbad, Ca, USA), 0.5 % Glutamax (Thermofisher Scientific, Waltham, MA), 0.5 % Antibiotic-Antimycotic (100×; Gibco, Gibco, Thermofisher Scientific, Massachusetts, USA). The cryopreserved vials were removed from liquid nitrogen and immediately thawed in a 37 ^oC water bath for 1.5 minutes. The thawed cells were then gently resuspended in 5 mL temperature equilibrated culture medium. These cells were centrifugation at 1500 rpm for 5 minutes at room temperature and the supernatant was replaced by fresh media. The cells were resuspended, and the number of live cells were estimated using by trypan blue exclusion in a haemocytometer. Cells were seeded at a density of 6000 cells/cm^2 and incubated at 37 ^oC in an atmosphere of humidified 5 % CO_2/ 95 % air. The cell culture media was changed on alternate days and the cells were cultured until they reached 75-80 % confluency. All experiments using hMSC were performed between passage 4-7. Repeated passaging was limited as stem cells show a significant reduction in differentiation potential and an increase in doubling time with increasing numbers of passages.

5.1.2 Preparation of Au NRs coated cell culture surface

All surfaces used for Au NRs coating were made of glass based material. The wells in a glass based 96-well plates (CellVis, USA) (for PrestoBlue assay) were coated with 30µl of ProA-Au NRs (0.31×10^{12} Au NRs/mL, 0.65×10^{12} Au NRs/mL, 1.25×10^{12} Au NRs/mL and 2.5×10^{12} Au NRs/mL) and PA-Au NRs (0.67×10^{12} Au

NRs/mL, 1.3 $\times 10^{12}$ Au NRs/mL and 2.6 $\times 10^{12}$ Au NRs/mL) individually. For Live/Dead assay and cell detachment studies, glass slides of 15 mm diameter (ProSci Tech, Thuringowa Central, Australia) were exposed to 80 µl of required Au NRs solution. The substrates were then air-dried overnight at room temperature, thereby allowing the Au NRs to be absorbed onto the surface. This was followed by rinsing the coated surfaces to remove any unattached Au NRs.

5.1.3 Cell detachment from Au NRs surface via NIR irradiation

NIR laser conditions

As described in chapter 3, section 3.1, all experiments were performed using 785 nm single mode fibre coupled continuous wave laser diode. All the experiments were undertaken with the fibre placed at a distance of 6±2 mm at the air/medium interface, to give a final irradiance of 566 mW/cm^2.

Cells were grown for 24 hours on Au NRs-coated and uncoated glass surfaces in 24 well tissue culture plates as described above. The glass surfaces were then washed with PBS to remove any loosely attached or non-adherent cells and 0.5 mL of fresh cell culture medium was added to each well. Samples were then aligned with the NIR laser source. The laser was positioned at a height of 6±2 mm at the air/medium interface (Figure 39). Cells were exposed to NIR irradiation for 15, 30, 45, and 60 minutes to determine the optimum exposure times for cell detachment and to ensure that cell viability was maintained throughout these exposure time periods.

Following NIR exposure, the media above each irradiated sample which contains cells detached from the Au NRs surface was collected by gentle aspiration and transferred to a new well in a fresh 24 well plate (Corning Costar, New York, USA). The irradiated Au NRs surfaces were then washed with 0.5 mL of fresh culture media to remove any remaining detached or loosely adherent cells. The wash was then collected by aspiration and transferred to a new well. The samples containing detached cells were then incubated for 24 hours at 37 ^{o}C, 5 % CO_2/ 95 % air. After this time cell proliferation and viability were measured in the irradiated and non-irradiated control samples. Proliferation and viability assays were performed on the cells that were non-irradiated and post NIR irradiation.

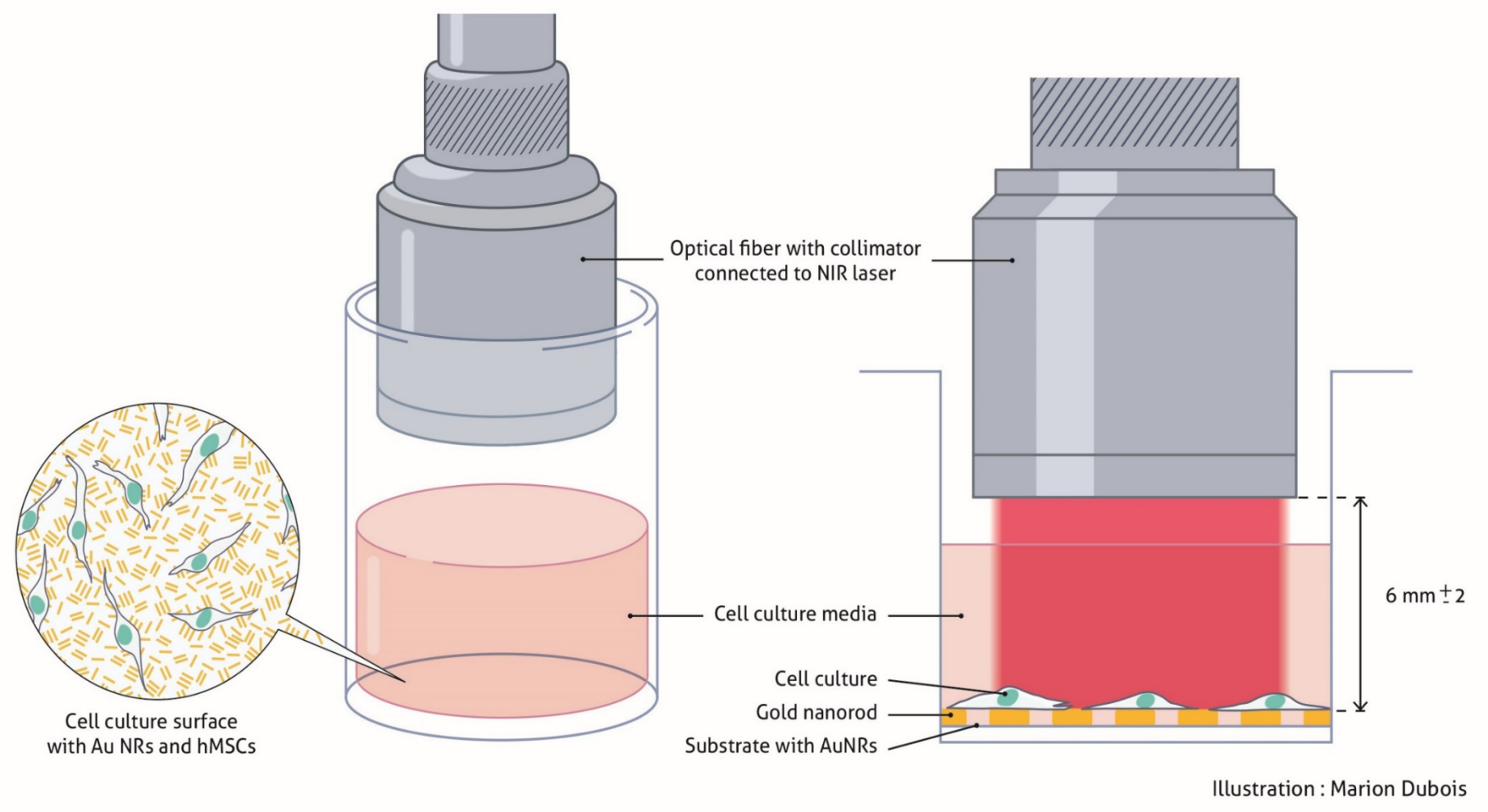

Figure 39: NIR laser set up from cell culture surface. The Optical fibre caped with collimator was set at a distance of 6±2 mm from cells cultured on Au NRs coated surface. The surface was irradiated for required amount of time until cell detachment is achieved.

5.1.4 Cell viability

Cell viability studies namely the PrestoBlue assay and Live/Dead staining were performed to determine the effect of Au NRs concentrations and NIR irradiation on NIH-3T3 fibroblasts and hMSCs viability. The working principles and mechanism of PrestoBlue are explained in chapter 3, section 3.5and 3.6.

5.1.4.1.NIH-3T3 cell viability

Au NRs coated and uncoated surface

Quantitative studies using PrestoBlue assay to analyse the cytotoxic effects of various concentrations of ProA-Au NRs and PA-Au NRs were performed. Au NRs samples for analysis were prepared in glass bottom 96 well plates (Nunc, Roskilde, Denmark). The well plates were coated individually with ProA-Au NRs (0.31×10^{12} Au NRs/mL, 0.65×10^{12} Au NRs/mL, 1.25×10^{12} Au NRs/mL and 2.5×10^{12} Au NRs/mL) or PA-Au NRs (0.67×10^{12} Au NRs/mL, 1.3×10^{12} Au NRs/mL and 2.6×10^{12} Au NRs/mL) (section 5.1.2). NIH-3T3 cells were seeded at a density of 10,000 cells/well and incubated at 37 ^{o}C in an atmosphere of humidified 5 % CO_2/ 95 % air for 24 hours. After the required time period, the culture media was removed, and the cells washed with PBS.

200 µL of a 10 % v/v PrestoBlue reagent (Invitrogen, California, USA) diluted in DMEM was added to the cell culture wells. The samples were incubated at 37 ^{o}C in an atmosphere of humidified 5 % CO_2/ 95 % air for 1 hour. Fluorescence was then measured using a POLARStar microplate reader (BMG, LabTech FluoStar Omega) at an excitation and emission wavelengths of λ_{ex}560 nm and λ_{em}590 nm respectively. Cells cultured in uncoated wells was considered as controls.

Qualitative studies on NIH-3T3 fibroblasts on coated and uncoated samples was performed using Live/Dead staining. Glass slides coated with ProA-Au NRs and PA-Au NRs (section 5.1.2) were placed in individual 24 well plates and seeded with NIH-3T3 fibroblasts at a density of 100,000 cells/well. The cultures were incubated for 24 hours at 37 °C in an atmosphere of humidified 5 % CO_2/ 95% air. After 24 hours, samples were then gently washed with warm PBS and the cell culture media was replaced with Live/Dead solution. A working solution of calcein AM/PI (Live/Dead Cell Double Staining Kit, Sigma) with a ratio of 2:1 was prepared for this assay (as per manufacturer's instructions). In order to make 10ml of working solution,

approximately 20 µl of Calcein AM and 10 µl of PI was added to 10 ml of PBS solution. This solution was then vortexed to ensure a through mixing of all the dyes.

500 µL of this working solution was added to each sample in a 24-well plate. The samples were then incubated in the dark at 37 ^{o}C in an atmosphere of humidified 5 % CO_2/ 95 % air for 30 minutes. After incubation, the samples were washed twice with PBS, to remove excess fluorophores. The labelled cells were imaged with a 40 × and 10 × magnification objective under an epifluroscent Nikon Eclipse Ti-E Inverted microscope system (DS-Qi1 fluorescent time lapse camera) using the wavelength configurations of λ_{ex}535 nm and λ_{em}617 nm for PI staining and λe_x490 nm and λ_{em}515 nm for Calcein AM staining.

Viability of detached NIH-3T3 fibroblasts post NIR-irradiation

Qualitative Live/Dead assay was performed on re-seeded NIH-3T3 fibroblasts detached via NIR irradiating from Au NRs coated surface. Samples for irradiation were prepared by seeding cells at a density of 100,000 cells/well on to a Au NRs coated glass surface (which was placed in a 24 well plate) (section 5.1.2). The cells were incubated for 24 hours at 37 ^{o}C in an atmosphere of humidified 5 % CO_2/ 95 % air. After 24 hours of cell culture, the cells were irradiated with NIR laser for 1 hour.

Following 1 hour of irradiation, the detached cells (post-NIR irradiation) were re-plated onto a 24 well plate and allowed to proliferate for 24 hours at 37 ^{o}C in an atmosphere of humidified 5 % CO_2/ 95% air. After 24 hours the cells were washed with PBS solution to remove any unattached cells or debris. 500 µL of Live/Dead working solution was added to each of these samples and incubated in dark at 37 ^{o}C in an atmosphere of humidified 5 % CO_2/ 95% air for 30 minutes. Following the 30 minutes incubation, the samples were washed with PBS and observed under an epifluroscent Nikon Eclipse Ti-E Inverted microscope system (DS-Qi1 fluorescent time lapse camera) with wavelengths of λ_{ex}490 nm and λ_{em}515 nm for Calcein AM and λ_{ex}535 nm and λ_{em}617 nm for PI.

5.1.4.2. hMSCs viability

Following the viability studies performed on NIH-3T3 fibroblasts, hMSCs viability studies were conducted on the final chosen Au NRs surface.

Viability of hMSCs on coated Au NRs and uncoated surface

PrestoBlue was use to qualitatively study the viability of hMSCs on PA-Au NRs coated surface. Viability of cells cultured on glass bottomed 96 well plates (Nunc, Roskilde, Denmark), coated with 2.6 $\times 10^{12}$ PA-Au NRs/mL (section 5.1.2), were studies against uncoated samples. hMSCs were seeded at a density of 10,000 cells/well and incubated at 37 ^{o}C in an atmosphere of humidified 5 % CO_2/ 95 % air for 24 hours. After the required time period, the culture media was removed, and the cells washed with PBS. 200 µL of a 10 % v/v PrestoBlue reagent (Invitrogen, California, USA) diluted in α-DMEM was added to the cell culture wells. The samples were incubated at 37 ^{o}C in an atmosphere of humidified 5 % CO_2/ 95 % air for 1 hour. Fluorescence was then measured using a POLARStar microplate reader (BMG, LabTech FluoStar Omega) at an excitation and emission wavelengths of λ_{ex}560 nm and λem590 nm respectively.

Live/Dead assay was performed on the hMSCs cultured on PA-Au NRs coated glass substrate (section 5.1.2) to qualitatively study the cell viability. hMSCs (seeding density of 100,000 cells/well) were cultured on glass slides coated with 2.6 $\times 10^{12}$ Au NRs/mL pf PA-Au NRs that were placed in 24 well plates. The cells were incubated for 24 hours at 37 °C in an atmosphere of humidified 5 % CO_2/ 95% air. Following the 24 hours cell culture, the hMSCs were washed with warm PBS followed by Live/Dead staining.

Live/Dead solution consisting of calcein AM/PI (Live/Dead Cell Double Staining Kit, Sigma) was prepared at a ratio of 2:1 (as per manufacturer's instructions). 500 µL of this working solution was added to each sample in a 24-well plate. The samples were then incubated in the dark at 37 ^{o}C in an atmosphere of humidified 5 % CO_2/ 95 % air for 30 minutes. Following the incubation, excess fluorophores were removed by washing the samples twice with warm PBS. The labelled hMSCs were imaged with a 40 × and 10 × magnification objective under a epifluroscent Nikon Eclipse Ti-E Inverted microscope system (DS-Qi1 fluorescent time lapse camera) using the wavelength configurations of λ_{ex}535 nm and λ_{em}617 nm for PI staining and λe_x 490 nm and λ_{em}515 nm for Calcein AM staining.

Viability of hMSCs detached post NIR-irradiation

The viability of hMSCs released via NIR irradiation and by trypsin was compared quantitatively using the PrestoBlue assay. PA-Au NRs coated glass

substrates (section 5.1.2) were seeded with hMSCs at a density of 100,000 cells/mL in a 24 well plate. The cells were incubated at 37^{o}C in an atmosphere of humidified 5 % CO_2/ 95 % air for 24 hours before being irradiated with NIR laser for 1 hour. Post NIR-irradiation the detached cells (an average of 70,000 cells/mL) were then re-seeded on 12 well plates and incubated for a time period ranging from 24 hours to 10 days. A parallel control experiment was performed were cells released via trypsin were reseeded, at the same cell count as to that of the laser detached cells, onto 12 well plates. On the day of the experiment, the cells were washed with PBS. A 10 % (v/v) solution of PrestoBlue was prepared by adding PrestoBlue dye to α-DMEM and added to the cells. 500 µl of PrestoBlue solution was added to the samples and incubated at 37 ^{o}C in an atmosphere of humidified 5 % CO_2/ 95 % air for 1 hour. The samples were then analysed using a POLARStar micro plate reader (BMG, LabTech FluoStar Omega) at excitation and emission wavelengths of λ_{ex}560 nm and λ_{em}590 nm. Cells released via irradiation and trypsinization were tested for viability on days 1, 3, and 7.

Qualitative analyses of re-seeded hMSCs detached via NIR irradiation was performed using Live/Dead assay. Cells released post irradiation were re-seeded in a 24 well plate and incubated for 24 hours at 37 ^{o}C in an atmosphere of humidified 5 % CO_2/ 95 % air. After the required time period, the cell culture media was removed and cells were washed with PBS. 500 µL of Live/Dead working solution was added to each of these samples and incubated in dark at 37 ^{o}C in an atmosphere of humidified 5 % CO_2/ 95% air for 30 minutes. Following the 30 minutes incubation, the samples were washed with PBS and observed under an epifluroscent Nikon Eclipse Ti-E Inverted microscope system (DS-Qi1 fluorescent time lapse camera) with wavelengths of λ_{ex}490 nm and λ_{em}515 nm for Calcein AM and λ_{ex}535 nm and λ_{em}617 nm for PI.

5.1.5 hMSCs differentiation and analyses

In order to determine if exposure of human mesenchymal stem cells to NIR irradiation influences the multipotency of the cells, NIR irradiated hMSCs and cells collected by trypsinization were provided with cues to differentiate into either adipocytes or osteocytes, and the extent of differentiation was quantified.

The following conditions were used for all the differentiation assays:

1. Mesenchymal stem cells released via NIR irradiation and cultured in differentiation promoting media.

2. Mesenchymal stem cells released via trypsin and cultured in differentiation promoting media.
3. Mesenchymal stem cells released via NIR irradiation and cultured in cell culture or maintenance media (controls).
4. Mesenchymal stem cells released via trypsin and cultured in cell culture or maintenance media (controls).

hMSCs were seeded on 15 mm PA-Au NRs coated samples (section 5.1.2) at a density of 100,000 cells/well in a 24 well plate and allowed to proliferate for 24 hours at 37^{o}C in an atmosphere of humidified 5 % CO_2/ 95 % air. The samples were then washed with PBS and replaced with fresh media. The cells were then either exposed to NIR irradiation for one hour or release by trypsinization. After one hour of NIR irradiation, the detached cells were re-seeded into a 12 well plate. Simultaneously, cells released via trypsin were also seeded on to a 12 well plate at a seeding density of similar to that of the NIR detached cells.

Adipogenic Differentiation

In order to induce Adipogenesis in hMSCs, hMSC Adipogenic Differentiation BulletKit™ (PT 3004, Lonza Poietics, Switzerland) was used. This kit contained Adipogenic Induction Medium basal medium ((PT-3102B) and SingleQuots (PT-4135)) and Adipogenic Maintenance Medium basal medium ((PT-3102A) and SingleQuots (PT-4122)). The Adipogenic Induction Media was supplemented with h-insulin (0.1%), L-glutamine, mesenchymal cell growth supplement (MCGS), dexamethasone, indomethacin, IBMX (3-isobuty-1-methyl-xanthine) and Gentamicin sulfate-Amphotericin (GA-1000). Adipogenic Maintenance media was supplemented with h-insulin, L-glutamine, mesenchymal cell growth supplement (MCGS), and GA-1000. Supplements were added according to a proprietary protocol defined by Lonza.

Cells released via trypsin and laser were seeded on to 12-well plates (as described above in section 5.1.3), were cultured in hMSC proliferation media for 7 days in order to reach confluency. After reaching 100 % confluency, the proliferation media was replaced with adipogenic induction media. The cells were subjected to three cycles of induction and maintenance to induce adipogenesis. Each cycle consisted of culturing the cells in adipogenic induction media for 3 days followed by culture in supplemented adipogenic maintenance media for 1-3 days. After 3 cycles, the cells

were cultured in maintenance media for 7 days, with media being replaced every 2-3 days. Care was taken to avoid drying out of cells during media replacement as this would disrupt lipid vacuoles in the differentiated cells.

For controls non-induced hMSCs were used. After 7 days of initial proliferation, hMSCs were cultured in only adipogenic maintenance media which was replaced every 2-3 days. The controls were cultured in parallel to the differentiation.

Levels of adipogenic differentiation were quantified in test and control cell samples. The quantification procedure is detailed in section 5.1.6

Osteogenic Differentiation

Osteogenic differentiation of hMSC was performed by using hMSC Osteogenic Differentiation BulletKit™ Medium (PT-3002, Lonza Poietics, Switzerland). Osteogenic induction media was supplemented with dexamethasone, L-glutamine, ascorbate, penicillin/streptomycin, MCGS, and β-glycerophosphate.

Cells released via trypsin and NIR irradiation were seeded separately in a 12 well plate as explained in section 5.1.3 and were incubated in hMSC media for 24 hours at 37 ^{o}C in an atmosphere of humidified 5 % CO_2/ 9 5% air. After 24 hours, cell culture media was replaced by 2 mL/well of Osteo Induction Media. Induction media was replaced with fresh induction media every 3-4 days for 3 weeks. Non-induced controls were cultured in parallel to the test samples in hMSC proliferation media for 3 weeks with media being replaced every 2-3 days.

After the completion of osteogenic induction, the extent of differentiation was quantified for all cells (section 5.1.6).

5.1.6 Differentiation Assays

Adipogenic differentiation assay

The extent of adipogenic differentiation in all samples was quantified using AdipoRed™ Adipogenesis Assay Reagent (PT-7009, Lonza Poietics, Switzerland). The Adipo red staining kit is based on Nile Red staining.

Cell samples were allowed to equilibrate to room temperature prior to commencement of the assay and washed with 1 mL of PBS. An AdipoRed staining solution (3% v/v in PBS) was freshly prepared, 2 mL was added to each test well and the samples were then incubated at 37 ^{o}C in an atmosphere of humidified 5 % CO_2/ 95

% air for 15 minutes.

For quantitative analysis, the plates were read at excitation/emission of $\lambda_{ex}485/\lambda_{ex}535$nm using a microplate reader (BMG, LabTech FluoStar Omega). Adipogenic differentiation was qualitatively confirmed by observing the cells using a fluorescent microscope (Nikon Eclipse T*i*-E Inverted microscope system) at 40 and 100 x magnification.

Osteogenic differentiation assay

The extent of osteogenisis, in differentiated and undifferentiated hMSC, released by NIR irradiation or trypsinization was determined using Alizarin Red S Staining Quantification Assay (#8678, ScienCell Research Laboratories, CA, USA).

Qualitative analyses:

Cell samples for analysis were gently washed 3 times with 1 mL PBS solution. The cells were then fixed using 4% paraformaldehyde solution for 30 minutes at room temperature. The fixative was carefully removed, and the samples were washed with de-ionised water 3 times. Alizarin Red S Stain Solution (2 %; 1 mL) was added to each well and the samples were incubated at room temperature for 20-30 minutes with gentle shaking. After this time, the dye was removed, and the samples were washed 5 times with de-ionised water to remove any excess dye. The samples were then stored in 1mL de-ionised water to prevent dehydration. The samples were studied under a light (Olympus CKX41, Japan) microscope to determine the osteogenic differentiation qualitatively.

Quantitative analyses:

For quantitative analyses, the samples were stained as described above, but were stored at -20 ^{o}C without a water overlay until required for analysis.

Preparation of samples for microplate reader

Samples to be analysed were removed from -20^{o}C prior to dye extraction and brought to room temperature. 800 µL of 10 % acetic acid was added to each well in a 6 well plate. These samples were placed on a shaker and incubated at room temperature for 30 minutes. The cells, along with the 10 % acetic acid, were transferred to a 1.5 ml microcentrifuge tube. The samples were then vortexed for 30 seconds before being heated to 85 °C for 10 minutes. Parafilm was used to seal the tubes to prevent evaporation of the samples. The tubes were then cooled for 5 minutes on ice and then

centrifuged at 20,000g for 15 minutes. After centrifugation, 500µl of supernatant was transferred to a new tube and care was taken not to disturb the pellet. The supernatant was neutralized by the addition of 200 µl of 10 % ammonium hydroxide solution. 150 µl of the above solution, from each sample, was aliquoted in to a 96 well plate in triplicates. The absorbance was measured at 405nm in a microplate reader (BMG, LabTech FluoStar Omega).

5.1.7 Fluorescence-Activated Cell Sorting (FACS)

The assessment of the expression of surface antigens for MSC, released via NIR irritation or trypsin, was carried out using a FACS (FACSAria™ III, BD Bioscience). Detection of cells positive for CD44,73, 90 and 105 would indicate the multi-lineage differentiation capacity of hMSC. Cells detached via NIR irradiation or trypsinization were seeded on separate 12 well plates and cultured to confluence at 37 ^{o}C in an atmosphere of humidified 5 % CO_2/ 95 % air. On reaching confluence, the cells detached by irradiation were gently scraped from the culture surface and transferred to an 1.5 mL Eppendorf tube. For the controls, each well of hMSCs, was washed with PBS and detached via 0.5 mL trypsin (TrypLE™ Express, Invitrogen, California, USA).

After the required time period cell culture media was added to each well to neutralize the trypsin. The well contents containing detached MSC was then transferred into 1.5ml Eppendorf tubes. The cells were collected by centrifugation at 1300 rpm at 23 ^{o}C for 5 minutes. Following centrifugation, the supernatant was aspirated and the cell resuspended in 2 % FBS in PBS (FACS buffer) and re-centrifuged.

The supernatant was then removed and the cells were resuspended in 100 µl FACS solution containing the following antibodies: FITC mouse anti-human CD44 antibody (1:400, Lot # 2748009) (BD Biosciences, NJ, USA), APC mouse anti-human CD90 antibody (1:2000; Lot # 5323878) (BD Biosciences, NJ, USA), PE-Cy7 mouse anti-human CD73 (1:2000) (BD Biosciences, NJ, USA), BV421 mouse anti-human CD105 (1:200) (BD Biosciences, NJ, USA) and propidium iodide solution (1:500). The cells were incubated on ice for one hour. After this time the stained cells were collected by centrifugation, then washed 3 times and re-suspended in FACS buffer to a final volume of 500 µl. The cell suspension was immediately analysed under BD FACSAria™ II flow cell cytometer.

5.1.8 Reverse transcription quantitative polymerase chain reaction (RT-qPCR)

Cell Culture

Cells detached via NIR irradiation or trypsin were re-seeded onto TCPS and differentiated into osteogenic and adipogenic cells as described in section 5.1.5. Parallel to these, undifferentiated cells were also maintained as controls. All cell culture was performed in 6 well plates. After the required time period (a total of approximately 3 weeks for osteogenic differentiation and 4 weeks for adipogenic differentiation) of differentiation into each cell type, RNA was extracted, and qPCR performed.

RNA Extraction, Reverse Transcription and qPCR

1. RNA extraction was performed using Trizol Reagent (Thermofisher Scientific, Massachusetts, USA) following manufacturer's instructions. Differentiated adipogenic or osteogenic and control hMSCs were resuspended in 500 µl of TRIZOL with relative controls.
2. 100 µl of chloroform was added to each sample, mixed and the RNA aqueous phase was separated by centrifugation at 12,000 RCF × 15 minutes.
3. The extracted RNA was then precipitated with 500 µl of isopropyl alcohol for 10 minutes at room temperature and pelleted by centrifugation at 12,000g × 10 minutes.
4. RNA was washed twice with EtOH 70% and resuspended in 10 µl of RNAse free Water.
5. Resuspended RNA was treated with 1 Unit of DNAse I for 15 minutes to remove any DNA contaminants. DNAse I reaction was ended by addition of 50mM EDTA and denaturation at 70°C degrees for 10 minutes.
6. After spectrophotometric quantification at 260 nm by a Clariostar plate reader (BMG labtech), the same amount for all the samples of RNA (500 ng) was reverse transcribed into cDNA using Omniscript reverse transcription kit (Quiagen, Hilden, Germany). The reverse transcription was performed with the recipe stated in Table 8.

Table 8: Components and recipe for reverse transcription

Component	Volume	Final concentration
Reaction mix	**20 ul**	
10× Buffer RT	2 µL	1×
dNTP Mix	2 µL	0.5 mM each dNTP
Oligo-dT primer (10 µM)	2 µL	1 µM
RNase inhibitor (10 units/µL)	1 µL	10 units
Reverse Transcriptase	1 µL	4 units
Template RNA	Variable	500 ng
H_20	Variable	Up to 20 µl

7. Each reaction tube was incubated at 37 ºC in an atmosphere of humidified 5 % CO_2/ 9 5% air for 1 hour.
8. At the end of the Reverse Transcription, qPCR was performed using Power UP SYBR Green Assay (Thermo Scientific) to analyse the expression of osteogenic or adipogenic markers.
9. Each condition was analysed with a technical triplicate for the selected gene.

The single reaction was prepared using the following recipe (Table 9):

Table 9: Components used in single reaction

Component	Volume	Final concentration
Reaction mix	**10 µL**	
2× SYBR GREEN	5 µL	1×
Forward Primer (5 µM)	0.5 µL	0.5 µM
Reverse Primer (5 µM)	0.5 µL	0.5 µM
cDNA	2 µL	N/D
H_20	2 µL	N/D

The primer sequences were used to specifically amplify the selected osteogenic and adipogenic markers are ash shown in Table 10 and Table 11.

Table 10: Primers sequences for osteogenic differentiation markers and the house keeping gene

OSTEOGENIC MARKER	**SEQUENCE**
ALP (Alkaline Phosphatase)	FORWARD ACGAGCTGAACAGGAACAACGT
	REVERSE CACCAGCAAGAAGAAGCCTTTG
RUNX2	FORWARD TCCCCGTCCATCCACTCTAC
	REVERSE CAGAGGTGGCAGTGTCATCA
HOUSEKEEPING	**SEQUENCE**
GAPDH	FORWARD AATTCCATGGCACCGTCAAG
	REVERSE AGGGATCTCGCTCCTGGAAG

Table 11: Primary sequences for adipogenic differentiation markers and the housekeeping gene

ADIPOGENIC MARKER	SEQUENCE
C/EBPα	FORWARD TATAGGCTGGGCTTCCCCTT
	REVERSE AGCTTTCTGGTGTGACTCGG
FABP4 (Fatty Acid Binding Protein)	FORWARD AACCTTAGATGGGGGTGTCCTG
	REVERSE TCGTGGAAGTGACGCCTTTC
HOUSEKEEPING	**SEQUENCE**
GAPDH	FORWARD AATTCCATGGCACCGTCAAG
	REVERSE AGGGATCTCGCTCCTGGAAG

The DNA amplification was performed with Quant Studio 6 Real Time PCR system (Thermofisher Scientific, Massachusetts, USA) using the following cycling steps as shown in Table 12.

Table 12: RT-qPCR cycle time

HOLD STAGE		PCR STAGE (×40)		MELT CURVE STAGE		
Decontamination 50 °C/2:00 minutes	Activation 95 °C /2:00 minutes	Denaturation 95 °C /0:01 second	Annealing 60 °C/1:00 minutes	95 °C/0:15 seconds	60 °C/1:00 minute	95 °C/0:15 seconds

The relative expression of each gene was quantified by using the 2e-ΔΔCT method. This was done by obtaining the Ct average value from the raw data followed by normalizing the Ct average value against the house keeping gene (GAPDH).

5.1.9 Detection of extra cellular matrix

Visualization of extra cellular matrix (ECM) proteins including fibronectin, laminin and collagen was performed by fluorescent based immunocytochemistry. Immunocytochemistry detects the presence and cellular location of the protein of interest by binding a labelled antibody to an antigen present usually on the surface of the cell. This study was performed to determine and compare the presence of major ECM proteins on the cells detached via laser irradiation or trypsinization. Cells

cultured for 24 hours and detached by both the methods were studied for the presence of the cell surface proteins fibronectin, laminin and collagen.

Method

Cells seeded on glass surfaces and PA-Au NRs surfaces were cultured for 24 hours prior detachment. hMSCs (70,000 cells/mL) detached via NIR irradiation or trypsinization were collected in separate 1.5 mL Eppendorf tubes. Cells were collected by centrifugation (1500 rpm/5 minutes/RT) and washed 3 times with PBS by repeated resuspension and centrifugation. Following the final wash step collected cells were resuspended in, 200 µL of 4 % paraformaldehyde (pH 7.4), mixed thoroughly and incubated at room temperature for 15 minutes. The cells were collected by centrifugation (1500 rpm/5 minutes/RT) and washed twice in 200 µl of PBS prior to resuspension in blocking solution (200uL; 2 % BSA v/v in PBS) to block non-specific binding sites on the cells. After incubating the cells in blocking solution for 60 minutes at room temperature, the samples were washed 3 times in PBS.

Laminin staining

In order to stain the detached cells for laminin, samples were exposed to the primary rabbit anti-human Laminin antibody (1:100 (v/v) in 0.1 % BSA, ab11575, Lot GR3180809, Ab-cam, Cambridge, UK). The samples were incubated overnight at 4 ^{o}C. Following the overnight incubation with anti-laminin antibodies, the cells were washed prior to incubation with Alexa Fluor 647 (Thermofisher Scientific, Massachusetts, USA) anti-rabbit IgG from goat (1:1000 (v/v) in 0.1 % BSA). The samples were incubated in the secondary antibody for 60 minutes at room temperature in the dark. The cells then washed three times with PBS and incubated in 4',6-diamidino-2-phenylindole, (DAPI; 300 nM in PBS, Sigma-Aldrich, Missouri, USA) for 30 minutes. After the required time the cells were washed and transferred to a 24 well plate. In order to image the cells using a 2D fluorescent microscope, it is necessary for the cells to be attached to the surface. In order to facilitate cell attachment, the well plates were centrifuged at 2000 RPM for 7 minutes (Thermo Scientific Heraeus® Multifuge® 3SR Plus Centrifuge). The samples were imaged in a confocal microscope (Olympus FV1000 Confocal Microscope). The nuclear location was confirmed by observation of DAPI fluorescence at λ_{ex}385 nm/λ_{em}420 nm and laminin was imaged by observation of Alexa 647 at λ_{ex}650 nm/λ_{em}665 nm.

Fibronectin staining

Following the washing step the cells were exposed to Anti-Fibronectin antibody (1:500 (v/v) in 0.1 % BSA, ab45688, Lot GR155478, AbCam, Cambridge, UK) and incubated at 4 ºC overnight. The following day the cells were washed with PBS and incubated with Alexa Flour 546 for 60 minutes at room temperature. Following a wash step the cells were incubated in DAPI (300 nM in PBS, Sigma-Aldrich, Missouri, USA) for 30 minutes. Following the incubation, the cells were washed and transferred onto a well plate. The well plates were centrifuged at 2000 RPM for 7 minutes (Thermo Scientific Heraeus® Multifuge® 3SR Plus Centrifuge). Under a confocal microscope the samples were imaged using rhodamine (TRITC) filter (λ_{ex}556 nm/λ_{em}573 nm) to image the fibronectin and DAPI filter (λ_{ex} 385 nm/λ_{em}420 nm) to image the nucleus of the cell.

Collagen staining

To stain the samples for collagen, the samples were exposed to Anti-Collagen I antibody (1:500 (v/v)) in 0.1 % BSA, ab138492, Lot GR247379, AbCam, Cambridge, UK) and incubated overnight at 4 ºC. After the required incubation time, the cells were washed with PBS and exposed to Alexa Flour 488 (AbCam, Cambridge, UK) anti-rabbit IgG from goat (1:1000 (v/v) in 0.1 % BSA) and incubated for 60 minutes, in the dark, at room temperature. This was followed by a wash step and exposure of the samples to DAPI (300 nM in PBS, Sigma-Aldrich, Missouri, USA) for 30 minutes. The samples were washed and transferred to a well plate. The well plates were centrifuged at 2000 rpm for 7 minutes (Thermo Scientific Heraeus® Multifuge® 3SR Plus Centrifuge). Under a confocal microscope the samples were imaged using FITC filter (λ_{ex}495 nm/λ_{em}519 nm) to image the Collagen and DAPI filter (λ_{ex}385 nm/λ_{em}420 nm) to image the nucleus of the cells.

5.2 RESULTS AND DISCUSSION

The following results and discussion is separated into two sections based on the cell types investigated, namely NIH-3T3 fibroblasts and hMSCs.

5.2.1 NIH-3T3 Fibroblast

Initially the cytocompatibility of NIH-3T3 fibroblasts on various concentrations and types of Au NRs coated surface was performed. Following this the, NIH-3T3 cells were cultured on selected Au NRs coated surfaces and irradiated with NIR laser to study if this technique would lead to cell detachment from the surface. The detached cells were then re-seeded and studies for cell viability.

Cell viability on Au NRs coated surface (non-NIR irradiated cells)

The effects ProA-Au NRs and PA-Au NRs coated surfaces had on NIH-3T3 fibroblast viability were initially explored by performing the quantitative PrestoBlue assay and the qualitative Live/Dead assay.

Viability on ProA-Au NRs coated surface

Figure 40 displays the results obtained by the quantitative PrestoBlue assay when NIH-3T3 fibroblasts were exposed to various concentrations of ProA-Au NRs coated surface and blank surface. The results were obtained in the form of fluorescence intensity measured in a microplate reader after exposure to PrestoBlue solution for 1 hour. The NIH-3T3 fibroblasts cultured on clean glass surfaces were used as positive controls. Cells grown on the ProA-Au NRs coated surface were compared with cells grown in the absence of Au NRs coating (Uncoated control; Figure 40). A trend towards reduced numbers of viable NIH-3T3 cells could be observed following 24 hours culture, for surfaces coated with higher concentrations of Au NRs and showed an approximate reduction of 25 % at the highest Au NRs surface coating. But Student's t-test showed no statistically significant difference when cell cultured on all the Au NRs were compared with the controls. However, although not significant, if there was an inhibitory effect on the metabolic activity of the cells this may have been caused due to the presence of Au NRs clumps observed on the surface coated with highest concentration of Au NRs (Figure 32 b). A study conducted by Grabinski *et al* ., showed that the proliferative capacity of HaCaT (human keratinocyte cell line) decrease by 10% when expose to high concentration of polyethylene glycol (PEG) functionalized Au NRs [521].

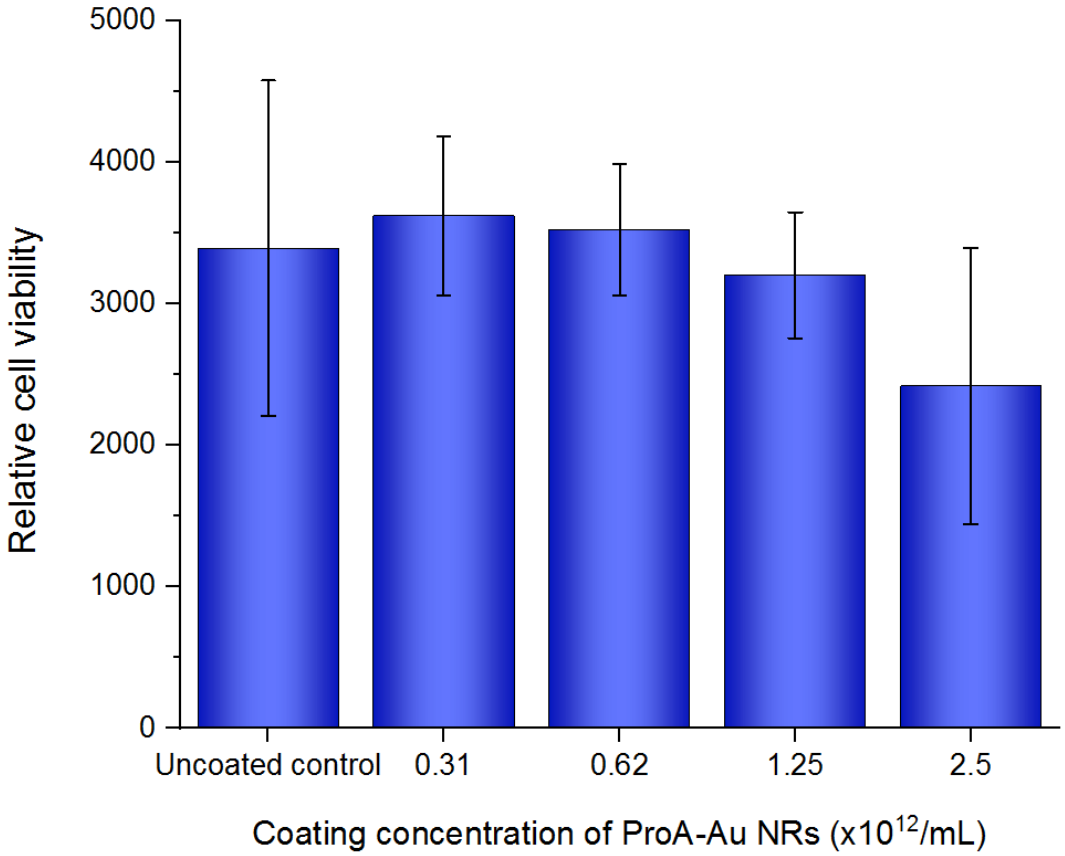

Figure 40: PrestoBlue analyses of NIH-3T3 fibroblast cell viability cultured for 24 hours on glass surfaces coated with varying concentrations of PA-Au NRs. Difference between the NIH-3T3 grown on the ProA-Au NRs coated and non-coated glass surfaces is statistically insignificant. Standard deviation was used. Error bars show ± 1 standard deviation from the mean.

NIH-3T3 fibroblasts grown on either control or ProA-Au NRs coated surface were observed using Live/Dead staining to visually compare the viability and morphology of the cells. Figure 41 shows representative photomicrographs of cells grown on surfaces coated with the highest concentration of Au NRs coated (2.5×10^{12} Au NRs/ml concentration of ProA-Au NRs). In both the control and coated surfaces large amounts of cells are stained green, indicating that the cells are intact and viable. The lack of large amounts red stained nuclei, compared to green stained cells, indicates that the ProA-Au NRs coated surface does not have a visible negatively effect on the NIH-3T3 fibroblast cell viability. The number of cells on both the surfaces were approximately the same (~135 cells per 500 μm^2) with no statistically significant difference.

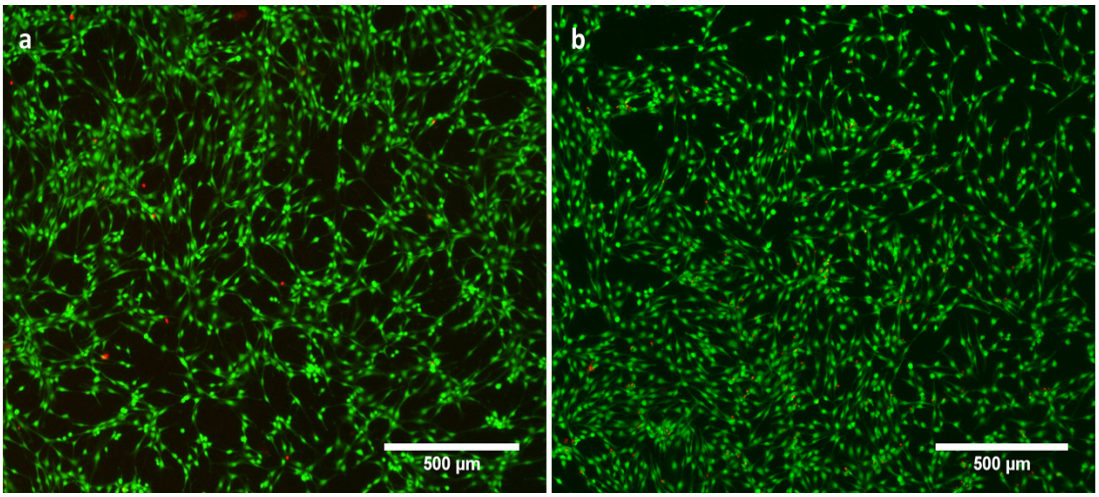

Figure 41: Live/Dead staining of NIH-3T3 fibroblasts (a) NIH-3T3 fibroblasts grown on glass surface. (b) NIH-3T3 fibroblasts grown on ProA-Au NRs coated surface (2.5 $\times 10^{12}$ Au NRs/ml concentration).

Since there was no statistically significant difference in the viability across the different concentrations, concentration of 2.5 $\times 10^{12}$ Au NRs/ml concentration was chosen for all the further experiments that dealt with ProA-Au NRs.

Viability on PA-Au NRs coated surfaces

Figure 42 shows the quantitative viability of the NIH-3T3 fibroblast cells cultured on uncoated glass (control) and glass coated with PA–Au NRs at concentrations ranging from 0.67 – 2.6 $\times 10^{12}$ Au NRs/mL. From the graph it can be observed that surface with the lowest concentration shows an equal metabolic activity when compared to the controls, surface covered with higher densities shows a slight drop. While the cells in 1.34 $\times 10^{12}$ Au NRs/mL shows the lowest metabolic activity (approximately 15%), the highest of concentration (2.6 $\times 10^{12}$ Au NRs/mL) is at 92 %. There was no statistically significant difference between any of the treatments and controls for all samples when measured by Student's t-test.

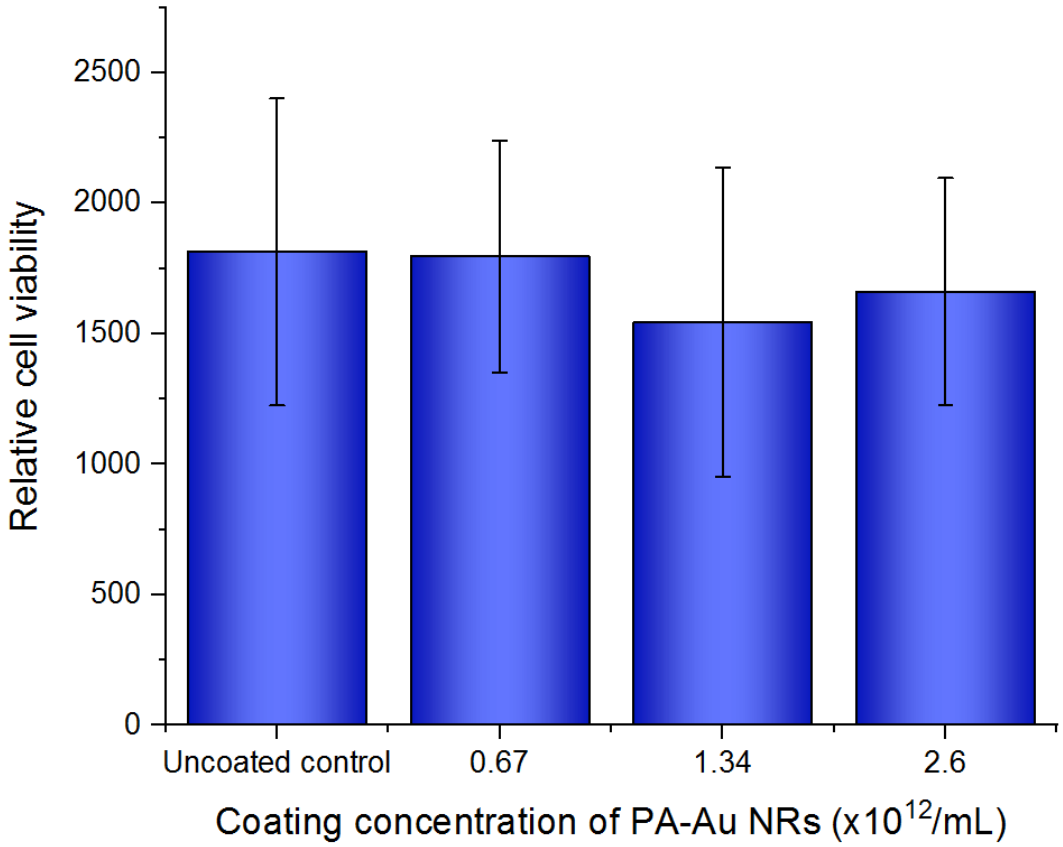

Figure 42: PrestoBlue analyses of NIH-3T3 fibroblast cell viability cultured for 24 hours on glass surfaces coated with varying concentrations of PA-Au NRs. Difference between the NIH-3T3 grown on the PA-Au NRs coated and non-coated surfaces is statistically insignificant. Standard deviation was used. Error bars show ± 1 standard deviation from the mean.

Observation of the cells on the control and PA-Au NRs coated surface (2.6×10^{12} Au NRs/mL) using a Live/Dead stain shows (Figure 43) that the cells are predominantly viable on both surface types after 24 hours of cell culture. Visual inspection of Figure 43 (a & b) is agrees with the PrestoBlue assay were the viability of the cells is shown to be consistent across all surfaces. The number on controls surface was slightly higher on the control surface (~125 cells per 500 μm^2) when compared to the PA-Au NRs coated surface (~110 cells per 500 μm^2) but there was no statistically significant difference between the cell counts. This result is in agreement with the PrestoBlue assay.

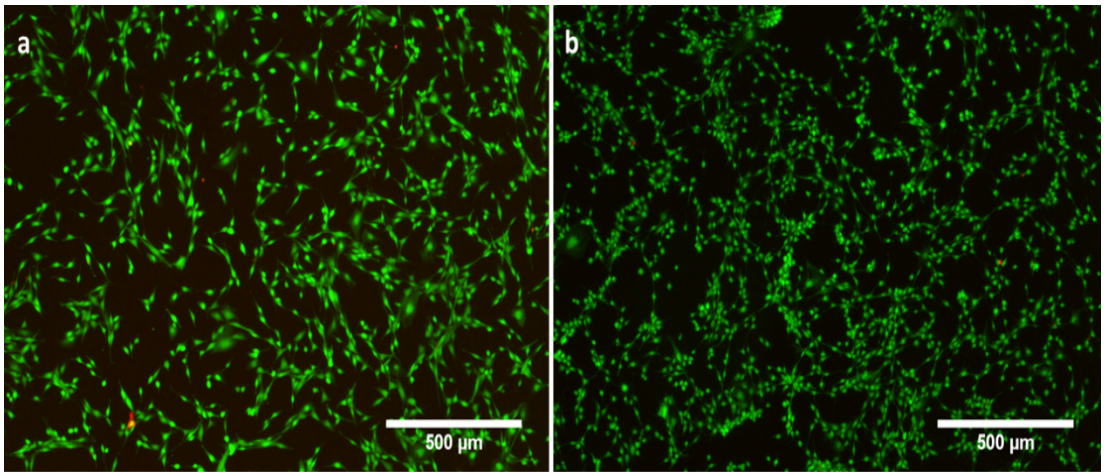

Figure 43: NIH-3T3 fibroblasts stained with Live/Dead stain after culture for 24 hours on (a) an uncoated glass surface (control) and (b) PA-Au NRs coated glass surface (2.6×10^{12} Au NRs/mL). Live cells are stained green (Calcein AM) and non-vi able cells are are stained red by propidium iodide.

5.2.2 NIR irradiation, cell detachment and cell viability of NIH-3T3 fibroblasts

There are very few studies investigating the application of gold nanostructures to cell detachment. The first study was published in 2012 by Kolesnikova *et al*., who demonstrated the detachment of NIH-3T3 fibroblasts, grown on gold nano particles, when exposed to visible light using a green laser (532 nm) [334]. The second study conducted by Giner-Casares *et al*., in 2016, developed plasmonic surfaces of dense gold nanostructures by the process of chemical growth [335]. Cells such as HeLa, A549, HUVEC, T3T and J774 were seeded on this surface, proliferated and then irradiated with near infrared radiation of 980nm. A successful detachment rate of 80-100% was seen for all cell types tested. Re-seeded cells were viable and proliferation of these re-seeded cells were observed. While both the studies showed successful cell detachment, there are some disadvantages to each of these approaches. Studies (examining the effects of 523 nm on cells) have shown that longer exposures not only decrease cell proliferation but also result in damage to cellular DNA [522, 523]. Additionally, chemical growth of gold nanostructures is a multi-step, time consuming process that would be costly to scale up. Here, a simple coating process was used to attach gold nanorods to culture surfaces and NIR irradiation at 785 nm to facilitate detachment as wavelengths in the NIR region have a low scattering coefficient and little consequence for biological tissues [524].

Studies on ProA-Au NRs surface

Cell detatchment studies were undertaken to compare the Au NRs attachment

chemistries on glass. These studies were initated after 24 hours of cell culture (Figure 44). Figure 44 a shows NIH-3T3 fibroblasts cultured on ProA-Au NRs coated surface for 24 hour pre-NIR irradiation. After 24 hours of culture the samples were exposed to NIR irradiation of 785 nm wavelength for 1 hour at 566 mW/cm^2. Post irradiation cell detachment can clearly be observed in Figure 44 (b). But few cells can still be seen attached to the ProA-Au NRs coated surface post irradiation. In Figure 32 of chapter 3, the SEM images shows ProA-Au NRs coverage over the entire surface area, however the extent of ProA-Au NRs attachment is not even across the substrate. This may explain why complete cell detachment cannot be observed from the ProA-Au NRs coated surface post NIR irradiation.

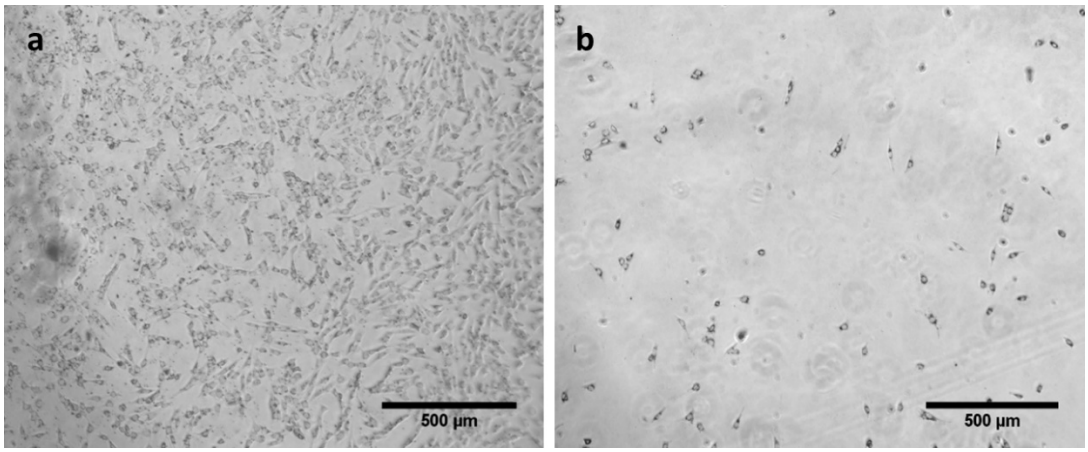

Figure 44: NIH-3T3 fibroblasts cultured on ProA-Au NRs (2.5 ×10^{12} Au NRs/ml) coated glass surface and irradiated with NIR laser. (a) Cell on the surface pre NIR - irradiation and (b) post NIR – irradiation. Post-irradiation, a clear detachment of cells from the surface can be observed.

NIH-3T3 fibroblasts detached via NIR irradiation were collected, re-seeded and cultured for 24 hours at 37 ºC in an atmosphere of humidified 5 % CO_2/ 95 % air. After 24 hours of culture. Live/Dead analyses was performed on the cells to investigate if the process of laser detachment may have induced apoptosis in the cells. From Figure 45 it can be observed that the majority of the cells, that adhered to the surface, are stained green. This indicates that a proportion of the cells, that were detached and re-seeded, have recovered and were viable even after being exposed to laser for 1 hour. The lack of red stained cells, after 24 hours, indicates that the irradiation may not have had negative implications on the viability of adhered NIH-3T3 fibroblasts.

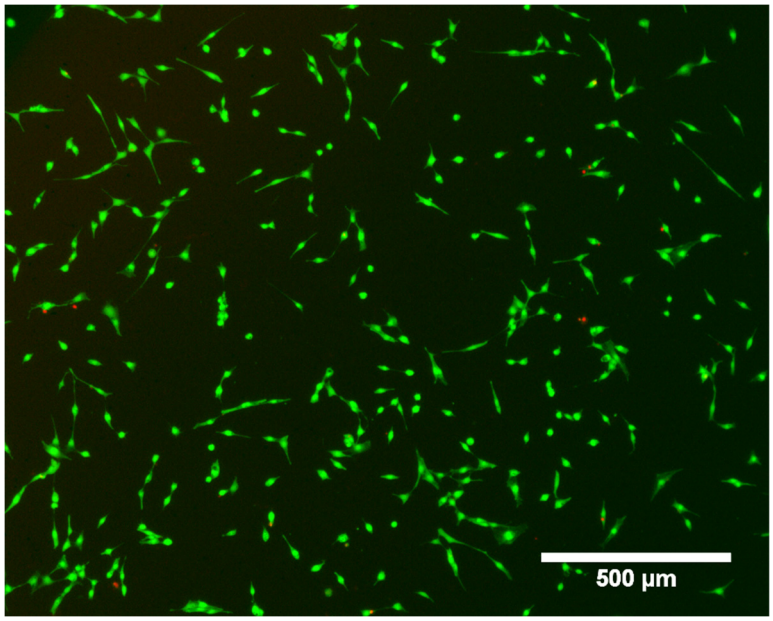

Figure 45: Live/Dead staining on NIH-3T3 cells detached via laser re-seeded after 24 hours. The cells can be observed to be viable and healthy.

Studies on PA-Au NRs surface

Figure 46 (a) displays the samples pre NIR irradiation and Figure 46 (b) shows the same sample, after being exposed to NIR irradiation of 785 nm wavelength for 1 hour at 566 mW/cm^2. Almost complete cell detachment from the PA-Au NRs coated substrate was seen to occur after NIR exposure (Figure 46 b). In comparison to the ProA-Au NRs coated surface (Figure 46 b), almost 100% cell detachment can be seen qualitatively post-irradiation.

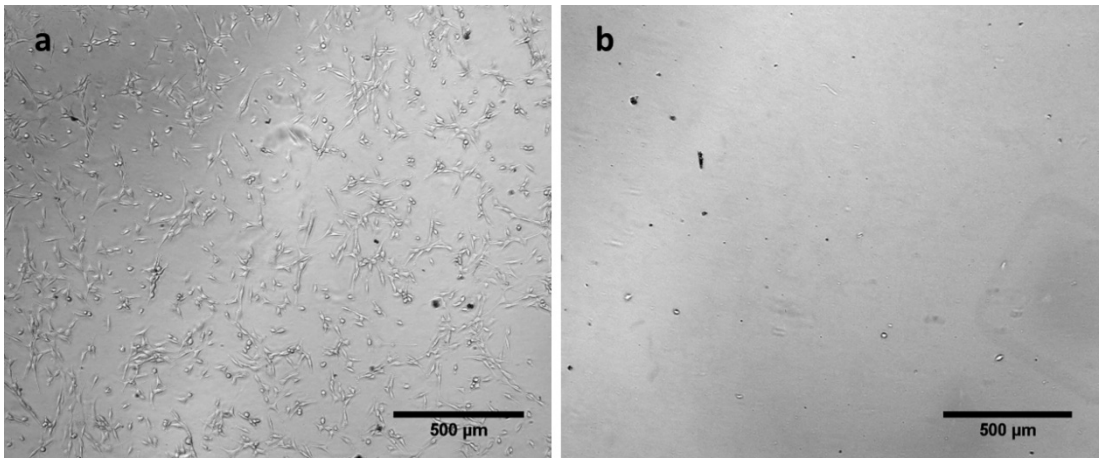

Figure 46: NIH –3T3 fibroblasts grown on PA - Au NRs (2.6 ×10^{12} Au NRs/mL) coated surface. (a) Before NIR irradiation and (b) 1 hour after NIR irradiation. Clear detachment of cell detachment was observed post-irradiation.

NIH-3T3 cells detached via NIR irradiation from PA-Au NRs coated surface were re-seeded onto a TCPS surface and cultured for 24 hours at 37 ºC in an

atmosphere of humidified 5 % CO_2/ 95 % air atmospheric pressure. Figure 47 shows the Live/Dead staining performed on these cells to investigate if detachment via laser irradiation was cytotoxic. The presence of green stained and lack of red stained cells indicates that the cells are viable and that the 1-hour irradiation has no negative effect on the proliferation and viability of the cells.

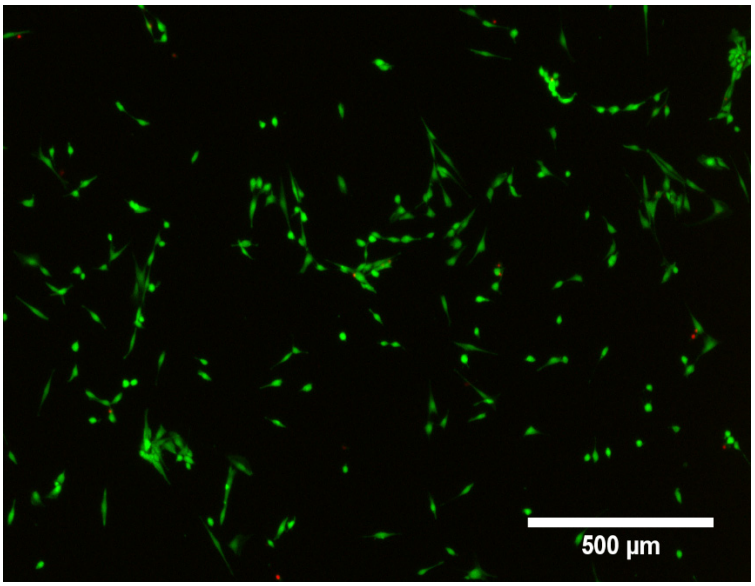

Figure 47: Live/Dead staining on NIH-3T3 cells detached via NIR irradiation and cultured for 24 hours. Green fluorescence indicate that the cells are viable and healthy.

The difference in detachment of NIH-3T3 fibroblasts from both the surfaces, post NIR-irradiation, may have been relative to the spread and density of the Au NRs present on the cell culture surface. The SEM images (Chapter 4, Figure 32) of the ProA-Au NRs coated surface shown an uneven distribution and large amounts of Au NRs aggregates across the cell culture surface. Opposed to this, the SEM images of PA-Au NRs coated surface (Chapter 4, Figure 34) show an even distribution of Au NRs coupled via of PA-chemistry with little or no aggregation. Calculations have shown that on a ProA-Au NRs surface, each NIH-3T3 fibroblast cell was exposed to approximately 38 gold nanorods. But when cultured on PA-Au NRs surface, each cell was exposed to nearly 1192 nanoparticles. The ratio of nanoparticles to cell exposure in case of PA-Au NRs surface was 31 times higher when compared with ProA-Au NRs surface. In addition to this, the Au NRs being more evenly distributed across the culture surface may have enabled the cells to have a larger contact area with the nanorods, which in turn allows a higher amount of cell detachment post-irradiation.

5.2.3 Human mesenchymal stem cells (hMSCs)

The methods developed for cell detachment via NIR irradiation using NIH-3T3 fibroblasts were then applied to hMSC. Here I examined in detail the viability, differentiation and gene expression of the cells before and following irradiation and re-cultured. In section 5.2.2 it was observed that a higher rate of NIH-3T3 fibroblasts detachment from PA-Au NRs coated surface when compared to ProA-Au NRs surface. Due to these results, all the hMSCs cell studies were performed on PA-Au NRs coated surface. The hMSCs were cultured on glass surfaces coated with PA-Au NRs (2.6 $\times 10^{12}$ Au NRs/mL) for 24 hours under standard conditions.

Cell viability on Au NRs coated surface on non-NIR irradiated cells

Here I explored effects of PA-Au NRs surface on hMSCs by performing the PrestoBlue assay (Figure 48) and Live/Dead assay (Figure 49). In this study, the cultured cells were not subjected to NIR stimulation.

The results obtained for 24-hour culture of hMSCs on PA-Au NRs coated glass surfaces compared to control surfaces are shown in Figure 48. There was no significant difference in levels of fluorescence (as a measure of cellular metabolic activity) at this time point between all samples. However, similarly to NIH-3T3 mouse fibroblasts grown on the same surfaces (Figure 42), hMSCs showed an approximately 10-15% reduction in fluorescence detected with increasing concentration of Au NRs. However, statistical comparison across all the PA-Au NRs coated surfaces (unpaired t-tests) revealed no significant differences between the metabolic activity of the cells cultured on any of the Au NRs functionalised substrates (Figure 48). The t-test done on the samples have shown that the difference among the samples are statistically insignificant ($p<0.05$).

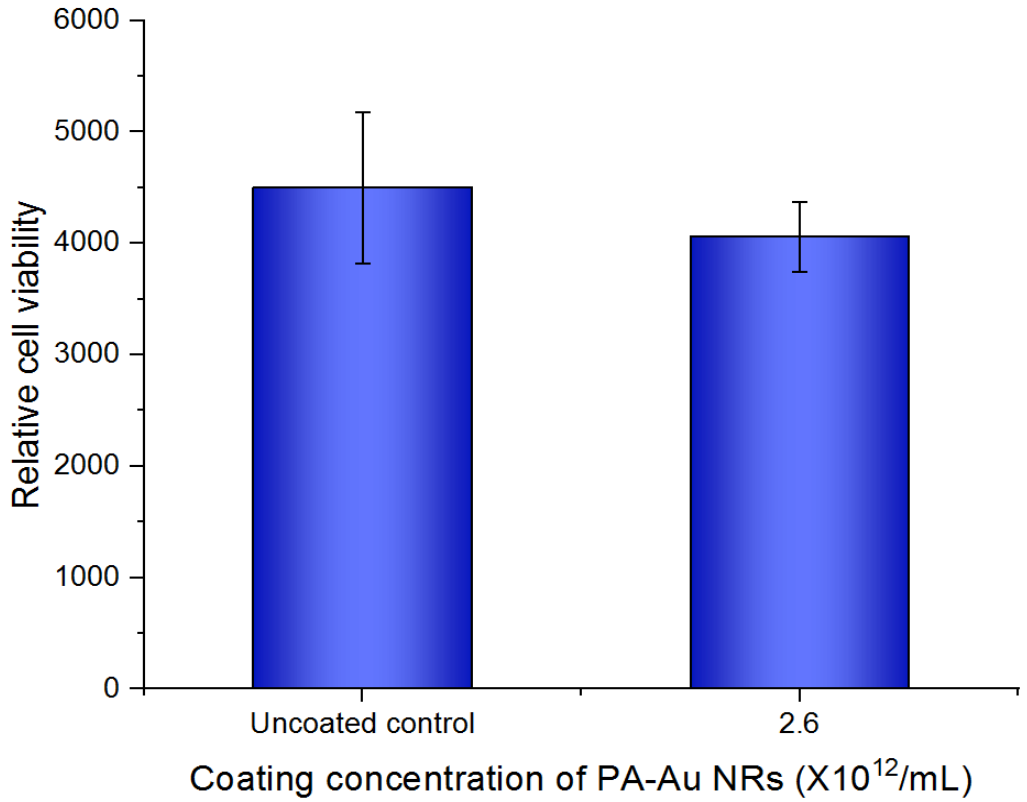

Figure 48: PrestoBlue assay comparing the viability between hMSCs cultured on uncoated control to PA-Au NRs coated surface. While a drop in viability is noted in hMSCs grown on PA-Au NRs coated surface, the difference was statistically insignificant. Standard deviation was used. Error bars show ± 1 standard deviation from the mean.

Figure 49 hMSCs cultured on glass surface (a) and on PA-Au NRs (b) for 24 hours. In both the cases the majority of the cells are stained green, confirming that the cells are healthy and viable. The lack of non-viable (red stained cells) indicates that the PA-Au NRs coated substrates were not cytotoxic to the cultured hMSCs.

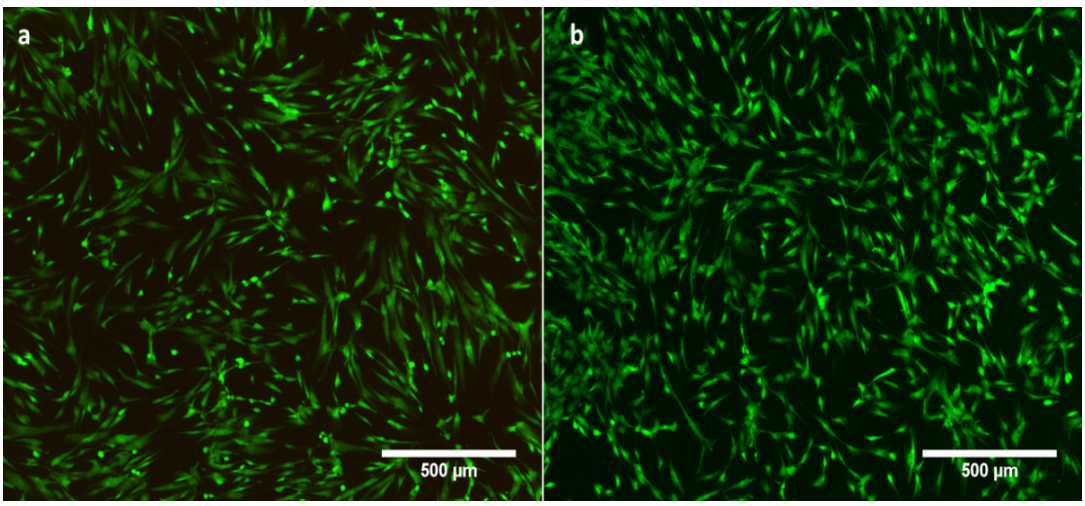

Figure 49: Live/Dead staining after 24 hours culture of hMSCs on (a) control glass surface and (b) PA-Au NRs coated glass surface. Cell in neither of the surface display red nuclei, thereby showing that all the cells imaged are viable.

Overall, the PrestoBlue assay and Live/Dead staining conducted on the NIH – 3T3 fibroblasts and hMSCs cultured on the various PA-Au NRs coated surfaces and glass shows that there is no decrease in metabolic activity of the cells regardless of the coating. The findings reported here (for the ability of the PA-Au NRs and the ProA-Au NRs surfaces to support growth of both fibroblasts and hMSCs) are consistent with studies reported in the literature examining the biocompatibility of surface-adsorbed Au NRs. These include studies examining a range of substrates and absorption chemistries. In various studies substrates including polystyrene sulfonate [490, 525], polycyclic aromatic hydrocarbon [525], polyacrylic acid, poly(allylamine) hydrochloride [491] and polyethylene glycol [526] were used to masking or completely remove CTAB present on the Au NRs surface. Studies were conducted on wide range of cell types such as human colon carcinoma cells (HT-29, HCT116), oral cancer cells, mammary adenocarcinoma (SKBR3), Chinese hamster ovary (CHO), mouse myoblast (C2C12), human leukaemia cell lines (HL60) and human gingival epithelioid cells. All the studies showed biocompatibility between the capped Au NRs and different cell types. While Parab *et al*., indicated an increase in cell proliferation in presence of the Au NRs [490], Rayavarapu *et al*., showed that the biocompatibility is also dependant on the cell type [526]. HL60, which is a less robust cell line, displayed high cytotoxicity which was not seen in other cell types to when exposed to PEG-Au NRs.

No such cytotoxic effect was seen in the data presented in this thesis which provide further confirmation that surface absorbed PA-Au NRs are suitable for development of platforms for both laboratory-based and industrial scale production of hMSCs and other cell types. Here I have further investigated their application to non-enzymatic cell detachment strategies using NIR.

Time measurement for total cell detachment

As previously mentioned, all hMSCs were cultured on PA-Au NRs coated surface (2.6×10^{12} Au NRs/mL) for 24 hours. After this time, the samples were exposed to NIR irradiation for different times up to 60 minutes to determine the minimum time needed to achieve complete detachment. This study was conducted to investigate the NIR laser exposure time required for hMSCs to detach from PA-Au NRs coated substrates. Four different time points were studied, namely 15 minutes, 30 minutes, 45 minutes and 60 minutes (Figure 50).

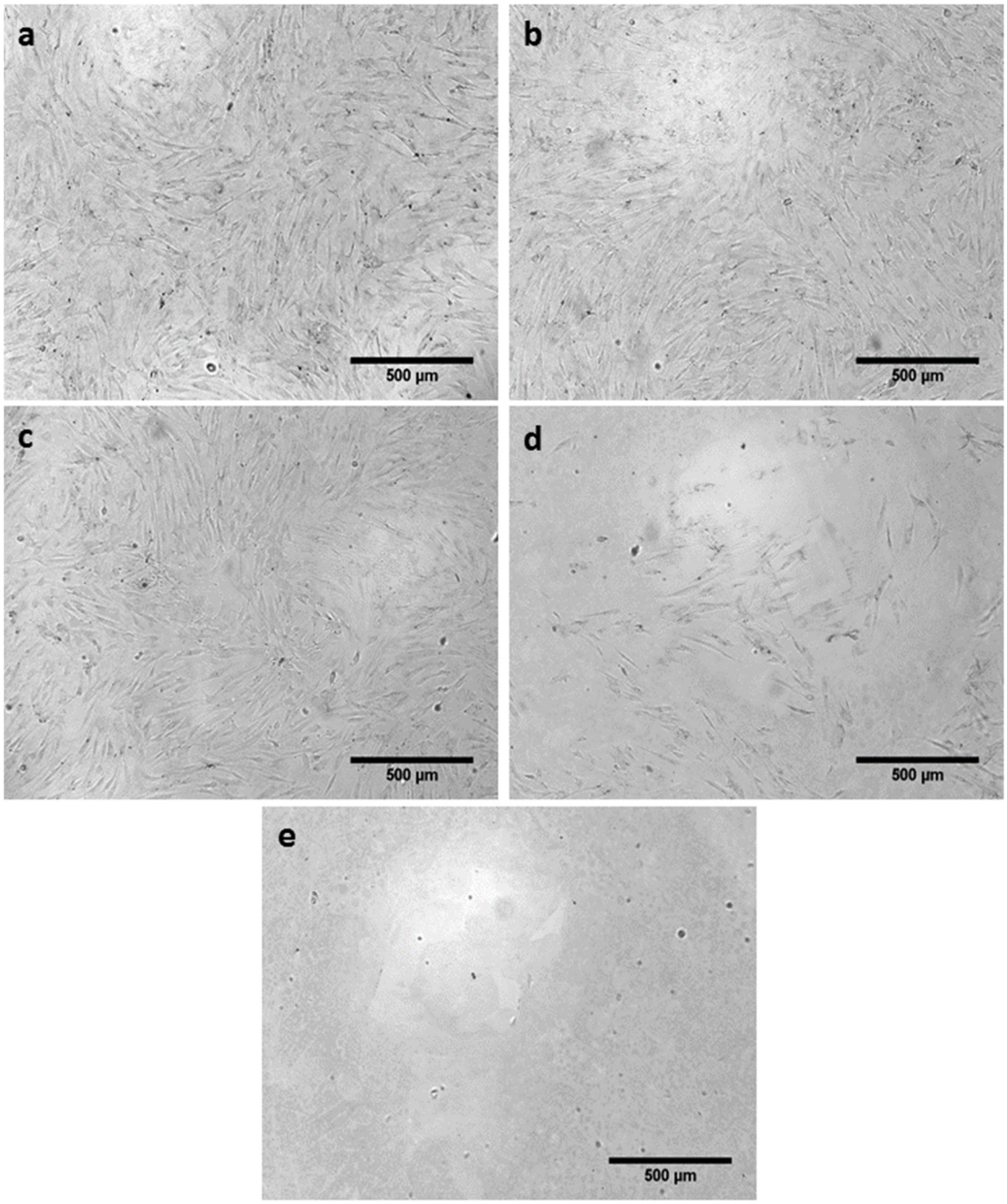

Figure 50: hMSCs cultured for 24 hours on PA-Au NRs coated surface (2.6×10^{12} Au NRS/mL) and exposed to NIR irradiation. (a) Before NIR irradiation, (b) 15 minutes of NIR irradiation, (c) 30 minutes of NIR irradiation, (d) 45 minutes of NIR irradiation and (e) 60 minutes of NIR irradiation. No cell detachment is seen at 15 minutes and 30 minutes. At 45 minutes partial detachment is observed. Complete cell detachment is seen at 60 minutes.

Figure 50 shows various NIR exposure times on hMSCs cultured on PA-Au NRs. Up to 30 minutes exposure very little cell detachment can be observed (Figure 50 b & c), at 45 minutes I observe partial cell detachment (Figure 50 d). At this Au NRs concentration and laser power density, NIR exposure times of 1 hour or more are required for complete cell detachment from the PA-Au NRs functionalised substrates (Figure 50). Thus, it was decided that for all future experiments 1-hour NIR exposure

would be used to ensure complete detachment.

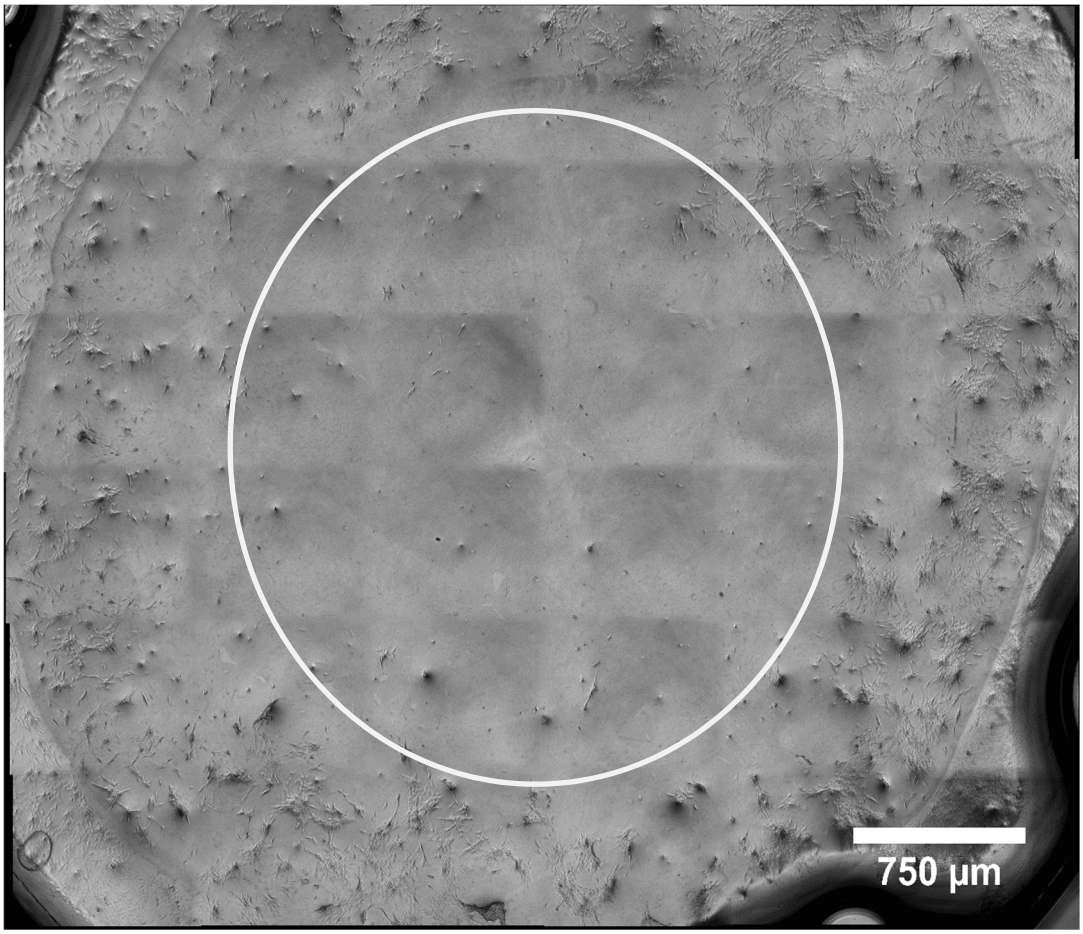

Figure 51: A composite image of hMSCs culture surface post NIR irradiation. An area almost devoid of attached cells can be observed in the centre of the image, co-incident with the area of NIR irradiation (white ellipse) showing the detachment of cells after the irradiation process.

Figure 51 shows stitched bright-field images of the total area of the PA-Au NRs substrate exposed to the NIR irradiation. An elliptical region that is almost devoid of attached cells can be observed in the centre of the image. This area is co-incident with the area of NIR irradiation and has a diameter of approximately 3 mm which corresponds to the expected/measured diameter of the NIR laser beam.

The exposure time, laser power density and the density of Au NRs are predominant factors for cell detachment. While the irradiation time varied between 5 – 40 minutes in the studies conducted by Giner-Casares *et al.*, Kolesnikova *et al*., had a maximum exposure time of 2 minutes [334, 335]. Though both the studies have shown successful cell detachment, it was observed that the power density varied widely. While Giner-Casares *et al*., used power density varying between 145 mW/cm^2 to 340 mW/cm^2 (NIR wavelength), Kolesnikova *et al*., used a power density of 1.5kW/cm^2 (green light). When compared to these two studies, the power density

produced by the NIR laser used in this thesis was recorded as 566 mW/cm^2. This was between 1.5 to 4 times higher than the studies conducted by Giner-Casares *et al.,* and 3 times lower than Kolesnikova *et al*. It should be kept in mind that Kolesnikova *et al* used light of green wavelength and not NIR wavelength. Since Giner-Casares *et al.,* showed that cell detachment is possible at less power densities and at lower time period, it was necessary to look at other parameters that might be different in these studies compared to theirs.

It was observed that the surface coverage of the gold nanoparticles produced by Giner-Casares *et al*., was high compared to the Au NRs covered surface used for this thesis. By using chemical growth process, a dense array of gold structures were developed on the cell culture surface by Giner-Casares *et al* [335]. While the study conducted by Giner-Casares *et al*., showed NIH-3T3 fibroblasts detaching after 40 minutes of NIR irradiation, the same cells had to be exposed for 60 minutes in my studies in order to gain total detachment. The increase in time of exposure may be due to the surface coverage of the Au NRs. This can be confirmed by comparing the detachment of cells from PA-Au NRs to ProA-Au NRs. While 100% detachment was observed in PA-Au NRs coated surface, some cells were undetached from ProA-Au NRs surface post irradiation. The difference was in the surface coverage of the Au NRs (as observed in the SEM images in chapter 3). While an even coverage of nanorods was obtain when using PA-Au NRs, this was not possible for ProA-Au NRs.

In addition to this, according to Giner-Casares *et al.,* the difference in the cell detachment time was also dependant on size of the cell. They observed a slower (30-40 minutes) and less efficient cell detachment (80% detachment) from cells with smaller surface area when compared to cells with larger surface area (5-20 minutes of irradiation with 100% detachment rate) [335]. This may have been due to the larger cells being exposed to higher number of gold structures compared to smaller cells, thus allowing the larger cells to experience higher localised surface plasmon resonance. An exposure time period of 60 minutes was required for both the cells types (hMSCs and NIH-T3T fibroblasts) used in this research. Calculation have shown that both the cell types have similar surface area (~254.5 μm^2) which justifies the requirement of needing similar time of exposure.

5.2.4 hMSCs viability post detachment

hMSCs detached via NIR irradiation were tested for their ability to be re-cultured and to evaluate their viability. Similar to NIH-3T3 fibroblasts, this study was performed to investigate if the laser exposure affected the ability of detached cells to proliferate. Three different assays were performed for these studies, namely: (i) the PrestoBlue Assay (ii) Live/Dead staining and (iii) Propidium iodide (PI) studies via FACS to test the cell viability. Cells released via trypsin were used as controls for all these studies.

PrestoBlue assay

Cell proliferation of hMSC following collection of cells after detachment by either NIR irradiation or trypsinization and subsequent subculture was confirmed over a 7 day period using the PrestoBlue assay described in section 5.1.4.

Figure 52 represents the viability of re-seeded detached (via trypsin (control) and NIR irradiation) hMSCs over 7-day time period. Data collected on day 1 confirms the recovery of the cells after 24 hours of incubation post NIR irradiation. The viability of the cells recovered via laser irradiation are almost equal to those detached by trypsin. Over the course of 7 days a steady significant increase in the proliferation of hMSCs released by both NIR irradiation and trypsinization can be observed. On day 7 it can be observed a statistically significant increase in the viability of the cells released via NIR irradiation when compared to trypsinization. This result is consistent with other studies that show an increased proliferative capacity in cells post NIR irradiation [280, 281]. Statistical analyses (Student's t-test) revealed a significant difference in the metabolic activity of the subcultured hMSCs released via laser irradiation or trypsinization. The difference in metabolic activity of the cell maybe due to the difference in the proliferative rate of the hMSCs post cell detachment.

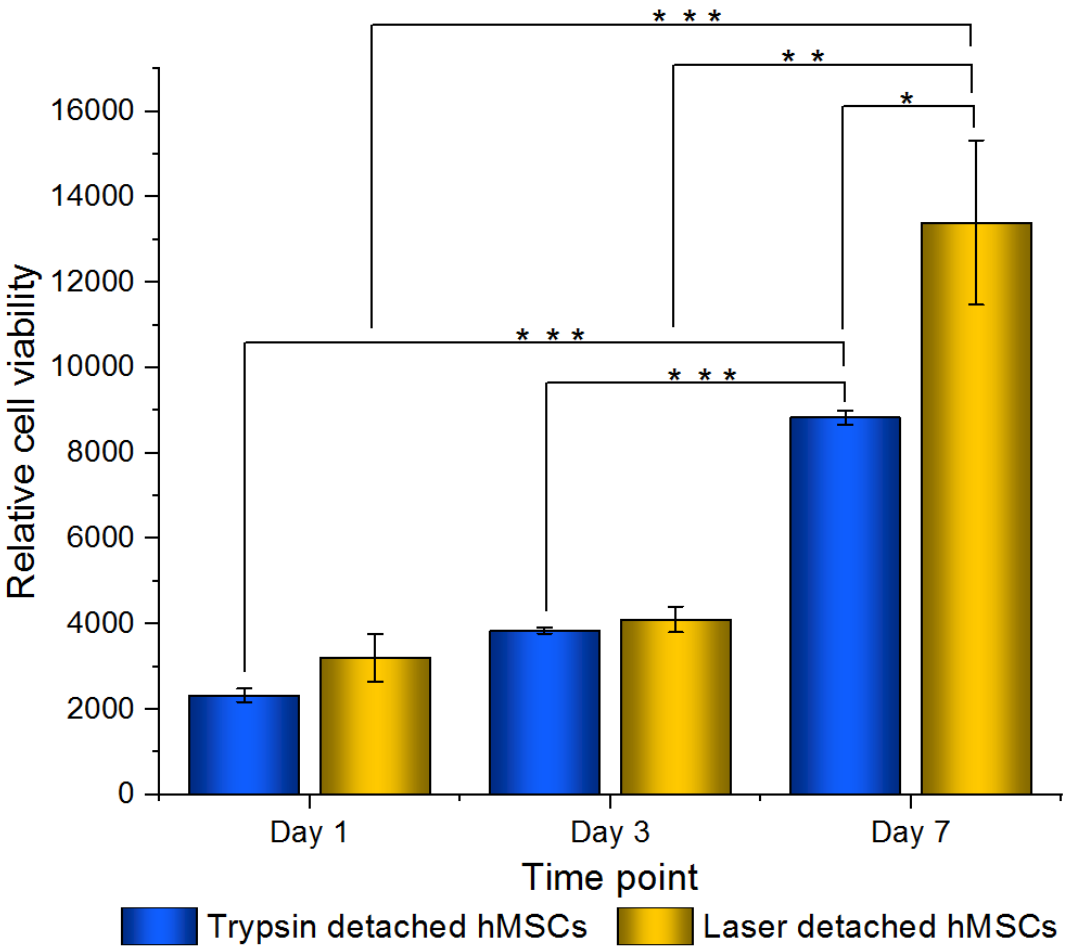

Figure 52: PrestoBlue analyses quantification of hMSCs detached via laser and trypsin and re-seeded over varying times. The hMSCs were observed to be viable and no statistical significance was seen over 7 days. Error bars represent the standard deviation between 3 independent experiments. Statistical analyses has shown significant difference between the cells. *p<0.05, **p<0.01 and ***p<0.001. Standard deviation was used. Error bars show ± 1 standard deviation from the mean.

Near infra-red lasers has been used for the past 40 years in clinical settings to stimulate various tissues to proliferate and regenerate at higher rates. Studies conducted by Tuby *et al*., demonstrated that pre-treating of hMSCs with NIR irradiation significantly increases the proliferative rate by two to five times [273] [280]. A 40% increase in proliferative capacity of hMSCs, in the first 24 hours, was noted by Károly Horvát-Karajz *et al*., after exposing the hMSCs to low powered laser irradiation [527]. It has been theorised that the ability of the NIR wavelength to easily penetrate the tissues cause a cascade of intra cellular reactions. The laser energy absorbed by intracellular chromophores is converted into metabolic energy which is used by the mitochondrial respiratory chain to create more ATP. The ATP generated is used to increase the DNA activity, synthesise proteins and RNA which may be responsible for increased tissue proliferation and regeneration [528].

Live/Dead assay

Figure 53 shows representative photomicrographs of hMSCs detached via trypsinization (Figure 53 a) and NIR irradiation (Figure 53 b & c) and re-cultured for 24 hours before staining with Live/Dead stain. Cells are predominately stained green indicating that they have intact membranes when detached and subcultured either by trypsinization or NIR irradiation. Cells subcultured following detachment by NIR were observed to be less evenly distributed over the culture well and formed cell clusters (Figure 53 c). This is likely to be a result of the observed detachment of cells in sheets rather than as individual cells as occurs during trypsinization. This suggests that the detachment of the cell by NIR irradiation on the Au NRs is mediated predominantly via disruption of basal surface attachment and that cell adhesion molecules (CAMs) on the baso-lateral and apical surfaces are unaffected by this method. In addition, it implies that other cell surface signalling molecules and receptors are also less likely to be affected by NIR than by exposure to the general protease trypsin.

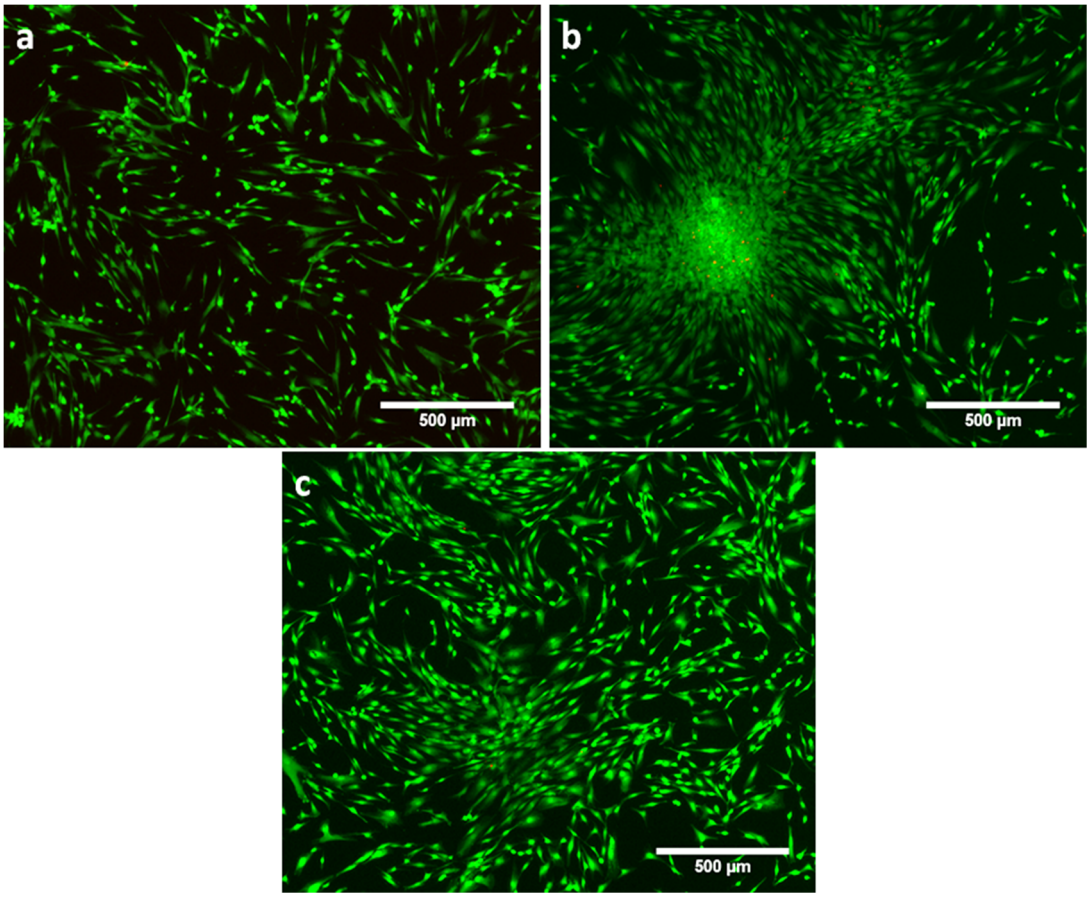

Figure 53: Live/Dead assay on re-seeded hMSCs after 24 hours of detachment. Detachment induced via (a) trypsinization, (b & c) NIR irradiation. A spread out of hMSCs is seen when detached via trypsin (a). When detached via NIR-irradiation, a cluster of hMSCs is formed due to the cells being released as sheets (b). These clusters can be dissociated by mechanical dissociation (c).

The cell clusters (Figure 53 b) could be mechanically disrupted by gently pipetting them multiple times in the well plates. This lead to the dissociation of the cells from the cell cluster allowing them to individually spread across the culture plate (Figure 53 c). To confirm the presence of CAMs in the NIR detached cells the presence of selected ECM and other surface molecules will be examined in trypsinized and NIR detached hMSCs in section 5.2.9.

PI FACS staining

In addition to PrestoBlue and Live/Dead assay, quantitative viability of the detached and re-seeded hMSCs were studied after 5 days of cell culture using PI staining. Studies conducted by Palankar *et al*., showed Au NRs coupled with NIR can induce nanopores formation in the lipid membrane structure of the cells due to thermal interaction [529]. Live/Dead assay conducted by Giner-Casares *et al*., on plasmon surface based NIR detached cells, showed a large proportion of dead cells, which was higher when compared to MTT assay [335]. The presence of metabolic activity suggests that the pore formation may have allowed the PI to pass through the ruptured membrane and that the nano pores may not be cytotoxic to the cells. All Live/Dead assays conducted in this study were performed 24 hours post cell detachment. This time period may have allowed the cells to recover from the nanopores formation leading to the observation of viable cells the following day. While PrestoBlue assay showed the viability of the cells over 7 days' time period, flow cytometry was used to quantify the percentage of cells staining positively for PI. This would quantitatively indicate if any disruption of the cell membrane persisted after 5 days post subculture.

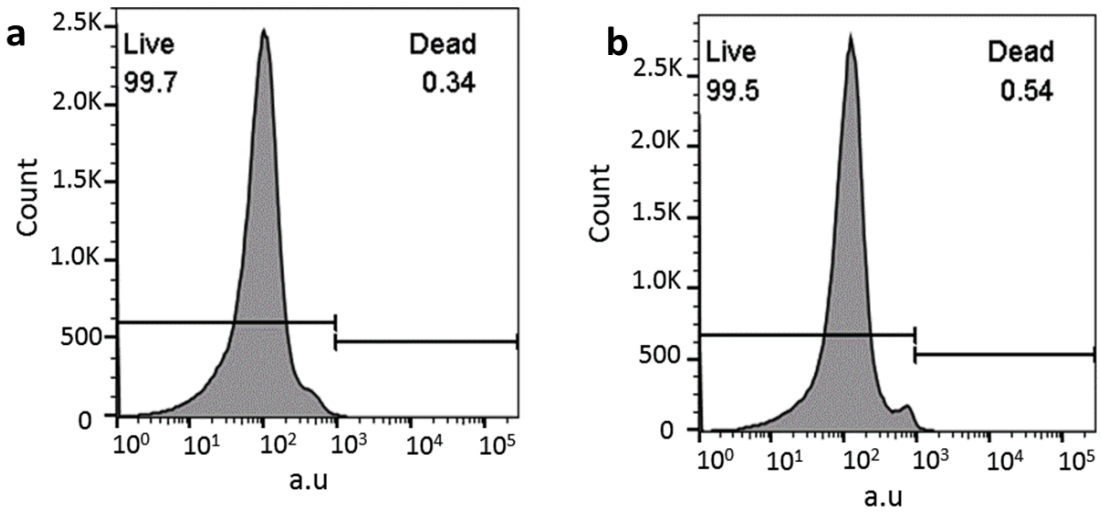

Figure 54: FACS analyses of PI stained sub-cultured cells (a) cells released via NIR Irradiation (b) cells detached via trypsin

Figure 54 shows the viability of cells released via NIR Irradiation and trypsin. The histograms show the number of cells displaying various amounts PI, at fluorescent intensities between 10^0 - 10^3 a.u the cells are considered viable and at fluorescent intensities greater than 10^3 a.u the cells are considered non-viable. Both histograms show that the overwhelming majority of the cells (in each case) are viable (99.7 % for laser detached and 99.5 % for trypsinized cells). This further proves that laser irradiation at the wavelength and power densities used here has no adverse effect on the cells viability of the cells when compared to trypsinization.

5.2.5 FACS: Immunophenotype of hMSCs

It should be noted that TrypLE express (as mentioned in 5.1.1) and not animal derived trypsin, was used to dissociate cells enzymatically for our studies. A study was conducted by Tsuji *et al*., to investigate the effects of various cell detachment reagents on the surface proteins of hMSCs [194]. These reagents included animal derived trypsin, TrypLE and collagenase. The study showed that of all the reagents used, animal derived trypsin had the most adverse effect on the cell surface proteins. All the positive markers expressed by the hMSCs were significantly reduced by animal derived trypsin. While markers such as CD140a disappeared during 5 minutes of exposure, markers such as CD55, CD105 and CD140b were negatively affected and almost disappeared after 30 minutes of exposure. Compared to animal derived trypsin, TrypLE and collagenase had a milder effect on the surface proteins.

In my studies, I have analysed if exposing and detaching the cells by NIR irradiation has any effect on the multipotency of the cells compared to trypsinization by TrypLE. Immunophenotypic characterization of hMSCs was achieved by analysing the expression of proteins that are known to be present on the surface of multipotent hMSCs. The cell surface proteins investigated were CD44, CD73, CD90 and CD105 [530, 531]. The use of this set of markers for characterization of multipotent hMSCs were proposed by International Society of cellular therapy [532]. Unstained subcultured laser detached cells and unstained trypsin cells were used as controls for cell detached via trypsin and NIR laser exposure.

Figure 55, shows the quantification of the extent of fluorescent antibody binding to the hMSCs markers described above, by FACS. Both the cells detached by NIR laser exposure and trypsinization show positive and identical expression of all the surface proteins tested. This suggests that cells released by NIR irradiation detachment

have very similar levels of surface protein expression to trypsinized cells and therefore retain their multipotency. This maintained multipotency after laser exposure validates the feasibility of further experiments investigating if laser exposure has any effects on their ability to differentiate into Adipocytes or Osteocytes.

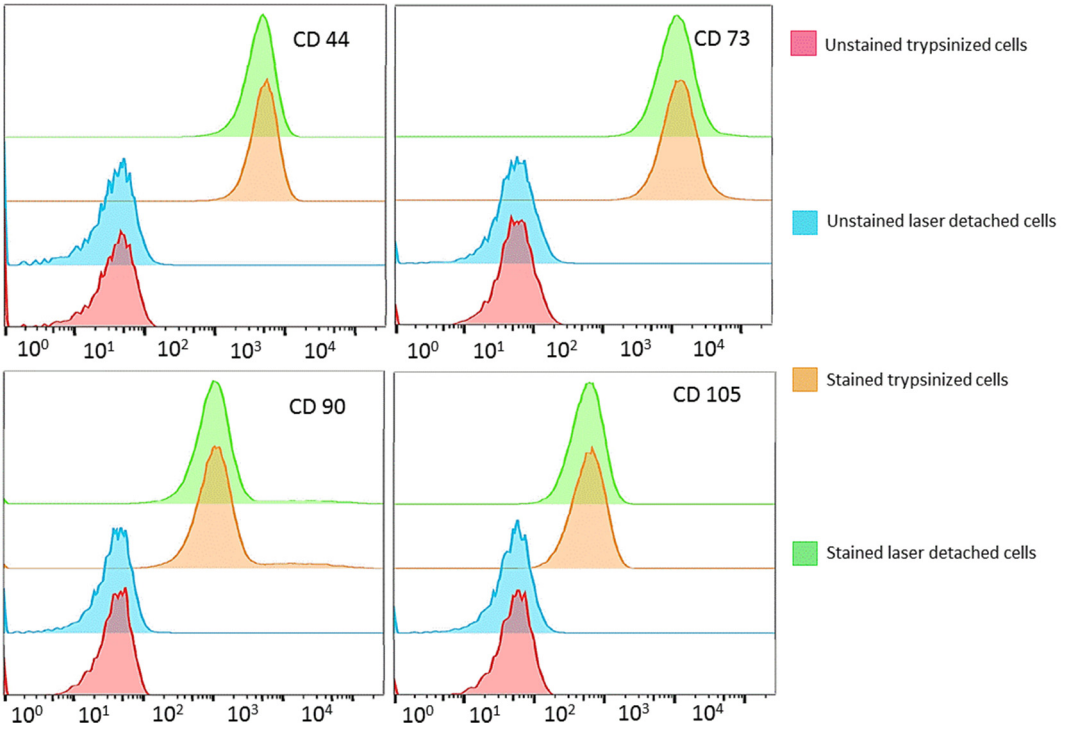

Figure 55: Comparison of surface markers expressed by trypsinized cells and detached via NIR irradiation. The histograms represent the surface markers on the hMSCs. The phenotype characterization does not show any difference for expression in all hMSC markers. (a) CD44, (b) CD73, (c) CD90 and (d) CD105.

5.2.6 Theory behind cell viability, cell detachment and post-detachment cell viability

While gold occurring in bulk is deemed to be chemically inert, nanoparticles such as gold nanorods have to be examined for biocompatibility and cellular toxicity when used in biological applications. A review conducted by Murphy *et al*., states that the surface chemistry of Au NRs can influence the biological behaviour and cytotoxicity in cells [533]. The synthesis and deposition of gold nanorods requires a structure-directing and stabilizing agent such as cetyltrimethylammonium bromide (CTAB). On gold nanorods, CTAB forms a tightly bound cationic bilayer and the presence of CTAB is stabilizes the gold nanorods preventing them from self-aggregation in solutions [534, 535]. But studies have shown that CTAB Au NRs have a cytotoxic effect on cultured cells [328, 536, 537]. In order to avoid the cytotoxic effect displayed by CTAB stabilized Au NRs, protein A coated Au NRs and polyamine

conjugated Au NRs were used in our studies. Studies on silicon coated gold nanorods were not undertaken due to non-reproducible and sparse surface coating displayed by the SiO_2-Au NRs.

From all the above experiments, successful detachment of cells was seen when the cells, cultured on Au NRs coated surface, were exposed to the NIR laser (Figure 44, Figure 46 and Figure 50). It is known that the cell detachment is mediated by the generation of localised surface plasmon resonance (LSPR) at the apex of Au NRs when irradiated with NIR radiation. The generation of LSPR is detailed in chapter 2, section 2.11.1. In non-spherical nanostructures such as Au NRs LSPR produces strong enhancement in the electromagnetic field that propagates across the nanoparticles and is concentrated at the apex of the nanostructures [293, 538, 539].

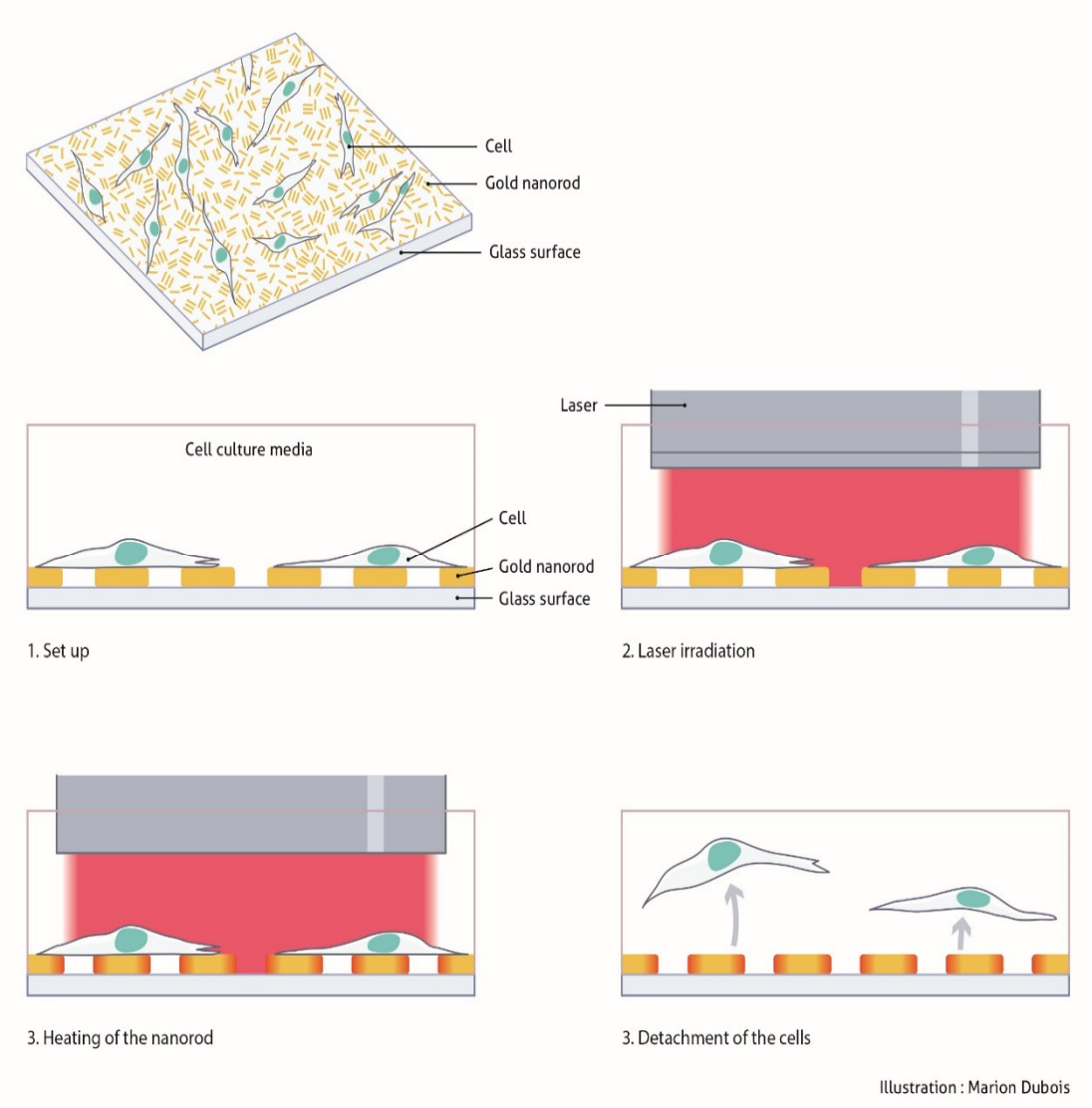

Figure 56: Cell detachment mechanism from Au NRs coated surface. The reactions taking place at the apex of the nanorods due to NIR irradiation leads to cell detachment.

It is this strong enhancement of the electromagnetic field generated by the LSPR that mediates cell detachment in our device. It is possible that this happens in one of two ways:

1. By a photothermal effect, caused when the LSPR effect results in a strong enhancement of the electromagnetic field at the apex of our Au NRs. The excess photon energy is rapidly converted to heat due to electron-photon coupling and electron-electron scattering, leading to nanoscale localised increases in temperature [485, 540]. These highly localised temperature spikes likely produce transient effect in the protein network that mediate cell:substrate effects weakening the cell adhesion and allowing cells to be easily removed.
2. By a photochemical effect, caused due to excess photon energy concentrated at the apex of the Au NRs due to the LSPR effect, which can also be converted into chemical forms. The LSPR triggers photochemical reactions with organic molecules in the cell culture media generating Reactive Oxygen Species (ROS). ROS themselves are highly reactive due to the presence of oxygen free radicals and can diffuse to the cell:substrate interface and damage the chemical bonds that mediate cell attachment, once again allowing cellular detachment [541]. Under normal circumstance, oxidative stress caused by high concentrations of ROS can trigger intracellular signalling pathways in the cells which causes mitochondrial fission (apoptosis) [542, 543]. Unregulated or higher concentrations of ROS can result in cytotoxicity, cellular dysfunction, mitochondrial DNA damage, cellular necrosis and ultimately apoptosis in cells [544-546].

In my studies, I hypothesize that the cellular detachment is caused mainly due to the photothermal effect. As described above, if the detachment was due to ROS effect, I would expect to see some cytotoxic effect due to oxidative stress resulting in a higher amount of cell death upon detachment. On the contrary in Figure 52, when the trypsinized cells are compared to the NIR-laser detached cells, it can be observed that the cell viability and proliferation rate are almost the same. Furthermore, the hMSCs have shown a steady growth rate over 7 days' indicating no permanent damage. Live/Dead assay performed after 24 hours also displayed healthy hMSCs. PI staining of hMSCs quantified by FACS (Figure 54), released by both the detachment technique,

have also shown a high cell viability rate with <1% apoptotic cells in either of the cases. Thus there is little or no evidence of ROS being involved in the detachment of cells from the Au NRs coated surfaces.

From these results I can conclude that, it is likely a photothermal effect taking place at the cell-substrate level may be leading to cell detachment and not ROS effect. Previous investigation (chapter 3, section 4.3.3) has shown a mild increase in the bulk heat of the CCM (present around the sample) during NIR irradiation. This also indicates an increase in the temperature at the nanoparticle level. Giner-Casares *et al*., states that, on a nanoscale level, there would have been a higher increase in temperature at the cell-nanoparticle interface causing a localized photothermal effect. Presumably this localized photothermal effect results in cellular detachment from the surface [335]. I theorise that the nanoscale heating effect between the cell:surface interface, maybe triggering a cascade reactions and this stimulates the cells to detach from the Au NRs coated surface.

The cell membrane or the plasma membrane is a semi permeable fluidic mosaic structure that is composed of protein, glycoproteins, lipids and phospholipids. Not only does the membrane helps in separated the cellular interior organelles form the outside environment but also in intercellular signal transduction, migration and cell adhesion [547]. Thermodynamic changes in the environment surrounding the cell is known to have an effect on the fluidic nature of the cell membrane. While low temperatures cause the membrane to become rigid and hypofluidic, increase in temperature leads hyperfluidization [548, 549]. Cellular adhesion to the ECM is mediated by CAMs such as integrins which are bound to the actin filament. The actin filaments along with other proteins form the cytoskeleton in the cells. Change in elasticity of the membrane due to hyperfluidization (as a result of thermal changes) can cause physical modification in the cell membrane. This may lead to the disruption of CAM clustering, thereby causing cell detachment.

As described earlier, I observed no cell detachment during first 30 minutes, partial cell detachment during 45 minutes and complete cell detachment after 60 minutes. This may be due to two reasons: the time required for the nanoparticles to reach an optimal temperature at the cell-nanoparticle interface and to stimulate cell detachment from the Au NRs coated surface. The dissipation of localized heating must be taken under consideration due to cell culture media.

5.2.7 hMSCs differentiation and gene expression

While researchers have shown that the NIR irradiation does have a positive effect on the ability of hMSCs to proliferate [280], some studies have also suggested NIR irradiation may also affect the ability of hMSCs to differentiate especially when differentiated into osteogenic cell line [275]. Studies were undertaken to determine if the hMSCs released via NIR irradiation would show the same differentiation potential as that of the trypsinized cells. This was done by differentiation of the detached hMSCs into adipogenic cells and osteogenic cells.

Adipogenic differentiation

hMSCs detached via trypsin and NIR irradiation were re-plated followed by adipogenesis induction for 25 days. Adipogenic induction and adipogenic maintenance media were cycled on cells cultured according to the manufactures protocol. After 25 days, the quantification of the extent of adipogenesis was achieved by investigating the triglyceride content of the cells using AdipoRed staining, fluorescent microscopy and UV Vis spectroscopy.

Representative micrographs of cells stained using AdipoRed are shown in Figure 57. As anticipated no triglycerides were observed in undifferentiated mesenchymal stem cell controls release via trypsin (Figure 57 a & b) and NIR irradiation (Figure 57 c & d). The red fluorescent fat vacuoles demonstrated in cells in Figure 57 (b & d) demonstrates that the cells detached by both NIR laser exposure and trypsinization have successfully differentiated into adipogenic cells.

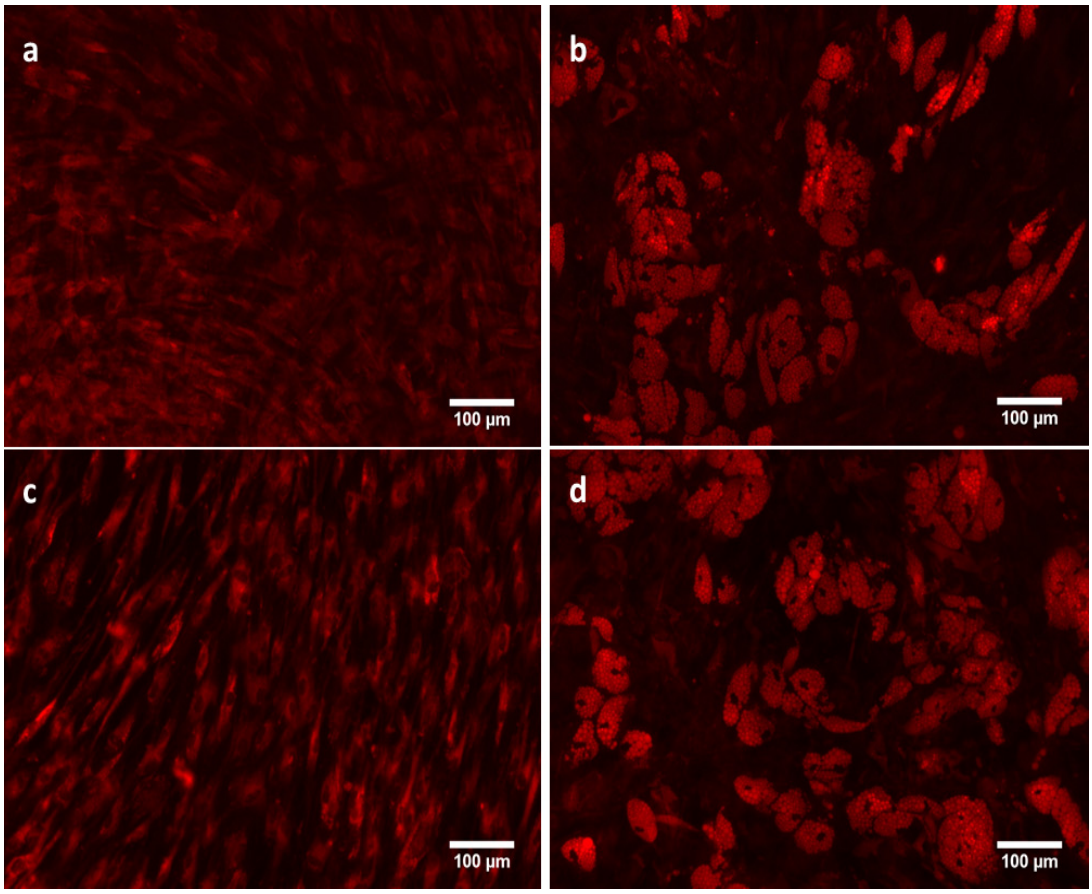

Figure 57: Adipogenic differentiation of (a) trypsin and (c) NIR laser detached cell controls showing no adipogenesis due to lack of adipogenic induction. Adipogenesis in (b) trypsinized hMSCs and (d) in hMSCs released via NIR-Irradiation after 25 days of adipogenic induction.

A quantitative analysis of the extent of adipogenesis for both laser detached and trypsinized cells was performed by fluorescence spectroscopy. Figure 58 shows the fluorescence intensity of AdipoRed stained hMSCs incubated in both differentiation and expansion media, for both the laser exposed and trypsinized cells.

From the graph in Figure 58 it can be observed that the NIR-detached cells show a slight increase in adipogenesis compared to the trypsinized cells. This difference was also shown to be statistically significant under Student's t-test.

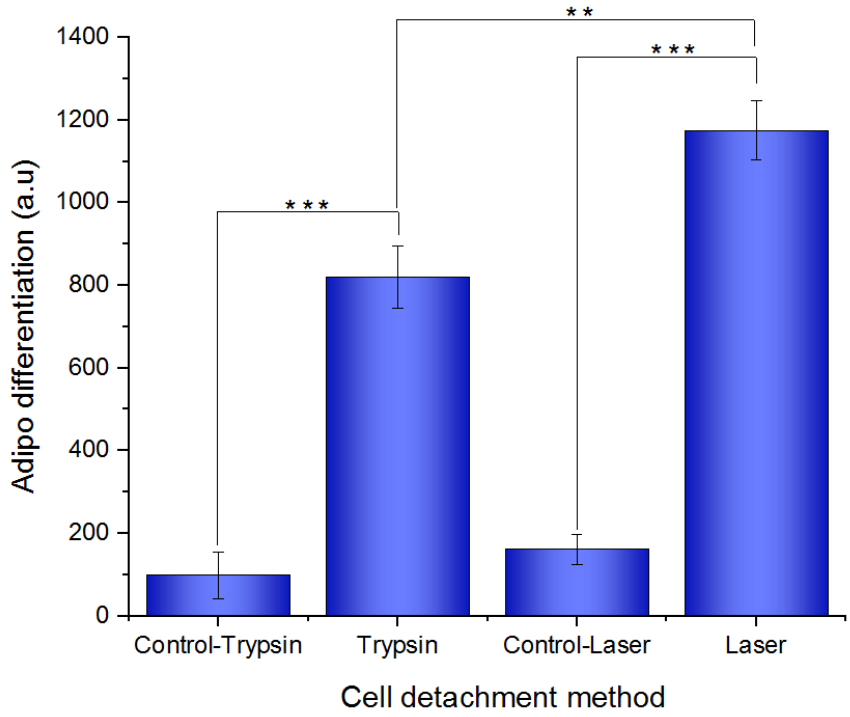

Figure 58: Fluorescent spectroscopy analyses of adipogenic differentiation in hMSC released via NIR irradiation and trypsin after 25 days of adipogenic induction *p<0.05, **p<0.01 and ***p<0.001. Standard deviation was used. Error bars show ± 1 standard deviation from the mean.

While red fluorescents can be qualitatively observed in the control non-adipo induced hMSCs (Figure 57 a & c), quantitative signals generated by undifferentiated control cells are also seen in Figure 58. This maybe mainly due to the intra cellular lipids that is present in all eukaryotic cells [550]. They can also be considered as background stains due to the possible presence of excess dye. Osteogenic differentiation

Following the adipogenic analyses, osteogenic analyses were performed in order to test the osteogenic potential of the hMSCs after NIR-exposure. hMSCs detached by laser irradiation were re-plated and cultured in osteogenic induction media. After 21 days, the cells were analysed by quantifying levels of calcium expression (by Alizarin Red S staining) in the laser detached cells and comparing it to levels in trypsinized cells.

Representative photomicrographs of Alizarin Red S staining of calcium deposits produced in hMSC after they have undergone osteogenic differentiation is shown in Figure 59. No Alizarin Red S staining can be seen in the undifferentiated controls (Figure 59 a & c) confirming the absence of osteogenesis. In Figure 59 (b & d) extensive Alizarin Red S staining can be seen in cells detached via NIR irradiation and

after trypsinization, that were cultured for 21 days in the osteogenic differentiation media.

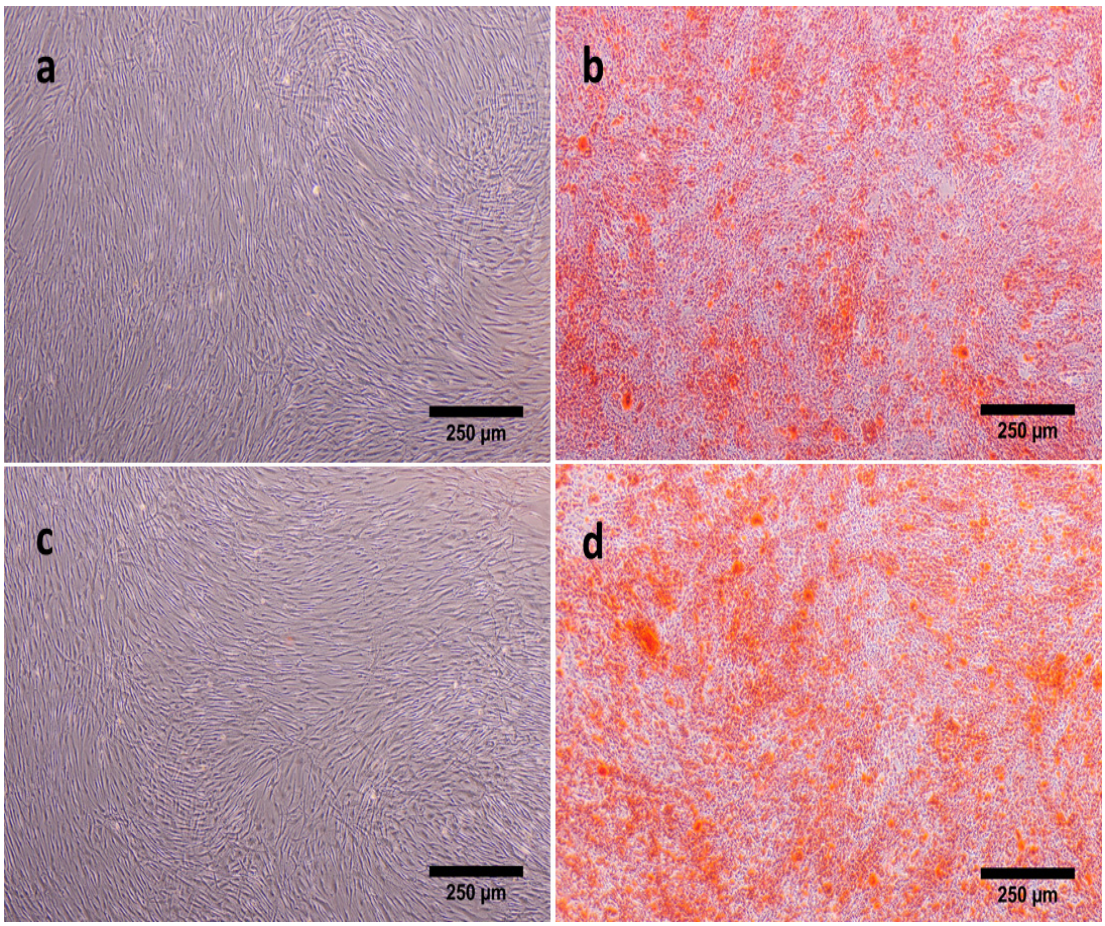

Figure 59: Alizarin Red S staining of (a) trypsinized and (c) NIR laser detached cell controls show no osteogenic differentiation. Osteogenesis can be observed in (b) trypsinized hMSCs and (d) NIR irradiation detached hMSCs after 21 days of osteogenic induction

A quantitative analysis of the above samples was performed using UV Vis spectroscopy. Figure 60 shows that, MSCs released by NIR irradiation show increased levels of osteogenisis compared to the trypsinized. The variation in differentiation capacity was also statistically confirmed via Student's t-test.

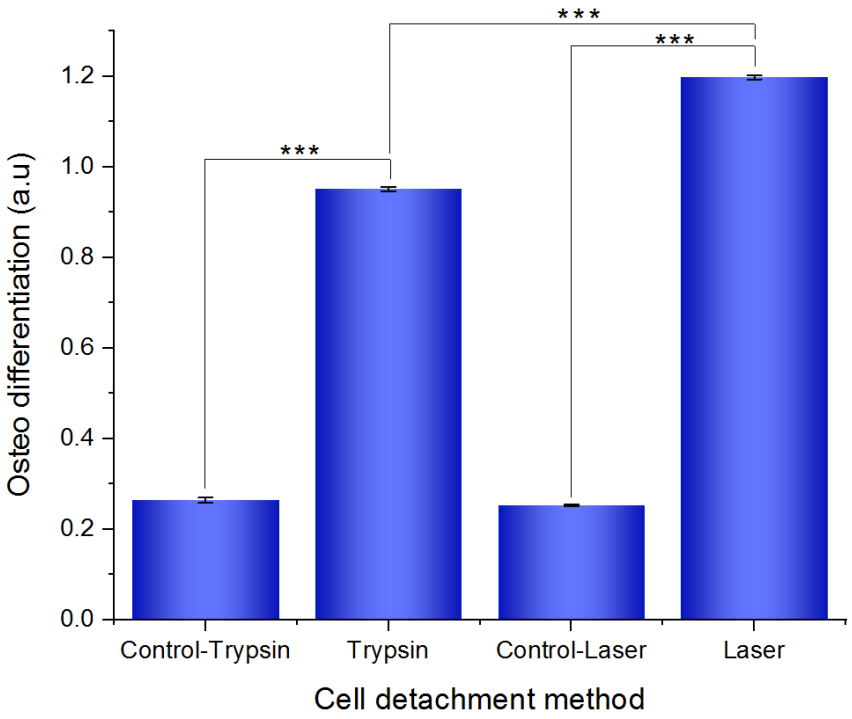

Figure 60: Absorbance spectroscopy analyses of Alizarin Red S stained osteogenic differentiated hMSCs detached via NIR laser irradiation and trypsinization after 21 days of osteogenic induction. Student t-test showed significant difference in osteogenesis between the cells detached via trypsin and laser. *p<0.05, **p<0.01 and ***p<0.001. Standard deviation was used. Error bars show ± 1 standard deviation from the mean.

While no red dye can be qualitatively observed in undifferentiated control hMSCs in Figure 59, signals can still be quantitatively observed in the plate reader assay as shown in Figure 60. This may be due to the presence of excess dye in the sample or background noise that may have been picked up by the sensitive plate reader.

The plate reader assays have shown that the hMSCs cultured on Au NRs and released via NIR irradiation have been successfully differentiated into osteogenic and adipogenic cell types just as those released via trypsin. In addition to this it was also observed that both the differentiation capacities were higher in the cells released by NIR irradiation, than those by trypsinization. The increase in osteogenic differentiation (in NIR detached cells) is in agreement with various other studies that have shown similar results after the MSCs were exposed to NIR irradiation [273, 275, 276]. All the studies have stated that NIR irradiation promotes osteogenesis in MSCs. Osteogenic differentiation in stem cells occurs when the cells switch from glycolydes to oxidative phosphorylation. According Wang *et al*., NIR irradiation of cells leads to an increase in the mitochondrial number. This may lead the metabolic profile in the cell to switch to oxidative phosphorylation from glycoses leading to the promotion in

cellular differentiation [284].

Not many studies have been found that have shown an upregulation in adipogenic differentiation post NIR irradiation. To confirm the microplate reader analyses on genetic level, qPCR was performed on the differentiated cells.

5.2.8 RT-qPCR Analyses

To gain more insight into the extent of differentiation in hMSCs converted to osteocytes or adipocytes, I performed an analysis of the differentiated cells expression of particular genes known to show upregulated expression during osteogenesis or adipogenesis. Osteogenesis and adipogenesis were separately induced in cells detached by trypsinization and NIR irradiation. These cells were then studied for specific gene expression using qPCR. The presence of C/EBPα and FABP4 was investigated in adipogenic cells, while osteogenic cells were tested for up regulation of ALP and RUNX2 gene.

Adipogenic Markers

CCAAT/Enhancer Binding Protein α (C/EBPα) is a pleiotropic transcription factor and a key regulator for adipogenesis. C/EBPα upregulation triggers adipogenic differentiation with increase in accumulation of lipid droplets in cytoplasm. Studies have shown that suppression of C/EBPα expression leads to the decrease in lipid formation and a reduction in adipogenesis [551-553]. Fatty acid binding protein 4 (FABP4) is a cytoplasmic fatty acid binding protein expressed mainly in adipocytes. It is associates with cyclooxygenases, long chain fatty acids and lipoxygenase metabolites. Studies has shown that the expression of FABP4 increases during adipogenic differentiation [554, 555].

From Figure 61 it can be observed that there is an upregulation in C/EBPα and FABP4 gene expression by the cells released via trypsin and NIR-irradiation after culture in adipogenic induction media. The up regulation of both genes is known to occur in cells undergoing adipogenesis, and no significant difference in expression levels between either of the cell detachment methods is observed. These Q-PCR results, match the adipo red staining results (Figure 61), confirming that there is no significant difference in the adipogenic differentiation capability of the hMSCs detached by NIR irradiation or by trypsin.

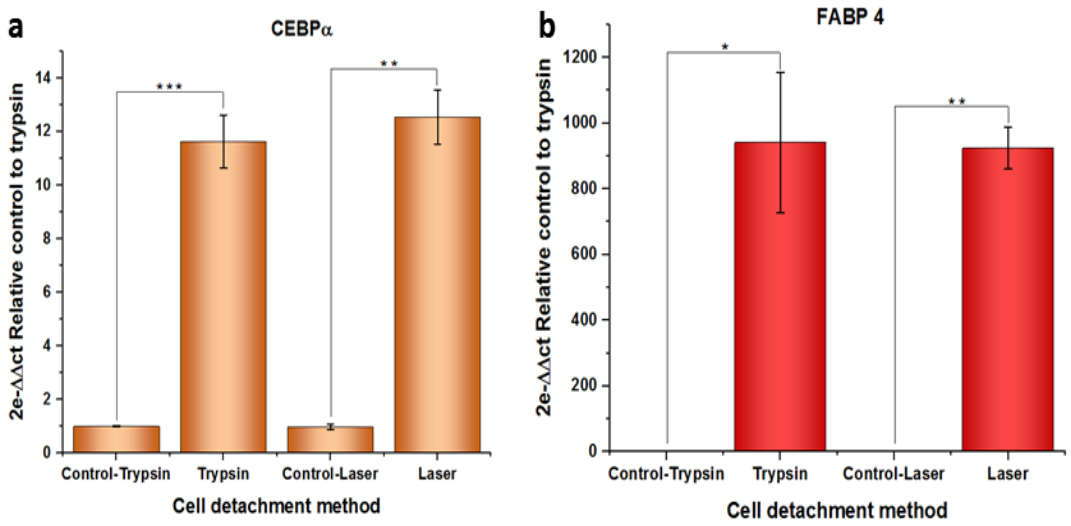

Figure 61: qPCR analyses for adipogenic markers (a) C/EBPα expression (b) FABP4 expression. *p<0.05, **p<0.01 and ***p<0.001. Standard deviation was used. Error bars show ± 1 standard deviation from the mean.

Osteogenic Markers

Also known as the master switch, Runt-related transcription factor 2 (RUNX2) is expressed in the early phase of osteogenic differentiation. RUNX2 is important for the generation of mineralization in tissues [556]. Alkaline phosphate or ALP also plays a crucial role in mineralization process especially in the early stages of differentiation [557]. The amount of ALP expressed during the differentiation process can be used to predict the *in vivo* bone forming capacity [558].

Looking at expression of genes typically upregulated in osteogenesis, for hMSCs cultured in osteogenic induction media we can see that levels of ALP up-regulation in trypsinized cells is identical to that of laser released cells in Figure 62 (a). We can see an increase in RUNX2 expressed by the NIR irradiated cells comparted to trypsinized cells in Figure 62 (b).

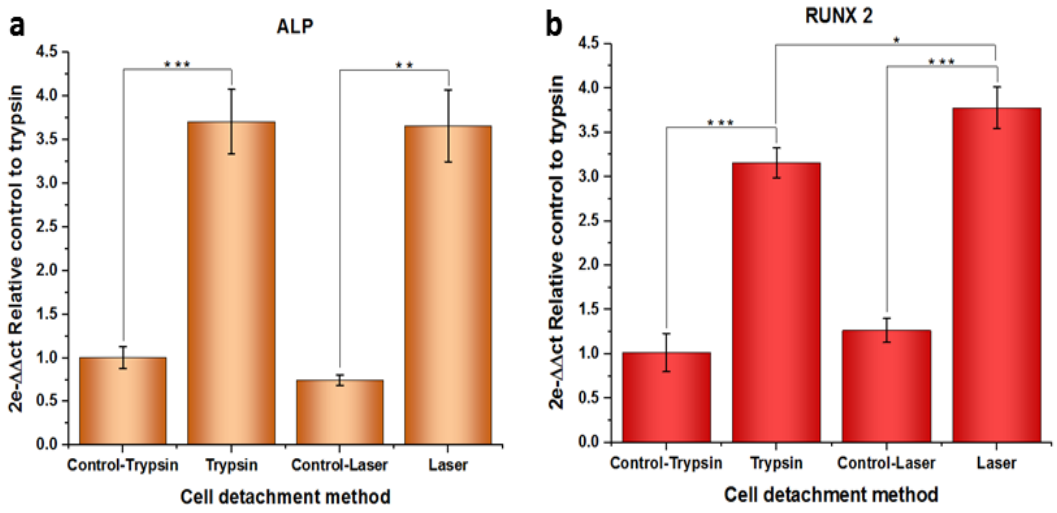

Figure 62: Q-PCR analyses for osteogenic markers (a) ALP expression (b) RUNX2 expression. *p<0.05, **p<0.01 and ***p<0.001. Standard deviation was used. Error bars show ± 1 standard deviation from the mean.

Q-PCR shows an upregulation in C/EBPα and FABP4 specifically expressed by adipogenic cells released via both cell detachment techniques. No statistically significant difference between the levels of C/EBBPα and FABP4 was noted in either of the release techniques.

However, a difference in osteogenic gene expression was observed between hMSCs released via NIR irradiation and trypsinization. Significant upregulation of ALP and RUNX2 gene was observed in differentiated cells released by both the techniques compared to undifferentiated ones. Several studies have shown that NIR irradiation does have an influence on the osteogenic differentiation of hMSCs. Evidence suggests that the osteogenic differentiation in cells irradiated in the NIR range presumably is higher when compared to trypsinized cells [273, 275, 559]. NIR irradiation has also been reported to promote significantly higher levels of ALP expression in the first 2-3 days of differentiation before returning to normal levels as seen in non-irradiated MSCs [275]. In these current studies, we have observed a higher expression of RUNX2 gene by laser detached cells in comparison to trypsinized cells. This is in agreement with other that have shown an increase in RUNX2 gene when the MSCs were NIR irradiated [560-562].

5.2.9 Extracellular matrix protein expression

The cells, in multi cellular organisms, are surrounded by non-cellular component made up of water, fibrous proteins, polysaccharides and various other biomolecules and form a scaffold-like substance called the extra cellular matrix (ECM) [563, 564].

Not only does the ECM give a structural scaffold like support to the cells, it also plays an important role in cell adhesion, polarity, migration, differentiation, proliferation, tissue organization, and intra cellular signalling. All these functions play an important role in maintaining the development, constant remodelling and homeostasis of an organism [565, 566]. Of all the functions listed above cellular adhesion and migration are among the most important of the extra cellular matrix of a cell. Adhesion between the cell to cell and cell to substrate is mediated by adhesive molecules on the cellular surface and the ECM proteins. Many of the functions previously described such as proliferation, differentiation and polarity are mainly dependent on cell adhesion. In a living organism, adhesion molecules are responsible for mediating cell migration during morphogenesis, wound healing and immune system responses [567].

The extracellular matrix of a cell is made up of many fibrillary protein aggregates that display short peptide sequences that promote cell adhesion through the formation of specific interactions with complimentary moieties on the exterior of a cell (e.g. integrin's) [566]. These proteins include: collagen, laminin, fibronectin and elastin. Of all these proteins, the triple helical structured collagen is one of the most abundant proteins in the extra cellular matrix of an animal tissue. A human body is made up of 25-30% collagen, this large family is subdivided into 28 different members [568]. Of all the different types of collagen, fibril forming collagen type I is the most abundant type found in a cell.

Laminin, found in the basal laminae of the ECM, is a heterotrimeric glycoprotein that is subdivided into 15 classes. It has a self-assembling mesh like structure which helps in reinforcing the ECM by binding to other laminin, collagen, the nidogens family of glycoproteins and other molecules [569, 570]. In addition to these functions laminin is known to participate in adhesion, proliferation, migration, differentiation and regeneration [571].

A master organizer in the ECM, fibronectin is a dimeric glycoprotein that is divided into two sub classes. Fibronectin has the ability to crosslink with collagen and glycosamino glycans (GAGs) as well as with itself in the form of fibrils due to the presence of disulfide bonds. Being an important adhesion molecule, fibronectin has been widely studied. It has been shown that the presence of fibronectin can induce fast migration of cells such as is needed during wound healing [563, 569, 572].

Immunofluorescent labelling of hMSCs, released via laser and trypsin, was

performed was performed immediately after cell detachment. This study was conducted to qualitatively analyse the effect these detachment process had on the extra cellular matrix of the cells. In the studies I used TrypLE express, a xeno free dissociation solution which, according to the manufacturer, is gentle and reduces damage to the cells.

Collagen

Qualitative analyses for the presence of collagen in hMSCs detached via NIR irradiation and trypsin are shown in Figure 63. While cells detached via NIR irradiation are shown in Figure 63 (a & b), trypsinized cells are represented in Figure 63 (c & d).

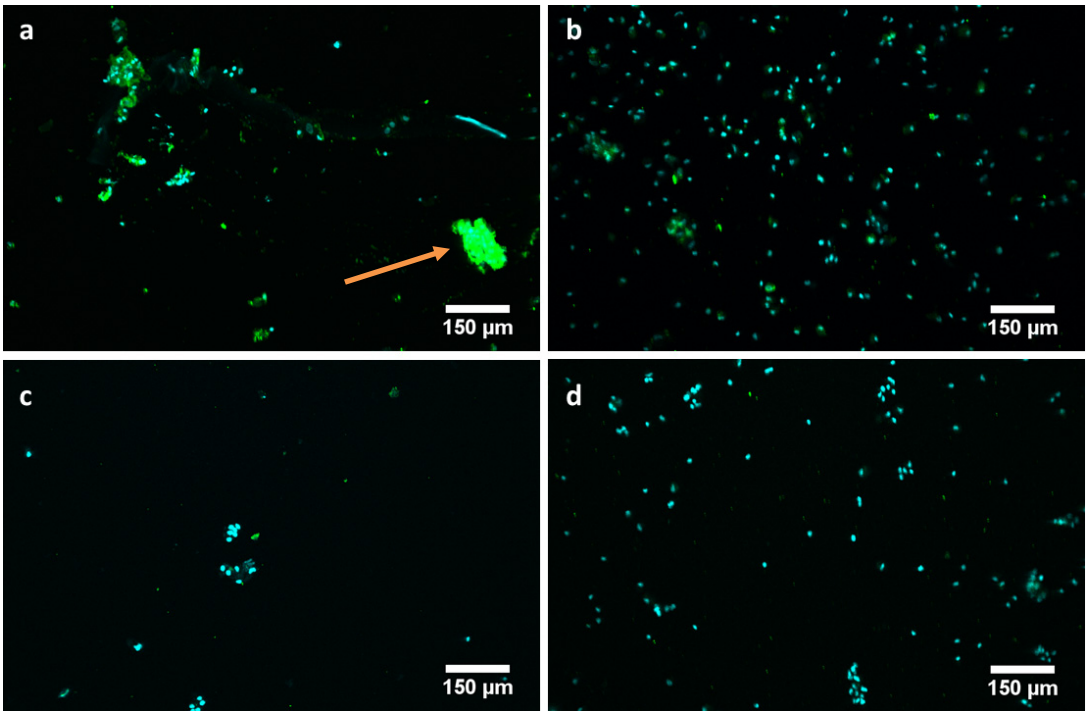

Figure 63: Immunostaining performed on hMSCs detached via NIR irradiation and trypsin to detect the presence of collagen on the extracellular matrix. The presence of green fluorescence around the cells, (a) released via NIR irradiation, indicates the presence of collagen. A cluster of cells is also pointed by the yellow arrow. (b) hMSCs detached via trypsin display less green fluorescence indicating less presence of collagen, (c) negative controls for cells released via laser and (d) negative controls for cells released via trypsin

A higher amount of green collagen fluorescent staining can be observed in hMSCs released via NIR irradiation when compared to trypsin released cells. Though cells detached by trypsin do display the green stain, it is shown to be diminished compared to its counterpart. The reduced amount of collagen displayed by the cell ECM released via trypsin may have been due to its digestion by the enzymes. This shows that trypsinization may have an effect on the collagen present on the ECM of the hMSCs while laser irradiation leaves it intact.

Fibronectin

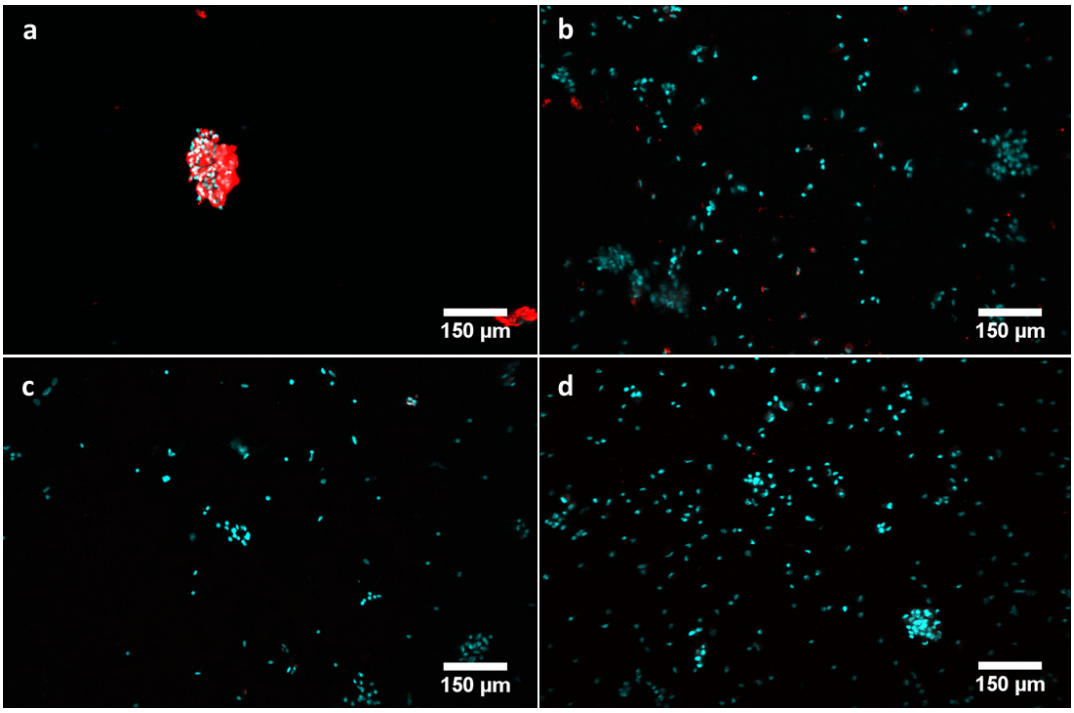

Figure 64: Immunofluorescence labelling of hMSCs to detect the presence of fibronectin in cells detached via trypsinization and NIR irradiation. (a) A cell cluster of hMSCs released via NIR irradiation with the red stain indicating the presence of fibronectin. (b) hMSCs released via trypsin with the reduction of red fluorescence indicated the absence of fibronectin. (c) negative controls for cells released via laser irradiation and (d) via trypsin.

Figure 64 shows the qualitative analyses of the presence of fibronectin on the surface of hMSCs released via IR irradiation and trypsinization. Figure 64 (a & c) shows hMSCs released via laser irradiation and Figure 64 (b & d) represent hMSCs released via trypsinization. In Figure 64 (a & b), the samples are exposed to both primary rabbit anti-fibronectin antibodies and secondary TRITC conjugated goat anti-rabbit IgG antibodies. Figure 64 (c & d) shows negative controls where the cells are exposed only to secondary TRITC conjugated goat anti-rabbit IgG antibodies. The nuclei of the cells are stained with DAPI (blue).

While Figure 64 (a) shows a cluster of cells which is clearly surrounded by fibronectin present on the extra cellular matrix of the hMSCs, a reduced amount of fibronectin is observed in Figure 64 (b). The lack of fibronectin on the hMSCs released via trypsinization demonstrates that trypsin may be responsible for stripping the cells of fibronectin. In contrast the fibronectin on the cells released via laser irradiation is found to be intact showing that laser irradiation may not have an adverse effect on the fibronectin.

Laminin

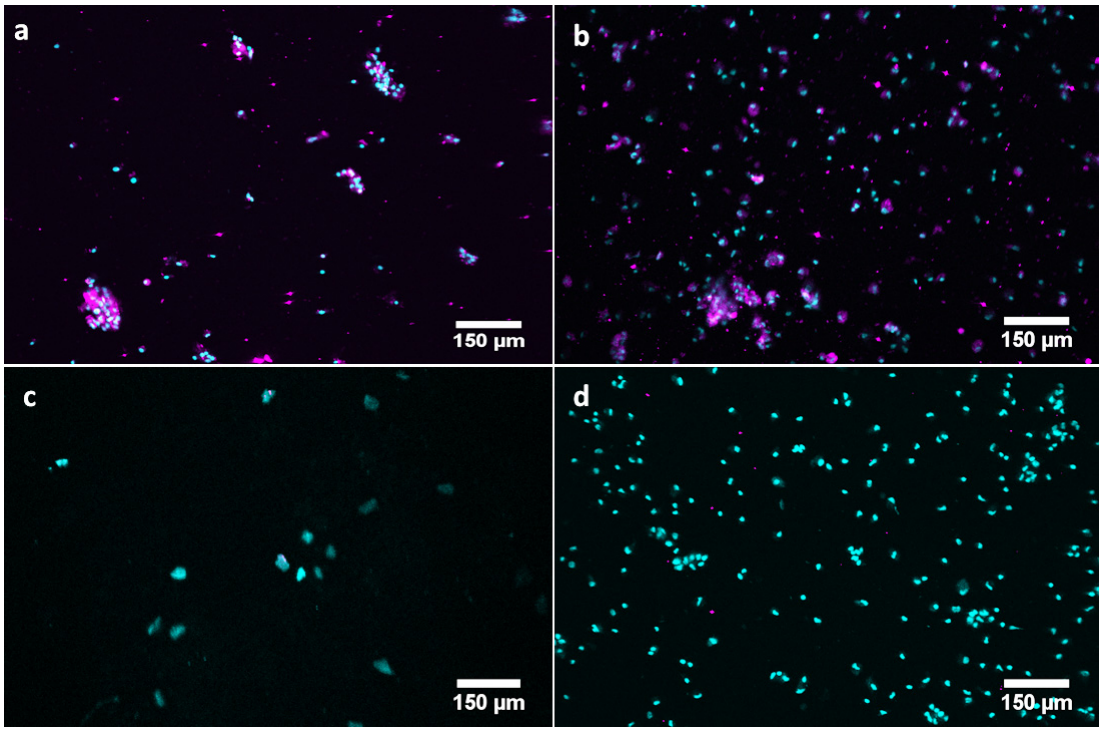

Figure 65: Immunofluorescence labelling of hMSCs released via trypsinization and NIR irradiation to detect the presence of laminin. (a) hMSCs released via laser irradiation. The magenta stain indicates the presence of fibronectin. (b) hMSCs released via trypsin. The cells display the presence of laminin. (c) Negative controls for cells released via laser irradiation and (d) negative controls for cells released via trypsin.

Figure 65 is a qualitative analysis for the presence of laminin on the extracellular cellular matrix of the hMSCs. While Figure 65 (a & c) are hMSCs released via NIR irradiation, Figure 65 (b & d) represent hMSCs released via trypsin. In Figure 65 (a & b), both the samples were exposed to primary Anti-Laminin antibodies and secondary DRAC goat anti-mouse antibodies. Figure 65 (c & d) represent control samples that were only exposed secondary DRAC goat anti-mouse antibodies.

The ECM of the hMSCs released by both the mechanisms display an equal amount of laminin. Unlike the collagen and fibronectin, trypsinization did not seem to have an effect on the laminin. This result is different to Yang *et al*., who conducted comparative studies on hMSCs released via trypsinization and from temperature responsive polymer [573]. Qualitative and quantitative measurements performed by Yang *et al*., saw a significant drop in the presence of laminin in the trypsinized cells. The difference in the results may be due to the type of trypsin used in this studies. While TrypLE express was used for the research conducted in this thesis, Yang *et al*., seem to have used porcine derive trypsin.

The immunocytochemistry for the ECM proteins shows that laminin was the least by the method of cell detachment. Few of the individual cells, released via trypsin, display collagen proteins around the cells. But the intensity of collagen displayed by the NIR detached cells are higher compared to the trypsin detached cells. All the three proteins that were released via trypsin, fibronectin was the most effected protein. While the hMSCs released via NIR irradiation shows a greater intensity of fibronectin around the cells, only traces of fibronectin can be observed trypsinized cells. The implications of trypsin on these three cellular proteins was also shown by Yang *et al*., and Canavan *et al*., whose studies were based on temperature responsive (ppNIPAM) cell detachment technique. In their studies, the cells dissociated via trypsin showed a significant damage to the proteins when compared with cells released via ppNIPAM [187, 573].Further studies are needed to confirm the qualitative findings.

While the effect of trypsin is to largely disaggregate cells, detachment by NIR appears to detach cells in small sheets. The sheet form of detachment is consistent with the earlier studies conducted by Giner-Casares *et al* [335]. These findings suggest that detachment of cells by NIR in small sheets may preserve the intracellular ECM to greater extent than enzymatic methods of detachment. This may have implications for other cell surface proteins and consequently for maintenance of hMSC phenotype and clinical applications. Studies conducted by Huang *et al*., have shown that 36 proteins that were responsible for cell metabolism, transportation, adhesion etc. were downregulated in the cells detached via trypsin [517]. Cells released as sheets have also found major medical applications. Human and animal studies are already under way to use the sheet as grafts in order to treat diseases related to corneal reconstruction [574], cardiac grafts [575], bladder augmentation [576], periodontal regeneration [577].

5.3 CONCLUSION

While trypsinization has been the “gold standard” for cell detachment for many years, it can have multiple deleterious effects on cells including cell apoptosis, ECM loss, and damage to the cells. Though there are many a number of commercially available alternatives such as non-enzymatic dissociative solutions and temperature responsive cell detachment technologies, they are unsuitable for scale-up to commercial levels either due to a decrease in cell viability or their prohibitive cost.

Through the experiments outlined in this chapter I have shown that it is possible to detach cells using Au NRs functionalised substrates by exposure to a NIR laser. I have also studied the effects the gold nanorods and NIR irradiation might have on the cell viability and differentiation capacity. These studies have shown high cell viability after laser exposure and cellular retention of multipotency similar to that of trypsinized cells. Cellular differentiation remains the same for adipogenesis, but osteogenic differentiation is higher in case of NIR detached cells. In addition, there are potential advantages in preservation of extra cellular matrix and other cell surface proteins which may contribute to greater therapeutic utility of cells, reducing the numbers required to treat a given condition.

The efficient and non-toxic nature of photothermal detachment of NIH-3T3 mouse fibroblasts and hMSCs from Au NRs coated surface via NIR irradiation can be seen as a promising alternative to trypsin. There is also an exciting prospect for future studies to scale-up this technology to provide a large number of hMSCs for therapeutic industries.

Chapter 6: Cell Culture and Detachment from Microcarrier Surface

New methods are required for the generation of large numbers of hMSCs (cell expansion) to ease bottlenecks preventing the widespread implication of stem cell therapies to treat a range of diseases, *in vivo* implantation and the restoration of tissue homeostasis [578]. Earlier in the literature review (chapter 2) it was discussed that vast number of cells are required for treating various diseases. For patient treatment, the cell numbers range from 10^6 to 10^{10} MSC/kg to treat disease such as autoimmune disease [359], cardiac repair [361] and diabetes [409].

Presently cell expansion for stem cell therapy is achieved by extracting stem cells from patients and culturing them in plastic 2D tissue culture T-flasks. T-flasks are flat containers made up of polystyrene and treated with oxygen plasma to make the container hydrophilic, thus more supportive of cell growth [579, 580]. Lab based T-flasks have a limited surface area ranging from 25 cm^2 to 175 cm^2 thus servery limiting the maximum available surface area for cell expansion. In order to overcome this limitation, automated stacked T-flasks are used in industrial processes [364]. However generating a sufficient number of cells using this process is slow and un-scalable if stem cell therapies are to have significant clinical impact on a large scale especially if the stem cells have are culture to be used autologously [364]. In addition to this studies have also shown that growing cells as a monolayer in a 2D surface causes the cells to lose their original in vivo properties such as cell-cell, cell-ECM signalling pathways that are necessary for an in vivo cell proliferation, differentiation and other functions [343]. Current alternatives for cell expansion such as hollow fibres and roller bottles exist but the scalability of these devices may also be limited which have been discussed in chapter 2 [365, 369].

In order to overcome these limitations 3D microcarrier system can be used to generate cells on a large scale. Microcarrier call culturing technique is based on culturing anchor dependant cells on a microcarrier in a fluid suspension [388]. In addition to high cell output this system has the advantage of being easily scalable, maintaining a dynamic and homogeneous system, ease of controlling various

parameters such as the pH, gas levels, shear rate, temperature and nutrient flow [376, 377].

Large scale culturing of cells on microcarriers also requires an effective method for detaching them from the microcarrier surface, without damaging the cells. As detailed in chapter 2, currently detachment of cells from microcarriers involves in the usage of trypsin, accutase, collagenase, and hypotonic treatment. While trypsin has shown an effective detachment of cells from the microcarriers, collagenase and hypotonic treatment resulted in reduced cell viability [410, 411, 413].

In chapter 5, I observed a successful detachment of hMSCs from Au NRs coated 2D surface post-NIR irradiation. Further studies showed that the detachment technique did not have a negative impact on the stem cell characteristics. The current chapter aims to investigate the possibility of detaching hMSCs from Au NRs coated 3D microcarriers upon NIR irradiation. In this chapter I will describe (i) the materials and methods used and discuss the results regarding (ii) the surface characterization of the coated and uncoated microcarriers (iii) cell viability on the Au NRs coated microcarriers (iv) cell structure on the Au NRs coated microcarriers (v) cell detachment and (vi) cell re-culture and viability.

6.1 MATERIALS AND METHODS

6.1.1 Microcarriers

All the previous studies, involving in cell detachment via NIR irradiation on 2D surfaces, were performed using silica-based surface (glass slides). In order to remain consistent with the base material used previously, glass microcarriers were opted for the following studies.

The microcarriers used in all the following experiments are acid washed glass beads obtained from Sigma-Aldrich (St. Louis, Missouri, USA). The diameter of the glass beads ranged between 212-300µm. Acid washed beads were chosen over untreated beads as the acid washing process removes contaminants such as dust, microbes and silica fragments which can detrimentally affect cellular viability and responses.

6.1.2 Gold nanorods

In the 2D studies it was observed that, compared to the other systems studied, polyamine conjugated Au NRs (PA-Au NR) successfully yielded the most evenly coated surface. Taking this result into account, I have decided to coat all microcarriers with PA-Au NRs.

6.1.3 PA-Au NRs coating on the Microcarriers

Polyamine conjugated Au NRs (PA-Au NRs) obtained from Nanopartz (C12-10-780-TA-50) (Loveland, CO, USA) were used for all the microcarrier based studies. The diameter of the nanorods was 10 nm and the length was 38 nm, thus possessing an aspect ratio of 3.8. The concentration of the stock solution of PA-Au NRs was 4.1 $\times 10^{13}$ Au NRs/mL. The stock solutions were diluted in PBS to either 2.6 $\times 10^{12}$ Au NRs/mL, and 1.34 $\times 10^{12}$ Au NRs/mL. The diluted solutions of Au NRs were stored at 4 ^{o}C until further use.

Prior to coating the microcarriers with PA-Au NRs, 500 mg of aliquots of microcarriers were placed in individual 1.5 mL Eppendorf tubes. PA-Au NRs solutions was sonicated for 360 seconds in a sonication bath (170W, 42kHz) (CODYSON Digital Ultrasonic Cleaner CD-4820) to separate aggregated nanorods. Two approaches were used to coat the microcarriers:

Sonicate-Rotate (SR): In this process 1 mL of PA-Au NRs solution (with concentration of either 2.6 $\times 10^{12}$ Au NRs/mL, or 1.34 $\times 10^{12}$ Au NRs/mL) was added to each of the Eppendorf tubes filled with 500 mg of microcarriers and sonicated for 360 seconds. These Eppendorf tubes were then placed on a roller and were allowed to roll for 24 hours at 60-65 rpm.

Sonicate-Rotate-Sonicate-Rotate (SRSR): This procedure follows the same protocol as above, except that after first 12 hours of rotation the samples are removed from the roller and sonicated for additional 360 seconds in a sonication bath and then placed back on the roller for another 12 hours.

Two methods of coatings were tested to evaluate which of the techniques would allow the microcarriers to retain higher amount of Au NRs on its surface. The additional sonication step in SRSR (after initial 12 hours of rotation) was added to disaggregate possible gold nanorods aggregation either on the microcarrier surface or in supernatant itself. After the SR or SRSR process, all the microcarriers were

sonicated for 180 seconds to separate unattached or weakly attached Au NRs. Immediately after sonication the microcarriers sediment to the bottom of the tube, following this, the supernatant (containing unattached PA-Au NRs) was carefully removed from Eppendorf, leaving only the Au NRs coated microcarriers. Care was taken to avoid accidental aspiration of the microcarriers. The samples were then dried in an oven for 3 hours at 40 ^{o}C and stored at RT until needed.

6.1.4 Surface characterization:

Scanning Electron microscopy

The surface of the microcarriers coated with Au NRs was investigated by scanning electron microscopy (SEM) (Carl Zeiss SUPRA 40VP SEM and RAITH 150 Two). A small amount of coated and uncoated microcarriers were carefully removed from the Eppendorf tubes and spread evenly on carbon tape, which was then glued on to a sample holder. For these SEM studies, we used both gold sputtered and unsputtered samples. Sputter coating of gold, onto the samples, was performed in order to reduce charging artefacts from the insulating glass microcarriers and was achieved by using Emitech K975X Turbo-pumped evaporator in sputtering configuration. The samples were then placed in the SEM for further studies. A magnification of 12,500 ×, 25,000 ×, 40,000 × and 60,000 × was used at 3-5 kV to obtain high-resolution images of the microcarriers.

Dark field microscopy

Due to the limitations of SEM imaging (discussed in the results section of this chapter), dark field microscopy was also used to study the PA-Au NRs coated surface of the microcarriers. An upright microscope, Nikon Eclipse LV 150NL (Melbourne Centre for Nanofabrication, Melbourne), was used to perform the microspectrometry. The principles and working of this technique are detailed in Chapter 3, section 3.13.

Method of imaging

A small amount of coated or uncoated microcarriers were spread evenly on a glass slides. Microscopic immersion oil was the applied onto the samples and were covered with a glass cover slip. The glass slides were placed under the dark field microscope (Nikon Eclipse LV 150NL, Melbourne Centre for Nanofabrication, Melbourne) and PA-Au NRs coated microcarriers were imaged.

Dark field microscopy was also used to obtain emission spectra of specific regions on the coated microcarriers for PA-Au NRs coating. A point of interest on the microcarriers was chosen and the spectral output of the chosen pixels was captured.

6.1.5 Inductively coupled plasma mass spectrometry (ICP-MS)

While dark field microscopy was used to qualitatively confirm the presence of Au NRs on the microcarrier surface, a quantitative analysis using ICP-MS was performed to obtain the number of Au NRs coated on the microcarrier surface.

Not only was this study performed to quantify the Au NRs numbers but also to determine which of the coating procedure (SR or SRSR) would be effective in allowing the microcarriers to retain the maximum number of nanoparticles on their surface. All the experiments involving generation of data using ICP-MS were performed at University of Technology Sydney, Sydney, Australia by Dr David Bishop. The data analyses was then performed at Swinburne University of Technology to discern the appropriate microcarriers for further experiments that involved cell culture and NIR irradiation based cell detachment.

6.1.6 Cell Culture

Human mesenchymal stem cells extracted from bone marrow were obtained from Lonza (PT – 2501, Basel, Switzerland) and stored in liquid nitrogen until required. Media required for hMSCs culture was made up of Alpha Minimum Essential Medium (α-MEM) (M4526, Sigma-Aldrich, St. Louis, Missouri, USA) supplemented with 10 % foetal bovine serum (FBS) (Life Technologies, CA, USA), 0.5 % Glutamax (Gibco, Thermo Fisher Scientific, MA, USA), 0.5 % Antibiotic-Antimycotic (100x) (Thermo Fisher Scientific, MA, USA). The cells were transferred from a cryovial to TCPS. The cells were thawed in a 37 ^{o}C water bath for 1.5 minutes. Using a micropipette, the thawed cells were gently resuspended and removed from the cryovial and suspended in 5 ml of temperature-equilibrated hMSCs cell culture media. This suspension was centrifuged at 1500 rpm for 5 minutes at room temperature. The suspension media is removed and the cells are re-suspended in the cell culture media. A seeding density of 6000 cells/cm^2 was used to culture the cells in T-75 tissue culture plastic. The cell lines were incubated at 37 °C in an atmosphere of humidified 5 % CO_2/ 95 % air. The media was changed every alternate day and the cells were cultured to 75-80 % confluence.

Cell Seeding on PA-Au NRs coated and uncoated microcarriers

35 mg aliquots of PA-Au NRs coated microspheres and uncoated microspheres were placed in separate wells in 96 well plates. 35 mg of samples was chosen as this amount was enough to cover the surface of the 96 well plate with a monolayer of microcarriers. The samples were then sterilized by exposing them to 2 % Anti-Anti in PBS (Antimycotic-Antibiotic 100×) solution for 60 minutes. The Anti-Anti solution was then removed from the samples and the microcarrier samples were thoroughly rinsed with PBS.

The cells used for seeding, were recovered via trypsinization (TrypLE™ Express, Invitrogen, CA, USA) for experimental studies. Cells were exposed to 1 mL TrypLE in a T-25 TCPS or 3mL for T-75 TCPS and incubated at 37 °C in an atmosphere of humidified 5 % CO_2/ 95% air for 5 minutes. The cells were then observed under a microscope to determine the level of cell detachment. The TCPS with cell culture was then washed by a twice repeated cycle of dilution in 5 mL of cell culture media. These cells were then centrifuged at 1500 rpm at 23 ^oC for 5 minutes and resuspended in fresh media. Cell counting was done by using a hemocytometer. The microcarriers, present in wells of a 96 well plate, were seeded with hMSCs at a seeding density of 10,000 cells/well and allowed to proliferate for 24 hours before the detachment experiments were performed, unless stated differently. All the microcarrier based cell culture performed in this thesis was done in static condition.

6.1.7 PrestoBlue assay

The viability of cells cultured on PA-Au NRs coated microcarriers, was investigated using the PrestoBlue assay. The working principle and mechanism behind PrestoBlue assay is described in chapter 3, section 3.6.

Viability of cells on Au NRs coated and uncoated microcarriers

The PrestoBlue assay was used to assess the viability of cells cultured on both the PA-Au NR coated and un-coated microcarriers. Cells were seeded at a density of 10,000 cells/well on 35 mg of microcarriers and incubated at 37 ^oC in an atmosphere of humidified 5 % CO_2/ 95% air for 24 hours to 7 days. Before adding the PrestoBlue solution, the samples were gently washed with PBS to remove unattached cells or debris. A 10 % (v/v) solution of PrestoBlue was prepared by diluting the stock solution of PrestoBlue (Invitrogen, CA, USA) in α-DMEM and 200 µl of the diluted solution

was added to each well containing the microcarriers. The samples were then incubated at 37 °C in an atmosphere of humidified 5 % CO_2/ 95% air for one hour. Following the required time period, the PrestoBlue media from the each sample was transferred to a fresh 96 well plate while taking care to avoid creating any bubbles in the well. The PrestoBlue media was then analysed under POLARStar micro plate reader (BMG, LabTech FluoStar Omega) at an excitation and emission wavelengths of λ_{ex}560 nm and λ_{em}590 nm.

6.1.8 Live/Dead Staining

Qualitative analyses of hMSCs viability was performed using the Live/Dead assay. The working principles and mechanism behind Liv/Dead assay is detailed in chapter 3, section 3.5.

A working solution of Calcein AM/PI (Live/Dead Cell Double Staining Kit, Sigma) with a ratio of 2:1 was prepared for this assay. In order to make 10 mL of working solution, 20 µl of Calcein AM and 10 µl of PI was added to 9.97 mL PBS. This solution was then vortexed to ensure complete mixing.

Live/Dead staining cells on Au NRs coated and uncoated microcarriers prior NIR irradiation

In order to prepare samples for the Live/Dead assay, the cells were seeded (10,000 cells/well) on uncoated and PA-Au NRs coated microcarriers (placed in 96 well plates) and were allowed to proliferate for 24 hours. The samples were then thoroughly washed with warm PBS and the cell culture media was replaced with Live/Dead solution. 100 µl of the live/dead working solution was added to each sample in a 96-well plate and the samples were incubated in the dark at 37 ^{o}C in an atmosphere of humidified 5 % CO_2/ 95 % air for 30 minutes. After the incubation, the samples were washed twice with PBS, to remove excess and unattached fluorophores. The labelled cells were imaged with a 40× and 100× magnification objective on a epifluroscent Nikon Eclipse Ti-E Inverted microscope system (DS-Qi1 fluorescent time lapse camera) using the wavelength configurations of λ_{ex}490 nm and λ_{em}515 nm for Calcine AM and λ_{ex}535 nm and λ_{em}617 nm for Propidium iodide (PI).

Live/Dead staining on hMSCs detached via NIR-Irradiation

Au NRs coated and uncoated microcarriers cultured with cells were exposed to the NIR irradiation as explained previously. After being exposed to the NIR irradiation

the samples were gently washed with cell culture media and the detached cells were aspirated from the samples and re-cultured in a 96 well plate. The cells were incubated for 24 hours at 37 ^{o}C in an atmosphere of humidified 5 % CO_2/ 95% air and washed with PBS. 100 µl of Live/Dead solution was added to each sample in the 96 well plate and incubated in the dark for at 37 ^{o}C in an atmosphere of humidified 5 % CO_2/ 95% air for 30 minutes. The samples were then rinsed with PBS and observed under a Nikon Eclipse Ti-E Inverted microscope system (DS-Qi1 fluorescent time lapse camera) at λ_{ex}490 nm and λ_{em}515 nm for Calcine AM and λ_{ex}535 nm and λ_{em}617 nm for Propidium iodide (PI).

6.1.9 Phalloidin Staining of hMSCs on Microcarrier surface

In eukaryotic cells, actin is found as a meshwork of membrane associated proteins which allow the cells to attach to associated substrates. Fluorescent staining of actin filaments with phalloidin is therefore a useful method of visualising the intra cellular resolution of the cytoskeleton, cellular attachment and the spread of cells across the microcarriers.

hMSCs were cultured on PA - Au NRs coated and uncoated microcarriers for 24 hours at 37 ^{o}C in an atmosphere of humidified 5 % CO_2/ 95 % air before staining with them phalloidin. The samples were washed with PBS to remove any unattached cells or debris and fixed in paraformaldehyde (4 % w/v in PBS) for 30 minutes at room temperature. The samples were once again washed with PBS and permeabilized with Triton X-100 (0.1 % v/v in PBS) for 15 minutes and washed again. Non-specific adsorption of phalloidin was minimized by blocking non-actin binding sites in 1 % bovine serum albumin (BSA, 1 % w/v in PBS, Life Technologies, CA, USA) for 60 minutes. The samples were then rinsed with PBS and incubated in Alexa Flour-488 conjugated phalloidin solution (1:20 dilution in 1 % BSA) (Life Technologies, CA, USA) for 60 minutes at room temperature. Finally, the samples were thoroughly rinsed in PBS to remove any un-attached phalloidin and their nuclei were stained with DAPI (1:1000 in PBS) (Life Technologies, CA, USA) for 5 minutes before being given a final rinse.

Images were captured using an epifluroscent microscope (Nikon Eclipse T*i*-E Inverted microscope system). The presence of Alexa488 conjugated phalloidin was identified in the FITC channel (λ_{ex}490 nm and λ_{em}523 nm) the nucleus of the cells were imaged in the DAPI channel (λ_{ex}385 nm and λ_{em}420 nm).

6.1.10 Laser irradiation

To study the detachment of cells from the PA-Au NRs conjugated microcarriers, a continuous wave near infra-red laser (NIR) of 785 nm wavelength, as explained in chapter 3, section 3.1, was used. All experiments were performed under a collimated laser beam. final power density of 566 mW/cm^2.

Laser irradiation was performed on cells cultured on Au NRs coated microcarriers and cells cultured on un-coated microcarriers. Prior to the laser exposure, the cell cultured on microspheres, were washed with PBS in order to remove any unattached or dead cells and fresh cell culture media was added to the samples. The samples were then placed under the laser beam. The laser was setup at a height of 6 ± 2 mm from the cell culture samples. Since we have already observed in 2D studies that complete cell detachment only occurs at laser exposure times of 1 hour or more, we used the same exposure times for these experiments.

After exposure, the samples were washed gently with cell culture media to remove the laser detached cells. These detached cells were re-seeded onto a tissue culture plastic and incubated at 37 ^{o}C in an atmosphere of humidified 5 % CO2/ 95 % air and were monitored regularly. Proliferation and viability assays were performed on the re-seeded cells to determine their continued viability after laser exposure.

6.2 RESULTS AND DISCUSSION

In the following section, the results pertaining to PA-Au NRs coating on microcarriers, culturing hMSCs on microcarriers, their viability pre and post-NIR irradiation and the success of hMSCs detachment from the PA-Au NRs coated microcarriers post NIR irradiation is detailed.

6.2.1 Surface characterization

Surface characterisation of the PA-Au NRs coated and uncoated microcarriers were qualitatively and quantitatively studied. While SEM and dark field microscopy were used for qualitative studies, ICP-MS was performed to determine the gold content present on the microcarriers.

SEM analyses

SEM was used to characterize the surface architecture of uncoated and Au NRs glass microcarriers.

Figure 66 shows representative SEM images of the surface of the glass microcarriers. Figure 66 (a) provides an overview image of the microcarriers whereas Figure 66 (b, c & d) show higher resolution images of the surface of individual microcarriers and the attached Au NRs. All images show microcarriers coated PA-Au NRs at concentration of 1.34 $\times 10^{12}$ Au NRs/mL. Au NRs can be observed on the surface of the micro-carriers, however significant charging artefacts prevented high quality SEM images being obtained.

Unlike 2D surface characterization under SEM, were we could clearly observe the Au NRs coated surface without any further surface treatment, it was almost impossible to image the surface of the glass microcarriers without significant charging effects. This charging phenomenon occurs due to the insulating nature of the glass microcarriers and is one of the most common imaging artefacts in SEM [581, 582].

To reduce charging effects, samples can be coated with gold or other conducting materials. This process is relatively straightforward on flat surfaces and very thin continuous gold layers can be applied to the surface. In the case of the microcarriers, their highly curved morphology makes it very challenging to deposit continuous thin conducting layers without obscuring nanoscale features (such as the Au NRs) on the surface of the microcarriers. Therefore, there is a trade-off between reduced charging

and obscuring the nanoscale features of the Au NRs. The images in Figure 66 (b, c & d) represent the best images obtained, here a thin layer of gold was sputtered on the surface eliminating the worst of the charging effects, thicker gold layers did further reduce these artefacts but at the expense of the ability to resolve the Au NRs. Whilst PA-Au NRs can be clearly observed on the microcarrier surface in Figure 66 (b, c & d) we cannot be sure that more of the Au NRs are not obscured by the presence of the gold conducting layer.

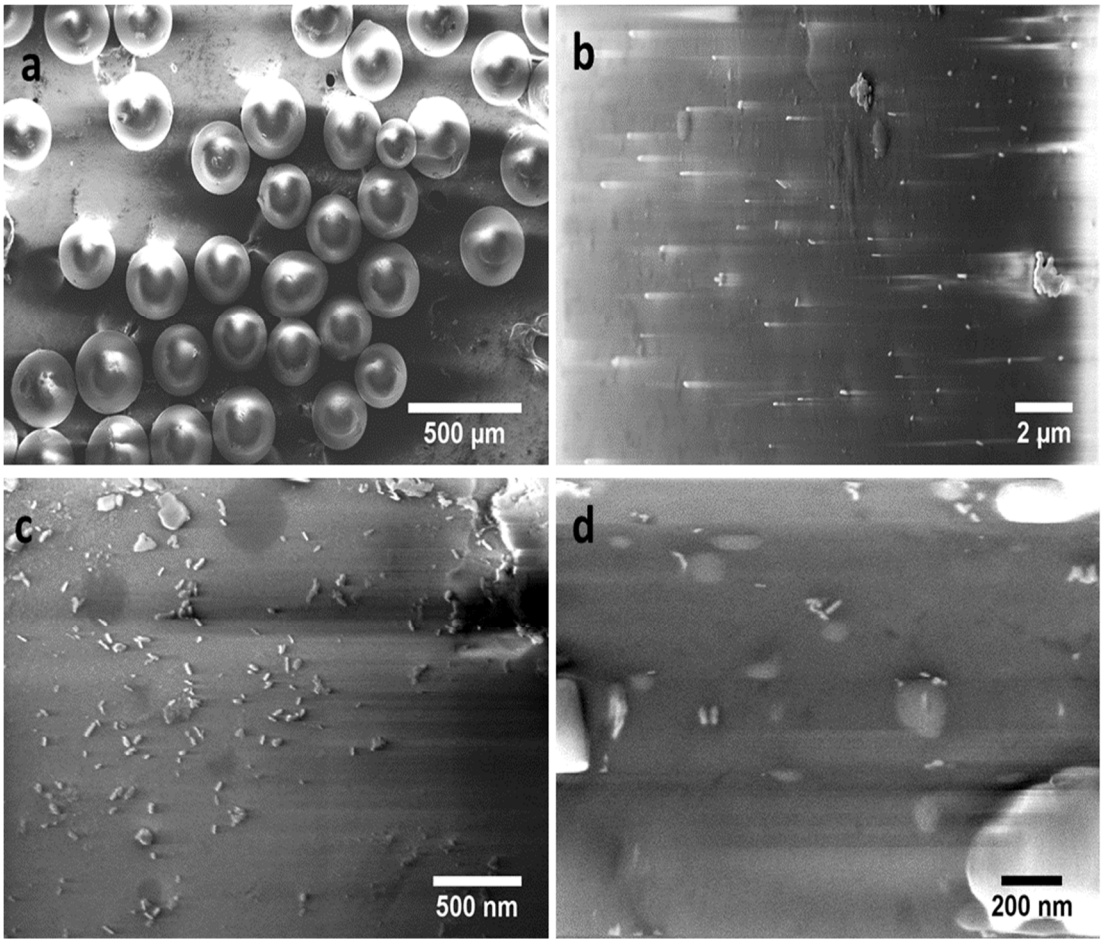

Figure 66: SEM images of nanorods coated microcarriers. (a) uncoated microcarriers, (b), (c) & (d) PA-Au NRs coated surface of the microcarriers.

Dark field microscopy

Since, SEM was not an ideal technique to characterise the surface of microcarriers, imaging via dark field microscopy was also investigated.

Figure 67 a shows dark field microscopy images of uncoated microcarrier, while Figure 67 (b, c, d & e) shows Au NRs coated microcarriers. Figure 67 (b & c) show representative images of the microcarriers coated by the SR process and Figure 67 (d

& e) by the SRSR process. The concentration of Au NRs exposed on to the microcarriers in each of the image are stated in Table 13:

Table 13: Coating method and figure legends

Concentration of gold nanorods/Coating process involved	**2.6 ×10^{12} Au NRs/mL**	**1.34 ×10^{12} Au NRs/mL**
Sonicate-Rotate (SR)	Figure 67 (b)	Figure 67 (c)
Sonicate-Rotate-Sonicate-Rotate (SRSR)	Figure 67 (d)	Figure 67 (e)

The presence of PA-Au NRs on all surfaces (except for the uncoated surface) in Figure 67 can be confirmed by the scattered light reflecting from the surface of the coated microcarriers. In contrast the controls (Figure 67 a) show much reduced scattered light which also has a different hue. These observations indicate good PA-Au NRs coverage on the microcarriers in Figure 67 (b, c, d & e). Qualitative analysis of Figure 67 (using software package Image J) suggests that the microcarriers coated using the SR coating technique (Figure 67 b & c) have more Au NRs present on their surface compared to the SRSR coated microcarriers (Figure 67 d & e). This result was confirmed by performing quantitative analyses – ICP-MS (Figure 69).

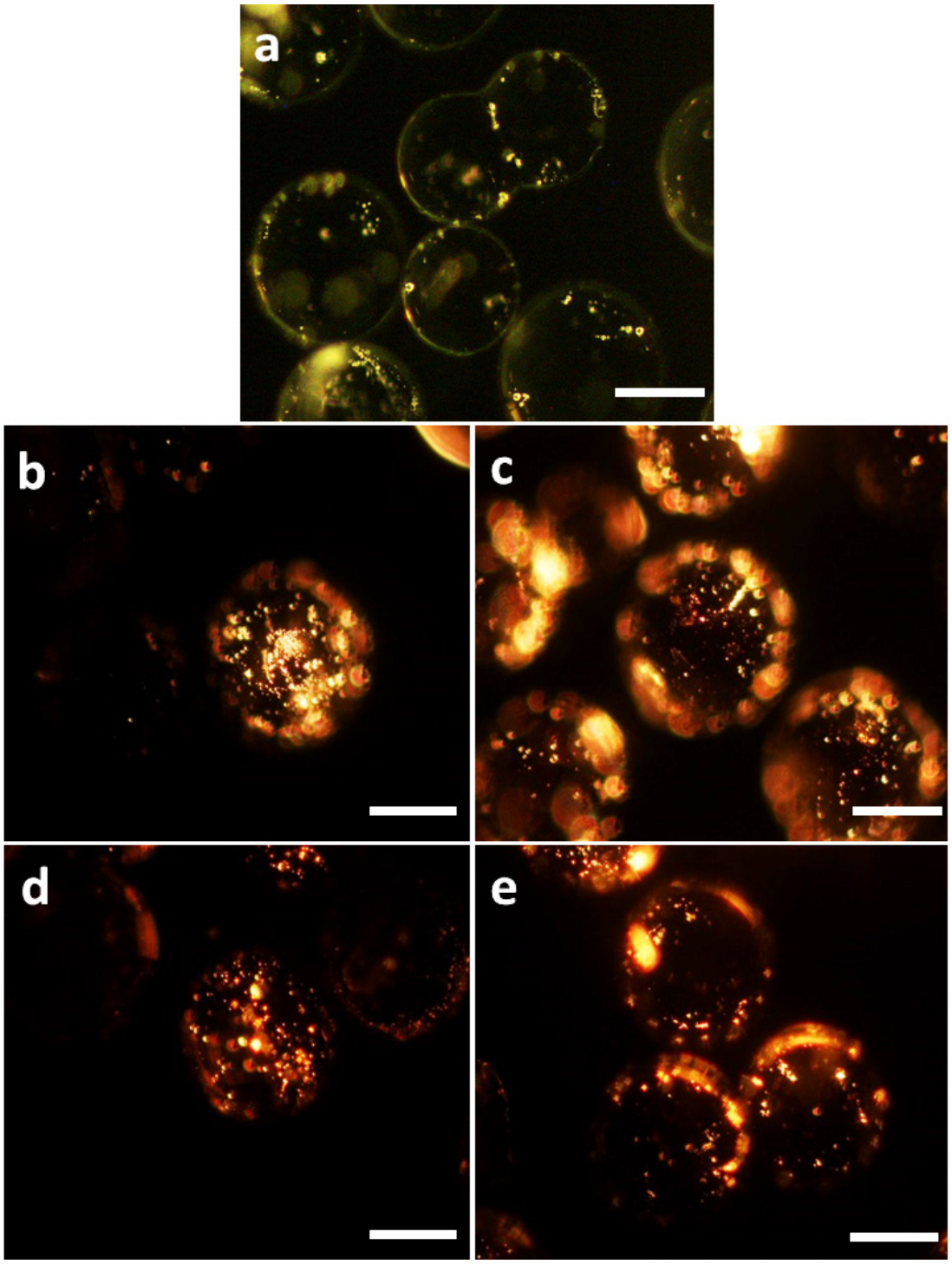

Figure 67: PA-Au NRs coated microcarriers. (a) uncoated microcarriers, (b) SR coated with 2.6 $\times 10^{12}$ Au NRs/mL, (c) SR coated with 1.34 $\times 10^{12}$ Au NRs/mL, (d) SRSR coated with 2.6 $\times 10^{12}$ Au NRs/mL and (e) SR coated with 1.34 $\times 10^{12}$ Au NRs/mL. Scale = 125 µm

Figure 68 (a & b) represents a selected point of interest on a PA-Au NR coated microcarrier that was used to generate an emission spectra of the Au NRs coated microcarriers as shown in Figure 68 (c). Emission spectra from the coated microcarriers were seen to possess a broad peak between 700-800 nm. Whilst this peak

is in the correct region for the Au NRs used, whose SPR excitation wavelength equals 780 nm, the peak is surprisingly broad. This is likely due to the reduced spectral resolution of the dark field microscope compared to the UV-Vis spectrometer used for the analysis of the Au NRs. Additionally, adhering the Au NRs to the microcarrier surface may have had small effect on the position of the SPR band of the Au NRs. If this was the case this shifting of the SPR band did not detrimentally effect their ability to mediate cell detachment via exposure to the NIR irradiation (as shown later in this chapter).

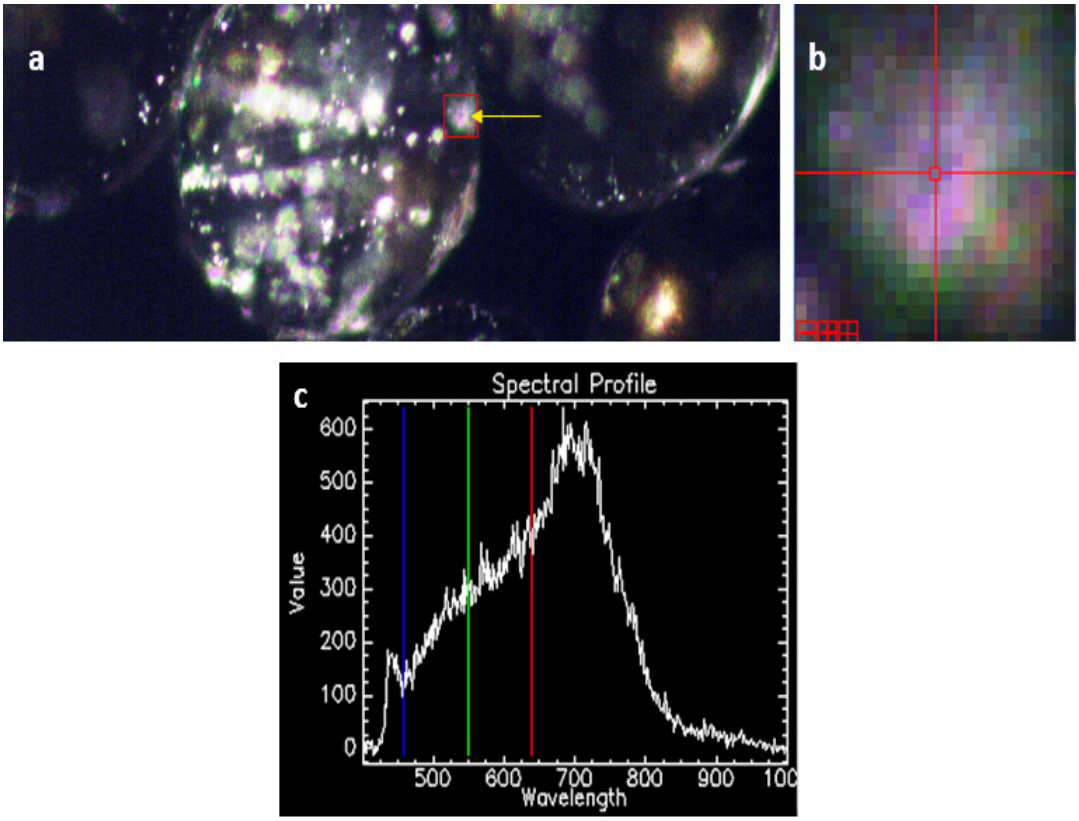

Figure 68: PA-Au NR coated microcarrier used for spectral studies (a) with the yellow arrow showing the area investigated spectroscopically. (b) Magnified view of point of interest and (c) spectral graph of PA-Au NRs coated on the microcarrier.

Quantitative analyses of gold on microcarriers using ICP-MS

In order to fully quantify the amount of PA-Au NRs present on the surface of the microcarriers, inductively coupled plasma mass spectroscopy (ICP-MS) was performed to measure gold content. ICP-MS uses a high energy plasma to ionize atoms in the sample and subsequently using mass spectrometry to quantify the amount of those ions present. Figure 69, shows that the microcarriers coated using 2.6×10^{12} Au NRs/mL possess more gold on their surface and therefore retain more PA-Au NRs regardless of the coating technique. But the microcarriers undergoing sonicate-rotate

coating technique (SR), retain higher amount of Au NRs on their surface compared to sonicate-rotate-sonicate-rotate (SRSR). In order to compare the quantity of coating across the different micro carriers, the data obtained were normalises. While the highest concentration of gold content was assigned as 100% (SR 2.6 $\times 10^{12}$/mL), other measurements were normalised against this. For example, when normalised to percentage, if microcarriers coated with SR 2.6 is assumed as 100%, microcarriers coated with SRSR 2.6 are shown to have 84% coverage of Au NRs on its surface. But this result was shown as statistically insignificant under Student's t-test. Microcarriers coated with SR 1.34 and SRSR 1.34 show the least amount of Au NRs (68% and 46%) and were statistically significant when compared with SR 2.6.

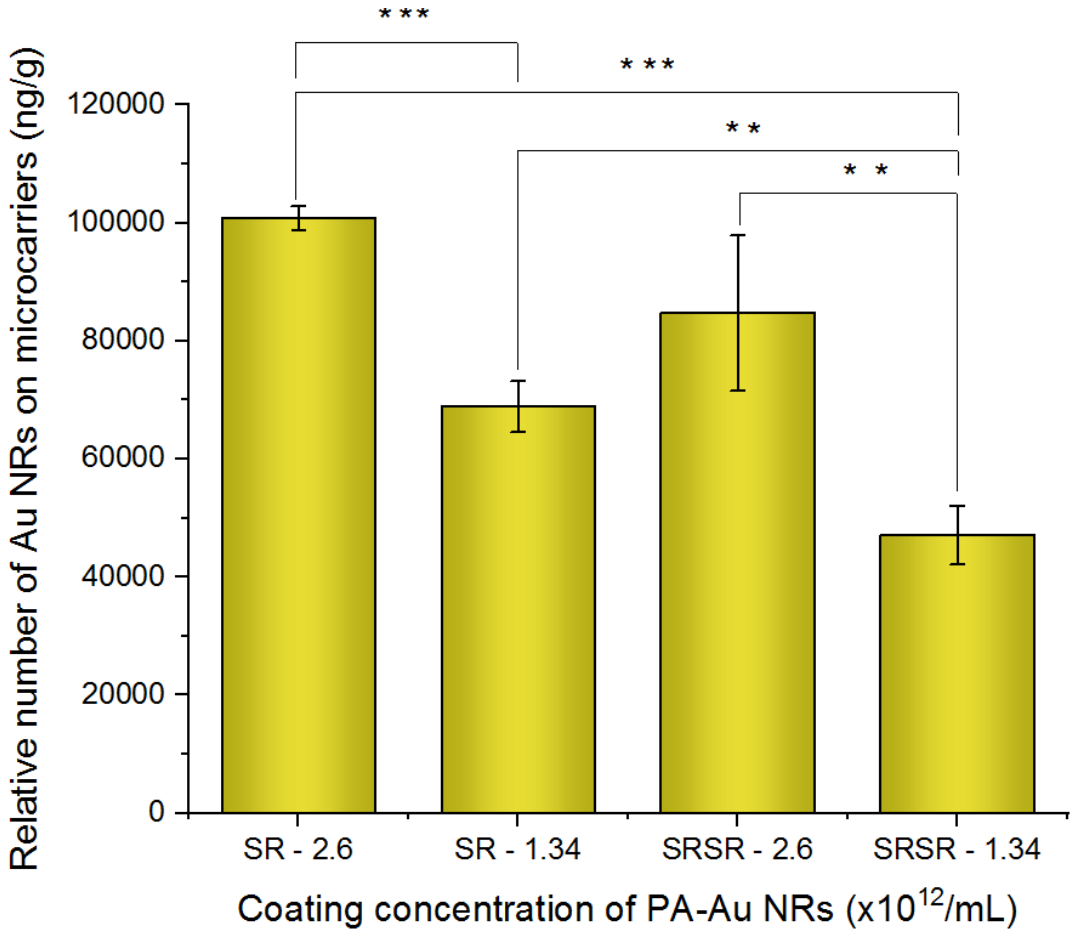

Figure 69: ICP-MS quantification of PA-Au NRs on microcarriers. Microcarriers coated with SR – 2.6 $\times 10^{12}$/mL displays higher concentration of gold compared to other PA-Au NRs coated microcarriers. The difference in the gold content on the microcarriers are statistically significant when compared to others. *p<0.05, **p<0.01 and ***p<0.001. Standard deviation was used. Error bars show ± 1 standard deviation from the mean.

The lower number of Au NRs on the SRSR coating based microcarriers may be due to the sonication step that was performed after 12 hours of rolling before placing

the samples back on the roller for further 12 hours of rolling. While this step was performed to disaggregate Au NRs in the solution or on the microcarriers, it might have resulted in the Au NRs attached to the microcarriers to dislodge from the surface. It should be noted all the coated microcarriers, regardless of the technique involved, were sonicated after the required time period of rolling before quantification and cell culture. This step was performed to separate unattached or weakly attached Au NRs from the microcarriers.

For all following experiments involving in cell culture, microcarriers coated with SR 2.6 $\times 10^{12}$ Au NRs/mL were used. This was due to presence of higher density of Au NRs on the microcarrier surface and limited steps involved in coating technique when compared to SRSR.

6.2.2 Cell viability of non-irradiated cells on Au NRs coated microcarriers

Similar to the experiments performed in 2D studies (Chapter 5), studies were performed to observe if the PA-Au NRs coated microcarriers had a negative impact on cell viability. PrestoBlue assay and Live/Dead assay was performed for these studies.

PrestoBlue assay

Figure 70 represents the quantitative analyses of the metabolic activity of the hMSCs cultured on uncoated and Au NRs coated microcarriers over 7 days' time period. From the graph it can be noted that there no statistically significant difference between the cells cultured on either of the microcarriers on a given day point. A significant increase in the metabolic activity of the cells between day 1 and day 3, followed by a sharp decline on day 7 can be observed from the graph. Though not statistically significant, the decline in metabolic activity of hMSCs may be as a result of contact inhibition due to high cell density. Contact inhibition can be defined as the decrease in the proliferative capacity of the cells due to increase in the cell density. Contact inhibition leads to an arrest in cell cycle and the cell cycle can be renewed by replating the cells at lower densities [583]. Studies have shown that the contact inhibition in hMSCs is also dependent on the origin of the cells. A study conducted by Zhu *et al*., showed that the adipo derived hMSCs show lower contact inhibition and higher proliferative capacity when compared to bone marrow derive hMSCs. Unlike the bone marrow derived hMSCs, which grow as a monolayer, the adipo derived

hMSCs continue to proliferate in multilayers [584]. All the stem cell studies conducted in this thesis used bone marrow derive hMSCs.

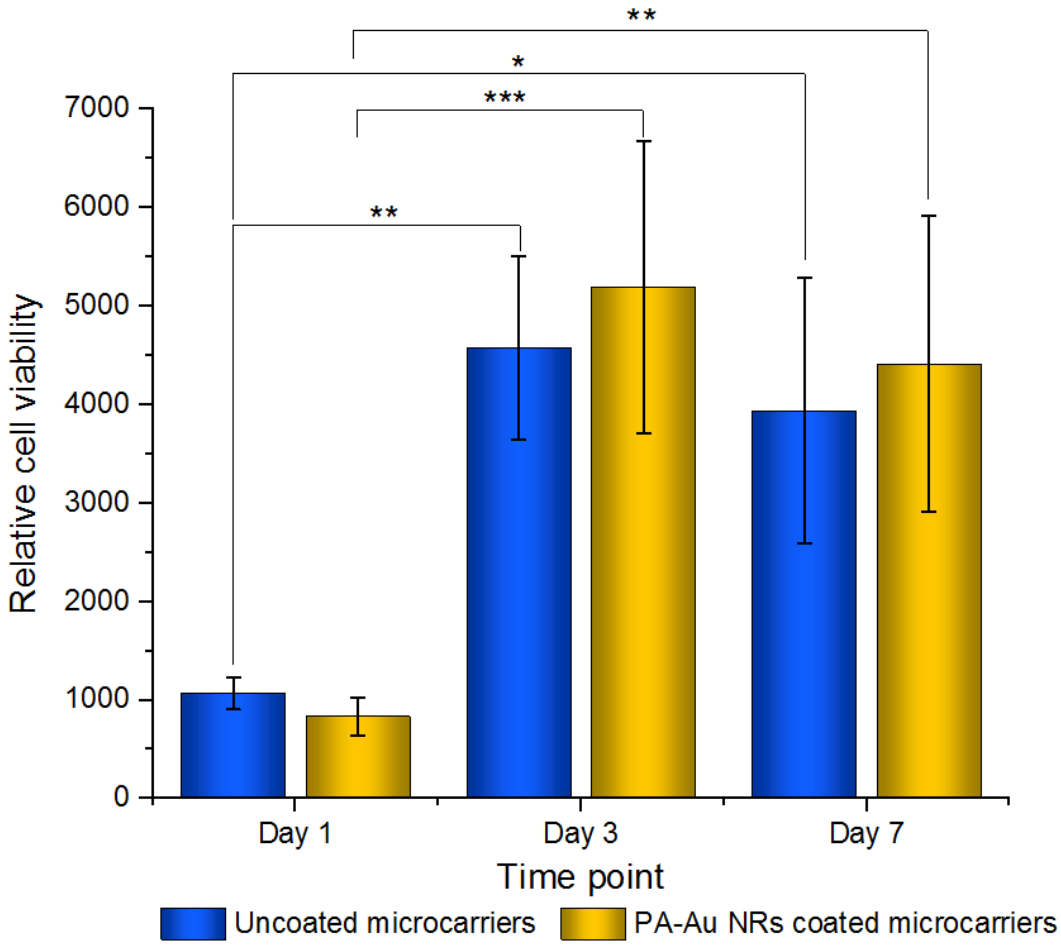

Figure 70: Quantification of viability of hMSCs on control surface (Uncoated microcarriers) and PA-Au NRs coated microcarriers via PrestoBlue assay. Statistical analyses show no significant difference between the cells grown on uncoated or Au NRs coated microcarriers when compared for the same day point. *p<0.05, **p<0.01 and ***p<0.001. Standard deviation was used. Error bars show ± 1 standard deviation from the mean.

Live/Dead assay

Due to the three-dimensional nature of the microcarrier system, the limited depth of focus of the fluorescent microscope and the diffuse staining used, it was difficult to resolve individual cells using the live/dead assay. The vast majority of fluorescence seen in these images arises from the Calcein AM (green) and almost no Propidium Iodide staining can be seen (red) (Figure 71 a & b) suggesting that the majority of cells cultured on the PA-Au NRs decorated microcarriers are viable. Due to the limitations in imaging it was not possible to comment on the viability of cells based on cell density

present on the microcarriers. However this limitation was overcome by performing the quantitative PrestoBlue assay as already shown in Figure 70.

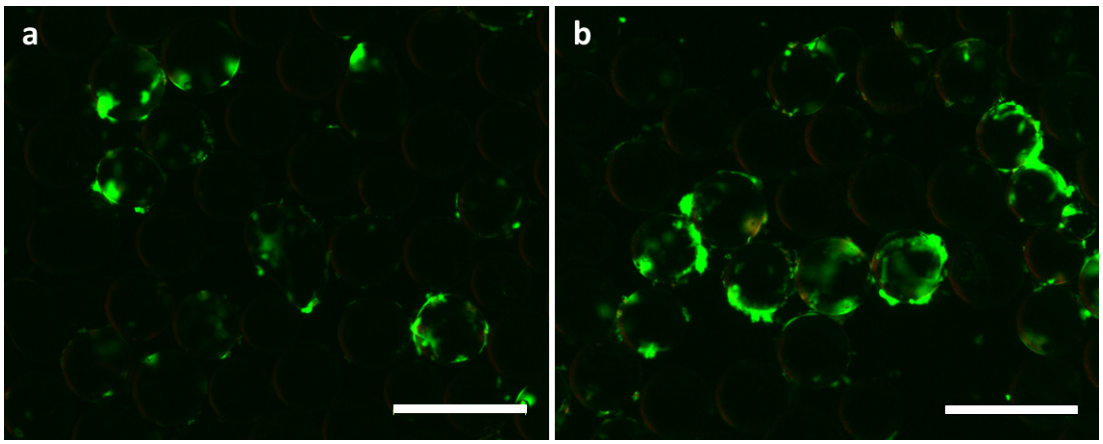

Figure 71: Live/Dead assay on (a) hMSCs on uncoated microcarriers and (b) hMSCs on PA-Au NRs coated microcarriers. Scale bar = 500 µm

Cell visualization was performed by using staining the actin filament in the cells by using phalloidin. These results are detailed in section 6.2.3.

6.2.3 Evaluation of cell distribution across microcarriers

As previously stated in chapter 2, adhesion of hMSCs on the cell culture surface are necessary in order for cell proliferation, maintaining viability and regulation of cellular activities. Actin filament plays a major structural role in this process and it forms the cytoskeletal network across the cell membrane. Cytoskeletal actin binding molecule phalloidin would help in characterizing the cellular spread across the microcarriers, which was not possible in Live/Dead staining.

Figure 72 is a representative image of hMSCs growing on uncoated microcarriers. Whilst it is hard to resolve individual actin fibres using a fluorescent microscope due to the depth of field created by the 3D microcarriers, the disperse green fluorescent stain clearly shows that actin producing cells are growing on the surface of the microcarriers. Some evidence of filamentous staining particularly on the microcarriers in the centre of the image suggest the formation of actin filaments generated due to strong adhesions to the microcarriers.

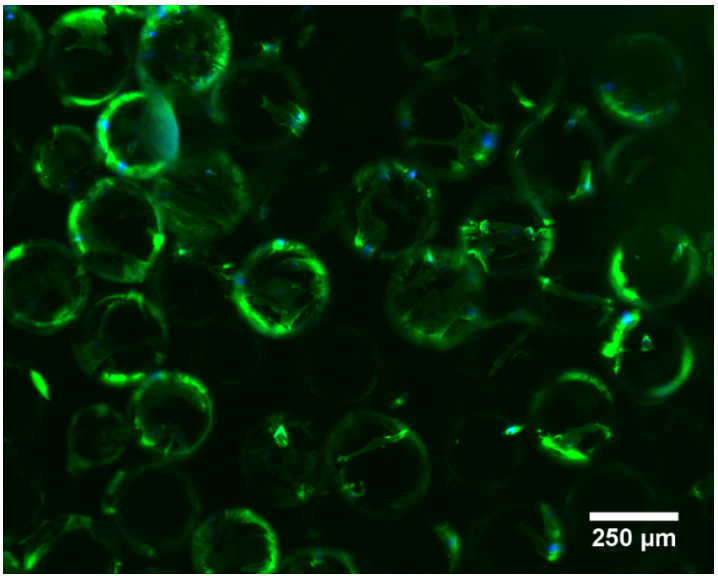

Figure 72: Actin staining of hMSCs by using fluorescent phalloidin. Cell growth around uncoated microcarrier surface can be observed.

Figure 73 are representative micrographs of hMSCs growth on PA-Au NRs coated microcarrier surfaces. The actin filament stained in the cells can clearly be seen coating the majority of the observable microcarriers, furthermore the clear nuclear staining from the DAPI shows high concentrations of cells on each microcarrier. Analysis of the DAPI stains (manual cell counting) showed that individual microcarriers could support the growth of up to 75 hMSCs. The expression of cytoskeletal staining shows a successful spread of cells across the Au NRs coated microcarriers. Typical stem cell expansion uses 2.5-4.3 mg/mL of microcarriers [585]. This is equivalent to approximately 7,500-13,500 microcarriers/mL. If 75 hMSCs per microcarriers is taken into consideration and calculated, a 100 mL spin flask lab based bioreactor would yield ~ 56.2 million to 101.25 million cells. Bioreactor tanks in industries can be made as large as 6000 litres which would lead to production of billions of cells that can be used to eased the bottle neck in the development of stem cell therapy [390].

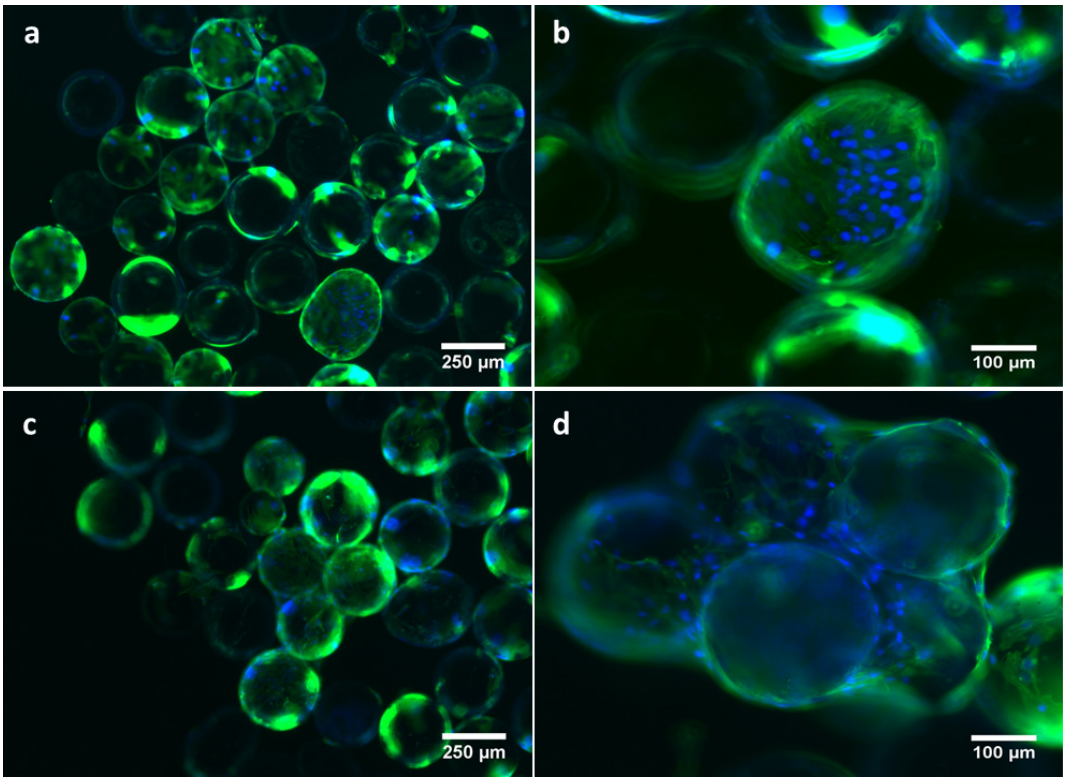

Figure 73: Actin staining (using phalloidin) of hMSCs cultured on PA-Au NR coated microcarriers for actin filaments to determine the structure and placement of the cells after 24 hours of incubation. (a & b) Cell growth can be noted around individual microcarriers. (c) & (d). Aggregation of microcarriers due to cell sheet growing around them.

When imaging the hMSCs grown on the Au NRs coated microcarriers, a frequent observation was the aggregation of microcarriers due to the growth of cells in the form of sheets across multiple microcarriers (Figure 73 c & d). This cell sheet growth is likely due to the presence of cadherin and other extracellular molecules being able to develop extensive networks of cell-cell interactions [586]. Studies conducted with cells and microcarriers cultured in bioreactors have stated that the formation of aggregation between the microcarriers is directly proportional to the agitation rate of the cell culture in the bioreactor system. While lower agitation rates leads the microcarriers to sediment and form aggregates due to cell-cell interaction, higher agitation speed leads to lower probability of aggregation as a result of hydrodynamic shear stress [587, 588]. The aggregation between the microcarriers, seen in Figure 73, may have been the result of the use of a static microcarrier cell culture system. Such cell sheet growth can be avoided by further developing this microcarrier cell culture system and eliminating the static culture conditions used for these initial experiments.

6.2.4 Cell Detachment

hMSCs, cultured on Au NRs coated and uncoated microcarriers, were irradiated with NIR laser for 1 hour to determine if cell detachment from the 3D microcarriers was possible. Due to technical challenges involved in imaging live cells attached to microcarriers (difference between cell and microcarrier refractive index), we evaluated cell detachment by immediately re-seeding the detached cells (or lack of) on 2D TCPS culture substrates and observing them as in previous chapters. The premise of this analysis is that if it is possible to observed cells growing in the re-seeded samples, then cell detachment from the microcarriers was achieved (Figure 74).

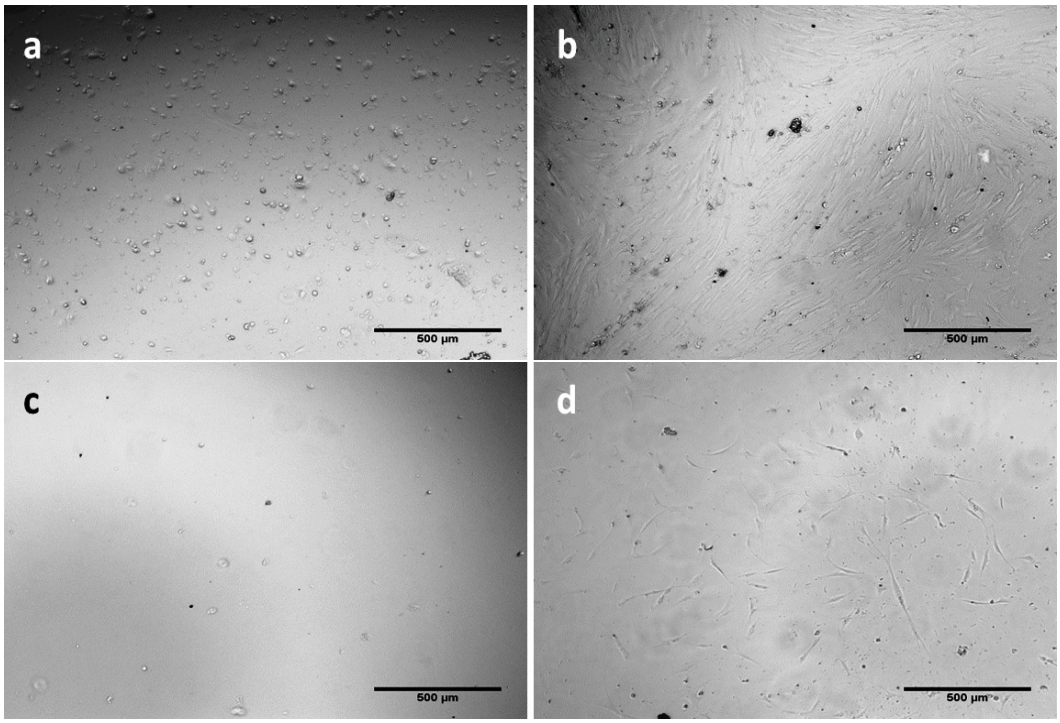

Figure 74: Re-seeded hMSCs detached post NIR-laser irradiation from (a) PA-Au NR coated microcarriers at t = 0 days, (b) coated microcarriers at t = 3 days, (c) un-coated microcarriers at t = 0 days and (d) un-coated microcarriers a t = 3 days. Scale bar = 500 µm.

Figure 74 (a) shows microscopic image of cells that have been detached from Au NRs coated microcarriers, re-seeded onto TCPS substrates and immediately imaged, whilst Figure 74 (b) shows the same TCPS substrate after 3 days cell growth. Figure 74 (a) clearly shows many rounded cells on the TCPS surface suggesting that NIR mediated cell detachment was successful. Encouragingly, after 3 days an almost confluent layer of well spread hMSCs can be seen on the TCPS substrates (Figure 74 b). Figure 74 (c) shows a representative image as in Figure 74 (a) but from microcarriers without the Au NRs coating that were NIR irradiated, here almost no rounded cells can be seen. Once again Figure 74 (d) shows this same substrate after 3

days, now only a few well spread can be seen on the surface however their number is much reduced compared to the cells detached from the Au NRs decorated microcarriers.

From Figure 74 (a & b) we can confirm that, similar to studies seen on 2D surfaces, detachment of cells from Au NRs coated microcarrier surface using NIR laser is feasible. The detachment of cells from the uncoated microcarriers is likely due to shear stress (and other) forces generated between colliding microcarriers during the washing steps causing a few weakly bound cells to detach.

Live/Dead assay were performed on hMSCs that were cultured on coated and uncoated microcarriers (before NIR irradiation) and also on the hMSCs that were detached from the microcarriers after the laser exposure in order to determine if either the microcarrier surface or the laser had any adverse effect on the hMSCs.

6.2.5 Live/Dead assay on cells detached by laser

Cells detached from coated and uncoated microcarriers were subjected to Live/Dead assay to test their viability 24 hours post-irradiation. It has already been stated in section 6.2.4 that the number of cells detached from PA-Au NR coated surface is substantially higher than from uncoated surfaces, this is further confirmed here (Figure 75 a & b). In Figure 75 (b) the amount of cells that have regrown, following detachment from the gold nanorod coated surface, is visibly higher compared to Figure 75 (a) which presents cells detached from uncoated surface. In both the figures, the lack of red fluorescence and presence of large quantities of green fluorescent stained cells confirms that the cells detached via NIR irradiation are viable.

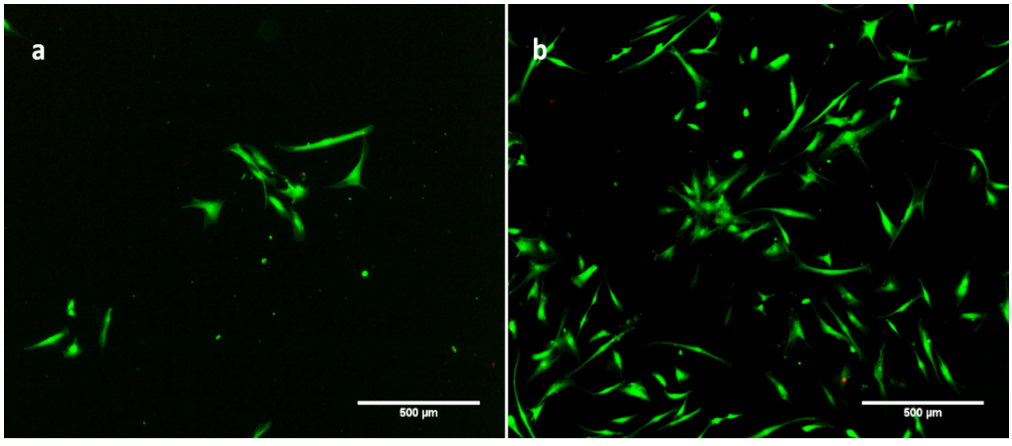

Figure 75: 24 hours after NIR irradiation (a) hMSCs detached from uncoated microcarriers and (b) hMSCs detached from PA-Au NR coated microcarriers

6.3 CONCLUSION

In cell therapeutic industries, it is essential to have a system were stem cells can be generated in large amounts in a short period of time. Though 2D surfaces like the T-flask stacks are standard procedure, we have seen that the quantity of stem cells generated can be limited due to limited surface area. Efforts have been made in the last two decades to make stem cell expansions using microcarriers feasible due to their large surface area, scalability, storage space and cost. One of the main hurdles faced is detachment of stem cells after expansion. Though trypsin is still being used as a main source for cell detachment, we have seen that the material and labour cost is high.

The studies presented in this chapter demonstrated the ability to coat the glass microcarriers with the PA-Au NRs and that these coated microcarriers were not cytotoxic to hMSCs. The hMSCs were able to attach and proliferate on both the coated and uncoated microcarriers. Irradiation of the microcarriers with NIR laser light successfully achieved cell detachment. And these hMSCs were shown to be viable through re-culture evaluation. All the studies were successful under static conditions.

Due to time constrains, it was not possible to evaluate the adipogenic and osteogenic differentiative capacity of the detached cells.

Chapter 7: Conclusion

7.1 CONCLUSION

There are very few studies which use surface plasmon resonance, generated through gold and NIR lasers, to detach cells from a surface. The ability to detach stem cells from an Au NRs coated surface using light has been reported for the first time in this thesis. As opposed to other studies, that use surface chemistry to "grow" gold nanostructures on the surface, this research used functionalized Au NRs that are readily available in the market. The efficiency and effects of surface plasmons and light based detachment on the stem cells was investigated.

Initially three different types of Au NRs were tested in this thesis: silica coated gold nanorods (SiO_2-Au NRs), Protein A functionalized gold nanorods (ProA-Au NRs) and amine terminated polymer functionalized gold nanorods (PA-Au NRs). Due to unreproducible surface coating SiO_2-Au NRs was rejected earlier on in the studies. ProA-Au NRs and PA-Au NRs were further tested. While both the particles had absorption spectra of approximately 785 nm in cell culture media, it was also possible to obtain a reproducible coated surface. While particle aggregation was observed on ProA-Au NRs coated surface, PA-Au NRs displayed an even coating across the surface with no aggregation of the Au NRs. Cell culture studies were performed on ProA-Au NRs, as well as PA-Au NRs coated surface.

NIH-3T3 mouse fibroblasts were initially used to study which of the particles would allow better cell viability and detachment when irradiated with NIR laser. Prior to cell detachment studies, the viability of the cells on various concentrations of Au NRs was assessed using PrestoBlue assay and Live/Dead staining. The data obtained confirmed no statistical difference either in the cell viability or proliferative capacity when cultured on different densities of Au NRs coated surface. Due to this result the surface coated with highest concentration of Au NRs (PA-Au NRs) were used for cell detachment studies. The cells, cultured on Au NRs coated surface, were irradiated with NIR laser for one hour and successful cell detachment was seen on both the Au NRs. While almost 100% cell detachment was possible using PA-Au NRs surface, some cells were left behind on the ProA-Au NRs coated surface. Viability of the cells were confirmed on the detached cells after re-culturing them for 24 hours using PrestoBlue

and Live/Dead assays. The cells detached via NIR irradiation were viable and healthy indicating that the laser and the Au NRs interaction did not cause an irreversible damage to the cells. Cell detachment is due to the localised surface plasmons resonance generated during NIR irradiation. As complete cell detachment was showed by the PA-Au NRs coated surface, these surfaces were chosen for hMSCs studies.

Similar to NIH-3T3 fibroblasts, the data obtained from hMSCs studies confirmed no statistical difference in cell viability or proliferative capacity on the PA-Au NRs coated surface. Complete cell detachment was observed by the cells from the Au NRs coated surface when exposed to NIR radiation. Cell viability and proliferative capacity was monitored for re-seeded cells for 7 days. The data showed that the cells were viable and healthy regardless of the irradiation time. In addition to this, a significant increase in the metabolic activity of the hMSCs were observed on the 7^{th} day when compared with the enzymatically detached cells. This result is consistent with other literature that have stated an increase in cell proliferative capacity post NIR irradiation. This maybe caused due to additional ATP generated in the cells exposed to NIR irradiation. Studies have also indicated the formation of nanopores on the cells membrane when irradiated with NIR laser [529]. But these nanopores are non-cytotoxic and cell membranes showed complete recovery when re-seeded. PI studies using FACS showed the re-cultured cells to be as viable as the trypsinized cells after 5 days of sub culture indicating showing that if there was nanopore formation, no irreversible damage to the cell membrane was done.

The cell immunophenotype of the laser detached undifferentiated hMSCs were compared with trypsinized cells by studying cell surface marker expression (CD 44, CD 73, CD90 and CD 105) by flow cytometry. Cells detached by both the methods showed similar level expression of surface markers. This data indicates that NIR exposure had no impact on the immunophenotype expression of the cells, and that cells detached using the NIR technique remained multipotent. When adipogenic and osteogenic differentiation ability was assessed using plate reader assay, a significant increase in both the differentiative capacity was observed in the NIR irradiated hMSCs compared to trypsinized cells. RT-qPCR was performed on the differentiated cells to confirm if there was any differences in the expression levels of a number of selected genes important in both adipogenesis and osteogenesis by irradiated cells when compared to trypsinized cells. Adipo differentiated cells were studied for the

expression of C/EBPα and FABP4. No statistically significant difference in either of the genes was observed between the trypsin released cells and laser detached cells. The expression of ALP and RUNX2 gene were studies for osteogenic differentiation. While the ALP expression was the similar for both the detachment techniques, an significant increase in RUNX2 gene was observed in NIR irradiated cells compared to trypsinized cells. Other studies have shown that NIR irradiation of hMSCs causes an upregulation both ALP and RUNX2 [275, 560-562]. Comparison of the presence of cell derived ECM proteins such as collagen, fibronectin and laminin after cell detachments was investigated for both NIR and enzymatically detached cells. Enzymatically detached cells (as expected) were stripped of the majority of their excreted ECM proteins. Conversely, NIR released cells retained a significant amount of their expressed ECM proteins after detachment. trypsin. These differences in ECM protein retention were most obvious for collagen and fibronectin and less of a difference was observed for laminin.

Since, surface plasmons and light-based cell detachment was successful on 2D surfaces, a proof-of-concept studies were conducted on 3D microcarriers. This was performed to see if the similar result could be replicated on 3D surfaces. Microcarriers, coated with different concentrations of PA-Au NRs, were studied by dark field microscopy and ICP-MS to qualitatively and quantitatively analyse the number of Au NRs on their surface. Microcarriers coated with highest concentration of PA-Au NRs (equivalent to that of 2D surface) were used for cell culture studies due to higher number of Au NRs on their surface. Cells viability studied using PrestoBlue assay and Live/Dead staining showed similar cell viability on uncoated and Au NRs coated microcarriers. Cells that were cultured on the PA-Au NRs coated microcarriers, when exposed to NIR irradiation for 1 hour, showed cell detachment. This was not observed from uncoated microcarriers post irradiation. Live/Dead assay showed that the cells detached from the PA-Au NRs coated microcarriers were viable. Thus, a successful detachment of hMSCs from PA-Au NRs was observed.

7.2 OUTLOOK AND FUTURE WORK

Overall, the research conducted in this thesis shows that it is possible to detach cells using Au NRs and NIR irradiation without detrimental impact to the fate of the stem cells. This technology can allow researchers to avoid the application of trypsin to

recover cells for therapeutic purposes. Further studies needs to be conducted if this technique is to be used for large scale cell detachment. While, it is theorized that the photothermal effect, caused due to the interaction between the surface plasmons and NIR irradiation, is responsible for cell detachment, this theory needs to be practically confirmed. This can be performed by (i) conducting nanoscale studies to detect the temperature elevation near the Au NRs (ii) testing hMSCs for increased production in ROS during NIR irradiation (iii) studying the cells for upregulation in heat shock proteins (HSP).

Future studies are also required to decrease the time required for the cells to detach from the Au NRs coated surface. Though the hMSCs released via NIR irradiation are viable and show improved proliferative and osteogenic differentiative capacity, each detachment process takes an hour while trypsinization process takes only 5-15 minutes. Studies can be conducted to observe if the time required can be reduced by increasing the power and energy density supplies to the Au NRs.

Microcarriers have the ability to generate large amount of cells, due to their higher surface to volume ratio when compared to flat surfaces. Microcarrier technologies are quite highly developed and have been implemented commercially for many cell based applications. For instance, microcarriers are used to amplify the volume of vaccines generated by cells in culture. However, for applications such as stem cell therapies were the cells need to be detached and recovered from the microcarriers intact (in vaccine production the cells are sacrificed and the vaccine is purified from the system), commercial development has been limited This is largely due to a lack of reliable and efficient methods for detaching and recovering adherent stem cells from microcarriers. While this thesis has demonstrated that it is possible to detach cells from Au NRs coated glass micro carrier surface via NIR irradiation, it is necessary to transfer this technology on to the microcarriers that are specifically designed for cell culture. Studies need to conducted on microcarriers that can be used in stirred tank bioreactors in order for the technology to be scaled up. An estimation of cost to see if it would be cheaper to use this Au NRs and NIR based cell detachment technique is outlined below:

7.2.1 Cost analysis of scale up of micro-carrier system

In current industrial environment trypsin is the gold standard for cell detachment. Data related to the cost and amount of trypsin used for industrial scale cell production

is not directly available. Here we performed a cost-analysis of the cost of cell detachment per m^2 of culture substrate for a number of different systems:

1. Cell detachment via trypsinization.

2. Cell detachment using the NIR-Au NRs system developed in this thesis, with Au NRs from a commercial source (Nanopartz).

3. Cell detachment using the NIR-Au NRs system, but with an estimation of the cost of synthesising the Au NRs in-house.

The results from this cost-analysis allow us to determine if industrial scale up of either method 2 (using commercial Au NRs) or method 3 (synthesising our own Au NRs) is feasible compared to the current costs of trypsinization.

Current cost analyses of trypsin used in industries

Industrial scale cell production is currently done using stacking technique were up to 40 flasks are stacked on top of each other (figure 1). Each flask has a surface area of 636 cm^2 and the total area of the entire setup (assuming 40 stacked flasks) is approximately 2.54 m^2. Typically, we use around 5 mL of trypsin for one t-75 flask (area 75 cm^2). Using these estimates we would require around 1.7 litres of trypsin per 2.54 m^2 (one stacked t-flask). In industries thousands of flasks are trypsinized daily.

The current market price of trypsin is approximately $50 for 100 mL (depending on the type of trypsin used). This means that for each stack requiring 1.7 litres of trypsin, the industries would be required to spend $850 i.e., $850 per 2.54 m^2 or $335 per m^2. When calculated for hundreds of stacks along with money spent on labour per hour, the cost increases greatly.

Cost analyses for using 2D Au NRs coated surface with commercially available Au NRs

As per our results, we require a density of 300 Au NRs/μm^2. The area of a stacked t-flask used in industry is 2.54 m^2 to coat an equivalent surface area (either t-flasks or microcarriers) in Au NRs would require 7.6×10^{14} Au NRs. One vial of Au NRs obtained commercially form Nanopartz, USA, contains 4.1×10^{13} Au NRs and costs $800. To cover the entire 2.54 m^2 we would require 185.36 vials of Au NRs from Nanopartz costing $148,000 per flask or $59,000 per m^2. The current form the costs associated with scaling up Au NRs from a commercial source makes it completely

unfeasible compared to the current costs of trypsinization. In fact, trypsinization is around 176 times less expensive.

Cost analyses of synthesizing Au NRs in private lab for scale up process

From above calculations we can state that it is not commercially viable to spend \$59,000 per m^2 to coat a cell culture substrate with Au NRs. As an alternative the cost of the raw materials required to synthesize the Au NRs in our lab was investigated. According to Xu *et al*., the cost of synthesizing one gram of Au NRs, using CTAB and obtaining 99% purity is \$2.5 [589]. As per to the above calculations, 760×10^{13} Au NRs is required to coat a 2.54 m^2 surface area which corresponds to 0.4g of Au NRs. So the cost of the raw materials for synthesising Au NRs for one stacked t-flask would cost be approximately \$0.92 or \$0.36 per m^2 of cell culture substrate. This does not include either the labour or the infrastructure required to make the Au NRs. However, based on raw materials alone I can observe that there is a 1000-fold drop in price when the Au NRs are fabricated in-house.

Bibliography

1. Phinney, D.G. and D.J. Prockop, *Concise Review: Mesenchymal Stem/Multipotent Stromal Cells: The State of Transdifferentiation and Modes of Tissue Repair—Current Views.* STEM CELLS, 2007. **25**(11): p. 2896-2902.
2. Pytlik, S., *Production of clinical grade mesenchymal stromal cells*, in *Regenerative Medicine and Tissue Engineering-Cells and Biomaterials*. 2011, InTech.
3. Menard, C., et al., *Clinical-grade mesenchymal stromal cells produced under various good manufacturing practice processes differ in their immunomodulatory properties: standardization of immune quality controls.* Stem cells and development, 2013. **22**(12): p. 1789-1801.
4. Lee, W.Y.-W. and B. Wang, *Cartilage repair by mesenchymal stem cells: Clinical trial update and perspectives.* Journal of orthopaedic translation, 2017. **9**: p. 76-88.
5. Ackerman, I.N., Bohensky, M. A., Pratt, C., Gorelik, A. & Liew, D, *Counting the Cost: the current and future burden of arthritis.* Arthritis Australia, 2016.
6. Mahla, R.S., *Stem cells applications in regenerative medicine and disease therapeutics.* International journal of cell biology, 2016. **2016**.
7. Yamasaki, S., et al., *Cartilage Repair With Autologous Bone Marrow Mesenchymal Stem Cell Transplantation: Review of Preclinical and Clinical Studies.* Cartilage, 2014. **5**(4): p. 196-202.
8. Orozco, L., et al., *Treatment of knee osteoarthritis with autologous mesenchymal stem cells: two-year follow-up results.* Transplantation, 2014. **97**(11): p. e66-e68.
9. Wang, L., et al., *Allogeneic bone marrow mesenchymal stem cell transplantation in patients with UDCA-resistant primary biliary cirrhosis.* Stem cells and development, 2014. **23**(20): p. 2482-2489.
10. Ismail, H.D., et al., *Mesenchymal stem cell implantation in atrophic nonunion of the long bones: A translational study.* Bone & Joint Research, 2016. **5**(7): p. 287-293.
11. Horwitz, E.M., et al., *Isolated allogeneic bone marrow-derived mesenchymal cells engraft and stimulate growth in children with osteogenesis imperfecta: Implications for cell therapy of bone.* Proceedings of the National Academy of Sciences of the United States of America, 2002. **99**(13): p. 8932-8937.
12. Broekman, W., et al., *Mesenchymal stromal cells: a novel therapy for the treatment of chronic obstructive pulmonary disease?* Thorax, 2018. **73**(6): p. 565-574.
13. Siminovitch, L., E.A. McCulloch, and J.E. Till, *The distribution of colony-forming cells among spleen colonies.* Journal of Cellular and Comparative Physiology, 1963. **62**(3): p. 327-336.
14. Hongbao, M., Y. Yan, and M. Ma, *The discovery history of stem cell*. Vol. 4. 2013. 4-6.
15. Prindull, G., B. Prindull, and N.v. Meulen, *Haematopoietic stem cells (CFUc) in human cord blood.* Acta Paediatrica, 1978. **67**(4): p. 413-416.
16. Thomson, J.A., et al., *Embryonic Stem Cell Lines Derived from Human Blastocysts.* Science, 1998. **282**(5391): p. 1145-1147.
17. Takahashi, K. and S. Yamanaka, *Induction of Pluripotent Stem Cells from Mouse Embryonic and Adult Fibroblast Cultures by Defined Factors.* Cell. **126**(4): p. 663-676.
18. Reya, T., et al., *Stem cells, cancer, and cancer stem cells.* Nature, 2001. **414**: p. 105.
19. Blanpain, C., et al., *Self-Renewal, Multipotency, and the Existence of Two Cell Populations within an Epithelial Stem Cell Niche.* Cell, 2004. **118**(5): p. 635-648.
20. Kolios, G. and Y. Moodley, *Introduction to Stem Cells and Regenerative Medicine.* Respiration, 2013. **85**(1): p. 3-10.

21. Blanpain, C., V. Horsley, and E. Fuchs, *Epithelial Stem Cells: Turning over New Leaves.* Cell, 2007. **128**(3): p. 445-458.
22. Kunisaki, Y., et al., *Arteriolar niches maintain haematopoietic stem cell quiescence.* Nature, 2013. **502**(7473): p. 637-643.
23. Sneddon, J.B. and Z. Werb, *Location, Location, Location: The Cancer Stem Cell Niche.* Cell Stem Cell, 2007. **1**(6): p. 607-611.
24. Schofield, R., *The relationship between the spleen colony-forming cell and the haemopoietic stem cell.* Blood cells, 1978. **4**(1-2): p. 7-25.
25. Yeung, T.M., et al., *Regulation of self-renewal and differentiation by the intestinal stem cell niche.* Cellular and Molecular Life Sciences, 2011. **68**(15): p. 2513-2523.
26. Kiefer, J.C., *Primer and interviews: the dynamic stem cell niche.* Developmental Dynamics, 2011. **240**(3): p. 737-743.
27. Wang, L.D. and A.J. Wagers, *Dynamic niches in the origination and differentiation of haematopoietic stem cells.* Nature reviews Molecular cell biology, 2011. **12**(10): p. 643.
28. Eseonu, O.I. and C. De Bari, *Homing of mesenchymal stem cells: mechanistic or stochastic? Implications for targeted delivery in arthritis.* Rheumatology, 2015. **54**(2): p. 210-218.
29. Biswas, A. and R. Hutchins, *Embryonic Stem Cells.* Stem Cells and Development, 2007. **16**(2): p. 213-222.
30. Bishop, A.E., L.D.K. Buttery, and J.M. Polak, *Embryonic stem cells.* The Journal of Pathology, 2002. **197**(4): p. 424-429.
31. Ilic, D. and J.M. Polak, *Stem cells in regenerative medicine: introduction.* British Medical Bulletin, 2011. **98**(1): p. 117-126.
32. Hayflick, L., *The limited in vitro lifetime of human diploid cell strains.* Experimental Cell Research, 1965. **37**(3): p. 614-636.
33. Amit, M., et al., *Human Feeder Layers for Human Embryonic Stem Cells1.* Biology of Reproduction, 2003. **68**(6): p. 2150-2156.
34. Richards, M., et al., *Human feeders support prolonged undifferentiated growth of human inner cell masses and embryonic stem cells.* Nature Biotechnology, 2002. **20**: p. 933.
35. Bongso, A. and M. Richards, *History and perspective of stem cell research.* Best Practice & Research Clinical Obstetrics & Gynaecology, 2004. **18**(6): p. 827-842.
36. Takahashi, K., et al., *Induction of Pluripotent Stem Cells from Adult Human Fibroblasts by Defined Factors.* Cell. **131**(5): p. 861-872.
37. Robert, C.G., *The First Human Retrovirus.* Scientific American, 1986. **255**(6): p. 88.
38. Yu, J., et al., *Induced Pluripotent Stem Cell Lines Derived from Human Somatic Cells.* Science, 2007. **318**(5858): p. 1917-1920.
39. Dang, C.V., et al., *Function of the c-Myc Oncogenic Transcription Factor.* Experimental Cell Research, 1999. **253**(1): p. 63-77.
40. Okita, K., T. Ichisaka, and S. Yamanaka, *Generation of germline-competent induced pluripotent stem cells.* Nature, 2007. **448**: p. 313.
41. Robey, P.G., *Series Introduction: Stem cells near the century mark.* Journal of Clinical Investigation, 2000. **105**(11): p. 1489-1491.
42. Lo, B. and L. Parham, *Ethical Issues in Stem Cell Research.* Endocrine Reviews, 2009. **30**(3): p. 204-213.
43. Obradović, S., et al., *Autologous bone marrow-derived progenitor cell transplantation for myocardial regeneration after acute infarction.* Vojnosanitetski pregled, 2004. **61**(5): p. 519-529.
44. Chimutengwende-Gordon, M. and W. S. Khan, *Advances in the Use of Stem Cells and Tissue Engineering Applications in Bone Repair.* Current Stem Cell Research & Therapy, 2012. **7**(2): p. 122-126.

45. Bang, O.Y., *Clinical Trials of Adult Stem Cell Therapy in Patients with Ischemic Stroke.* Journal of Clinical Neurology (Seoul, Korea), 2016. **12**(1): p. 14-20.
46. Mead, B., et al., *Stem cell treatment of degenerative eye disease.* Stem Cell Research, 2015. **14**(3): p. 243-257.
47. Nishida, S., et al., *Number of osteoprogenitor cells in human bone marrow markedly decreases after skeletal maturation.* Journal of bone and mineral metabolism, 1999. **17**(3): p. 171-177.
48. Estes, B.T., et al., *Isolation of adipose-derived stem cells and their induction to a chondrogenic phenotype.* Nature protocols, 2010. **5**(7): p. 1294.
49. Boquest, A.C., et al., *Isolation of stromal stem cells from human adipose tissue*, in *Nuclear Reprogramming*. 2006, Springer. p. 35-46.
50. Mizuno, H., M. Tobita, and A.C. Uysal, *Concise Review: Adipose-Derived Stem Cells as a Novel Tool for Future Regenerative Medicine.* STEM CELLS, 2012. **30**(5): p. 804-810.
51. Hindle, P., et al., *The Infrapatellar Fat Pad as a Source of Perivascular Stem Cells with Increased Chondrogenic Potential for Regenerative Medicine.* STEM CELLS Translational Medicine, 2017. **6**(1): p. 77-87.
52. De Bari, C., et al., *Multipotent mesenchymal stem cells from adult human synovial membrane.* Arthritis & Rheumatism, 2001. **44**(8): p. 1928-1942.
53. Seo, B.-M., et al., *Investigation of multipotent postnatal stem cells from human periodontal ligament.* The Lancet, 2004. **364**(9429): p. 149-155.
54. Aasen, T. and J.C.I. Belmonte, *Isolation and cultivation of human keratinocytes from skin or plucked hair for the generation of induced pluripotent stem cells.* Nature protocols, 2010. **5**(2): p. 371.
55. Bieback, K., et al., *Critical Parameters for the Isolation of Mesenchymal Stem Cells from Umbilical Cord Blood.* STEM CELLS, 2004. **22**(4): p. 625-634.
56. Williams, J.T., et al., *Cells isolated from adult human skeletal muscle capable of differentiating into multiple mesodermal phenotypes.* The American Surgeon, 1999. **65**(1): p. 22.
57. Itskovitz-Eldor, J., et al., *Differentiation of Human Embryonic Stem Cells into Embryoid Bodies Comprising the Three Embryonic Germ Layers.* Molecular Medicine, 2000. **6**(2): p. 88-95.
58. Amit, M., et al., *Clonally derived human embryonic stem cell lines maintain pluripotency and proliferative potential for prolonged periods of culture.* Developmental biology, 2000. **227**(2): p. 271-278.
59. Eriksson, P.S., et al., *Neurogenesis in the adult human hippocampus.* Nature Medicine, 1998. **4**(11): p. 1313-1317.
60. Johansson, C.B., et al., *Neural stem cells in the adult human brain.* Experimental cell research, 1999. **253**(2): p. 733-736.
61. Kirschenbaum, B., et al., *In vitro neuronal production and differentiation by precursor cells derived from the adult human forebrain.* Cerebral Cortex, 1994. **4**(6): p. 576-589.
62. Carleton, A., et al., *Becoming a new neuron in the adult olfactory bulb.* Nature Neuroscience, 2003. **6**(5): p. 507-518.
63. Pittenger, M.F., et al., *Multilineage Potential of Adult Human Mesenchymal Stem Cells.* Science, 1999. **284**(5411): p. 143-147.
64. Mackay, A.M., et al., *Chondrogenic differentiation of cultured human mesenchymal stem cells from marrow.* Tissue engineering, 1998. **4**(4): p. 415-428.
65. Prockop, D.J., *Marrow stromal cells as stem cells for nonhematopoietic tissues.* Science, 1997. **276**(5309): p. 71-74.
66. Baksh, D., R. Yao, and R.S. Tuan, *Comparison of Proliferative and Multilineage Differentiation Potential of Human Mesenchymal Stem Cells Derived from Umbilical Cord and Bone Marrow.* STEM CELLS, 2007. **25**(6): p. 1384-1392.

67. Fu, Y.-S., et al., *Conversion of Human Umbilical Cord Mesenchymal Stem Cells in Wharton's Jelly to Dopaminergic Neurons In Vitro: Potential Therapeutic Application for Parkinsonism.* STEM CELLS, 2006. **24**(1): p. 115-124.
68. Mitchell, K.E., et al., *Matrix cells from Wharton's jelly form neurons and glia.* Stem cells, 2003. **21**(1): p. 50-60.
69. Wang, H.-S., et al., *Mesenchymal Stem Cells in the Wharton's Jelly of the Human Umbilical Cord.* STEM CELLS, 2004. **22**(7): p. 1330-1337.
70. Gimble, J.M. and F. Guilak, *Adipose-derived adult stem cells: isolation, characterization, and differentiation potential.* Cytotherapy, 2003. **5**(5): p. 362-369.
71. Mizuno, H., et al., *Myogenic differentiation by human processed lipoaspirate cells.* Plastic and reconstructive surgery, 2002. **109**(1): p. 199-209.
72. L., D.J., et al., *Tissue-engineered cartilage and bone using stem cells from human infrapatellar fat pads.* The Journal of Bone and Joint Surgery. British volume, 2003. **85-B**(5): p. 740-747.
73. Ashjian, P.H., et al., *In vitro differentiation of human processed lipoaspirate cells into early neural progenitors.* Plastic and reconstructive surgery, 2003. **111**(6): p. 1922-1931.
74. de Sousa, E.B., et al., *Synovial fluid and synovial membrane mesenchymal stem cells: latest discoveries and therapeutic perspectives.* Stem Cell Research & Therapy, 2014. **5**(5): p. 112.
75. De Bari, C., et al., *Skeletal muscle repair by adult human mesenchymal stem cells from synovial membrane.* The Journal of Cell Biology, 2003. **160**(6): p. 909-918.
76. Miura, M., et al., *SHED: stem cells from human exfoliated deciduous teeth.* Proceedings of the National Academy of Sciences, 2003. **100**(10): p. 5807-5812.
77. Gronthos, S., et al., *Postnatal human dental pulp stem cells (DPSCs) in vitro and in vivo.* Proceedings of the National Academy of Sciences, 2000. **97**(25): p. 13625-13630.
78. Gronthos, S., et al., *Stem cell properties of human dental pulp stem cells.* Journal of dental research, 2002. **81**(8): p. 531-535.
79. Joannides, A., et al., *Efficient generation of neural precursors from adult human skin: astrocytes promote neurogenesis from skin-derived stem cells.* The Lancet, 2004. **364**(9429): p. 172-178.
80. Toma, J.G., et al., *Isolation of multipotent adult stem cells from the dermis of mammalian skin.* Nature cell biology, 2001. **3**(9): p. 778.
81. Belicchi, M., et al., *Human skin-derived stem cells migrate throughout forebrain and differentiate into astrocytes after injection into adult mouse brain.* Journal of neuroscience research, 2004. **77**(4): p. 475-486.
82. Zvaifler, N.J., et al., *Mesenchymal precursor cells in the blood of normal individuals.* Arthritis Research & Therapy, 2000. **2**(6): p. 477.
83. Pesce, M., et al., *Myoendothelial Differentiation of Human Umbilical Cord Blood Derived Stem Cells in Ischemic Limb Tissues.* Circulation Research, 2003. **93**(5): p. e51-e62.
84. Sun, B., et al., *Induction of human umbilical cord blood-derived stem cells with embryonic stem cell phenotypes into insulin producing islet-like structure.* Biochemical and biophysical research communications, 2007. **354**(4): p. 919-923.
85. Zhao, Y., H. Wang, and T. Mazzone, *Identification of stem cells from human umbilical cord blood with embryonic and hematopoietic characteristics.* Experimental cell research, 2006. **312**(13): p. 2454-2464.
86. Jankowski, R.J., B.M. Deasy, and J. Huard, *Muscle-derived stem cells.* Gene Therapy, 2002. **9**(10): p. 642-647.

87. Schultz, S.S. and P.A. Lucas, *Human stem cells isolated from adult skeletal muscle differentiate into neural phenotypes.* Journal of neuroscience methods, 2006. **152**(1-2): p. 144-155.
88. Alessandri, G., et al., *Isolation and culture of human muscle-derived stem cells able to differentiate into myogenic and neurogenic cell lineages.* The lancet, 2004. **364**(9448): p. 1872-1883.
89. De Coppi, P., et al., *Rosiglitazone modifies the adipogenic potential of human muscle satellite cells.* Diabetologia, 2006. **49**(8): p. 1962-1973.
90. Mastrogiacomo, M., A. Derubeis, and R. Cancedda, *Bone and cartilage formation by skeletal muscle derived cells.* Journal of cellular physiology, 2005. **204**(2): p. 594-603.
91. Malik, N.N. and M.B. Durdy, *Chapter 7 - Cell Therapy Landscape: Autologous and Allogeneic Approaches*, in *Translational Regenerative Medicine*, A. Atala and J.G. Allickson, Editors. 2015, Academic Press: Boston. p. 87-106.
92. Friedenstein, A., R. Chailakhjan, and K. Lalykina, *The development of fibroblast colonies in monolayer cultures of guinea-pig bone marrow and spleen cells.* Cell Proliferation, 1970. **3**(4): p. 393-403.
93. Friedenstein, A., R. Chailakhyan, and U. Gerasimov, *Bone marrow osteogenic stem cells: in vitro cultivation and transplantation in diffusion chambers.* Cell proliferation, 1987. **20**(3): p. 263-272.
94. Ashton, B.A., et al., *Formation of bone and cartilage by marrow stromal cells in diffusion chambers in vivo.* Clinical Orthopaedics and Related Research, 1980(151): p. 294-307.
95. Wakitani, S., T. Saito, and A.I. Caplan, *Myogenic cells derived from rat bone marrow mesenchymal stem cells exposed to 5-azacytidine.* Muscle & nerve, 1995. **18**(12): p. 1417-1426.
96. Gang, E.J., et al., *Skeletal myogenic differentiation of mesenchymal stem cells isolated from human umbilical cord blood.* Stem cells, 2004. **22**(4): p. 617-624.
97. Caplan, A.I., *Mesenchymal stem cells.* Journal of Orthopaedic Research, 1991. **9**(5): p. 641-650.
98. Sanchez-Ramos, J., et al., *Adult Bone Marrow Stromal Cells Differentiate into Neural Cells in Vitro.* Experimental Neurology, 2000. **164**(2): p. 247-256.
99. Ni, W.-F., et al., *In vitro neural differentiation of bone marrow stromal cells induced by cocultured olfactory ensheathing cells.* Neuroscience Letters, 2010. **475**(2): p. 99-103.
100. Petersen, B.E., et al., *Bone Marrow as a Potential Source of Hepatic Oval Cells.* Science, 1999. **284**(5417): p. 1168-1170.
101. Jopling, C., S. Boue, and J.C.I. Belmonte, *Dedifferentiation, transdifferentiation and reprogramming: three routes to regeneration.* Nature Reviews Molecular Cell Biology, 2011. **12**: p. 79.
102. Murray, I.R., et al., *Natural history of mesenchymal stem cells, from vessel walls to culture vessels.* Cellular and Molecular Life Sciences, 2014. **71**(8): p. 1353-1374.
103. Fraser, J.K., et al., *Fat tissue: an underappreciated source of stem cells for biotechnology.* Trends in Biotechnology. **24**(4): p. 150-154.
104. Uccelli, A., L. Moretta, and V. Pistoia, *Mesenchymal stem cells in health and disease.* Nature Reviews Immunology, 2008. **8**: p. 726.
105. Soleimani, M. and S. Nadri, *A protocol for isolation and culture of mesenchymal stem cells from mouse bone marrow.* Nature Protocols, 2009. **4**: p. 102.
106. Bara, J.J., et al., *Concise Review: Bone Marrow-Derived Mesenchymal Stem Cells Change Phenotype Following In Vitro Culture: Implications for Basic Research and the Clinic.* STEM CELLS, 2014. **32**(7): p. 1713-1723.

107. Dominici, M., et al., *Minimal criteria for defining multipotent mesenchymal stromal cells. The International Society for Cellular Therapy position statement.* Cytotherapy, 2006, Vol.8(4), p.315-317, 2006. **8**(4): p. 315-317.
108. Chen, Q., et al., *Fate decision of mesenchymal stem cells: adipocytes or osteoblasts?* Cell Death And Differentiation, 2016. **23**: p. 1128.
109. Samsonraj, R.M., et al., *Concise Review: Multifaceted Characterization of Human Mesenchymal Stem Cells for Use in Regenerative Medicine.* STEM CELLS Translational Medicine, 2017. **6**(12): p. 2173-2185.
110. Quirici, N., et al., *Isolation of bone marrow mesenchymal stem cells by anti-nerve growth factor receptor antibodies.* Experimental Hematology, 2002. **30**(7): p. 783-791.
111. BÜHRING, H.J., et al., *Novel Markers for the Prospective Isolation of Human MSC.* Annals of the New York Academy of Sciences, 2007. **1106**(1): p. 262-271.
112. Boxall, S.A. and E. Jones, *Markers for characterization of bone marrow multipotential stromal cells.* Stem cells international, 2012. **2012**.
113. Niehage, C., et al., *The cell surface proteome of human mesenchymal stromal cells.* PloS one, 2011. **6**(5): p. e20399-e20399.
114. Choi, K.-M., et al., *Effect of ascorbic acid on bone marrow-derived mesenchymal stem cell proliferation and differentiation.* Journal of Bioscience and Bioengineering, 2008. **105**(6): p. 586-594.
115. Song, I.H., A.I. Caplan, and J.E. Dennis, *In vitro dexamethasone pretreatment enhances bone formation of human mesenchymal stem cells in vivo.* Journal of Orthopaedic Research, 2009. **27**(7): p. 916-921.
116. Jaiswal, N., et al., *Osteogenic differentiation of purified, culture-expanded human mesenchymal stem cells in vitro.* Journal of cellular biochemistry, 1997. **64**(2): p. 295-312.
117. Simann, M., et al., *Heparin affects human bone marrow stromal cell fate: Promoting osteogenic and reducing adipogenic differentiation and conversion.* Bone, 2015. **78**: p. 102-113.
118. Hitomi, K. and N. Tsukagoshi, *Role of ascorbic acid in modulation of gene expression*, in *Subcellular biochemistry*. 1996, Springer. p. 41-56.
119. Walsh, S., et al., *High concentrations of dexamethasone suppress the proliferation but not the differentiation or further maturation of human osteoblast precursors in vitro: relevance to glucocorticoid-induced osteoporosis.* Rheumatology, 2001. **40**(1): p. 74-83.
120. Cheng, S.L., et al., *Differentiation of human bone marrow osteogenic stromal cells in vitro: induction of the osteoblast phenotype by dexamethasone.* Endocrinology, 1994. **134**(1): p. 277-286.
121. Langenbach, F. and J. Handschel, *Effects of dexamethasone, ascorbic acid and β-glycerophosphate on the osteogenic differentiation of stem cells in vitro.* Stem cell research & therapy, 2013. **4**(5): p. 117-117.
122. Tada, H., et al., *Phosphate increases bone morphogenetic protein-2 expression through cAMP-dependent protein kinase and ERK1/2 pathways in human dental pulp cells.* Bone, 2011. **48**(6): p. 1409-1416.
123. Kulterer, B., et al., *Gene expression profiling of human mesenchymal stem cells derived from bone marrow during expansion and osteoblast differentiation.* BMC Genomics, 2007. **8**(1): p. 70.
124. Waymire, K.G., et al., *Mice lacking tissue non–specific alkaline phosphatase die from seizures due to defective metabolism of vitamin B–6.* Nature Genetics, 1995. **11**: p. 45.

125. Narisawa, S., N. Fröhlander, and J.L. Millán, *Inactivation of two mouse alkaline phosphatase genes and establishment of a model of infantile hypophosphatasia.* Developmental Dynamics, 1997. **208**(3): p. 432-446.
126. Narisawa, S., et al., *Accelerated fat absorption in intestinal alkaline phosphatase knockout mice.* Molecular and cellular biology, 2003. **23**(21): p. 7525-7530.
127. Wysokinski, D., E. Pawlowska, and J. Blasiak, *RUNX2: A master bone growth regulator that may be involved in the DNA damage response.* DNA and cell biology, 2015. **34**(5): p. 305-315.
128. Rawadi, G., et al., *BMP-2 Controls Alkaline Phosphatase Expression and Osteoblast Mineralization by a Wnt Autocrine Loop.* Journal of Bone and Mineral Research, 2003. **18**(10): p. 1842-1853.
129. Ducy, P., *CBFA1: A molecular switch in osteoblast biology.* Developmental Dynamics, 2000. **219**(4): p. 461-471.
130. Komori, T., et al., *Targeted Disruption of Cbfa1 Results in a Complete Lack of Bone Formation owing to Maturational Arrest of Osteoblasts.* Cell, 1997. **89**(5): p. 755-764.
131. Ghali, O., et al., *Dexamethasone in osteogenic medium strongly induces adipocyte differentiation of mouse bone marrow stromal cells and increases osteoblast differentiation.* BMC Cell Biology, 2015. **16**: p. 9.
132. Klemm, D.J., et al., *Insulin-induced Adipocyte Differentiation activation of CREB rescues adipogenesis from the arrest caused by inhibition of prenylation.* Journal of Biological Chemistry, 2001. **276**(30): p. 28430-28435.
133. Lehmann, J.M., et al., *Peroxisome proliferator-activated receptors α and γ are activated by indomethacin and other non-steroidal anti-inflammatory drugs.* Journal of Biological Chemistry, 1997. **272**(6): p. 3406-3410.
134. Petersen, R.K., et al., *Cyclic AMP (cAMP)-Mediated Stimulation of Adipocyte Differentiation Requires the Synergistic Action of Epac- and cAMP-Dependent Protein Kinase-Dependent Processes.* Molecular and Cellular Biology, 2008. **28**(11): p. 3804-3816.
135. Hudak, C.S. and H.S. Sul, *Pref-1, a gatekeeper of adipogenesis.* Frontiers in endocrinology, 2013. **4**: p. 79-79.
136. Zhang, H.H., et al., *Insulin Stimulates Adipogenesis through the Akt-TSC2-mTORC1 Pathway.* PLOS ONE, 2009. **4**(7): p. e6189.
137. Niemelä, S., et al., *Adipose tissue and adipocyte differentiation: molecular and cellular aspects and tissue engineering applications.* Topics in tissue engineering, 2008. **4**(1): p. 26.
138. Wu, Z., et al., *Cross-regulation of C/EBPα and PPARγ controls the transcriptional pathway of adipogenesis and insulin sensitivity.* Molecular cell, 1999. **3**(2): p. 151-158.
139. GREGOIRE, F.M., C.M. SMAS, and H.S. SUL, *Understanding Adipocyte Differentiation.* Physiological Reviews, 1998. **78**(3): p. 783-809.
140. James, A.W., *Review of signaling pathways governing MSC osteogenic and adipogenic differentiation.* Scientifica, 2013. **2013**.
141. Johnstone, B., et al., *In VitroChondrogenesis of Bone Marrow-Derived Mesenchymal Progenitor Cells.* Experimental Cell Research, 1998. **238**(1): p. 265-272.
142. Tuli, R., et al., *Transforming growth factor-β-mediated chondrogenesis of human mesenchymal progenitor cells involves N-cadherin and mitogen-activated protein kinase and Wnt signaling cross-talk.* Journal of Biological Chemistry, 2003. **278**(42): p. 41227-41236.
143. Lefebvre, V., R. Behringer, and B. De Crombrugghe, *L-Sox5, Sox6 and Sox9 control essential steps of the chondrocyte differentiation pathway.* Osteoarthritis and Cartilage, 2001. **9**: p. S69-S75.

144. Jo, A., et al., *The versatile functions of Sox9 in development, stem cells, and human diseases.* Genes & Diseases, 2014. **1**(2): p. 149-161.
145. Lefebvre, V., et al., *SOX9 is a potent activator of the chondrocyte-specific enhancer of the pro alpha1 (II) collagen gene.* Molecular and cellular biology, 1997. **17**(4): p. 2336-2346.
146. Savvatis, K., et al., *Mesenchymal stromal cells but not cardiac fibroblasts exert beneficial systemic immunomodulatory effects in experimental myocarditis.* PLoS One, 2012. **7**(7): p. e41047.
147. Krampera, M., et al., *Role for Interferon-γ in the Immunomodulatory Activity of Human Bone Marrow Mesenchymal Stem Cells.* STEM CELLS, 2006. **24**(2): p. 386-398.
148. Gea-Banacloche, J.C., *Immunomodulation*, in *Principles of Molecular Medicine*, M.S. Runge and C. Patterson, Editors. 2006, Humana Press: Totowa, NJ. p. 893-904.
149. William, T.T., et al., *Suppression of allogeneic T-cell proliferation by human marrow stromal cells: implications in transplantation.* Transplantation, 2003. **75**(3): p. 389-397.
150. Beyth, S., et al., *Human mesenchymal stem cells alter antigen-presenting cell maturation and induce T-cell unresponsiveness.* Blood, 2005. **105**(5): p. 2214-2219.
151. Jo, C.H., et al., *Intra-Articular Injection of Mesenchymal Stem Cells for the Treatment of Osteoarthritis of the Knee: A Proof-of-Concept Clinical Trial.* STEM CELLS, 2014. **32**(5): p. 1254-1266.
152. Wakitani, S., et al., *Human autologous culture expanded bone marrow mesenchymal cell transplantation for repair of cartilage defects in osteoarthritic knees.* Osteoarthritis and Cartilage, 2002. **10**(3): p. 199-206.
153. Orozco, L., et al., *Treatment of knee osteoarthritis with autologous mesenchymal stem cells: a pilot study.* Transplantation, 2013. **95**(12): p. 1535-1541.
154. Vega, A., et al., *Treatment of knee osteoarthritis with allogeneic bone marrow mesenchymal stem cells: a randomized controlled trial.* Transplantation, 2015. **99**(8): p. 1681-1690.
155. Horwitz, E.M., et al., *Transplantability and therapeutic effects of bone marrow-derived mesenchymal cells in children with osteogenesis imperfecta.* Nature Medicine, 1999. **5**: p. 309.
156. Figueroa, F.E., et al., *Mesenchymal stem cell treatment for autoimmune diseases: a critical review.* Biological research, 2012. **45**(3): p. 269-277.
157. Shi, M., et al., *Human mesenchymal stem cell transfusion is safe and improves liver function in acute-on-chronic liver failure patients.* Stem cells translational medicine, 2012. **1**(10): p. 725-731.
158. Florian, E.T. and W. Christof, *Mesenchymal stem cells: a new therapeutic tool for AKI.* Nature Reviews Nephrology, 2010. **6**(3): p. 179.
159. Chiarugi, P. and E. Giannoni, *Anoikis: A necessary death program for anchorage-dependent cells.* Biochemical Pharmacology, 2008. **76**(11): p. 1352-1364.
160. Lee, S., et al., *Cell adhesion and long-term survival of transplanted mesenchymal stem cells: a prerequisite for cell therapy.* Oxidative medicine and cellular longevity, 2015. **2015**: p. 632902-632902.
161. Zaidel-Bar, R., et al., *Hierarchical assembly of cell-matrix adhesion complexes.* Biochemical Society Transactions, 2004. **32**: p. 416-420.
162. Gumbiner, B.M., *Cell adhesion: The molecular basis of tissue architecture and morphogenesis.* Cell, 1996. **84**(3): p. 345-357.
163. Santini, M.T., G. Rainaldi, and P.L. Indovina, *Apoptosis, cell adhesion and the extracellular matrix in the three-dimensional growth of multicellular tumor spheroids.* Critical reviews in oncology/hematology, 2000. **36**(2-3): p. 75-87.

164. Aplin, A.E., et al., *Signal transduction and signal modulation by cell adhesion receptors: The role of integrins, cadherins, immunoglobulin-cell adhesion molecules, and selectins.* Pharmacological Reviews, 1998. **50**(2): p. 197-263.
165. Hood, J.D. and D.A. Cheresh, *Role of integrins in cell invasion and migration.* Nature Reviews Cancer, 2002. **2**: p. 91.
166. Lodish, H., et al., *Molecular cell biology*. Vol. 3. 1995: WH Freeman New York.
167. Knight, C.G., et al., *The Collagen-binding A-domains of Integrins α1β1 and α2β1recognize the same specific amino acid sequence, GFOGER, in native (Triple-helical) collagens.* Journal of Biological Chemistry, 2000. **275**(1): p. 35-40.
168. Humphries, J.D., A. Byron, and M.J. Humphries, *Integrin ligands at a glance.* Journal of Cell Science, 2006. **119**(19): p. 3901-3903.
169. Dalby, M.J., N. Gadegaard, and R.O.C. Oreffo, *Harnessing nanotopography and integrin-matrix interactions to influence stem cell fate.* Nature Materials, 2014. **13**(6): p. 558-569.
170. O'Connor, C.M., J.U. Adams, and J. Fairman, *Essentials of cell biology.* Cambridge, MA: NPG Education, 2010. **1**.
171. Delon, I. and N.H. Brown, *Integrins and the actin cytoskeleton.* Current Opinion in Cell Biology, 2007. **19**(1): p. 43-50.
172. Chen, C.S., et al., *Cell shape provides global control of focal adhesion assembly.* Biochemical and Biophysical Research Communications, 2003. **307**(2): p. 355-361.
173. Corina Ciobanasu, B.F., Christophe Le Clainche, *Actin Dynamics Associated with Focal Adhesions.* International Journal of Cell Biology, 2012. **2012**.
174. Parsons, J.T., A.R. Horwitz, and M.A. Schwartz, *Cell adhesion: integrating cytoskeletal dynamics and cellular tension.* Nature reviews. Molecular cell biology, 2010. **11**(9): p. 633-643.
175. Cavalcanti-Adam, E.A., et al., *Cell spreading and focal adhesion dynamics are regulated by spacing of integrin ligands.* Biophysical Journal, 2007. **92**(8): p. 2964-2974.
176. Cavalcanti-Adam, E.A., et al., *Cell adhesion and response to synthetic nanopatterned environments by steering receptor clustering and spatial location.* Hfsp Journal, 2008. **2**(5): p. 276-285.
177. Takeichi, M., *Cadherins: a molecular family important in selective cell-cell adhesion.* Annual review of biochemistry, 1990. **59**(1): p. 237-252.
178. Grossmann, J., *Molecular mechanisms of "detachment-induced apoptosis—Anoikis".* Apoptosis, 2002. **7**(3): p. 247-260.
179. Hartsock, A. and W.J. Nelson, *Adherens and tight junctions: structure, function and connections to the actin cytoskeleton.* Biochimica et biophysica acta, 2008. **1778**(3): p. 660-669.
180. Alberts, B., et al., *Molecular Biology of the Cell 4th Edition: International Student Edition*. 2002, Routledge.
181. Garrod, D. and M. Chidgey, *Desmosome structure, composition and function.* Biochimica et Biophysica Acta (BBA) - Biomembranes, 2008. **1778**(3): p. 572-587.
182. Hirota, M., M. Ohmuraya, and H. Baba, *The role of trypsin, trypsin inhibitor, and trypsin receptor in the onset and aggravation of pancreatitis.* Journal of Gastroenterology, 2006. **41**(9): p. 832-836.
183. McDowall, J. *Trypsin and Chymotrypsin*. Available from: https://www.ebi.ac.uk/interpro/potm/2003_5/Page1.htm.
184. Olsen, J.V., S.-E. Ong, and M. Mann, *Trypsin Cleaves Exclusively C-terminal to Arginine and Lysine Residues.* Molecular & Cellular Proteomics, 2004. **3**(6): p. 608-614.
185. Sigma-Aldrich. *Cell Dissociation*. Sigma-Aldrich; Enzyme explorer:[Available from: http://www.sigmaaldrich.com/life-science/metabolomics/enzyme-explorer/analytical-enzymes/trypsin/cell-dissociation.html.

186. BI-BiologicalIndustries. *Trypsin & Cell Dissociation*. BI-Biological Industries; Available from: http://www.bioind.com/page_13947.
187. Canavan, H.E., et al., *Cell sheet detachment affects the extracellular matrix: A surface science study comparing thermal liftoff, enzymatic, and mechanical methods.* Journal of Biomedical Materials Research Part A, 2005. **75A**(1): p. 1-13.
188. Anglhileri, L.J. and Dermietzel, *Cell coat in tumor cells -- effects of trypsin and EDTA: a biochemical and morphological study.* Oncology, 1976. **33**(1): p. 17-23.
189. Huang, H.-L., et al., *Trypsin-induced proteome alteration during cell subculture in mammalian cells.* Journal of Biomedical Science, 2010. **17**.
190. Rosivatz, E., et al., *Neoexpression of N-cadherin in E-cadherin positive colon cancers.* International Journal of Cancer, 2004. **111**(5): p. 711-719.
191. Kuphal, S.B., A. K., *Influence of the cytoplasmic domain of E-cadherin on endogenous N-cadherin expression in malignant melanoma.* Oncogene, 2006. **25**(2): p. 248-259.
192. Ito, Y., et al., *Expression and clinical significance of erb-B receptor family in hepatocellular carcinoma.* British Journal of Cancer, 2001. **84**(10): p. 1377-1383.
193. Lee, J.W., et al., *ERBB2 kinase domain mutation in a gastric cancer metastasis.* Apmis, 2005. **113**(10): p. 683-687.
194. Tsuji, K., et al., *Effects of Different Cell-Detaching Methods on the Viability and Cell Surface Antigen Expression of Synovial Mesenchymal Stem Cells.* Cell Transplantation, 2017. **26**(6): p. 1089-1102.
195. Petricciani, J., et al., *Adventitious agents in viral vaccines: Lessons learned from 4 case studies.* Biologicals, 2014. **42**(5): p. 223-236.
196. Nathalie Meuleman, T.T., Alain Delforge, Marielle Dejeneffe, Martine Massy, Mark Libertalis, Dominique Bron and Laurence Lagneaux, *Human marrow mesenchymal stem cell culture: serum-free medium allows better expansion than classical α-MEM medium.* European Journal of Haematology, 2006. **76**(4): p. 309-316.
197. Canavan, H.E., et al., *Cell sheet detachment affects the extracellular matrix: A surface science study comparing thermal liftoff, enzymatic, and mechanical methods.* Journal of Biomedical Materials Research Part A, 2005. **75A**(1): p. 1-13.
198. Heng, B.C., C.M. Cowan, and S. Basu, *Comparison of Enzymatic and Non-Enzymatic Means of Dissociating Adherent Monolayers of Mesenchymal Stem Cells.* Biological Procedures Online, 2009. **11**(1): p. 161-169.
199. Industries, B.-B. *Non-Enzymatic Cell Dissociation Solution*. Available from: http://www.bioind.com/page_13948.
200. Alstem-CellAdvancements. *EZStem™ Enzyme-free Stem Cell Dissociation Solution*. Available from: EZStem™ Enzyme-free Stem Cell Dissociation Solution.
201. DNR-MolecularBiology. *Animal Component-Free Cell Dissociation Solution Non-enzymatic*. Available from: http://www.dnr-is.com/src/ACF%20Cell%20Dissociation%20Solution.pdf.
202. PromoCell. *Cell Dissociation Solution ACF*. Available from: http://www.promocell.com/products/reagents-and-supplements/detachment-reagents/cell-dissociation-solution-acf/.
203. ThermoFischerScientifics. *Cell Dissociation Buffer, enzyme-free*. Available from: https://www.thermofisher.com/order/catalog/product/13151014.
204. Sigma-Aldrich. *Cell Dissociation Solution Non-enzymatic 1x*. Available from: http://www.sigmaaldrich.com/catalog/product/sigma/c5789?lang=en&region=AU.
205. Stemmera. *Non-Enzymatic Cell Dissociation Solution (1X)*. Available from: http://www.stemmera.com/index.php/product/8-stemmera/37-non-enzymatic-cell-dissociation-solution-1x.
206. Stemcell-Technologies. *Gentle Cell Dissociation Reagent*. Available from: http://www.stemcell.com/en/Products/All-Products/Gentle-Cell-Dissociation-Reagent.aspx.

207. ThermoScientific, *Thermo Scientific Nunc UpCell Surface*. p. 1-12.
208. SigmaAldrich. *Nunc® UpCell™ Surface cell culture dish*. 6 cm culture dish, 60 x 15 mm, 21.5 cm2/well, w/ lid and airvent, 30/cs]. Available from: http://www.sigmaaldrich.com/catalog/product/sigma/z688835?lang=en&region=AU.
209. SigmaAldrich. *Nunc® UpCell™ Surface cell culture dish*. 3.5 cm culture dish, 40 x 12 mm, 8.8 cm2/well, w/ lid and airvent, 30/cs]. Available from: http://www.sigmaaldrich.com/catalog/product/sigma/z688851?lang=en&region=AU&cm_sp=Insite-_-prodRecCold_xviews-_-prodRecCold10-1.
210. Nishida, K., et al., *Functional bioengineered corneal epithelial sheet grafts from corneal stem cells expanded ex vivo on a temperature-responsieve cell culture surface.* Transplantation, 2004. **77**(3): p. 379-385.
211. Ohashi, K., et al., *Engineering functional two- and three-dimensional liver systems in vivo using hepatic tissue sheets.* Nature Medicine, 2007. **13**(7): p. 880-885.
212. Kushida, A., et al., *A noninvasive transfer system for polarized renal tubule epithelial cell sheets using temperature-responsive culture dishes.* European cells & materials, 2005. **10**: p. 23-30; discussion 23-30.
213. Kushida, A., et al., *Two-dimensional manipulation of differentiated Madin-Darby canine kidney (MDCK) cell sheets: The noninvasive harvest from temperature-responsive culture dishes and transfer to other surfaces.* Journal of Biomedical Materials Research, 2001. **54**(1): p. 37-46.
214. Masayuki Yamato, M.O., Fumiko Karikusa, Akihiko Kikuchi, Yasuhisa Sakurai and Teruo Okano, *Signal transduction and cytoskeletal reorganization are required for cell detachment from cell culture surfaces grafted with a temperature-responsive polymer.* Journal of Biomedical Materials Research, 1999. **44**(1): p. 44-52.
215. Yamato, M., et al., *Thermo-responsive culture dishes allow the intact harvest of multilayered keratinocyte sheets without dispase by reducing temperature.* Tissue Engineering, 2001. **7**(4): p. 473-480.
216. Shimizu, T., et al., *Two-dimensional manipulation of cardiac myocyte sheets utilizing temperature-responsive culture dishes augments the pulsatile amplitude.* Tissue Engineering, 2001. **7**(2): p. 141-151.
217. Hasegawa, M., et al., *Human periodontal ligament cell sheets can regenerate periodontal ligament tissue in an athymic rat model.* Tissue Engineering, 2005. **11**(3-4): p. 469-478.
218. Noriko Yamada, T.O., Hideaki Sakai, Fumiko Karikusa, Yoshio Sawasaki and Yasuhisa Sakurai, *Thermo-responsive polymeric surfaces; control of attachment and detachment of cultured cells.* Die Makromolekulare Chemie, Rapid Communications, 1990. **11**(11): p. 571-576.
219. Okano, T., et al., *A novel recovery system for cultured cells using plasma- treated polystyrene dishes grafted with Poly (N-Isopropylacrylamide).* Journal of Biomedical Materials Research, 1993. **27**(10): p. 1243-1251.
220. Okano, T., et al., *Mechanism of cell detachment from temperature-modulated, hydrophillic-hydrophobic polymer surface.* Biomaterials, 1995. **16**(4): p. 297-303.
221. Ito, Y., et al., *Patterned immobilization of thermoresponsive polymer.* Langmuir, 1997. **13**(10): p. 2756-2759.
222. Chen, G.P., Y. Imanishi, and Y. Ito, *Effect of protein and cell behavior on pattern-grafted thermoresponsive polymer.* Journal of Biomedical Materials Research, 1998. **42**(1): p. 38-44.
223. Reed, J.A., et al., *The effects of cell culture parameters on cell release kinetics from thermoresponsive surfaces.* Journal of Applied Biomaterials & Biomechanics, 2008. **6**(2): p. 81-88.

224. Cooperstein, M.A., P.A.H. Nguyen, and H.E. Canavan, *Poly(N-isopropyl acrylamide)-coated surfaces: Investigation of the mechanism of cell detachment.* Biointerphases, 2017. **12**(2): p. 02C401.
225. Persson, K.M., et al., *Electronic Control of Cell Detachment Using a Self-Doped Conducting Polymer.* Advanced Materials, 2011. **23**(38): p. 4403-4408.
226. Karlsson, R.H., et al., *Iron-Catalyzed Polymerization of Alkoxysulfonate-Functionalized 3,4-Ethylenedioxythiophene Gives Water-Soluble Poly(3,4-ethylenedioxythiophene) of High Conductivity.* Chemistry of Materials, 2009. **21**(9): p. 1815-1821.
227. Sada, T., et al., *Near-IR laser-triggered target cell collection using a carbon nanotube-based cell-cultured substrate.* ACS nano, 2011. **5**(6): p. 4414-4421.
228. Shi Kam, N.W., et al., *Nanotube Molecular Transporters: Internalization of Carbon Nanotube–Protein Conjugates into Mammalian Cells.* Journal of the American Chemical Society, 2004. **126**(22): p. 6850-6851.
229. Klumpp, C., et al., *Functionalized carbon nanotubes as emerging nanovectors for the delivery of therapeutics.* Biochimica et Biophysica Acta (BBA) - Biomembranes, 2006. **1758**(3): p. 404-412.
230. Cui, D., et al., *Effect of single wall carbon nanotubes on human HEK293 cells.* Toxicology Letters, 2005. **155**(1): p. 73-85.
231. Manna, S.K., et al., *Single-walled carbon nanotube induces oxidative stress and activates nuclear transcription factor-κB in human keratinocytes.* Nano letters, 2005. **5**(9): p. 1676-1684.
232. Wang, X., et al., *Visible-Light-Responsive Surfaces for Efficient, Noninvasive Cell Sheet Harvesting.* ACS applied materials & interfaces, 2017. **9**(34): p. 28250-28259.
233. *Introduction to Biophotonics*, in *Handbook of Biophotonics*. 2013.
234. Prasad, P.N.a., *Introduction to biophotonics*, ed. W. John and e. Sons. 2003, Hoboken, NJ: Hoboken, NJ : Wiley-Interscience.
235. Mobley, J. and T. Vo-Dinh, *Optical properties of tissue.* Biomedical photonics handbook, 2003. **2**: p. 1-2.
236. Tuchin, V.V. and V. Tuchin, *Tissue optics: light scattering methods and instruments for medical diagnosis.* 2007.
237. Niemz, M.H., *Laser-tissue interactions: fundamentals and applications*. 2013: Springer Science & Business Media.
238. Steiner, R., *Laser-tissue interactions*, in *Laser and IPL technology in dermatology and aesthetic medicine*. 2011, Springer. p. 23-36.
239. Hecht, J. *Short history of laser development*. 2010. SPIE.
240. Berger, N. and P.H. Eeg, *Veterinary Laser Surgery: A Practical Guide*. 2008, Ames, Iowa, USA: Ames, Iowa, USA: Blackwell Publishing Professional.
241. Matys, J., M. Dominiak, and R. Flieger, *Energy and Power Density: A Key Factor in Lasers Studies.* Journal of Clinical and Diagnostic Research : JCDR, 2015. **9**(12): p. ZL01-ZL02.
242. Millington, K.R., *9 - Improving the whiteness and photostability of wool*, in *Advances in Wool Technology*, N.A.G. Johnson and I.M. Russell, Editors. 2009, Woodhead Publishing. p. 217-247.
243. Jawad, M.M., et al., *An overview of laser principle, laser-tissue interaction mechanisms and laser safety precautions for medical laser users.* Int J Pharmacol, 2011. **7**(2): p. 149-160.
244. Henderson, B.W. and T.J. Dougherty, *How does photodynamic therapy work?* Photochemistry and Photobiology, 1992. **55**(1): p. 145-157.
245. Dougherty, T.J., et al., *Photodynamic Therapy.* JNCI: Journal of the National Cancer Institute, 1998. **90**(12): p. 889-905.

246. Schindl, A., et al., *Direct stimulatory effect of low-intensity 670 nm laser irradiation on human endothelial cell proliferation.* British Journal of Dermatology, 2003. **148**(2): p. 334-336.
247. Ma, H., et al., *Effect of Low-Level Laser Therapy on Proliferation and Collagen Synthesis of Human Fibroblasts in Vitro*. Vol. 14. 2018. 1-6.
248. Houreld, N. and H. Abrahamse, *Low-Intensity Laser Irradiation Stimulates Wound Healing in Diabetic Wounded Fibroblast Cells (WS1).* Diabetes Technology & Therapeutics, 2010. **12**(12): p. 971-978.
249. Schindl, A., et al., *Low-intensity laser irradiation improves skin circulation in patients with diabetic microangiopathy.* Diabetes care, 1998. **21**(4): p. 580-584.
250. Naeser, M.A., et al., *Carpal tunnel syndrome pain treated with low-level laser and microamperes transcutaneous electric nerve stimulation: A controlled study*. Archives of Physical Medicine and Rehabilitation, 2002. **83**(7): p. 978-988.
251. Chang, W.-D., et al., *Carpal tunnel syndrome treated with a diode laser: a controlled treatment of the transverse carpal ligament.* Photomedicine and laser surgery, 2008. **26**(6): p. 551-557.
252. Gur, A., et al., *Efficacy of different therapy regimes of low-power laser in painful osteoarthritis of the knee: A double-blind and randomized-controlled trial.* Lasers in Surgery and Medicine: The Official Journal of the American Society for Laser Medicine and Surgery, 2003. **33**(5): p. 330-338.
253. Hawkind, D., N. Houreld, and H. Abrahamse, *Low Level Laser Therapy (LLLT) as an Effective Therapeutic Modality for Delayed Wound Healing.* Annals of the New York Academy of Sciences, 2005. **1056**(1): p. 486-493.
254. Shaimova, V.A., E.V. Boyko, and O.G. Pozdeeva, *Retinal Laser Photocoagulation in Peripheral Retinal Degenerations*, in *Peripheral Retinal Degenerations: Optical Coherence Tomography and Retinal Laser Coagulation*, V.A. Shaimova, Editor. 2017, Springer International Publishing: Cham. p. 209-227.
255. Ogan, K., et al., *Sutureless laparoscopic heminephrectomy using laser tissue soldering.* Journal of endourology, 2003. **17**(5): p. 295-300.
256. Riordan, M. and Z. Tovar-Spinoza, *Laser induced thermal therapy (LITT) for pediatric brain tumors: case-based review.* Translational pediatrics, 2014. **3**(3): p. 229-235.
257. Ashraf, O., et al., *Laser-Induced Thermal Therapy in Neuro-Oncology: A Review.* World Neurosurgery, 2018. **112**: p. 166-177.
258. Moreno-Barriuso, E., et al., *Ocular Aberrations before and after Myopic Corneal Refractive Surgery: LASIK-Induced Changes Measured with Laser Ray Tracing.* Investigative Ophthalmology & Visual Science, 2001. **42**(6): p. 1396-1403.
259. *Chapter 5 - CORNEA*, in *Moorfields Manual of Ophthalmology*, T.L. Jackson, Editor. 2008, Mosby: Edinburgh. p. 144-221.
260. Salomão, M.Q. and S.E. Wilson, *Femtosecond laser in laser in situ keratomileusis.* Journal of cataract and refractive surgery, 2010. **36**(6): p. 1024-1032.
261. Huang, Y.-Y., *Low-level laser therapy: an emerging clinical paradigm*. 2009.
262. Tuchin, V.V. *Light interaction with biological tissues: overview*. in *OE/LASE'93: Optics, Electro-Optics, and Laser Applications in Scienceand Engineering*. 1993. SPIE.
263. Anderson, R.R. and J.A. Parrish, *The Optics of Human Skin.* Journal of Investigative Dermatology, 1981. **77**(1): p. 13-19.
264. Poyton, R.O. and K.A. Ball, *Therapeutic photobiomodulation: nitric oxide and a novel function of mitochondrial cytochrome c oxidase.* Discovery medicine, 2011. **11**(57): p. 154-159.
265. Chen, C.-H., et al., *Low-level laser irradiation promotes cell proliferation and mRNA expression of type I collagen and decorin in porcine achilles tendon fibroblasts In Vitro.* Journal of Orthopaedic Research, 2009. **27**(5): p. 646-650.

266. Ayuk, S.M., N.N. Houreld, and H. Abrahamse, *Effect of 660 nm visible red light on cell proliferation and viability in diabetic models in vitro under stressed conditions.* Lasers in Medical Science, 2018. **33**(5): p. 1085-1093.
267. Taniguchi, D., et al., *Low-energy laser irradiation promotes synovial fibroblast proliferation by modulating p15 subcellular localization.* Lasers in Surgery and Medicine, 2009. **41**(3): p. 232-239.
268. Gavish, L., et al., *Low level laser irradiation stimulates mitochondrial membrane potential and disperses subnuclear promyelocytic leukemia protein.* Lasers in Surgery and Medicine: The Official Journal of the American Society for Laser Medicine and Surgery, 2004. **35**(5): p. 369-376.
269. Ben-Dov, N., et al., *Low-energy laser irradiation affects satellite cell proliferation and differentiation in vitro.* Biochimica et Biophysica Acta (BBA)-Molecular Cell Research, 1999. **1448**(3): p. 372-380.
270. Zhang, J., D. Xing, and X. Gao, *Low-power laser irradiation activates Src tyrosine kinase through reactive oxygen species-mediated signaling pathway.* Journal of cellular physiology, 2008. **217**(2): p. 518-528.
271. Stadler, I., et al., *In vitro effects of low-level laser irradiation at 660 nm on peripheral blood lymphocytes.* Lasers in Surgery and Medicine: The Official Journal of the American Society for Laser Medicine and Surgery, 2000. **27**(3): p. 255-261.
272. Yang, D., et al., *Effects of light-emitting diode irradiation on the osteogenesis of human umbilical cord mesenchymal stem cells in vitro.* Scientific Reports, 2016. **6**: p. 37370.
273. Soleimani, M., et al., *The effects of low-level laser irradiation on differentiation and proliferation of human bone marrow mesenchymal stem cells into neurons and osteoblasts—an in vitro study.* Lasers in Medical Science, 2012. **27**(2): p. 423-430.
274. de Villiers, J.A., N.N. Houreld, and H. Abrahamse, *Influence of Low Intensity Laser Irradiation on Isolated Human Adipose Derived Stem Cells Over 72 Hours and Their Differentiation Potential into Smooth Muscle Cells Using Retinoic Acid.* Stem Cell Reviews and Reports, 2011. **7**(4): p. 869-882.
275. Abramovitch-Gottlib, L., et al., *Low level laser irradiation stimulates osteogenic phenotype of mesenchymal stem cells seeded on a three-dimensional biomatrix.* Lasers in Medical Science, 2005. **20**(3): p. 138-146.
276. Peng, F., et al., *The effect of noncoherent red light irradiation on proliferation and osteogenic differentiation of bone marrow mesenchymal stem cells.* Lasers in medical science, 2012. **27**(3): p. 645-653.
277. Li, W.-T., Y.-C. Leu, and J.-L. Wu, *Red-light light-emitting diode irradiation increases the proliferation and osteogenic differentiation of rat bone marrow mesenchymal stem cells.* Photomedicine and laser surgery, 2010. **28**(S1): p. S-157-S-165.
278. AlGhamdi, K.M., A. Kumar, and N.A. Moussa, *Low-level laser therapy: a useful technique for enhancing the proliferation of various cultured cells.* Lasers in Medical Science, 2012. **27**(1): p. 237-249.
279. Evans, D.H. and H. Abrahamse, *Efficacy of three different laser wavelengths for in vitro wound healing.* Photodermatology, photoimmunology & photomedicine, 2008. **24**(4): p. 199-210.
280. Tuby, H., L. Maltz, and U. Oron, *Low-level laser irradiation (LLLI) promotes proliferation of mesenchymal and cardiac stem cells in culture.* Lasers in Surgery and Medicine, 2007. **39**(4): p. 373-378.
281. Li, W., H. Chen, and C. Wang, *Effect of light emitting diode irradiation on proliferation of human bone marrow mesenchymal stem cells.* Journal of Medical and Biological Engineering, 2006. **26**(1): p. 35.
282. Chung, H., et al., *The Nuts and Bolts of Low-level Laser (Light) Therapy.* Annals of Biomedical Engineering, 2012. **40**(2): p. 516-533.

283. Li, W.-T. and Y.-C. Leu. *Effects of low level red-light irradiation on the proliferation of mesenchymal stem cells derived from rat bone marrow*. in *Engineering in Medicine and Biology Society, 2007. EMBS 2007. 29th Annual International Conference of the IEEE*. 2007. IEEE.
284. Wang, Y., et al., *Photobiomodulation (blue and green light) encourages osteoblastic-differentiation of human adipose-derived stem cells: role of intracellular calcium and light-gated ion channels.* Scientific Reports, 2016. **6**: p. 33719.
285. Schroeder, P., et al., *Cellular response to infrared radiation involves retrograde mitochondrial signaling.* Free Radical Biology and Medicine, 2007. **43**(1): p. 128-135.
286. Shirata, C., et al., *Near-infrared photothermal/photodynamic therapy with indocyanine green induces apoptosis of hepatocellular carcinoma cells through oxidative stress.* Scientific Reports, 2017. **7**(1): p. 13958.
287. Urao, N. and M. Ushio-Fukai, *Redox regulation of stem/progenitor cells and bone marrow niche.* Free Radical Biology and Medicine, 2013. **54**: p. 26-39.
288. Prigione, A., et al., *The Senescence-Related Mitochondrial/Oxidative Stress Pathway is Repressed in Human Induced Pluripotent Stem Cells.* STEM CELLS, 2010. **28**(4): p. 721-733.
289. Standardization, I.O.f., *ISO/TS 80004-2 (2015). Nanotechnologies-Vocabulary-Part 2: Nano-Objects. Geneva: International Organization for Standardization.* International Organization for Standardization, 2015.
290. Strambeanu, N., et al., *Nanoparticles: Definition, Classification and General Physical Properties*, in *Nanoparticles' Promises and Risks: Characterization, Manipulation, and Potential Hazards to Humanity and the Environment*, M. Lungu, et al., Editors. 2015, Springer International Publishing: Cham. p. 3-8.
291. Yang, X., et al., *Gold Nanomaterials at Work in Biomedicine.* Chemical Reviews, 2015. **115**(19): p. 10410-10488.
292. Weissleder, R., *A clearer vision for in vivo imaging.* Nature Biotechnology, 2001. **19**: p. 316.
293. El-Sayed, M.A., *Some interesting properties of metals confined in time and nanometer space of different shapes.* Accounts of Chemical Research, 2001. **34**(4): p. 257-264.
294. Huang, X., S. Neretina, and M.A. El-Sayed, *Gold nanorods: from synthesis and properties to biological and biomedical applications.* Advanced Materials, 2009. **21**(48): p. 4880-4910.
295. Cao, J., T. Sun, and K.T.V. Grattan, *Gold nanorod-based localized surface plasmon resonance biosensors: A review.* Sensors and Actuators B: Chemical, 2014. **195**: p. 332-351.
296. Vigderman, L., B.P. Khanal, and E.R. Zubarev, *Functional Gold Nanorods: Synthesis, Self-Assembly, and Sensing Applications.* Advanced Materials, 2012. **24**(36): p. 4811-4841.
297. Li, J., H. Guo, and Z.-Y. Li, *Microscopic and macroscopic manipulation of gold nanorod and its hybrid nanostructures.* Photonics Research, 2013. **1**(1): p. 28-41.
298. Yu, et al., *Gold Nanorods: Electrochemical Synthesis and Optical Properties.* The Journal of Physical Chemistry B, 1997. **101**(34): p. 6661-6664.
299. Chang, S.-S., et al., *The Shape Transition of Gold Nanorods.* Langmuir, 1999. **15**(3): p. 701-709.
300. Nikoobakht, B. and M.A. El-Sayed, *Preparation and growth mechanism of gold nanorods (NRs) using seed-mediated growth method.* Chemistry of Materials, 2003. **15**(10): p. 1957-1962.
301. Pérez-Juste, J., et al., *Gold nanorods: Synthesis, characterization and applications.* Coordination Chemistry Reviews, 2005. **249**(17): p. 1870-1901.

302. Kim, F., J.H. Song, and P. Yang, *Photochemical Synthesis of Gold Nanorods.* Journal of the American Chemical Society, 2002. **124**(48): p. 14316-14317.
303. Nishioka, K., Y. Niidome, and S. Yamada, *Photochemical Reactions of Ketones to Synthesize Gold Nanorods.* Langmuir, 2007. **23**(20): p. 10353-10356.
304. Jana, N.R., L. Gearheart, and C.J. Murphy, *Wet Chemical Synthesis of High Aspect Ratio Cylindrical Gold Nanorods.* The Journal of Physical Chemistry B, 2001. **105**(19): p. 4065-4067.
305. Jana, N.R., L. Gearheart, and C.J. Murphy, *Seed-Mediated Growth Approach for Shape-Controlled Synthesis of Spheroidal and Rod-like Gold Nanoparticles Using a Surfactant Template.* Advanced Materials, 2001. **13**(18): p. 1389-1393.
306. Busbee, B.D., S.O. Obare, and C.J. Murphy, *An Improved Synthesis of High-Aspect-Ratio Gold Nanorods.* Advanced Materials, 2003. **15**(5): p. 414-416.
307. Pérez-Juste, J., et al., *Electric-Field-Directed Growth of Gold Nanorods in Aqueous Surfactant Solutions.* Advanced Functional Materials, 2004. **14**(6): p. 571-579.
308. Gao, J., C.M. Bender, and C.J. Murphy, *Dependence of the Gold Nanorod Aspect Ratio on the Nature of the Directing Surfactant in Aqueous Solution.* Langmuir, 2003. **19**(21): p. 9065-9070.
309. Cheng, Y.-T., et al., *Laser annealing of gold nanoparticles thin film using photothermal effect.* Microelectronic Engineering, 2009. **86**(4): p. 865-867.
310. Link, S., et al., *Laser Photothermal Melting and Fragmentation of Gold Nanorods: Energy and Laser Pulse-Width Dependence.* The Journal of Physical Chemistry A, 1999. **103**(9): p. 1165-1170.
311. Harris-Birtill, D., et al., *Gold nanorod reshaping in vitro and in vivo using a continuous wave laser.* PLOS ONE, 2017. **12**(10): p. e0185990.
312. Pissuwan, D., T. Niidome, and M.B. Cortie, *The forthcoming applications of gold nanoparticles in drug and gene delivery systems.* Journal of Controlled Release, 2011. **149**(1): p. 65-71.
313. Alkilany, A.M., et al., *Gold nanorods: Their potential for photothermal therapeutics and drug delivery, tempered by the complexity of their biological interactions.* Advanced Drug Delivery Reviews, 2012. **64**(2): p. 190-199.
314. Chen, H., et al., *Drug loaded multilayered gold nanorods for combined photothermal and chemotherapy.* Biomaterials Science, 2014. **2**(7): p. 996-1006.
315. Wei, Q., J. Ji, and J. Shen, *Synthesis of Near-Infrared Responsive Gold Nanorod/PNIPAAm Core/Shell Nanohybrids via Surface Initiated ATRP for Smart Drug Delivery.* Macromolecular Rapid Communications, 2008. **29**(8): p. 645-650.
316. Xiao, Y., et al., *Gold Nanorods Conjugated with Doxorubicin and cRGD for Combined Anticancer Drug Delivery and PET Imaging.* Theranostics, 2012. **2**(8): p. 757-768.
317. Norman, R.S., et al., *Targeted Photothermal Lysis of the Pathogenic Bacteria, Pseudomonas aeruginosa, with Gold Nanorods.* Nano Letters, 2008. **8**(1): p. 302-306.
318. Paciotti, G.F., et al., *Colloidal Gold: A Novel Nanoparticle Vector for Tumor Directed Drug Delivery.* Drug Delivery, 2004. **11**(3): p. 169-183.
319. Partha, G., et al., *Gold nanoparticles in delivery applications.* Advanced Drug Delivery Reviews, 2008. **60**(11): p. 1307–1315.
320. Galvin, P., et al., *Nanoparticle-based drug delivery: case studies for cancer and cardiovascular applications.* Cellular and Molecular Life Sciences, 2012. **69**(3): p. 389-404.
321. Luo, D. and W.M. Saltzman, *Synthetic DNA delivery systems.* Nature Biotechnology, 2000. **18**(1): p. 33-37.
322. Chen, C.C., et al., *DNA-gold nanorod conjugates for remote control of localized gene expression by near infrared irradiation.* Journal of the American Chemical Society, 2006. **128**(11): p. 3709-3715.

323. Xiaohua, H. and A.E.-S. Mostafa, *Plasmonic photo-thermal therapy (PPTT).* Alexandria Journal of Medicine, 2011. **47**: p. 1-9.
324. Huang, X., et al., *Plasmonic photothermal therapy (PPTT) using gold nanoparticles.* Lasers in Medical Science, 2008. **23**(3): p. 217-228.
325. Sau, T.K. and C.J. Murphy, *Seeded high yield synthesis of short Au nanorods in aqueous solution.* Langmuir, 2004. **20**(15): p. 6414-6420.
326. Huang, X., S. Neretina, and M.A. El-Sayed, *Gold Nanorods: From Synthesis and Properties to Biological and Biomedical Applications.* Advanced Materials, 2009. **21**(48): p. 4880-4910.
327. Zhan, Q., et al., *A study of mesoporous silica-encapsulated gold nanorods as enhanced light scattering probes for cancer cell imaging.* Nanotechnology, 2009. **21**(5): p. 055704.
328. Niidome, T., et al., *PEG-modified gold nanorods with a stealth character for in vivo applications.* Journal of Controlled Release, 2006. **114**(3): p. 343-347.
329. Huff, T.B., et al., *Controlling the cellular uptake of gold nanorods.* Langmuir, 2007. **23**(4): p. 1596-1599.
330. Pan, Y., et al., *CTAB induced mitochondrial apoptosis by activating the AMPK–p53 pathway in hepatocarcinoma cells.* Toxicology Research, 2015. **4**(5): p. 1359-1365.
331. Adamovich, Y., et al., *AMPK couples p73 with p53 in cell fate decision.* Cell Death And Differentiation, 2014. **21**: p. 1451.
332. Zhang, Z., et al., *Mesoporous Silica-Coated Gold Nanorods as a Light-Mediated Multifunctional Theranostic Platform for Cancer Treatment.* Advanced Materials, 2012. **24**(11): p. 1418-1423.
333. Bartczak, D. and A.G. Kanaras, *Preparation of Peptide-Functionalized Gold Nanoparticles Using One Pot EDC/Sulfo-NHS Coupling.* Langmuir, 2011. **27**(16): p. 10119-10123.
334. Kolesnikova, T.A., et al., *Laser-induced cell detachment, patterning, and regrowth on gold nanoparticle functionalized surfaces.* ACS nano, 2012. **6**(11): p. 9585-9595.
335. Giner-Casares, J.J., et al., *Plasmonic Surfaces for Cell Growth and Retrieval Triggered by Near-Infrared Light.* Angewandte Chemie, 2016. **128**(3): p. 986-990.
336. Duval, K., et al., *Modeling Physiological Events in 2D vs. 3D Cell Culture.* Physiology, 2017. **32**(4): p. 266-277.
337. Kolenda, T., et al., *2D and 3D cell cultures – a comparison of different types of cancer cell cultures*. Vol. 14. 2016.
338. Hynes, R.O., *Cell adhesion: old and new questions.* Trends in Cell Biology, 1999. **9**(12): p. M33-M37.
339. Birgersdotter, A., R. Sandberg, and I. Ernberg, *Gene expression perturbation in vitro—A growing case for three-dimensional (3D) culture systems.* Seminars in Cancer Biology, 2005. **15**(5): p. 405-412.
340. Mazzoleni, G., D. Di Lorenzo, and N. Steimberg, *Modelling tissues in 3D: the next future of pharmaco-toxicology and food research?* Genes & Nutrition, 2009. **4**(1): p. 13-22.
341. Honek, J., *Preclinical research in drug development.* Medical Writing, 2017. **26**: p. 5-8.
342. Friedman, L.M., et al., *Fundamentals of clinical trials*. Vol. 3. 1998: Springer.
343. Breslin, S. and L. O'Driscoll, *Three-dimensional cell culture: the missing link in drug discovery.* Drug Discovery Today, 2013. **18**(5): p. 240-249.
344. Kola, I. and J. Landis, *Can the pharmaceutical industry reduce attrition rates?* Nature Reviews Drug Discovery, 2004. **3**: p. 711.
345. Edmondson, R., et al., *Three-Dimensional Cell Culture Systems and Their Applications in Drug Discovery and Cell-Based Biosensors.* Assay and Drug Development Technologies, 2014. **12**(4): p. 207-218.

346. Hamburger, A. and S. Salmon, *Primary bioassay of human tumor stem cells.* Science, 1977. **197**(4302): p. 461-463.
347. Geckil, H., et al., *Engineering hydrogels as extracellular matrix mimics.* Nanomedicine (London, England), 2010. **5**(3): p. 469-484.
348. Katritsis, D.G., et al., *Transcoronary transplantation of autologous mesenchymal stem cells and endothelial progenitors into infarcted human myocardium.* Catheterization and Cardiovascular Interventions, 2005. **65**(3): p. 321-329.
349. Mathiasen, A.B., et al., *Rationale and design of the first randomized, double-blind, placebo-controlled trial of intramyocardial injection of autologous bone-marrow derived Mesenchymal Stromal Cells in chronic ischemic Heart Failure (MSC-HF Trial).* American Heart Journal, 2012. **164**(3): p. 285-291.
350. Mazzini, L., et al., *Mesenchymal stem cell transplantation in amyotrophic lateral sclerosis: A Phase I clinical trial.* Experimental Neurology, 2010. **223**(1): p. 229-237.
351. Mohyeddin Bonab, M., et al., *Does Mesenchymal Stem Cell Therapy Help Multiple Sclerosis Patients? Report of a Pilot Study.* Iranian Journal of Immunology, 2007. **4**(1): p. 50-57.
352. Kharaziha, P., et al., *Improvement of liver function in liver cirrhosis patients after autologous mesenchymal stem cell injection: a phase I–II clinical trial.* European journal of gastroenterology & hepatology, 2009. **21**(10): p. 1199-1205.
353. Zhang, Z., et al., *Human umbilical cord mesenchymal stem cells improve liver function and ascites in decompensated liver cirrhosis patients.* Journal of Gastroenterology and Hepatology, 2012. **27**(s2): p. 112-120.
354. Ciccocioppo, R., et al., *Long-Term Follow-Up of Crohn Disease Fistulas After Local Injections of Bone Marrow–Derived Mesenchymal Stem Cells.* Mayo Clinic Proceedings, 2015. **90**(6): p. 747-755.
355. Colter, D.C., et al., *Rapid expansion of recycling stem cells in cultures of plastic-adherent cells from human bone marrow.* Proceedings of the National Academy of Sciences, 2000. **97**(7): p. 3213-3218.
356. Wagner, W., et al., *Replicative Senescence of Mesenchymal Stem Cells: A Continuous and Organized Process.* PLOS ONE, 2008. **3**(5): p. e2213.
357. Bruder, S.P., N. Jaiswal, and S.E. Haynesworth, *Growth kinetics, self-renewal, and the osteogenic potential of purified human mesenchymal stem cells during extensive subcultivation and following cryopreservation.* Journal of cellular biochemistry, 1997. **64**(2): p. 278-294.
358. DiGirolamo, C.M., et al., *Propagation and senescence of human marrow stromal cells in culture: a simple colony-forming assay identifies samples with the greatest potential to propagate and differentiate.* British Journal of Haematology, 1999. **107**(2): p. 275-281.
359. Zhao, K., et al., *Immunomodulation Effects of Mesenchymal Stromal Cells on Acute Graft-versus-Host Disease after Hematopoietic Stem Cell Transplantation.* Biology of Blood and Marrow Transplantation, 2015. **21**(1): p. 97-104.
360. Ringdén, O., et al., *Mesenchymal stem cells for treatment of therapy-resistant graft-versus-host disease.* Transplantation, 2006. **81**(10): p. 1390-1397.
361. Kirouac, D.C. and P.W. Zandstra, *The Systematic Production of Cells for Cell Therapies.* Cell Stem Cell, 2008. **3**(4): p. 369-381.
362. Lock, L.T. and E.S. Tzanakakis, *Stem/Progenitor Cell Sources of Insulin-Producing Cells for the Treatment of Diabetes.* Tissue Engineering, 2007. **13**(7): p. 1399-1412.
363. Ryan, J.A., *Growing more cells: A simple guide to small volume cell culture scale-up*. 2005.
364. Nienow, A.W., et al., *Chapter 3 - Bioreactor Engineering Fundamentals for Stem Cell Manufacturing*, in *Stem Cell Manufacturing*, J.M.S. Cabral, et al., Editors. 2016, Elsevier: Boston. p. 43-75.

365. Chen, A.K.-L., S. Reuveny, and S.K.W. Oh, *Application of human mesenchymal and pluripotent stem cell microcarrier cultures in cellular therapy: Achievements and future direction.* Biotechnology Advances, 2013. **31**(7): p. 1032-1046.
366. Scientific, T. *Nunc™ Cell Factory™ Incubators*. Cell Factory BioProcessing Systems; Available from: https://www.thermofisher.com/order/catalog/product/120100.
367. Want, A.J., et al., *Large-scale expansion and exploitation of pluripotent stem cells for regenerative medicine purposes: beyond the T flask*, in *Regenerative Medicine*. 2012. p. 71+.
368. Schop, D., et al., *Expansion of mesenchymal stem cells using a microcarrier-based cultivation system: growth and metabolism.* Journal of tissue engineering and regenerative medicine, 2008. **2**(2-3): p. 126-135.
369. Glacken, M., R. Fleischaker, and A. Sinskey, *Mammalian cell culture: engineering principles and scale-up.* Trends in Biotechnology, 1983. **1**(4): p. 102-108.
370. Hu, A.Y.-C., et al., *Microcarrier-based MDCK cell culture system for the production of influenza H5N1 vaccines.* Vaccine, 2008. **26**(45): p. 5736-5740.
371. Knazek, R.A., et al., *Cell Culture on Artificial Capillaries: An Approach to Tissue Growth in vitro.* Science, 1972. **178**(4056): p. 65-67.
372. Whitford, W. and J. Cadwell, *The potential application of hollow fiber bioreactors to large-scale production: A hollow fiber matrix can be used for large-scale cell culture, and allows for efficient harvest of secreted proteins*. Vol. 24. 2011. s21-s26.
373. Systems, F. *The Advantages of Hollow Fiber Bioreactors in Cell Culture*. Available from: https://www.fibercellsystems.com/advantage/.
374. Van Wezel, A.L., *Growth of Cell-strains and Primary Cells on Micro-carriers in Homogeneous Culture.* Nature, 1967. **216**: p. 64.
375. Frauenschuh, S., et al., *A Microcarrier-Based Cultivation System for Expansion of Primary Mesenchymal Stem Cells.* Biotechnology Progress, 2007. **23**(1): p. 187-193.
376. Kehoe, D.E., et al., *Scalable Stirred-Suspension Bioreactor Culture of Human Pluripotent Stem Cells.* Tissue Engineering. Part A, 2010. **16**(2): p. 405-421.
377. Malda, J. and C.G. Frondoza, *Microcarriers in the engineering of cartilage and bone.* Trends in Biotechnology, 2006. **24**(7): p. 299-304.
378. Tsai, A.-C. and T. Ma, *Expansion of Human Mesenchymal Stem Cells in a Microcarrier Bioreactor*, in *Bioreactors in Stem Cell Biology: Methods and Protocols*, K. Turksen, Editor. 2016, Springer New York: New York, NY. p. 77-86.
379. Malda, J., et al., *Expansion of Bovine Chondrocytes on Microcarriers Enhances Redifferentiation.* Tissue Engineering, 2003. **9**(5): p. 939-948.
380. Melero-Martin, J.M., et al., *Expansion of chondroprogenitor cells on macroporous microcarriers as an alternative to conventional monolayer systems.* Biomaterials, 2006. **27**(15): p. 2970-2979.
381. Storm, M.P., et al., *Three-dimensional culture systems for the expansion of pluripotent embryonic stem cells.* Biotechnology and Bioengineering, 2010. **107**(4): p. 683-695.
382. Phillips, B.W., et al., *Attachment and growth of human embryonic stem cells on microcarriers.* Journal of Biotechnology, 2008. **138**(1): p. 24-32.
383. Badenes, S.M., et al., *Chapter 4 - Microcarrier Culture Systems for Stem Cell Manufacturing*, in *Stem Cell Manufacturing*. 2016, Elsevier: Boston. p. 77-104.
384. Hill, S.
385. SoloHill. *SoloHill® Microcarriers – Animal Product Free*. Available from: https://shop.pall.com/us/en/biotech/cell-culture/microcarriers/solohill-microcarriers-animal-product-free-zidhscbdxjn.
386. Scientific, T.F. *Corning™ Synthemax™ II Microcarriers* Available from: https://www.fishersci.com/shop/products/corning-synthemax-ii-microcarriers-synthemax-ii-microcarrier/13700506.

387. Li, B., et al., *Past, present, and future of microcarrier-based tissue engineering.* Journal of Orthopaedic Translation, 2015. **3**(2): p. 51-57.
388. Jenkins, N., *Animal cell biotechnology: Methods and protocols*. Vol. 8. 1999: Springer.
389. Rowley, J., et al., *Meeting lot-size challenges of manufacturing adherent cells for therapy.* BioProcess Int, 2012. **10**(3): p. 7.
390. Merten, O.-W., *Advances in cell culture: anchorage dependence.* Philosophical Transactions of the Royal Society B: Biological Sciences, 2015. **370**(1661): p. 20140040.
391. Frazzati-Gallina, N.M., et al., *Higher production of rabies virus in serum-free medium cell cultures on microcarriers.* Journal of Biotechnology, 2001. **92**(1): p. 67-72.
392. Montagnon, B., *The large-scale cultivation of Vero cells in micro-carrier culture for virus vaccine production preliminary results for killed poliovirus vaccine.* Dev. Biol. Stand., 1981. **47**: p. 55-64.
393. Montagnon, B.J., B. Fanget, and J.C. Vincent-Falquet, *Industrial-Scale Production of Inactivated Poliovirus Vaccine Prepared by Culture of Vero Cells on Microcarrier.* Reviews of Infectious Diseases, 1984. **6**: p. S341-S344.
394. Kistner, O., et al., *Development of a mammalian cell (Vero) derived candidate influenza virus vaccine.* Vaccine, 1998. **16**(9-10): p. 960-968.
395. Trabelsi, K., et al., *Optimization of virus yield as a strategy to improve rabies vaccine production by Vero cells in a bioreactor.* Journal of Biotechnology, 2006. **121**(2): p. 261-271.
396. Trabelsi, K., et al., *Development of a measles vaccine production process in MRC-5 cells grown on Cytodex1 microcarriers and in a stirred bioreactor.* Applied Microbiology and Biotechnology, 2012. **93**(3): p. 1031-1040.
397. Sugawara, K., et al., *Development of Vero Cell-Derived Inactivated Japanese Encephalitis Vaccine.* Biologicals, 2002. **30**(4): p. 303-314.
398. Structural Genomics, C., et al., *Protein production and purification.* Nature methods, 2008. **5**(2): p. 135-146.
399. Knibbs, R.N., et al., *Sustained High-Yield Production of Recombinant Proteins in Transiently Transfected COS-7 Cells Grown on Trimethylamine-Coated (Hillex) Microcarrier Beads.* Biotechnology Progress, 2003. **19**(1): p. 9-13.
400. Wurm, F.M., *Production of recombinant protein therapeutics in cultivated mammalian cells.* Nature Biotechnology, 2004. **22**: p. 1393.
401. Schnitzler, A.C., et al., *Bioprocessing of human mesenchymal stem/stromal cells for therapeutic use: Current technologies and challenges.* Biochemical Engineering Journal, 2016. **108**: p. 3-13.
402. Panchalingam, K.M., et al., *Bioprocessing strategies for the large-scale production of human mesenchymal stem cells: a review.* Stem cell research & therapy, 2015. **6**: p. 225-225.
403. Chisti, Y., *Hydrodynamic Damage to Animal Cells.* Critical Reviews in Biotechnology, 2001. **21**(2): p. 67-110.
404. Cherry, R.S. and E.T. Papoutsakis, *Physical mechanisms of cell damage in microcarrier cell culture bioreactors.* Biotechnology and Bioengineering, 1988. **32**(8): p. 1001-1014.
405. Wu, S.-C., *Influence of hydrodynamic shear stress on microcarrier-attached cell growth: cell line dependency and surfactant protection.* Bioprocess Engineering, 1999. **21**(3): p. 201-206.
406. Cormier, J.T., et al., *Expansion of undifferentiated murine embryonic stem cells as aggregates in suspension culture bioreactors.* Tissue engineering, 2006. **12**(11): p. 3233-3245.

407. Liu, L., et al., *Different effects of intermittent and continuous fluid shear stresses on osteogenic differentiation of human mesenchymal stem cells.* Biomechanics and Modeling in Mechanobiology, 2012. **11**(3): p. 391-401.
408. Leung, H., et al., *Agitation can Induce Differentiation of Human Pluripotent Stem Cells in Microcarrier Cultures.* Tissue Engineering Part C: Methods, 2011. **17**(2): p. 165-72.
409. Lock, L. and E. Tzanakakis, *Expansion and Differentiation of Human Embryonic Stem Cells to Endoderm Progeny in a Microcarrier Stirred-Suspension Culture*. Vol. 15. 2009. 2051-63.
410. Nienow, A.W., et al., *A potentially scalable method for the harvesting of hMSCs from microcarriers.* Biochemical Engineering Journal, 2014. **85**: p. 79-88.
411. Weber, C., et al., *Expansion and Harvesting of hMSC-TERT.* The Open Biomedical Engineering Journal, 2007. **1**: p. 38-46.
412. dos Santos, F., et al., *Toward a Clinical-Grade Expansion of Mesenchymal Stem Cells from Human Sources: A Microcarrier-Based Culture System Under Xeno-Free Conditions.* Tissue Engineering. Part C, Methods, 2011. **17**(12): p. 1201-1210.
413. Lai, C.-S., L.E. Hopwood, and H.M. Swartz, *ESR studies on membrane fluidity of Chinese hamster ovary cells grown on microcarriers and in suspension.* Experimental Cell Research, 1980. **130**(2): p. 437-442.
414. Yang, H.S., et al., *Suspension culture of mammalian cells using thermosensitive microcarrier that allows cell detachment without proteolytic enzyme treatment.* Cell transplantation, 2010. **19**(9): p. 1123-1132.
415. Okano, T., et al., *A NOVEL RECOVERY-SYSTEM FOR CULTURED-CELLS USING PLASMA-TREATED POLYSTYRENE DISHES GRAFTED WITH POLY(N-ISOPROPYLACRYLAMIDE).* Journal of Biomedical Materials Research, 1993. **27**(10): p. 1243-1251.
416. Krpetic, Z., et al., *Inflicting controlled nonthermal damage to subcellular structures by laser-activated gold nanoparticles.* Nano letters, 2010. **10**(11): p. 4549-4554.
417. Penner, M.H., *Basic Principles of Spectroscopy*, in *Food Analysis*. 2010, Springer US: Boston, MA. p. 375-385.
418. College, M. *Using the Cary 50, UV Vis Spectrometer Operations*. Available from: http://faculty.sdmiramar.edu/fgarces/ChemComon/Tutorial/Cary50/index.html.
419. Instrumentation, L.R., *User Guidelines & Standard Operating Procedure for the Cary 50 UV-Vis Spectrophotometer.* 2007.
420. Jayabal, S., et al., *A gold nanorod-based localized surface plasmon resonance platform for the detection of environmentally toxic metal ions.* Analyst, 2015. **140**(8): p. 2540-2555.
421. Cobley, C.M., et al., *Gold nanostructures: a class of multifunctional materials for biomedical applications.* Chemical Society Reviews, 2011. **40**(1): p. 44-56.
422. Takahata, R., et al., *Gold Ultrathin Nanorods with Controlled Aspect Ratios and Surface Modifications: Formation Mechanism and Localized Surface Plasmon Resonance.* Journal of the American Chemical Society, 2018. **140**(21): p. 6640-6647.
423. Jo, W., J.H. Lee, and M.J. Kim, *Temperature measurement in a single patterned gold nanorod cluster using laser-induced fluorescence.* Journal of Nanoparticle Research, 2012. **14**(1): p. 699.
424. Li, C., et al., *Dynamic microscale temperature gradient in a gold nanorod solution measured by diffraction-limited nanothermometry.* Applied Physics Letters, 2015. **107**(12): p. 121105.
425. Howarth, J.V., R.D. Keynes, and J.M. Ritchie, *The origin of the initial heat associated with a single impulse in mammalian non-myelinated nerve fibres.* The Journal of Physiology, 1968. **194**(3): p. 745-793.
426. Buttemere, C.R., et al. *In vivo assessment of thermal damage in the liver using optical spectroscopy*. 2004. SPIE.

427. Usamentiaga, R., et al., *Infrared Thermography for Temperature Measurement and Non-Destructive Testing.* Sensors (Basel, Switzerland), 2014. **14**(7): p. 12305-12348.
428. Wells, J., et al., *Biophysical Mechanisms of Transient Optical Stimulation of Peripheral Nerve.* Biophysical Journal, 2007. **93**(7): p. 2567-2580.
429. Bratosin, D., et al., *Novel fluorescence assay using calcein-AM for the determination of human erythrocyte viability and aging.* Cytometry Part A, 2005. **66A**(1): p. 78-84.
430. Decherchi, P., P. Cochard, and P. Gauthier, *Dual staining assessment of Schwann cell viability within whole peripheral nerves using calcein-AM and ethidium homodimer.* Journal of Neuroscience Methods, 1997. **71**(2): p. 205-213.
431. Dojindo Molecular Technologies, I. *Cellstain- Double Staining Kit*. 2016; Available from: https://www.dojindo.com/store/p/190-Cellstain-Double-Staining-Kit.html.
432. Ansar Ahmed, S., R.M. Gogal, and J.E. Walsh, *A new rapid and simple non-radioactive assay to monitor and determine the proliferation of lymphocytes: an alternative to [3H]thymidine incorporation assay.* Journal of Immunological Methods, 1994. **170**(2): p. 211-224.
433. Byth, H.-A., et al., *Assessment of a simple, non-toxic alamar blue cell survival assay to monitor tomato cell viability.* Phytochemical Analysis, 2001. **12**(5): p. 340-346.
434. Bueno, C., et al., *The Excited-State Interaction of Resazurin and Resorufin with Aminesin Aqueous Solutions. Photophysics and Photochemical Reaction¶.* Photochemistry and Photobiology, 2002. **76**(4): p. 385-390.
435. Al-Nasiry, S., et al., *The use of Alamar Blue assay for quantitative analysis of viability, migration and invasion of choriocarcinoma cells.* Human Reproduction, 2007. **22**(5): p. 1304-1309.
436. Bioscience, A. *Cell Viability Assay based on Metabolic Activity*. Available from: http://www.abpbio.com/product/cell-viability-assay-based-on-metabolic-activity/.
437. Xu, M., D.J. McCanna, and J.G. Sivak, *Use of the viability reagent PrestoBlue in comparison with alamarBlue and MTT to assess the viability of human corneal epithelial cells.* Journal of Pharmacological and Toxicological Methods, 2015. **71**: p. 1-7.
438. Padlan, E.A., *Anatomy of the antibody molecule.* Molecular Immunology, 1994. **31**(3): p. 169-217.
439. Janeway, C.A., et al., *Immunobiology: the immune system in health and disease.* 2005.
440. Koivunen, M.E. and R.L. Krogsrud, *Principles of immunochemical techniques used in clinical laboratories.* Laboratory Medicine, 2006. **37**(8): p. 490-497.
441. Delves, P.J., et al., *Essential immunology*. 2017: John Wiley & Sons.
442. Adan, A., et al., *Flow cytometry: basic principles and applications.* Critical Reviews in Biotechnology, 2017. **37**(2): p. 163-176.
443. Brown, M. and C. Wittwer, *Flow cytometry: principles and clinical applications in hematology.* Clinical chemistry, 2000. **46**(8): p. 1221-1229.
444. Technology, B.B. *Flow Cytometry Fundamental Principle, How FACS Works*. Available from: https://www.bosterbio.com/protocol-and-troubleshooting/flow-cytometry-principle.
445. Cam, A. *Introduction to flow cytometry*. Available from: http://www.abcam.com/protocols/introduction-to-flow-cytometry.
446. SINO BIOLOGICAL, I., *Flow Cytometry (FCM) /FACS | Fluorescence-activated cell sorting (FACS).*
447. Clark, G., et al., *Nomenclature of CD molecules from the Tenth Human Leucocyte Differentiation Antigen Workshop.* Clinical & Translational Immunology, 2016. **5**(1): p. e57.
448. Uccelli, A., L. Moretta, and V. Pistoia, *Mesenchymal stem cells in health and disease.* Nat Rev Immunol, 2008. **8**(9): p. 726-736.

449. Dominici, M., et al., *Minimal criteria for defining multipotent mesenchymal stromal cells. The International Society for Cellular Therapy position statement.* Cytotherapy, 2006. **8**(4): p. 315-317.
450. T, L.R., et al., *MSC surface markers (CD44, CD73, and CD90) can identify human MSC-derived extracellular vesicles by conventional flow cytometry.* Cell Commun Signal, 2016. **14**.
451. Qian, H., K. Le Blanc, and M. Sigvardsson, *Primary Mesenchymal Stem and Progenitor Cells from Bone Marrow Lack Expression of CD44 Protein.* J Biol Chem, 2012. **287**(31): p. 25795-807.
452. Delorme, B., et al., *Specific plasma membrane protein phenotype of culture-amplified and native human bone marrow mesenchymal stem cells.* Blood, 2008. **111**(5): p. 2631-2635.
453. Sibov, T.T., et al., *Mesenchymal stem cells from umbilical cord blood: parameters for isolation, characterization and adipogenic differentiation.* Cytotechnology, 2012. **64**(5): p. 511-521.
454. Boxall, S.A. and E. Jones, *Markers for Characterization of Bone Marrow Multipotential Stromal Cells.* Stem Cells International, 2012. **2012**: p. 12.
455. Ode, A., et al., *CD73 and CD29 concurrently mediate the mechanically induced decrease of migratory capacity of mesenchymal stromal cells.* Eur Cell Mater, 2011. **22**: p. 26-42.
456. Lin, C.-S., et al., *Commonly Used Mesenchymal Stem Cell Markers and Tracking Labels: Limitations and Challenges.* Histology and histopathology, 2013. **28**(9): p. 1109-1116.
457. Greenspan, P., E.P. Mayer, and S.D. Fowler, *Nile red: a selective fluorescent stain for intracellular lipid droplets.* The Journal of Cell Biology, 1985. **100**(3): p. 965-973.
458. Chemistry, C.-R.S.O. *Nile Red Chemical Structure - Chemspider*. Available from: http://www.chemspider.com/Chemical-Structure.58681.html.
459. *National Center for Biotechnology Information. PubChem Compound Database; CID=3955344, https://pubchem.ncbi.nlm.nih.gov/compound/3955344 (accessed Sept. 4, 2018).*
460. Moriguchi, T., et al., *Elucidation of adsorption mechanism of bone-staining agent alizarin red S on hydroxyapatite by FT-IR microspectroscopy.* Journal of Colloid and Interface Science, 2003. **260**(1): p. 19-25.
461. Bej, A.K., M.H. Mahbubani, and R.M. Atlas, *Amplification of Nucleic Acids by Polymerase Chain Reaction (PCR) and Other Methods and their Applications.* Critical Reviews in Biochemistry and Molecular Biology, 1991. **26**(3-4): p. 301-334.
462. Page, R.B. and A.J. Stromberg, *Linear methods for analysis and quality control of relative expression ratios from quantitative real-time polymerase chain reaction experiments.* The scientific world journal, 2011. **11**: p. 1383-1393.
463. Taylor, H.E., *Inductively coupled plasma-mass spectrometry: practices and techniques*. 2001: Academic press.
464. Singh, A.K., *Chapter 4 - Experimental Methodologies for the Characterization of Nanoparticles*, in *Engineered Nanoparticles*, A.K. Singh, Editor. 2016, Academic Press: Boston. p. 125-170.
465. Oishi, M. and K. Fukuda, *Analysis of Electroceramics by Laser Ablation ICP-MS.* Agilent Technologies publication.
466. Sept, D., et al., *Annealing Accounts for the Length of Actin Filaments Formed by Spontaneous Polymerization.* Biophysical Journal, 1999. **77**(6): p. 2911-2919.
467. Dominguez, R. and K.C. Holmes, *Actin Structure and Function.* Annual review of biophysics, 2011. **40**: p. 169-186.

468. Manautou, J.E., S.N. Campion, and L.M. Aleksunes, *9.08 - Regulation of Hepatobiliary Transporters during Liver Injury A2 - McQueen, Charlene A*, in *Comprehensive Toxicology (Second Edition)*. 2010, Elsevier: Oxford. p. 175-220.
469. Verderame, M., et al., *Cytoskeletal F-actin patterns quantitated with fluorescein isothiocyanate-phalloidin in normal and transformed cells.* Proceedings of the National Academy of Sciences, 1980. **77**(11): p. 6624-6628.
470. Cooper, J.A., *Effects of cytochalasin and phalloidin on actin.* The Journal of Cell Biology, 1987. **105**(4): p. 1473-1478.
471. Barden, J.A., et al., *Localization of the phalloidin and nucleotide-binding sites on actin.* European Journal of Biochemistry, 1987. **162**(3): p. 583-588.
472. Cuenca, A.G., et al., *Emerging implications of nanotechnology on cancer diagnostics and therapeutics.* Cancer, 2006. **107**(3): p. 459-466.
473. Wijaya, A., et al., *Selective Release of Multiple DNA Oligonucleotides from Gold Nanorods.* ACS Nano, 2009. **3**(1): p. 80-86.
474. Galvin, P., et al., *Nanoparticle-based drug delivery: case studies for cancer and cardiovascular applications.* Cellular and Molecular Life Sciences, 2012. **69**(3): p. 389-404.
475. Agarwal, A., et al., *Targeted gold nanorod contrast agent for prostate cancer detection by photoacoustic imaging.* Journal of applied physics, 2007. **102**(6): p. 064701.
476. Jokerst, J.V., et al., *Photoacoustic Imaging of Mesenchymal Stem Cells in Living Mice via Silica-Coated Gold Nanorods.* ACS Nano, 2012. **6**(7): p. 5920-5930.
477. Johnsson, B., S. Löfås, and G. Lindquist, *Immobilization of proteins to a carboxymethyldextran-modified gold surface for biospecific interaction analysis in surface plasmon resonance sensors.* Analytical Biochemistry, 1991. **198**(2): p. 268-277.
478. Boussif, O., et al., *A versatile vector for gene and oligonucleotide transfer into cells in culture and in vivo: polyethylenimine.* Proceedings of the National Academy of Sciences, 1995. **92**(16): p. 7297-7301.
479. Zhang, X.Z., et al., *8 - Bioactive materials in gene therapy*, in *Bioactive Materials in Medicine*, X. Zhao, J.M. Courtney, and H. Qian, Editors. 2011, Woodhead Publishing. p. 179-219.
480. R Vancha, A., et al., *Use of polyethyleneimine polymer in cell culture as adhesion factor and lipofection enhancer*. Vol. 4. 2004. 23.
481. Curtis, K.A., et al., *Unusual salt and pH induced changes in polyethylenimine solutions.* PloS one, 2016. **11**(9): p. e0158147.
482. Lim, C.Y., et al., *Succinimidyl Ester Surface Chemistry: Implications of the Competition between Aminolysis and Hydrolysis on Covalent Protein Immobilization.* Langmuir, 2014. **30**(43): p. 12868-12878.
483. Jonkheijm, P., et al., *Chemical Strategies for Generating Protein Biochips.* Angewandte Chemie International Edition, 2008. **47**(50): p. 9618-9647.
484. Israelachvili, J.N., *21 - Interactions of Biological Membranes and Structures*, in *Intermolecular and Surface Forces (Third Edition)*, J.N. Israelachvili, Editor. 2011, Academic Press: San Diego. p. 577-616.
485. Mackey, M.A., et al., *The Most Effective Gold Nanorod Size for Plasmonic Photothermal Therapy: Theory and In Vitro Experiments.* The Journal of Physical Chemistry B, 2014. **118**(5): p. 1319-1326.
486. Gu, X., et al., *The Effect of Gold Nanorods Clustering on Near-Infrared Radiation Absorption.* Applied Sciences, 2018. **8**(7): p. 1132.
487. Marcon, G., G. Plakoutsi, and F. Chiti, *Protein Aggregation Starting From The Native Globular State1*, in *Methods in Enzymology*. 2006, Academic Press. p. 75-91.

488. Kettiger, H., et al., *Interactions between silica nanoparticles and phospholipid membranes.* Biochimica et Biophysica Acta (BBA) - Biomembranes, 2016. **1858**(9): p. 2163-2170.
489. Tong, W., et al., *Control of Symmetry Breaking Size and Aspect Ratio in Gold Nanorods: Underlying Role of Silver Nitrate.* The Journal of Physical Chemistry C, 2017. **121**(6): p. 3549-3559.
490. Parab, H.J., et al., *Biosensing, cytotoxicity, and cellular uptake studies of surface-modified gold nanorods.* The Journal of Physical Chemistry C, 2009. **113**(18): p. 7574-7578.
491. Alkilany, A.M., et al., *Cellular Uptake and Cytotoxicity of Gold Nanorods: Molecular Origin of Cytotoxicity and Surface Effects.* Small, 2009. **5**(6): p. 701-708.
492. Iosin, M., et al., *Study of protein–gold nanoparticle conjugates by fluorescence and surface-enhanced Raman scattering.* Journal of Molecular Structure, 2009. **924**: p. 196-200.
493. Rovati, L., et al., *Plastic optical fiber pH sensor using a sol-gel sensing matrix*, in *Fiber Optic Sensors*. 2012, InTech.
494. Ekici, O., et al., *Thermal analysis of gold nanorods heated with femtosecond laser pulses.* Journal of physics D: Applied physics, 2008. **41**(18): p. 185501.
495. Laszlo, A., *The effects of hyperthermia on mammalian cell structure and function.* Cell Proliferation, 1992. **25**(2): p. 59-87.
496. Lepock, J.R., *Cellular effects of hyperthermia: relevance to the minimum dose for thermal damage.* International Journal of Hyperthermia, 2003. **19**(3): p. 252-266.
497. Vidair, C.A., S.J. Doxsey, and W.C. Dewey, *Heat shock alters centrosome organization leading to mitotic dysfunction and cell death.* Journal of Cellular Physiology, 1993. **154**(3): p. 443-455.
498. Rieder, C.L. and R.W. Cole, *Cold-shock and the Mammalian cell cycle.* Cell cycle, 2002. **1**(3): p. 168-174.
499. Shen, S., et al., *Targeting mesoporous silica-encapsulated gold nanorods for chemo-photothermal therapy with near-infrared radiation.* Biomaterials, 2013. **34**(12): p. 3150-3158.
500. Jackson, J., et al., *Design and Near-Infrared Actuation of a Gold Nanorod–Polymer Microelectromechanical Device for On-Demand Drug Delivery.* Micromachines, 2018. **9**(1): p. 28.
501. Mooney, R., et al. *Internal temperature increase during photothermal tumour ablation in mice using gold nanorods*. in *EMBC*. 2015.
502. Zuk, P.A., et al., *Multilineage cells from human adipose tissue: implications for cell-based therapies.* Tissue engineering, 2001. **7**(2): p. 211-228.
503. Horwitz, E.M., et al., *Isolated allogeneic bone marrow-derived mesenchymal cells engraft and stimulate growth in children with osteogenesis imperfecta: Implications for cell therapy of bone.* Proceedings of the National Academy of Sciences, 2002. **99**(13): p. 8932.
504. Jarvinen, L., et al., *Lung Resident Mesenchymal Stem Cells Isolated From Human Lung Allografts Inhibit T Cell Proliferation via a Soluble Mediator.* Journal of immunology (Baltimore, Md. : 1950), 2008. **181**(6): p. 4389-4396.
505. Lee, O.K., et al., *Isolation of multipotent mesenchymal stem cells from umbilical cord blood.* Blood, 2004. **103**(5): p. 1669-1675.
506. Ra, J.C., et al., *Stem cell treatment for patients with autoimmune disease by systemic infusion of culture-expanded autologous adipose tissue derived mesenchymal stem cells.* Journal of Translational Medicine, 2011. **9**(1): p. 181.
507. Roddy, G.W., et al., *Action at a Distance: Systemically Administered Adult Stem/Progenitor Cells (MSCs) Reduce Inflammatory Damage to the Cornea Without*

Engraftment and Primarily by Secretion of TNF-α Stimulated Gene/Protein 6. STEM CELLS, 2011. **29**(10): p. 1572-1579.
508. Orlic, D., et al., *Bone marrow cells regenerate infarcted myocardium.* Nature, 2001. **410**(6829): p. 701.
509. Xiang, Z., et al., *Bone Marrow Mesenchymal Stem Cells in a Three-Dimensional Gelatin Sponge Scaffold Attenuate Inflammation, Promote Angiogenesis, and Reduce Cavity Formation in Experimental Spinal Cord Injury.* Cell Transplantation, 2011. **20**(11-12): p. 1881-1899.
510. Ortiz, L.A., et al., *Interleukin 1 receptor antagonist mediates the antiinflammatory and antifibrotic effect of mesenchymal stem cells during lung injury.* Proceedings of the National Academy of Sciences, 2007. **104**(26): p. 11002-11007.
511. Kharaziha, P., et al., *Improvement of liver function in liver cirrhosis patients after autologous mesenchymal stem cell injection: a phase I–II clinical trial.* European Journal of Gastroenterology & Hepatology, 2009. **21**(10): p. 1199-1205.
512. Hernigou, P., et al., *Osteonecrosis repair with bone marrow cell therapies: State of the clinical art.* Bone, 2015. **70**: p. 102-109.
513. Rasulov, M.F., et al., *First experience in the use of bone marrow mesenchymal stem cells for the treatment of a patient with deep skin burns.* Bulletin of Experimental Biology and Medicine, 2005. **139**(1): p. 141-144.
514. Yamada, Y., et al., *A novel approach to periodontal tissue regeneration with mesenchymal stem cells and platelet-rich plasma using tissue engineering technology: A clinical case report*. Vol. 26. 2006. 363-9.
515. Lu, D., et al., *Comparison of bone marrow mesenchymal stem cells with bone marrow-derived mononuclear cells for treatment of diabetic critical limb ischemia and foot ulcer: A double-blind, randomized, controlled trial.* Diabetes Research and Clinical Practice, 2011. **92**(1): p. 26-36.
516. Gazit, Z., et al., *Chapter 19 - Mesenchymal Stem Cells*, in *Essentials of Stem Cell Biology (Third Edition)*, R. Lanza and A. Atala, Editors. 2014, Academic Press: Boston. p. 255-266.
517. Huang, H.-L., et al., *Trypsin-induced proteome alteration during cell subculture in mammalian cells.* Journal of Biomedical Science, 2010. **17**(1): p. 36-36.
518. Anghileri, L.J. and D. Dermietzel, *Cell Coat in Tumor Cells – Effects of Trypsin and EDTA: A Biochemical and Morphological Study.* Oncology, 1976. **33**(1): p. 17-23.
519. Gallant, N.D., et al., *Micropatterned Surfaces to Engineer Focal Adhesions for Analysis of Cell Adhesion Strengthening.* Langmuir, 2002. **18**(14): p. 5579-5584.
520. Todaro, G.J. and H. Green, *QUANTITATIVE STUDIES OF THE GROWTH OF MOUSE EMBRYO CELLS IN CULTURE AND THEIR DEVELOPMENT INTO ESTABLISHED LINES.* The Journal of Cell Biology, 1963. **17**(2): p. 299-313.
521. Grabinski, C., et al., *Effect of Gold Nanorod Surface Chemistry on Cellular Response.* ACS Nano, 2011. **5**(4): p. 2870-2879.
522. Anwer, A.G., et al., *Visible 532 nm laser irradiation of human adipose tissue-derived stem cells: Effect on proliferation rates, mitochondria membrane potential and autofluorescence.* Lasers in surgery and medicine, 2012. **44**(9): p. 769-778.
523. Ravi, M., et al., *In vitro Immunogenetic Effects of 532 nm Short YAG Laser Pulses on Human Lymphocytes.* International Journal of Human Genetics, 2002. **2**(1): p. 15-18.
524. Roggan, A., et al. *Optical properties of circulating human blood in the wavelength range 400-2500 nm*. 1999. SPIE.
525. Wan, J., et al., *Surface chemistry but not aspect ratio mediates the biological toxicity of gold nanorods in vitro and in vivo.* Scientific Reports, 2015. **5**: p. 11398.
526. Rayavarapu, R.G., et al., *In vitro toxicity studies of polymer-coated gold nanorods.* Nanotechnology, 2010. **21**(14): p. 145101.

527. Horvát-Karajz, K., et al., *In vitro effect of carboplatin, cytarabine, paclitaxel, vincristine, and low-power laser irradiation on murine mesenchymal stem cells.* Lasers in Surgery and Medicine, 2009. **41**(6): p. 463-469.
528. Karu, T., *Primary and secondary mechanisms of action of visible to near-IR radiation on cells.* Journal of Photochemistry and photobiology B: Biology, 1999. **49**(1): p. 1-17.
529. Palankar, R., et al., *Nanoplasmonically-Induced Defects in Lipid Membrane Monitored by Ion Current: Transient Nanopores versus Membrane Rupture.* Nano Letters, 2014. **14**(8): p. 4273-4279.
530. Samsonraj, R.M., et al., *Establishing Criteria for Human Mesenchymal Stem Cell Potency.* Stem Cells (Dayton, Ohio), 2015. **33**(6): p. 1878-1891.
531. L. Ramos, T., et al., *MSC surface markers (CD44, CD73, and CD90) can identify human MSC-derived extracellular vesicles by conventional flow cytometry.* Cell Communication and Signaling : CCS, 2016. **14**: p. 2.
532. Dominici, M., et al., *Minimal criteria for defining multipotent mesenchymal stromal cells. The International Society for Cellular Therapy position statement.* Cytotherapy. **8**(4): p. 315-317.
533. Murphy, C.J., et al., *Gold Nanoparticles in Biology: Beyond Toxicity to Cellular Imaging.* Accounts of Chemical Research, 2008. **41**(12): p. 1721-1730.
534. Nikoobakht, B. and M.A. El-Sayed, *Evidence for Bilayer Assembly of Cationic Surfactants on the Surface of Gold Nanorods.* Langmuir, 2001. **17**(20): p. 6368-6374.
535. Yu, et al., *Gold Nanorods: Electrochemical Synthesis and Optical Properties.* The Journal of Physical Chemistry B, 1997. **101**(34): p. 6661-6664.
536. Lewinski, N., V. Colvin, and R. Drezek, *Cytotoxicity of Nanoparticles.* Small, 2008. **4**(1): p. 26-49.
537. Takahashi, H., et al., *Modification of Gold Nanorods Using Phosphatidylcholine to Reduce Cytotoxicity.* Langmuir, 2006. **22**(1): p. 2-5.
538. Jain, P.K., W. Huang, and M.A. El-Sayed, *On the Universal Scaling Behavior of the Distance Decay of Plasmon Coupling in Metal Nanoparticle Pairs: A Plasmon Ruler Equation.* Nano Letters, 2007. **7**(7): p. 2080-2088.
539. Stiles, P.L., et al., *Surface-Enhanced Raman Spectroscopy.* Annual Review of Analytical Chemistry, 2008. **1**(1): p. 601-626.
540. Tsai, S.-W., et al., *Photothermal effects of laser-activated surface plasmonic gold nanoparticles on the apoptosis and osteogenesis of osteoblast-like cells*. Vol. Volume 11. 2016. 3461-3473.
541. Turrens, J.F., *Mitochondrial formation of reactive oxygen species.* The Journal of Physiology, 2003. **552**(2): p. 335-344.
542. Dröge, W., *Free Radicals in the Physiological Control of Cell Function.* Physiological Reviews, 2002. **82**(1): p. 47-95.
543. Zorov, D.B., et al., *Reactive oxygen and nitrogen species: Friends or foes?* Biochemistry (Moscow), 2005. **70**(2): p. 215-221.
544. Dai, D.-F., P.S. Rabinovitch, and Z. Ungvari, *Mitochondria and Cardiovascular Aging.* Circulation Research, 2012. **110**(8): p. 1109-1124.
545. Fiers, W., et al., *More than one way to die: apoptosis, necrosis and reactive oxygen damage.* Oncogene, 1999. **18**: p. 7719.
546. Matés, J.M., et al., *Intracellular redox status and oxidative stress: implications for cell proliferation, apoptosis, and carcinogenesis.* Archives of Toxicology, 2008. **82**(5): p. 273-299.
547. Singer, S.J. and G.L. Nicolson, *The Fluid Mosaic Model of the Structure of Cell Membranes.* Science, 1972. **175**(4023): p. 720-731.
548. Vigh, L., B. Maresca, and J.L. Harwood, *Does the membrane's physical state control the expression of heat shock and other genes?* Trends in biochemical sciences, 1998. **23**(10): p. 369-374.

549. Balogh, G., et al., *The hyperfluidization of mammalian cell membranes acts as a signal to initiate the heat shock protein response.* The FEBS Journal, 2005. **272**(23): p. 6077-6086.
550. Zweytick, D., K. Athenstaedt, and G. Daum, *Intracellular lipid particles of eukaryotic cells.* Biochimica et Biophysica Acta (BBA) - Reviews on Biomembranes, 2000. **1469**(2): p. 101-120.
551. Lin, F.-T. and M.D. Lane, *Antisense CCAAT/enhancer-binding protein RNA suppresses coordinate gene expression and triglyceride accumulation during differentiation of 3T3-L1 preadipocytes.* Genes & development, 1992. **6**(4): p. 533-544.
552. Samuelsson, L., et al., *The CCAAT/enhancer binding protein and its role in adipocyte differentiation: evidence for direct involvement in terminal adipocyte development.* The EMBO Journal, 1991. **10**(12): p. 3787-3793.
553. Jiang, M.-S., et al., *Derepression of the C/EBPα gene during adipogenesis: identification of AP-2α as a repressor.* Proceedings of the National Academy of Sciences, 1998. **95**(7): p. 3467-3471.
554. Gargiulo, C.E., S.M. Stuhlsatz-Krouper, and J.E. Schaffer, *Localization of adipocyte long-chain fatty acyl-CoA synthetase at the plasma membrane.* Journal of lipid research, 1999. **40**(5): p. 881-892.
555. Gan, L., et al., *FABP4 reversed the regulation of leptin on mitochondrial fatty acid oxidation in mice adipocytes.* Scientific Reports, 2015. **5**: p. 13588.
556. Kirkham, G. and S. Cartmell, *Genes and proteins involved in the regulation of osteogenesis.* Ashammakhi N, Reis R, Chiellini E, editores. Topics in Tissue Engineering, 2007. **3**.
557. Golub, E.E. and K. Boesze-Battaglia, *The role of alkaline phosphatase in mineralization.* Current Opinion in Orthopaedics, 2007. **18**(5): p. 444-448.
558. Prins, H.-J., et al., *In vitro induction of alkaline phosphatase levels predicts in vivo bone forming capacity of human bone marrow stromal cells.* Stem Cell Research, 2014. **12**(2): p. 428-440.
559. Renno, A.C.M., et al., *The Effects of Laser Irradiation on Osteoblast and Osteosarcoma Cell Proliferation and Differentiation in Vitro.* Photomedicine and Laser Surgery, 2007. **25**(4): p. 275-280.
560. Hamblin, M.R., *Introduction to Experimental and Clinical Studies Using Low-Level Laser (Light) Therapy (LLLT).* Lasers in surgery and medicine, 2010. **42**(6): p. 447-449.
561. Ma, H., et al., *A Bifunctional Biomaterial with Photothermal Effect for Tumor Therapy and Bone Regeneration.* Advanced Functional Materials, 2016. **26**(8): p. 1197-1208.
562. Kajiya, H., et al., *Photothermal stress triggered by near-infrared-irradiated carbon nanotubes up-regulates osteogenesis and mineral deposition in tooth-extracted sockets.* International Journal of Hyperthermia, 2015. **31**(6): p. 635-642.
563. Cooper, G.M. and R.E. Hausman, *The cell: Molecular approach*. 2004: Medicinska naklada.
564. Frantz, C., K.M. Stewart, and V.M. Weaver, *The extracellular matrix at a glance.* Journal of Cell Science, 2010. **123**(24): p. 4195-4200.
565. Meredith Jr, J., B. Fazeli, and M. Schwartz, *The extracellular matrix as a cell survival factor.* Molecular biology of the cell, 1993. **4**(9): p. 953-961.
566. Berrier, A.L. and K.M. Yamada, *Cell–matrix adhesion.* Journal of Cellular Physiology, 2007. **213**(3): p. 565-573.
567. Schmidt, S. and P. Friedl, *Interstitial cell migration: integrin-dependent and alternative adhesion mechanisms.* Cell and Tissue Research, 2009. **339**(1): p. 83.
568. Silvipriya, K., et al., *Collagen: Animal sources and biomedical application.* J App Pharm Sci, 2015. **5**(3): p. 123-127.

569. Willerth, S., *Chapter 4 - Design considerations when engineering neural tissue from stem cells*, in *Engineering Neural Tissue from Stem Cells*, S. Willerth, Editor. 2017, Academic Press. p. 65-88.
570. Colognato, H. and P.D. Yurchenco, *Form and function: The laminin family of heterotrimers.* Developmental Dynamics, 2000. **218**(2): p. 213-234.
571. Ryan, M.C. and A.M. Christiano, *The functions of laminins: Lessons from in vivo studies.* Matrix Biology, 1996. **15**(6): p. 369-381.
572. Ramos, G.d.O., et al., *Fibronectin Modulates Cell Adhesion and Signaling to Promote Single Cell Migration of Highly Invasive Oral Squamous Cell Carcinoma.* PLOS ONE, 2016. **11**(3): p. e0151338.
573. Yang, L., et al., *Comparison of mesenchymal stem cells released from poly (N-isopropylacrylamide) copolymer film and by trypsinization.* Biomedical Materials, 2012. **7**(3): p. 035003.
574. Nishida, K., et al., *Corneal reconstruction with tissue-engineered cell sheets composed of autologous oral mucosal epithelium.* New England Journal of Medicine, 2004. **351**(12): p. 1187-1196.
575. Sekine, H., et al., *Cardiac Cell Sheet Transplantation Improves Damaged Heart Function via Superior Cell Survival in Comparison with Dissociated Cell Injection.* Tissue Engineering Part A, 2011. **17**(23-24): p. 2973-2980.
576. Shiroyanagi, Y., et al., *Transplantable urothelial cell sheets harvested noninvasively from temperature-responsive culture surfaces by reducing temperature.* Tissue Engineering, 2003. **9**(5): p. 1005-1012.
577. Iwata, T., et al., *Cell sheet engineering and its application for periodontal regeneration.* Journal of tissue engineering and regenerative medicine, 2015. **9**(4): p. 343-356.
578. Sart, S., et al., *Controlled expansion and differentiation of mesenchymal stem cells in a microcarrier based stirred bioreactor.* BMC Proceedings, 2011. **5**(8): p. P55.
579. Ramsey, W.S., et al., *Surface treatments and cell attachment.* In Vitro, 1984. **20**(10): p. 802-808.
580. Ryan, J.A., *Evolution of cell culture surfaces.* BioFiles, 2008. **3**(8): p. 21.
581. Joy, D.C. and C.S. Joy, *Study of the Dependence of E2 Energies on Sample Chemistry.* Microscopy and Microanalysis, 2005. **4**(5): p. 475-480.
582. FlatabØ, R., A. Coste, and M.M. Greve, *A systematic investigation of the charging effect in scanning electron microscopy for metal nanostructures on insulating substrates.* Journal of Microscopy, 2017. **265**(3): p. 287-297.
583. Leontieva, O.V., Z.N. Demidenko, and M.V. Blagosklonny, *Contact inhibition and high cell density deactivate the mammalian target of rapamycin pathway, thus suppressing the senescence program.* Proceedings of the National Academy of Sciences, 2014. **111**(24): p. 8832-8837.
584. Zhu, Y., et al., *Adipose-derived stem cell: a better stem cell than BMSC.* Cell Biochemistry and Function, 2008. **26**(6): p. 664-675.
585. Goh, T.K.-P., et al., *Microcarrier culture for efficient expansion and osteogenic differentiation of human fetal mesenchymal stem cells.* BioResearch open access, 2013. **2**(2): p. 84-97.
586. Levenberg, S., et al., *Long-range and selective autoregulation of cell-cell or cell-matrix adhesions by cadherin or integrin ligands.* Journal of Cell Science, 1998. **111**(3): p. 347-357.
587. Ferrari, C., et al., *Limiting cell aggregation during mesenchymal stem cell expansion on microcarriers.* Biotechnology Progress, 2012. **28**(3): p. 780-787.
588. Borys, M.C. and E.T. Papoutsakis, *Formation of bridges and large cellular clumps in CHO-cell microcarrier cultures: Effects of agitation dimethyl sulfoxide and calf serum.* Cytotechnology, 1992. **8**(3): p. 237-248.

589. Xu, Y., et al., *Large-scale, low-cost synthesis of monodispersed gold nanorods using a gemini surfactant.* Nanoscale, 2015. **7**(15): p. 6790-6797.